INFORMATION TO USERS

This manuscript has been reproduced from the microfilm master. UMI films the text directly from the original or copy submitted. Thus, some thesis and dissertation copies are in typewriter face, while others may be from any type of computer printer.

The quality of this reproduction is dependent upon the quality of the copy submitted. Broken or indistinct print, colored or poor quality illustrations and photographs, print bleedthrough, substandard margins, and improper alignment can adversely affect reproduction.

In the unlikely event that the author did not send UMI a complete manuscript and there are missing pages, these will be noted. Also, if unauthorized copyright material had to be removed, a note will indicate the deletion.

Oversize materials (e.g., maps, drawings, charts) are reproduced by sectioning the original, beginning at the upper left-hand corner and continuing from left to right in equal sections with small overlaps.

Photographs included in the original manuscript have been reproduced xerographically in this copy. Higher quality 6" x 9" black and white photographic prints are available for any photographs or illustrations appearing in this copy for an additional charge. Contact UMI directly to order.

ProQuest Information and Learning
300 North Zeeb Road, Ann Arbor, MI 48106-1346 USA
800-521-0600

THE MOLECULAR DYNAMICS AND REACTIVITY OF TRANSITION METAL AND MAIN GROUP η^1-INDENYL COMPLEXES

By

MARK J. STRADIOTTO, B.Sc.

A Thesis

Submitted to the School of Graduate Studies

in Partial Fulfillment of the Requirements

for the Degree

Doctor of Philosophy

McMaster University

THE DYNAMICS AND REACTIVITY OF η^1-INDENYL COMPLEXES

DOCTOR OF PHILOSOPHY (1999) McMaster University

(Chemistry) Hamilton, Ontario

TITLE: The Molecular Dynamics and Reactivity of Transition Metal and Main Group η^1-Indenyl Complexes

AUTHOR: Mark J. Stradiotto

SUPERVISORS: Dr. M. J. McGlinchey and Dr. M. A. Brook

NUMBER OF PAGES: xiv, 228

ABSTRACT

The molecular dynamics of a landmark compound in fluxional organometallic chemistry, $(\eta^5\text{-}C_5H_5)Fe(CO)_2(\eta^1\text{-}C_9H_7)$, **1.9**, were reexamined by use of 2D-EXSY and single selective inversion NMR techniques. Contrary to an important early report, the present work establishes unambiguously that this compound is quasi-fluxional. The barrier ($\Delta G^{\ddagger}$) to [1,5] iron shifts in **1.9** is 20 ± 2 kcal mol^{-1} and the intermediate isoindene, **1.10**, is sufficiently long-lived so as to yield a [4+2] cycloadduct, **2.2**, with tetracyanoethylene.

The tris(σ-indenyl)silanes, $(1\text{-}C_9H_7)_3SiX$ where X = H, Me or allyl (**3.18**, **3.19** and **3.20**, respectively) undergo a series of [1,5] silatropic shifts which interconvert the *RRR*, *RRS*, *RSS*, and *SSS* isomers, where the *R* and *S* labels refer to the absolute configuration of C(1) in each indenyl ring. The molecular dynamics of these tris(σ-indenyl)silanes have been elucidated by means of selective inversion experiments together with 2D-EXSY data; the barrier ($\Delta G^{\ddagger}$) to [1,5] silicon shifts in these compounds is ~ 24 kcal mol^{-1}, and the exchange pathways between indenyl sites can be conveniently mapped onto a hypercube. Moreover, each of the three tris(σ-indenyl)silanes examined yielded the corresponding triple Diels-Alder adduct, **3.21**, **3.22** and **3.23**, respectively, upon reaction with tetracyanoethylene. Despite the steric demands of the ligands in these tris(σ-indenyl)silanes and tris(benzonorbornyl)silanes, it has been demonstrated that chemical reactions can still be carried out at the silicon centers in these molecules.

Whilst examining the factors which affect silicon migrations in indenylsilanes, the silicon-substituted dibenzo[*a*,*d*]fulvalene, **4.24**, was unexpectedly obtained in low yield from the reaction of indene and chlorotrimethylsilane in the presence of excess base. This compound has been characterized by use of both NMR spectroscopy and X-ray crystallography, and can be rationally prepared in acceptable yield starting from the dimer of trimethylsilylindene, **4.31**. In continuation of these studies, a series of indenylsilanes bearing methyl substituents (**4.7**) and a π-bonded

chromium fragment (**4.38**) on indene have been prepared, as has a compound in which a dicobalt cluster is situated adjacent to the migrating silicon center (**4.52**). Data obtained from 2D-EXSY and single selective inversion NMR studies involving these complexes demonstrated that such structural perturbations have little impact on the barrier to [1,5] silicon shifts ($\Delta G^{\ddagger}$ ~ 24 kcal mol^{-1}) in this class of compounds.

Finally, in an attempt to generate a compound capable of participating in intramolecular Diels-Alder reactions, the indenylsilanes, **5.15-5.17**, were prepared; the quasi-fluxional nature of this molecular system was revealed by 2D-EXSY NMR. Preliminary reactivity studies demonstrated that the unactivated dienophiles tethered to the indenyl framework in these molecules do not undergo the desired intramolecular [4+2] cycloaddition process.

ACKNOWLEDGMENTS

First and foremost I wish to thank my co-supervisors, Dr. Michael McGlinchey and Dr. Michael Brook, not only for their guidance, but also for providing me with the opportunity to explore areas of chemistry that intrigued me. Their support of my personal and professional efforts has helped me to grow both as a scientist, and as an individual. I am grateful for having had the opportunity to work with them, and consider them to be friends. I would also like to thank the other member of my Ph.D. thesis committee, Dr. Gary Schrobilgen, for his careful critique of my graduate research, and for his many valuable suggestions.

I am indebted to the facilities staff in the Department of Chemistry, including Dr. Donald Hughes (NMR), Brian Sayer (NMR), and Dr. James Britten (X-ray). In addition to providing a wealth of knowledge and expertise, these 'unsung heroes' ensure that our research time is spent solving chemical problems, not technical ones. I am especially thankful to Dr. Britten for his patience in teaching me some of the technical and theoretical aspects of X-ray crystallography; Jim has forgotten more about crystallography than I could ever hope to learn and working with him (in the X-ray lab, and on the blue line) has been a pleasure. I would also like to recognize the efforts of the office staff and Mike Malott; your work 'behind the scenes' keeps the department running smoothly and is greatly appreciated.

Throughout the course of my graduate studies, I have had the opportunity to work with and learn from several researchers, both from within the department, and from other academic institutions. I would like to thank Dr. Hughes, Dr. Alex Bain and Paul Hazendonk for their assistance in some of the NMR investigations. Dr. Suzie Rigby served not only as an important collaborator, but also as a mentor during my early days in graduate school; to her I owe much of my hands-on understanding of NMR spectroscopy. I am grateful to Dr. Lijuan Li and Dr. William Leigh for providing me with the opportunity to work on projects outside of my thesis research.

These studies afforded me exposure to areas of chemistry that I might not otherwise have delved into, and I have gained valuable experience from these endeavors.

Financial assistance, including scholarships from Imperial Chemical Industries, Dow Canada, NSERC Canada and McMaster University, was gratefully received.

I have met many wonderful people and made many friends during my time at McMaster – far too many to mention here. To the people who have passed through Dr. McGlinchey's lab during my stay – Suzie, Ralph, Jamie, Pippa, Stacey, Chris, John, Nada and Hari – your camaraderie made the lab an enjoyable place in which to work. To Ed and Pat – thanks for the many wonderful nights of food, cards and laughter. To the 'Charmers' – Rich, Sean and Tim – what can I say, other than I had the time of my life! I am especially indebted to Sean for showing me what life 'north of 60' is like. I would be remiss in not thanking the staff at the Rat, the John, and of course, the Phoenix.

For her encouragement, companionship, laughter, insight and patience, I would like to thank Stacey. You are my labmate, my teammate, my colleague, and most importantly, my best friend. You have a wonderful way of gently reminding me about the 'little things' and are truly an inspiration. Thank you for revealing the people and pleasures of the Valley to me.

Finally, to my sisters, Jennifer and Cynthia, and to my parents, Margaret and Elio, who provide unwavering support in all that I do, thank you. You are the platform from which I reach for the stars, while somehow always keeping my feet on the ground. I love you all very much and am proud to count you among my closest friends.

TABLE OF CONTENTS

LIST OF TABLES

LIST OF FIGURES

LIST OF COMMONLY USED SYMBOLS AND ACRONYMS

NMR:	Nuclear Magnetic Resonance
EXSY:	Exchange Spectroscopy
COSY:	Correlated Spectroscopy
HSQC:	Heteronuclear Single Quantum Coherence
HMBC:	Heteronuclear Multiple Bond Correlation
TCNE:	Tetracyanoethylene
IMDA:	Intramolecular Diels-Alder
T:	Temperature
E_a:	Activation Energy (Arrhenius)
$\Delta G^{\ddagger}$:	Gibb's Free Energy of Activation (Eyring)

CHAPTER ONE

Introduction

1.1 Molecular Dynamics: An Overview

The structure and properties of molecules are often rationalized based on a rigid point group formalism. Although in the majority of instances this approach is a valid one, some molecules possess a number of thermally accessible structures that, under energetically-favorable conditions, may interconvert *via* an *intra*molecular rearrangement pathway. Such dynamic compounds are defined as being *stereochemically non-rigid*,[1] and in the special case when all of the interconverting species are chemically and structurally equivalent, the compound is deemed *fluxional*.[2] In evaluating the features of a given compound, it is critical that the effects of dynamic processes on stereochemistry not be neglected. As will be delineated in the following sections, such oversights can lead to serious misconceptions about the nature of the structure and bonding in a given molecular system.

It is important to recognize that stereochemically non-rigid compounds occur widely and studies involving these molecules have played an important role in advancing our understanding in numerous chemical sub-disciplines. A myriad of fluxional inorganic compounds have been examined, including PF_5, **1.1**, in which the two axial and three equatorial fluorine atoms undergo chemical exchange as a result of a pseudorotation process.[3] Examples from organic chemistry are equally plentiful, and include the dynamic hydrocarbon, tricyclo[3.3.2.$0^{4,6}$]deca-2,7,9-triene ("bullvalene"), **1.2**, originally proposed by Doering,[2] and later synthesized and examined spectroscopically by Schröder[4] and Saunders.[5] At low temperature (-85 °C), the ^{1}H Nuclear Magnetic Resonance (NMR) spectrum of **1.2** is consistent with the *instantaneous* structure of **1.2**, while above 100 °C, only a sharp singlet (corresponding to the *dynamic* structure) is observed, due to the rapid intramolecular rearrangement process depicted in Scheme 1.1.

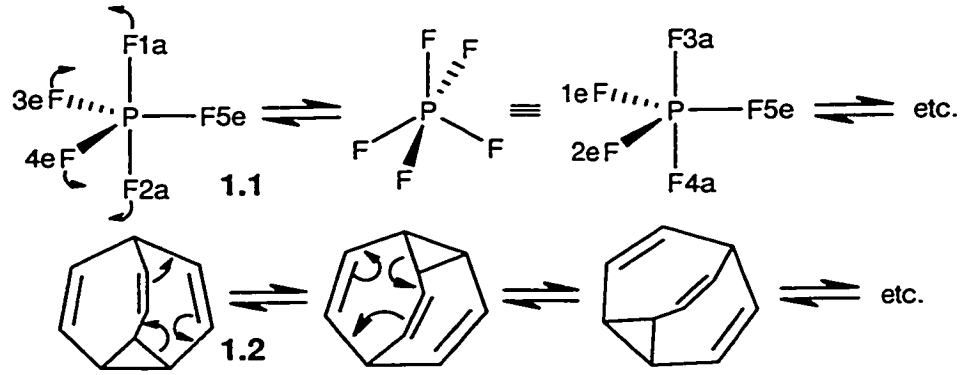

Scheme 1.1: *Intramolecular rearrangement processes involving **1.1** and **1.2** (for **1.1**, the atomic labels "a" and "e" denote axial and equatorial positions, respectively).*

The temperature-dependence of the ^{1}H NMR spectrum of **1.2** highlights the fact that the observed spectroscopic properties of a molecule will depend both on the lifetime of the molecular configurations present (Δt_{mc}) and on the time scale of the spectroscopic technique employed (Δt_{st}).[1,6] In the case of X-ray crystallographic studies, an *instantaneous* structure is invariably obtained because the interaction of the molecule with the X-ray radiation ($\Delta t_{st} \sim 10^{-18}$ s) is much faster than the time required for molecular rearrangements; in most cases, vibrational spectra ($\Delta t_{st} \sim 10^{-13}$ s) can similarly be rationalized as arising due to a superposition of the sub-spectra derived from all of the molecular configurations present. In contrast, the chemical shift data obtained from NMR spectroscopic experiments ($\Delta t_{st} \sim 10^{-1}$ to 10^{-9} s) correspond to a time scale of interaction which is comparable with the time required for molecular rearrangements to occur ($\Delta t_{st} \sim \Delta t_{mc}$), allowing for the application of this technique to the study of chemical exchange phenomena. Indeed, since the routine availability of Fourier-transform multi-NMR spectrometers in the mid-1970's, dynamic NMR spectroscopy has become the most common general method of detecting stereochemical non-rigidity in molecular species.[7]

1.2 Probing Chemical Exchange By Use of NMR Spectroscopy

In examining stereochemically non-rigid systems, chemists are often interested both in determining the energy required for the rearrangement and in obtaining information about the

mechanistic pathway(s) involved. Dynamic NMR spectroscopy is ideal in this regard, in that it is one of the few methods available for studying rates of reactions in systems at equilibrium. Under conditions of dynamic equilibrium when a chemical exchange process is proceeding at a detectable rate, kinetic processes can result in NMR spectral changes which may be utilized in the determination of rate constants for the chemical exchange process; the statistical analysis of rate data collected over a range of temperatures allows for an estimation of the energy barrier (E_a or $\Delta G^{\ddagger}$) for the rearrangement. Moreover, careful evaluation of the spectral changes noted above can be used in the elucidation of the rearrangement pathway(s).[7]

The numerous dynamic NMR techniques that have been developed for the evaluation of rates associated with chemically exchanging systems can be classified according to the magnitude of the rates of exchange that they are effective in measuring. Systems in the fast exchange regime ($k_{rate} \geq 10^5$ s^{-1}) can be studied by an evaluation of molecular correlation times obtained from relaxation or cross-relaxation experiments, while systems that fall in the intermediate exchange regime ($k_{rate} \sim 1$ to 10^5 s^{-1}) may be measured by use of total band-shape analysis. Slow rate constants ($k_{rate} \sim 10^{-3}$ to 10^2 s^{-1}), which are of comparable magnitude to the spin-lattice relaxation times for the exchanging sites, may be measured by use of one-dimensional magnetization transfer methods; two-dimensional exchange spectroscopy (2D-EXSY) is also useful in the slow exchange regime ($k_{rate} \sim 10^{-2}$ to 10^2 s^{-1}). In combination, these techniques allow for the determination of activation energies in the range of 5 to 25 kcal mol^{-1}.[6,7] A brief overview of these dynamic NMR techniques is presented in the following sections.

1.2.1 One-Dimensional Total Band-Shape Analysis

Total band-shape analysis makes use of the fact that passage from the slow through the intermediate to the fast chemical exchange regime is accompanied by characteristic changes in the shape of the NMR signal. Qualitatively, the spectral features of the exchanging system will vary according to the rate of the exchange process, and the frequency difference ($\Delta\nu$) between the permuted signals of the exchanging species. In the case of a two-site process when

exchange is rapid, the spectrum yields only the average of the two resonances; conversely, when the exchange is slow, individual signals are found. In the intermediate exchange regime, the extent of signal broadening varies, reaching a maximum at the coalescence temperature, T_c. In comparing the experimentally obtained NMR spectra (recorded at various temperatures) with a series of simulated spectra generated using assigned rate values, it is possible to visually match the experimental and simulated spectra, thus allowing for an estimation of the rearrangement rate at each temperature.[7,8]

1.2.1.1 Coalescence Temperature Approximation

The easiest and most widely used method of estimating the free energy of activation ($\Delta G^{\ddagger}$) for a chemical exchange process exploits the coalescence point, at which the two peaks combine so that there is only a single maximum. For two equally populated sites (at equilibrium) separated by a frequency difference, $\Delta\nu$, in the absence of exchange, the rate constant, k_c, at the coalescence temperature, T_c, is given by Equation 1:

$$k_c = \pi\Delta\nu / 2^{0.5} \qquad (1)$$

From this single rate constant, an estimation of the free energy of activation at the coalescence temperature, $\Delta G_c^{\ddagger}$, may be obtained by use of the Eyring Equation 2:

$$k_c = \kappa(k_b T_c / h) \exp(-\Delta G_c^{\ddagger} / RT_c) \qquad (2)$$

Rearranging Equation 2 leads to Equation 3:

$$\Delta G_c^{\ddagger} = (-RT_c) \ln[k_c h / (\kappa k_b T_c)] \qquad (3)$$

Finally, substitution for k_c in Equation 3 using Equation 1:

$$\Delta G_c^{\ddagger} = (-RT_c) \ln[(h\pi\Delta\nu / 2^{0.5}) / (\kappa k_b T_c)] \qquad (4)$$

It is evident from Equation 4 that after inputting values for the transmission coefficient, κ (usually assumed to be unity), the Boltzmann constant, k_b (1.3807×10^{-23} JK^{-1}), the Planck constant, h (6.6262×10^{-34} Js), and the ideal gas constant, R (8.3144 $JK^{-1}mol^{-1}$), the free energy of activation in Joules can be determined directly as a function of $\Delta\nu$ and T_c. Historically, such free energies of activation are often quoted in units of kilocalories per mole (1 J = 0.23901 cal).[7]

1.2.2 One-Dimensional Magnetization Transfer: Selective Inversion NMR

Although processes that occur with rate constants between 10^{-2} s^{-1} and 10^{2} s^{-1} are too slow to affect the NMR line-shape, they still may be probed using saturation transfer or magnetization transfer techniques. In general, these experiments involve the irradiation of one or more resonances of an exchanging system, followed by examination of the effect of that perturbation on the remaining sites. If the exchange rate is not much less than the spin-lattice relaxation rate (T_1), then the saturation or magnetization is transferred from the irradiated site to the sites that are chemically exchanging with it, allowing for the elucidation of chemical exchange pathways and the determination of the temperature-dependent rate constants associated with these processes. Stated differently, in such experiments, one of the exchange sites is "labeled" with a non-equilibrium Boltzmann population; chemical exchange phenomena result in a transfer of this label to the other exchanging sites in the molecule, where it can be detected in the form of a time-dependent change in the intensity of the signals associated with these chemical environments.[6,7]

In the two-site saturation transfer experiment first introduced by Forsén and Hoffman,[9] the required non-equilibrium Boltzmann population is generated by saturation of a given signal implicated in the exchange process by steady state irradiation. This technique was supplanted by the selective inversion experiment,[10,11] in which the resonance of interest is excited through inversion, by the application of a long, soft pulse to the signal prior to the required hard 90° observation pulse. Non-linear least squares fitting algorithms,[12] including the SIFIT program provided by McClung,[13] allow for the experimental selective inversion NMR data to be fit to different mechanistic pathways. The inversion approach is superior to the saturation technique in that the time allowed for chemical exchange is lengthened, and the intensities of both the inverted signal and those involved in the chemical exchange process can be measured; the intensity of the excited resonance in saturation transfer experiments is necessarily zero.

More recently, Bain and Cramer[14,15] developed the *single* selective inversion methodology, which makes use of the fact that any initial spin state can be created and fitted with the SIFIT

program. In contrast to previous methods which required multiple inversions,[11] the single selective inversion recovery approach requires that only one experiment be performed in order to obtain rate constants for all exchange processes occurring, provided that one can excite at least one site for each process. The pulse sequence used in the single selective inversion experiment is as follows:

$$D1 - 90° - D2 - 90° - VD - 90° - FID \qquad (5)$$

Following a fixed delay, D1, which ensures that the Boltzmann populations have returned to equilibrium, selective inversion of the NMR signal, which is on resonance, is achieved with the 90° - D2 - 90° sequence, where D2 is $\Delta\nu/2$, and $\Delta\nu$ is the frequency difference between the signal being inverted and the signal left unperturbed.[14,15] The return to equilibrium of the z-magnetization for the inverted peak can occur *via* chemical exchange and spin-lattice relaxation. If relaxation is more rapid than chemical exchange, then the population distribution at the unperturbed site will remain unaffected; in contrast, rapid exchange will result in complete saturation of the initially uninverted peak. However, when the rates are comparable, significant but incomplete population changes are induced at the uninverted site, allowing the rate of exchange to be measured. The growth or decay of the z-magnetization during the evolution time is monitored by conducting a series of experiments (at a given temperature) which utilize an incremented variable delay (VD). Numerical analysis[13] of these time-dependent signal intensity data ultimately yield the required temperature-dependent rate constants.

1.2.3 Two-Dimensional Exchange Spectroscopy (2D-EXSY)

The application of two-dimensional NMR techniques to the study of chemical exchange phenomena was first carried out by Ernst and co-workers.[16] Since then, the 2D-EXSY (EXchange SpectroscopY) technique, which has also been called 2D-EXCTSY (EXchange-CorrelaTed SpectroscopY), has gained widespread acceptance as an alternative to qualitative one-dimensional magnetization transfer experiments, because all exchange pathways can be elucidated simultaneously upon examination of a single two-dimensional spectrum. Moreover,

2D-EXSY can provide quantitative information about site-to-site rate constants, which is especially advantageous in the study of multisite exchange processes.[17] The 2D-EXSY pulse sequence commonly employed is:

$$\text{preparation - } 90° - t_1 - 90° - t_m - 90° - t_2 \qquad (6)$$

As in numerous other two-dimensional NMR experiments, the pulse sequence consists of three 90° pulses delimiting four periods of time: the preparation, evolution (t_1), and detection (t_2) periods. In addition, a mixing period, t_m, during which chemical exchange occurs, is introduced between the evolution and the detection periods. For a given 2D-EXSY experiment the mixing time is fixed, and by regularly incrementing t_1 and t_2 in the usual manner, the measured magnetization is a function of both t_1 and t_2; double Fourier transformation of the time domain converts this into a two-dimensional spectrum that is a function of two frequency variables (ω_1 and ω_2), with off-diagonal cross-peaks linking sites which are involved in chemical exchange.[18] It noteworthy that the 2D-EXSY experiment is commonly, and inappropriately, referred to as 2D-NOESY (Nuclear Overhauser Effect SpectroscopY), because the two experiments utilize identical pulse sequences to obtain different information. While the 2D-EXSY experiment provides information about chemically exchanging sites, the 2D-NOESY experiment provides a map of nuclei which are in close proximity to one another. The important difference between the two experiments arises as a result of the time increments employed in the pulse sequence.[8]

1.2.4 Selecting a Dynamic NMR Technique

Each of the aforementioned dynamic NMR methods has its own strengths, some of which were highlighted in the previous sections. However, each of these techniques have their drawbacks, which must be taken into consideration when choosing a methodology to apply in a given chemical exchange study. In some cases, the accessible rates of exchange dictate the techniques that may be utilized; for other systems, whereby slow through to fast exchange regimes are accessible, a combination of experiments can, and should, be used.

Total band-shape analysis is generally effective only for the determination of free energies in the range of 5 to 20 kcal mol^{-1}, primarily due to instrumental limitations; the operational range of most NMR spectrometers is from -150 to +150 °C. The elevated temperatures sometimes required to induce coalescence may be prohibitive, if thermal instability is a concern for the compound under examination. Moreover, for multisite systems, the total band-shape analysis becomes quite complex. In these instances, computer simulations are often required for the extraction of kinetic data, and spectral resolution must be sufficiently high so as to allow for the accurate determination of all the rate constants.

The coalescence temperature approximation approach is particularly appealing in that the time required to conduct the experiment and interpret the acquired data is minimal. An obvious disadvantage of this method is that it requires the temperature at which coalescence occurs to be qualitatively identified from experimental spectra, and subsequently permits the determination of a rate constant and the associated free energy of activation at a single temperature. For more rigorous analyses, methods that allow for the derivation of activation parameters ($\Delta H^{\ddagger}$ and $\Delta S^{\ddagger}$) based on the analysis of rate data obtained over a wide range of temperatures are often preferred.

Techniques based upon one-dimensional magnetization transfer have the advantage of detecting slow rates of exchange, and are therefore amenable to the study of dynamic systems at temperatures that are lower than would otherwise be required using the total band-shape analysis method. Nevertheless, the data obtained from these magnetization transfer experiments are often more time consuming to analyze. Experimental limitations must also be considered, because, as the resonances of interest increase in number or decrease in chemical shift separation, the technique becomes increasingly difficult to perform with a high degree of precision.

The beauty of two-dimensional magnetization transfer experiments, including 2D-EXSY, is that they qualitatively probe all of the operational exchange pathways for a given molecular

system, and the total time required to conduct such experiments is independent of the number of sites involved. In comparison to the available one-dimensional techniques, such approaches may not be as efficient in terms of the time required to obtain kinetic data. Additionally, the effective use of 2D-EXSY, especially in quantitative kinetic studies, requires that the optimal mixing time be determined (t_m in Equation 6). The choice of mixing time is often based on an estimate of the rate constant for the exchange process; if the mixing time is too short, insufficient magnetization transfer will prevent the observation of cross-peaks. In the case of multisite exchanges, second-order cross-peaks may be observed if the mixing time is too long. Difficulties can also arise in systems where the rate constants for multisite exchange are not equal. If the rates are considerably different, a single mixing time will not suffice and multiple 2D-EXSY experiments will be required in order to properly examine the kinetics of the system.[19,20]

1.2.5 Data Analysis and Evaluation of Activation Parameters

The temperature-dependent rate constants obtained *via* dynamic NMR studies can be used directly in the computation of chemically meaningful quantities, such as the activation parameters associated with a chemical exchange process under examination. Early approaches in this direction employed the Arrhenius activation theory, which is based on the assumption that molecules must acquire a certain surplus of energy, the activation energy E_a, in order to react, and that activated and unactivated molecules exist in equilibrium. The Arrhenius equation appears below as Equation 7, with the activation energy and the pre-exponential factor, A, being readily obtained from a linear plot of $\ln(k_{rate})$ versus T^{-1}:

$$\ln(k_{rate}) = \ln(A) - E_a / RT \qquad (7)$$

The absolute rate theory developed by Eyring, a more rigorous treatment founded in statistical mechanics, is currently the most popular technique for the derivation of activation parameters. The Eyring equation, originally presented as Equation 2, can be separated into the individual enthalpic and entropic terms based on the relationship given in Equation 8, leading to Equation 9:

$$\Delta G^{\ddagger} = \Delta H^{\ddagger} - T\Delta S^{\ddagger} \quad (8)$$

$$k_{rate} = \kappa(k_b T / h) \exp(-(\Delta H^{\ddagger} - T\Delta S^{\ddagger}) / RT) \quad (9)$$

If the transmission coefficient, κ, is assumed to be unity, then manipulation of Equation 9 yields Equation 10:

$$\ln(k_{rate} / T) = (-\Delta H^{\ddagger} / R)(1/T) + (\Delta S^{\ddagger} / R + \ln(k_b / h)) \quad (10)$$

It is evident that a linear plot of $\ln(k_{rate} / T)$ versus $1 / T$ provides a slope of $-\Delta H^{\ddagger} / R$, and an intercept of $(\Delta S^{\ddagger} / R + \ln(k_b / h))$, from which can be calculated the free energy of activation, $\Delta G^{\ddagger}$, at a specified temperature. Alternatively, $\Delta G^{\ddagger}$ can be determined from the values of $\Delta H^{\ddagger}$ and $\Delta S^{\ddagger}$ at a given temperature if the related Arrhenius parameters are known, using a combination of Equations 11 and 12:

$$\Delta H^{\ddagger} = E_a - RT \quad (11)$$

$$\Delta S^{\ddagger} = R (\ln (A) - \ln (e k_b / h)) \quad (12)$$

It is interesting to note that the Arrhenius equation is based on the temperature independence of E_a and A, and the Eyring equation on $\Delta H^{\ddagger}$ and $\Delta S^{\ddagger}$.

1.3 Fluxional σ-Cyclopentadienyl-Based Organometallic Complexes

It is not surprising, given the innumerable combinations of ligand sets and metal(loid) coordination motifs available, that organometallic chemistry is rich in examples of stereochemically non-rigid species. Over the past four decades, studies in this area have resulted in the identification of numerous dynamic processes, including: (a) the rotation or rearrangement of ligands on metals; (b) ligand scrambling on a metal; (c) the intermetallic, intramolecular exchange of ligands; and, (d) rearrangements of metal(s) on π-systems.[21-26] However, perhaps the most widely studied class of dynamic compounds are those in which a metal(loid) fragment is σ-bonded to a cyclopentadienyl ligand. In addition to providing the first examples of fluxional organometallic species, this class of compounds was among the first to be mechanistically

evaluated by use of dynamic NMR, in combination with the theoretical concepts of orbital symmetry conservation.

1.3.1 The Conservation of Orbital Symmetry

Over three decades ago, Woodward and Hoffmann[27,28] introduced one of the most useful theoretical approaches to the qualitative description of thermally or photochemically promoted reactions in the form of a set of predictive "rules" based on orbital symmetry considerations. Although these rules have found their widest application in organic chemistry, they may also be applied to inorganic and organometallic processes. The fundamental characteristic of a *concerted* process, as defined by Woodward and Hoffmann, is that in certain well-defined circumstances it is possible to transform *continuously* the molecular orbitals of reactants into those of the product in such a way as to preserve the bonding character of all occupied molecular orbitals along the entire reaction coordinate. Such concerted reactions are referred to as *symmetry allowed* and, since no filled orbitals are significantly destabilized in the transition state, a relatively low activation energy is observed. This simple, yet elegant theoretical approach has contributed significantly to our understanding of the nature of numerous concerted chemical processes, including sigmatropic rearrangements.[29] However, it is important to be cognizant of the fact that the dictates of orbital symmetry need not be adhered to in every chemical transformation. Not all reactions involve concerted mechanisms, and even when they are concerted, the principles of least motion[30] and subjacent orbital control[31] become increasingly relevant when steric factors become unfavorable to the operation of orbital symmetry control.

1.3.2 Thermal [1,m] Sigmatropic Rearrangements

McKinney and Haworth[32] have provided a succinct introduction to the elementary theoretical framework governing thermal sigmatropic [1,m] migrations in σ-bonded cyclopolyenyl organometallic complexes by considering the interaction of a metal(loid) group with the highest occupied molecular orbital (HOMO) of an acyclic polyene. One can naïvely envisage the migratory process as proceeding *via* homolytic cleavage of the metal fragment and the polyene; of

course, by definition this bonding interaction is maintained throughout the entire concerted rearrangement process. The HOMO of the polyenyl fragment can then be used to predict to which carbon atoms the metal can pass while maintaining bonding interactions with the polyene. When an *s*-orbital on the metal is employed, the [1,5] suprafacial shift is found to be a symmetry allowed process, while the corresponding [1,3] suprafacial shift is forbidden based on orbital symmetry rules. If the migrating metal utilizes a *p*, *d* or hybrid orbital, a different scenario emerges in which both [1,3] and [1,5] suprafacial shifts are permitted. In the case of the [1,5] suprafacial shift, the migration is anticipated to occur with retention of configuration at the migrating center, while for the [1,3] suprafacial shift, inversion of configuration is required. Although the [1,3] antarafacial migration is also theoretically permitted by the symmetry rules, spatial constraints make a concerted reaction in which the metal group moves from one side of the ligand to the other very difficult. The selection rules for allowed neutral [1,m] thermal migrations appear as part of Scheme 1.2.[27,28]

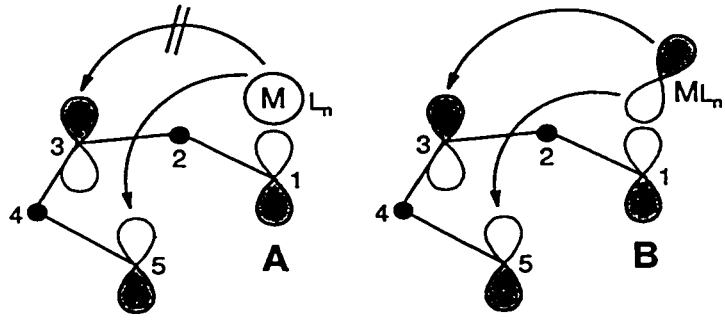

Selection Rules for [1,m] Sigmatropic Migrations

m = 3	*Antara*-retention *Supra*-inversion
m = 5	Antara-inversion Supra-retention
m = 7	Antara-retention Supra-inversion

Scheme 1.2: *Suprafacial migrations involving an acyclic metal-polyene complex, in which the metal interacts with the HOMO of the polyene using either an s- (**A**) or a p- (**B**) orbital.*

In extending these concepts to cyclopolyenes, it is necessary to take into account the cyclic π-interaction introduced by the development of a *p*-orbital at the migration origin. For odd-membered monocyclic C_nH_n π-systems, the HOMO must, in principle, be chosen from one of two degenerate molecular orbitals. In actuality, the cyclic C_nH_n π-system is perturbed due to interactions with the metal, thus lifting the degeneracy of these molecular orbitals.[33] As depicted in Scheme 1.3, the resulting allowed [1,5] and [1,3] shifts in σ-bonded cyclopentadienyl-based

organometallic systems (n = 5) are the same as described previously for the corresponding acyclic C_5 system.

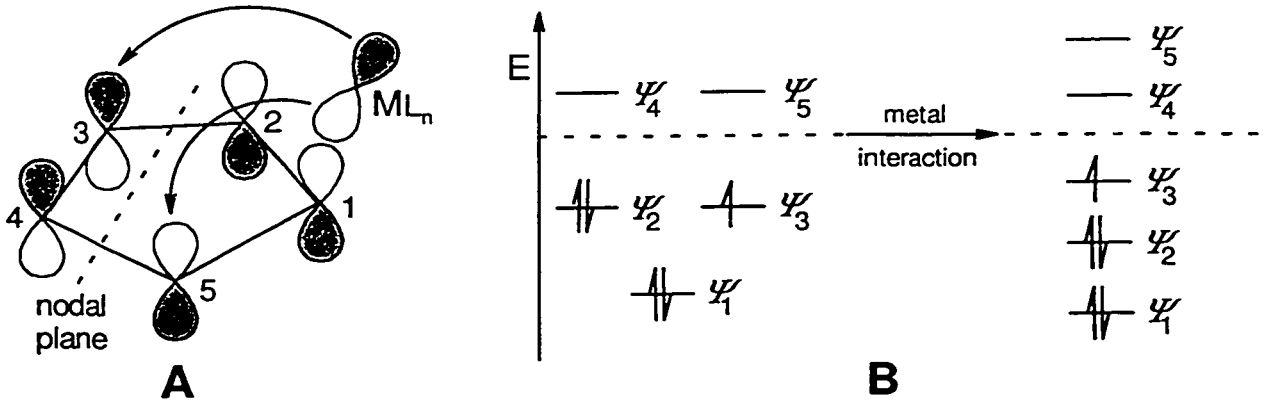

Scheme 1.3: *Suprafacial migrations involving the HOMO (Ψ_3) of a metallocyclopolyenyl complex (**A**); a qualitative molecular orbital scheme depicting the effect of metal interaction on the degeneracy of the orbitals in the C_5H_5 radical (**B**).*

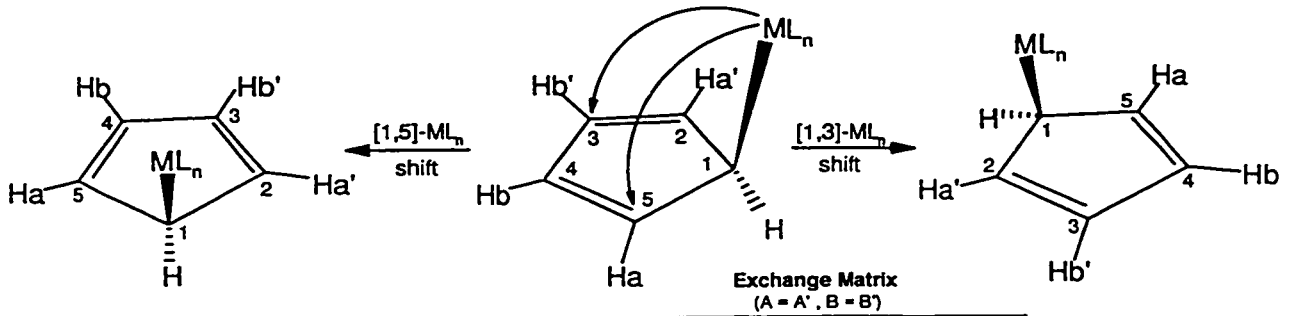

1.3: $ML_n = Fe(CO)_2(\eta^5\text{-}C_5H_5)$
1.4: $ML_n = Hg(\eta^1\text{-}C_5H_5)$
1.5: $ML_n = CuP(C_2H_5)_3$
1.6: $ML_n = Cr(NO)_2(\eta^5\text{-}C_5H_5)$
1.7: $ML_n = Ru(CO)_2(\eta^5\text{-}C_5H_5)$
1.8: $ML_n = Mo(NO)(\eta^5\text{-}C_5H_5)_2$

Exchange Matrix
(A = A', B = B')

Initial carbon atom label	Initial site label	After [1,5] Metal shift	After [1,3] Metal shift
1	H	A	B
2	A	H	A
3	B	A	H
4	B'	B	A
5	A'	B	B

Scheme 1.4: *Sigmatropic shifts in σ-cyclopentadienyl metal complexes and the corresponding exchange matrix for the [1,3] and [1,5] pathways.*

1.3.3 Transition Metal and Related Complexes

The non-rigid nature of organometallic compounds was first identified by Wilkinson and Piper[34-36] in 1956, during an examination of the σ-cyclopentadienyl metal complexes **1.3** to **1.5**. In each case, infrared evidence and chemical reactivity supported the σ-cyclopentadiene structures depicted in Scheme 1.4, which are entirely reasonable on the basis of valence concepts and comparison with analogous compounds. However, the ^{1}H NMR spectra obtained contained a single peak for each of the two rings in **1.3**, a single peak for **1.4**, and only one signal for the cyclopentadiene ring protons in **1.5**. In the absence of crystallographic data, and with extraordinary intuition, the authors attributed the appearance of a single ring proton resonance in each case to a rapid shifting of the metal-carbon linkage among the five possible positions, with concomitant rearrangement of the double bond system. As remarkable and unprecedented as this phenomenon was, ten years would pass before a subsequent report on such "ring-whizzing" would appear in the literature.[21]

In 1966, Bennett, Cotton and co-workers[37] published what is now a landmark article in the fields of organometallic chemistry and dynamic NMR spectroscopy. In this report, crystallographic data for **1.3** were provided, which verified the η^5/η^1 structure suggested by Wilkinson and Piper (Scheme 1.4). Moreover, these workers demonstrated that a ^{1}H NMR spectrum consistent with this structure could be observed if the data were collected below -80 °C; as the temperature was raised, the signals attributable to the two types of olefinic protons and the aliphatic proton broadened, leading to a collapsed single line spectrum at room temperature. In addition to validating the proposal put forth by Wilkinson and Piper, these preliminary spectroscopic data provided the basis for the first mechanistic analysis of NMR line-shape changes. Although the idea that rapid site exchange could lead to signal averaging had been known for several years,[38] the concept that the qualitative behavior of the line-shapes could yield mechanistic information had not previously been demonstrated.[22]

Bennett *et al.* skillfully recognized that three intramolecular mechanistic pathways could, in principle, lead to the observed signal averaging in the NMR spectra of compounds **1.3** to **1.8**, including 1,2 shifts, 1,3 shifts and random shifts (Scheme 1.4); since this work pre-dates the Woodward-Hoffmann rules, these transitions are conveniently reformulated in orbital symmetry terms as [1,5] and [1,3] suprafacial shifts. Careful examination of the variable-temperature ^{1}H NMR spectra of **1.3** revealed that the high-frequency portion of the AA'BB' multiplet (corresponding to the two pairs of equivalent sp^2-hybridized nuclei in the cyclopentadienyl ring) broadened faster than the other as the temperature was raised.[37] This allowed for the immediate exclusion of a dominant random shift pathway or one involving dissociation and recombination, since these processes would require that the two kinds of olefinic protons be permuted at the same rate. The problem was then reduced to that of differentiating between the [1,5] and [1,3] suprafacial pathways.

That the operation of a dominant migratory pathway involving either [1,3] or [1,5] shifts would lead to the broadening of one of the two vinylic multiplets more rapidly than the other is demonstrated by monitoring the site permutation process. A column matrix can be written listing the cyclopentadiene ring sites in the order in which they are initially occupied by the protons. Following either a [1,3] or [1,5] shift of the metal fragment (with simultaneous reorganization of the diene π-system), a given ring proton will occupy the same type of site that it was in previously (A = A' and B = B'), or it will reside in a new environment. Two new column matrices can then be written to describe the new locations of the protons after each type of transit; these three matrices are provided in tabular form as part of Scheme 1.4. It is readily observable that for each [1,5] shift, both protons initially in "A" sites change to other sites ("H" or "B"), whereas only half of the initial "B" protons change; on average, protons in the "A" sites reside in this location half as long as do those in the "B" sites. For [1,3] shifts the situation is reversed and protons in site "B" have mean residence times that are fifty percent shorter than those initially in the "A" sites. In either case more rapid broadening of one-half of the AA'BB' multiplet is predicted, which is in agreement with the experimental results.[23]

Having rigorously demonstrated that the dynamic behavior of **1.3** (and its analogues) can be rationalized in terms of either [1,3] or [1,5] suprafacial shifts, Bennett and co-workers were faced with the problem of selecting between these two mechanistic options; the solution of which depends on entirely on the proper assignment of the AA'BB' multiplet attributable to the two pairs of equivalent sp^2-hybridized nuclei in the cyclopentadienyl ring. Given the weighty mechanistic implications associated with this non-trivial chemical shift assignment, several different lines of independent supporting evidence for the assignment were sought. The initial criterion used by the authors in assigning the high-frequency portion of the multiplet to the "A" sites was based on the assumption that $|J_{HA}| > |J_{HB}|$, leading to the conclusion that **1.3** undergoes [1,5] shifts. Two lines of support for this choice were provided in a subsequent publication,[39] in which Cotton *et al.* reported on studies involving the analogous η^1-1*H*-inden-1-yl (herein referred to as σ-indenyl or η^1-indenyl) complex $(\eta^5\text{-}C_5H_5)Fe(CO)_2(\eta^1\text{-}C_9H_7)$, **1.9**, for which a [1,5] shift would require the intermediacy of the isoindene **1.10** (Scheme 1.5). It is evident that such a process would at least partially disrupt the aromatic character of the system, resulting in an increased barrier to migration relative to **1.3** (10.7 kcal mol^{-1}).[40,41] In contrast, if the "ring-whizzing" in **1.3** were to occur *via* a series of [1,3] shifts, then the indenyl analogue should exhibit fluxional behavior similar to **1.3**, since no disruption of the aromaticity in the six-membered ring is required. Based on the lack of observable ^1H NMR line-broadening up to 70 °C (above which **1.11** is rapidly generated) Cotton and co-workers claimed the indenyl compound, **1.9**, to be non-fluxional, an assertion which has been reiterated by Cotton in numerous subsequent reports.[21-23] Moreover, in examining isotopically labeled derivatives of **1.9** the chemical shifts assigned to the "A" and "B" sites were found to be in agreement with the previously invoked [1,5] shift mechanism. Soon after, a number of other reports appeared in the literature which also confirmed this choice of mechanistic pathway for **1.3** and **1.6** to **1.8**.[42]

Not long after Bennett and co-workers initially reported on the fluxional behavior of **1.3**, Whitesides and Fleming[43] published an analogous dynamic NMR examination of the copper system, **1.5**. These workers also observed a low-temperature ^1H NMR spectrum of **1.5** consistent with a

rigid instantaneous structure, which in turn coalesced to a single line when the sample was warmed room temperature. Yet, the behavior of **1.5** was found to differ from **1.3** at intermediate temperatures, in that the low-frequency portion of the AA'BB' multiplet collapsed more rapidly. Confronted with the daunting task of differentiating between these vinylic resonances, Whitesides provided an argument based primarily on the evaluation of chemical shift data, which led to an assignment identical to that put forth by Bennett *et al.* for **1.3**, and ultimately to the deduction of a [1,3] shift mechanism involving **1.5**. In contrast, when the coupling constant approach is applied to this problem, the chemical shift assignments in the AA'BB' multiplet are reversed, leading to the conclusion that [1,5] shifts are occurring. Ensuing studies involving related compounds and their indenyl analogues (for which the "A" and "B" protons can be unequivocally assigned) reveal that *a priori* it is extremely difficult to predict the relative ordering of the vinylic protons in these systems, and that chemical shift arguments based on solely inductive effects are ambiguous.[23]

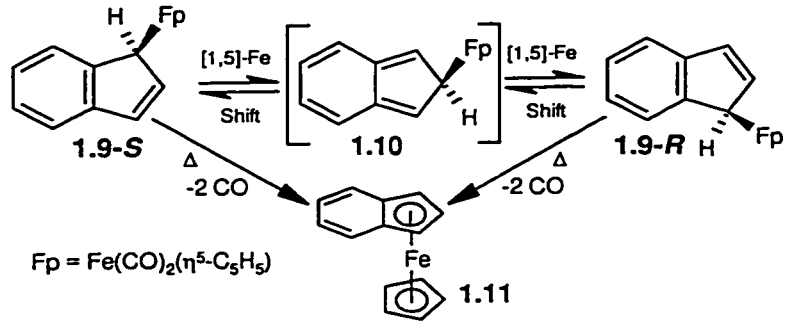

Scheme 1.5: *[1,5]-Suprafacial shifts in the η^1-indenyl system,* ***1.9****, showing the formation of the isoindene,* ***1.10****, and benzoferrocene,* ***1.11****.*

Numerous other transition metal complexes containing η^1-C_5H_5 rings are known, and in several cases their "ring-whizzing" behavior has been examined by dynamic NMR. Noteworthy examples of such compounds include the monocyclopentadienyl analogues[44] of **1.4** and the tetra(cyclopentadienyl) metal complexes of Group 4; the latter series of molecules is particularly fascinating as all four rings participate in chemical exchange processes which interconvert σ-C_5H_5 and π-C_5H_5 rings.[45] In light of the preceding examples, and in consideration of the conservation of orbital symmetry and the principle of "least action",[21,25] the most probable mechanism to account

for the fluxional behavior of all such η^1-C_5H_5 transition metal compounds is a [1,5] suprafacial, sigmatropic shift, which should proceed with retention of configuration at the metal center.

1.3.4 Main Group Complexes

Shortly after the discovery of "ring-whizzing" involving η^1-C_5H_5 transition metal complexes, it was recognized that the related main group species represented further examples of this special class of dynamic compounds. Although early studies were restricted primarily to the Group 14 elements, a variety of σ-cyclopentadienyl main group compounds have been prepared and their dynamic behavior examined over the past two decades. The factors that influence the dynamics of this group of compounds appear to be more numerous than in the corresponding transition metal systems, and in some cases, the operation of multiple rearrangement processes leads to complicated systems which require quite detailed stereochemical interpretation. One such distinction between the transition metal and main group series is that, in addition to elementotropic shifts, competitive prototropic shifts can lead to the formation of isomers in which the main group fragment (ER_x) resides in allylic or vinylic positions. Furthermore, the migratory aptitude of the main group elements differ greatly, and for a given element the rate can vary significantly with the "R" substituents and the substituents on the cyclopentadienyl ring. In keeping with the processes detailed in Section 1.3.3, the migrations of main group fragments are most commonly characterized as [1,5] sigmatropic shifts, which can proceed either with retention or inversion of configuration at the metalloid center.[46,47]

Much of the pioneering work in the field of fluxional cyclopolyenyl main group compounds involved the heavier Group 14 η^1-C_5H_5 compounds, and therefore an overview of this subject fittingly begins with a discussion of their dynamic behavior. Whereas the circumambulatory rearrangement of carbon fragments in substituted cyclopentadiene and related polyene ring systems has been extensively examined and reviewed,[48] the barriers to these processes are quite high, and accordingly will not be described here.

The occurrence of [1,5] metallotropic migrations in cyclopentadienyl compounds of silicon, germanium and tin was first noted in 1965,[49] and later examined in detail by Davison and Rakita.[50] In examining trimethyl derivatives of the aforementioned Group 14 elements, in combination with unsubstituted and substituted ring systems, the authors noted that these molecules undergo "ring-whizzing" with migratory rates in the order of Sn >> Ge > Si. For the silicon compounds, including **1.12**, the excessive heating required to induce line-broadening led to irreversible isomerizations due to competing hydrogen shifts, resulting in the generation of the vinylic isomers **1.13** and **1.14** (Scheme 1.6). However, given that the rate of hydrogen migration in these systems is approximately 10^6 times slower than that of silicon, contributions of hydrogen shifts to the observable NMR line-broadening were unequivocally ruled out.[51]

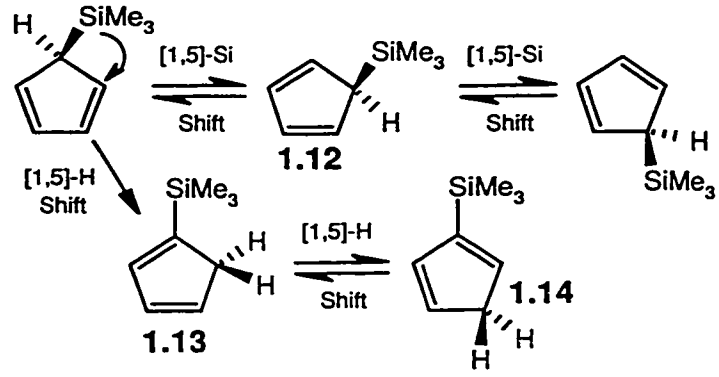

Scheme 1.6: *Silicon and hydrogen sigmatropic shifts in* ***1.12****, leading to* ***1.13*** *and* ***1.14****.*

Using the approach employed by Bennett *et al.* in the study of **1.3**, Davison and Rakita utilized data obtained from the corresponding silicon, germanium and tin indenyl derivatives to aid in the assignment of the vinylic AA'BB' multiplets in the corresponding C_5H_5 series. The more rapid collapse of the low-frequency portion of the multiplet, which was identified as the "A" protons (see Scheme 1.4), led to the conclusion that [1,5] metalloid shifts were occurring.[23] Spectroscopic data provided in a subsequent report by Sergeyev *et al.*[52] appeared to contradict this result. However, after careful scrutiny, Cotton *et al.*[53] demonstrated that these data were initially misinterpreted, and that the results actually provided support for the proposal of [1,5] shifts in these Group 14 compounds.

Many other important studies involving cyclopentadienyl Group 14 compounds have provided insight into the mechanism of these rearrangements, two of which are worthy of mention here. The assumed intramolecularity of these dynamic processes was verified by Davison *et al.*,[54] who noted that for the tin complexes, the Sn-H and Sn-C couplings could be observed in the fast exchange limit. In a later report, Stobart and co-workers[55] elegantly demonstrated that these Group 14 fragments migrate with retention of configuration at the metal center. For chiral compounds of the type $C_5H_5E(Me)(i\text{-}Pr)(Ph)$ (E = Si, Ge and Sn), ^1H and ^{13}C NMR spectral data revealed magnetically non-equivalent methyl resonances for the prochiral isopropyl substituent; as the temperature was raised and the cyclopentadienyl ring protons were equilibrated *via* [1,5] metallotropic shifts, the isopropyl methyl signals did not coalesce, thus establishing the retention of configuration at the migrating center. In light of the fluxional nature of Group 14 complexes, it is not surprising that other main group σ-cyclopentadienyl complexes are also stereochemically non-rigid. Even so, reports pertaining to non-Group 14 systems are scarce in comparison, and are primarily restricted to boron, phosphorus and their heavier congeners; selected examples of these are presented below.

Cyclopentadienyl complexes of Group 13 are also fluxional, and due to the potential for donation from the vinylic π-system into a vacant orbital at the main group element, sp^2-bonded isomers are thermodynamically favored over the allylic isomer. Since the barrier to [1,5] elementotropic migrations is lower than that of hydrogen shifts, only the allylic isomer is observed at reduced temperatures. This scenario is typified by $C_5H_5BMe_2$,[56] which exists as the fluxional sp^3-bonded isomer at low temperature (-80 °C), but is readily transformed (> -15 °C) to the corresponding vinylic complexes (analogous to **1.13** and **1.14**) *via* hydrogen shifts.[46] Interestingly, theoretical studies published by Schoeller[57] suggest that in the [1,5] sigmatropic rearrangements of cyclopentadienylboranes, *inversion* of configuration is favored over retention. The availability of such an inversion pathway is rationalized based on an alternative molecular orbital description of the element-cyclopentadiene interaction to that presented in Section 1.3.2 (see Scheme 1.3). The

author argues that processes involving inversion of configuration at the Group 13 center are viable (and even preferred), as the transition state can be looked upon as involving the mutual interaction of both a σ-orbital on the migrating fragment and its unhybridized *p*-orbital, with the π-system of the cyclopentadiene unit; as yet, such predictions await experimental authentication.

In addition to studies involving cyclopentadienyl[58] and pentamethylcyclopentadienyl complexes of boron,[46] the related aluminum compounds have also received considerable attention. An early study in this area involved the family of dialkylalanes, $C_5H_5AlR_2$,[59] and in each case the cyclopentadienyl resonance was observed as a single sharp line as low as -90 °C. The authors rationalized these spectroscopic results in terms of systems containing σ-bonded C_5H_5 rings and a fluxional aluminum center; however, in the absence of low-temperature limiting NMR spectra, these conclusions are speculative at best. More recently, tris(cyclopentadienyl)alane was examined, both spectroscopically and by use of X-ray crystallography;[60] similarly, an averaged signal for the C_5H_5 unit was observed at all temperatures. Based on the η^1, $\eta^{1.5}$ and η^2 cyclopentadienyl coordination geometries observed in the solid state, the NMR spectroscopic features were interpreted in terms of rapid [1,5] shifts of the aluminum fragment. Other combined NMR spectroscopic and X-ray crystallographic studies involving tris(cyclopentadienyl) complexes of gallium[61] and indium[62] also reveal averaged ring proton signals in solution and η^1-C_5H_5 geometries in the solid state.

Perhaps the most diverse classes of main group σ-cyclopentadienyl complexes are those of the Group 15 elements. As described previously for the η^1-C_5H_5 compounds of boron, allylic isomers of cyclopentadienylphosphorus compounds generally suffer from thermal instability, thus preventing an extensive comparative study of their dynamic behavior. However, the high barrier to non-degenerate methyl migrations has allowed for the examination of the related pentamethylcyclopentadienyl species, in which activation energies for sigmatropic migrations in the range of ≤ 5 to ≥ 35 kcal mol^{-1} have been observed.[46] That the migratory aptitude of these complexes depends heavily on coordination number at the metalloid center is evident in

comparing molecules of coordination number two, such as the multiply bonded compound, **1.15**, with tetra-coordinated species, including phosphonium salts and phosphane oxides, sulfides and selenides; the former are highly fluxional (E_a ~ 8 kcal mol^{-1}), while potential rearrangements involving the latter are not sufficiently rapid so as to cause observable changes to the NMR line-shape.[46] Moreover, the profound effect of migrating element substituents on the rearrangement rate is brought to light in the examination of tri-coordinate η^1-C_5Me_5 complexes; the barrier to [1,5] phosphorus shifts in the cyclic alkyl complex, **1.16** (E_a ~ 27 kcal mol^{-1}), is substantially larger than that found for the corresponding dibromo species, **1.17** (E_a ~ 5 kcal mol^{-1}).[63] Similar trends have been observed for the heavier Group 15 elements, although such compounds which have been prepared and studied by use of NMR are relatively few.[64]

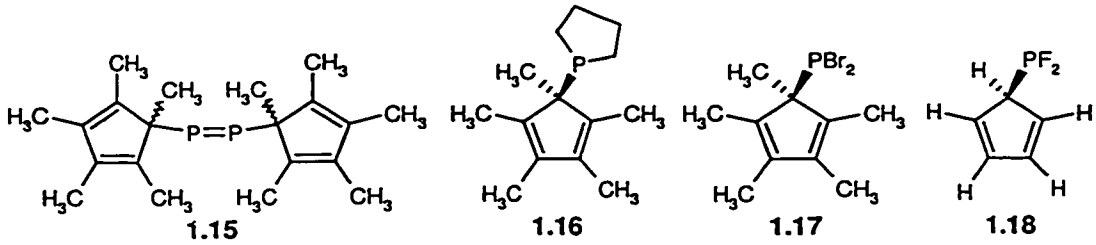

Scheme 1.7: *Selected examples of fluxional η^1-C_5R_5 (R = Me, H) phosphorus compounds.*

Despite the aforementioned thermal instability of the allylic isomers of phosphorus η^1-C_5H_5 compounds, examples of these do exist, and in some cases their dynamic behavior has been investigated. An early example includes $C_5H_5PF_2$, **1.18**, the non-rigidity of which was exquisitely demonstrated by use of ^{19}F NMR spectroscopy.[65] At low temperatures (-85 °C), the appearance of the ^{19}F resonance as a doublet of doublets (attributable to coupling with the phosphorus atom and the ring methine proton) is consistent with the instantaneous η^1-C_5H_5 structure depicted in Scheme 1.7. Upon warming to -30 °C the J_{HF} coupling collapses, and at ambient temperature a sextet pattern emerges and sharpens above 50 °C. These data indicate that on the NMR time scale, the PF_2 fragment in **1.18** resides on each of the cyclopentadienyl ring carbon atoms for an equivalent period of time, resulting in the observation of fluorine nuclei which couple equivalently to each of the five ring protons. While these findings can be rationalized in

terms of sigmatropic shifts involving the phosphorus unit, no facts pertaining to the rearrangement pathway were provided by the authors.

The viability of circumambulatory rearrangement pathways involving inversion of configuration at phosphorus has been examined by Schoeller.[66] Based on data obtained from Extended Hückel Molecular Orbital (EHMO) calculations, the potentiality of such stereochemical transformations in $C_5(R')_5PR_2$ complexes appears to be ligand-dependent; electropositive ligands on phosphorus favor inversion, whereas electronegative ligands promote retention. The stereochemistry in these rearrangements is also apparently influenced by the substituents attached to the cyclopentadienyl framework, as this ring is differently polarized in the transition state for the inversion and retention processes.

Experimental data acquired for tris(cyclopentadienyl) complexes of arsenic, antimony and bismuth (-70 °C to 35 °C) are in keeping with the previously observed trend of incrementally reduced migratory barriers upon descending the main group.[67] Proton NMR spectra obtained for the bismuth compound contain a single sharp line over the entire temperature range; a single line is also observed for the antimony complex, which broadens considerably at low temperatures. Conversely, the corresponding arsenic complex yields a low-temperature limiting ^1H NMR spectrum consistent with an $(\eta^1\text{-}C_5H_5)_3As$ structure, which subsequently coalesces to a single line spectrum above 35 °C. It is likely in the case of the arsenic compound that the equilibration of the ring protons occurs *via* sigmatropic migrations; such a scenario is also plausible for the heavier elements, but definitive mechanistic data remain elusive.

The rates of sigmatropic shifts among the Group 13, 14 and 15 cyclopentadienyl and pentamethylcyclopentadienyl complexes vary significantly; the experimentally derived activation energies (E_a) for selected examples are collected in Table 1.1 (Section 1.3.5). Attempts have been made to ascertain the origin of these differences using theoretical and computational methods, and some general conclusions derived from these investigations are deserving of mention. In a given instance, the barrier to sigmatropic shifts is determined by the relative

difference in energy between the η^1 ground state and the η^2 transition state. On descending the main group, the σ-bond between the migrating element and the cyclopentadienyl ring is weakened, while at the same time the orbital overlap between the migrating element and the carbon atoms at the migration termini is enhanced, due to the increased spatial extent of the valence orbitals on the heavier elements. The result is an overall reduction in the energy difference between the ground and transition states, and thus, reduced activation energies for migrations involving the heavier homologues are predicted.

The considerable variation in the rate of sigmatropic shifts and sensitivity to substituent effects between trivalent compounds of Groups 13 and 15, and tetravalent compounds of Group 14 has also been rationalized based on the nature of the frontier molecular orbitals involved in these systems.[68] In analogy to the previously described boron-based BR_2 fragments, the frontier orbital system of the PR_2 unit is characterized by a σ-orbital and a *p*-orbital, the latter of which interacts predominantly with the cyclopentadienyl fragment. This creates a situation in which the ligands can have a profound effect on the electronic character of the phosphorus center, and in the case of "R" substituents bearing lone pairs, the relevant *p*-orbital is perturbed in such a way as to lead to a drop in the transition state energy. Similarly, the migration rates of the related boron species can be correlated with the Lewis acidity of the boron center; rapid migrations are observed when "R" is chloro or methyl, rather low rates are observed for amino-substituted boranes, and static behavior (on the NMR time scale) is found for tetra-coordinate nitrogen-donor Lewis adducts. Much less dramatic substituent effects have been observed for the Group 14 cyclopentadienyl complexes. For example, the replacement of hydrogen by halogen atoms in cyclopentadienylsilanes marginally lowers the corresponding activation energy (~ 2 kcal mol^{-1}); the same is true for the introduction of methyl substituents. These observations can again be understood in terms of the bonding interactions in the ground and transition states. In contrast to the Group 13 and 15 elements, for which large differences in migratory rates are observed,

mesomeric effects cannot occur in tetra-valent Group 14 compounds, and therefore, a marked ligand influence on the barrier to sigmatropic shifts is not predicted.[46]

1.3.5 Concluding Remarks

In the more than forty years since the dynamic nature of σ-cyclopentadienyls was first postulated by Wilkinson, the synthetic, mechanistic and theoretical studies involving such complexes have played an important role, both in furthering our understanding of circumambulatory rearrangements and in emphasizing the significance of orbital symmetry conservation in chemical processes. The synthetic utility of the cyclopentadienyl group and its metal(loid) derivatives, coupled with the development of increasingly sensitive spectroscopic instrumentation, has led to continued interest in this burgeoning field of organometallic chemistry. It is evident that a distinction need not be made between transition metal and main group σ-cyclopentadienyl compounds, and that the preponderance of experimental evidence suggests that their fluxional behavior can be rationalized in terms of concerted, suprafacial [1,5] sigmatropic shifts. The barrier to elementotropic shifts in these complexes is most conveniently estimated by use of variable temperature NMR spectroscopic techniques, and careful interpretation of these spectral data can also yield mechanistic information about the rearrangement pathway(s) involved.

Table 1.1. Experimentally Determined Activation Energies (kcal mol^{-1}) for [1,5] Element Shifts in Selected Cyclopentadienyl and Pentamethylcyclopentadienyl Complexes of Groups 13, 14 and 15.[a]

$C_5H_5CMe_3$	> 40	$C_5Me_5NMe_2$	> 25
$C_5H_5SiMe_3$	13.0 ± 1	$C_5Me_5PMe_2$	23.0 ± 0.5
$C_5H_5GeMe_3$	9.2 ± 1	$C_5Me_5AsMe_2$	17.1 ± 0.4
$C_5H_5SnMe_3$	7.8 ± 1	$C_5Me_5SbMe_2$	11.3 ± 1.4
$C_5Me_5CMe_3$	> 40	$C_5Me_5BMe_2$	< 5
$C_5Me_5SiMe_3$	15.3 ± 0.2	$C_5Me_5BF_2$	12.8 ± 2.0
$C_5Me_5GeMe_3$	11.4 ± 1.3	$C_5Me_5BN(Me_2)_2$	20.6 ± 1.2
$C_5Me_5SnMe_3$	< 5	$C_5Me_5BCl_2$(pyridine)	> 25

[a]Data transcribed from Tables 11 and 15 in Jutzi, P. *Chem. Rev.* **1986**, *86*, 983.

1.4 Transition Metal and Main Group η^1-Indenyl Compounds

1.4.1 The Relationship Between Cyclopentadienyl and Indenyl Systems

The intrinsic relationship between σ-cyclopentadienyl complexes and their "benzannulated" indenyl counterparts has been alluded to in the foregoing sections; in several cases, the rigorous analysis of a σ-cyclopentadienyl metal(loid) system has relied heavily on data obtained from an examination of the analogous σ-indenyl compound. In fact, the similarity between circumambulations in fluxional cyclopentadienyls and those involving indenyl complexes has led to a description of the latter class of dynamic molecules as "quasi-fluxional". Such a distinction is necessary, because in contrast to the degeneracy of sequential [1,5] sigmatropic shifts involving σ-cyclopentadienyls, similar transitions in σ-indenyl systems proceed *via* non-degenerate migratory pathways involving short-lived isoindene intermediates; these processes are depicted in Scheme 1.8. The simplistic "diradical" rationale, used in Section 1.3.2 to schematically represent symmetry-allowed [1,5] sigmatropic migrations involving metal(loid) σ-cyclopentadienyl complexes, cannot *prima facie* be utilized in describing related processes in substituted indenes, due to the nodal properties of the HOMO of the indenyl radical (Scheme 1.9).[69] However, if the indene framework is instead regarded as a perturbed cyclopentadienyl fragment (i.e. cyclopentadiene containing an adjacent diene unit), the Woodward-Hoffmann selection rules governing concerted sigmatropic processes should effectively serve as a predictive guide.

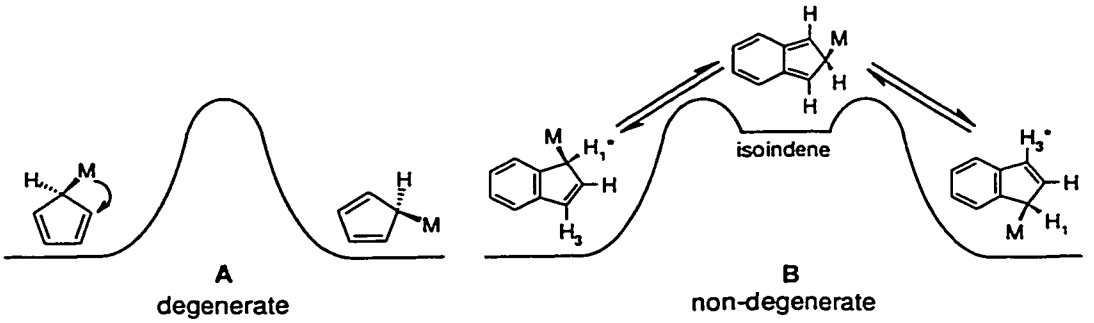

Scheme 1.8: *Reaction coordinate diagrams for the [1,5] sigmatropic shift pathway in fluxional σ-cyclopentadienyl (**A**) and quasi-fluxional σ-indenyl (**B**) complexes.*

An early estimate of the energetic cost of transforming an indenyl complex into the corresponding isoindenyl species was provided by Cotton (~ 8.5 kcal mol^{-1}).[37,39] This value was later verified experimentally through a comparative study of Group 14 fragment migrations in η^1-C_5H_5 and η^1-C_9H_7 complexes, in which it was observed that the barriers to sigmatropic shifts in the indenyl species were on average about 9 kcal mol^{-1} higher than in the related cyclopentadienyl complexes.[70] Historically, this heightened activation energy for sigmatropic shifts has presented a formidable barrier to the widespread examination of such migrations in transition metal and main group σ-indenyl compounds not comprised of the heavier Group 14 elements. Indeed, in the vast majority of cases, the conditions required to induce changes in the NMR line shape fell outside of the operational range of the instrumentation and/or resulted in extensive sample degradation. The advent of high-field spectrometers equipped with multi-pulse capability has provided a sensitive means of probing these chemical transformations under somewhat milder experimental conditions.

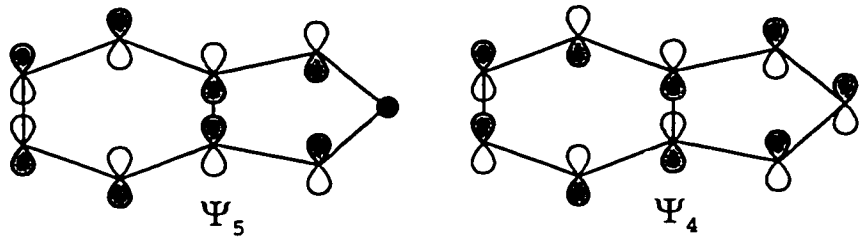

Scheme 1.9: *The HOMO (Ψ_5) and HOMO-1 (Ψ_4) of the indenyl radical.*

1.4.2 Impetus for a Review of η^1-Indenyl Complexes

Recently, η^1-indenyl transition metal and main group complexes have been the focus of numerous studies; the former have been identified as important intermediates in transition metal-based chemical transformations, while the latter have proven effective in the development of chiral catalytic systems. Despite the multitude of publications that have recently appeared detailing the preparation and characterization of such complexes, in the majority of cases, the potential for dynamic behavior has been overlooked. Moreover, a number of the studies that do include examinations of these dynamic processes are marred with misconceptions and often fail to recognize the possible significance of orbital symmetry conservation in these rearrangements.

Given the strong likelihood that molecular rearrangements involving transition metal and main group σ-indenyls are mechanistically related, and in light of the sporadic and disjointed nature of the reports pertaining to the dynamics of these compounds, a review of the entire area would be advantageous; unfortunately, no such survey has been published thus far. Within the following sections is provided a current summary of σ-indenyl compounds, with particular attention given to reports in which sigmatropic rearrangement processes are examined. Although a conscientious attempt has been made to cite all such dynamic studies, the goal of this critical review is not to serve as a comprehensive survey of the entire field, but rather to highlight the breadth and depth of this area, and to bring to the forefront the studies that provide a context for the thesis work to follow.

1.4.3 Transition Metal Complexes

1.4.3.1 The Generation of η^1-Indenyl Complexes Via "Ring-Slippage"

The ability of polyhapto (i.e. multi-coordinated) transition metal ligands to undergo changes in connectivity in response to electronic changes at the metal center is well documented. In the case of species bearing η^5-cyclopentadienyl fragments, such haptotropic isomerizations are common and are usually initiated by the addition of one or more two-electron donor ligand(s) to the metal center during thermally promoted associative substitution reactions; electrochemically and photochemically initiated processes are also known.[71] Remarkably, these "ring slippage" processes occur much more rapidly[72] in the corresponding η^5-indenyl complexes ($k_{ind} / k_{cp} \sim 10^8$), presumably because the η^3-coordination mode is stabilized *via* aromatization of the C_6 ring (Scheme 1.10).[73] This phenomenon, deemed the "kinetic indenyl ligand effect" by Basolo and co-workers,[74] has figured prominently in the design and mechanistic rationalization of numerous stoichiometric and catalytic processes that require the generation of an available coordination site *in situ*.[75] The significance of transition metal complexes containing η^3-indenyl ligands as purported reactive intermediates has lead to their widespread examination; to date, several trihapto species have been prepared and structurally characterized, including (but not restricted to) complexes of vanadium,[76] molybdenum,[77] tungsten,[78] and iridium.[79,80] Although stable η^1

indenyl species appear to be less common, these too have been examined and will be described throughout the following sections.

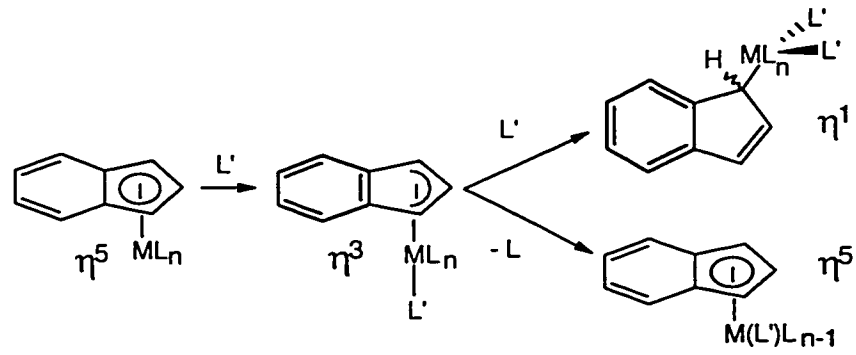

Scheme 1.10: *Ligand "slip" rearrangements involving an η^5-indenyl transition metal complex, giving rise to η^3 and η^1 species in which the aromatic character of the C_6 ring is recovered.*

1.4.3.2 Groups 4 and 6

A series of novel η^1-indenyl compounds comprising Group 4 elements has been prepared by Alt and co-workers.[81] Starting from the appropriate metal dichloride, the tris(indenyl) complexes, **1.19** and **1.20**, and the mono- and bis-indenyl metallocenes, **1.25** and **1.26**, were prepared *via* addition of indenyllithium. The stereochemically non-rigid nature of the tris(indenyl) species is evident upon examination of their temperature-dependent ^{1}H and ^{13}C NMR spectra. Under ambient conditions, NMR spectral data obtained from samples of these complexes reveal effective C_{3v} geometries in solution; the authors attribute these spectral features to a static η^5-η^5-η^5 structural formulation, as depicted for **1.19** and **1.20** in Scheme 1.11. At reduced temperatures (-100 °C for **1.19**; -40 °C for **1.20**) the acquired NMR spectra coincide with structures possessing effective C_3 molecular symmetries, in which all three indenyl ring environments are again equivalent. In the case of **1.19**, these variable temperature NMR data yield $\Delta G^{\ddagger}$ ~ 14.4 kcal mol^{-1}. Alt and co-workers rationalize the equilibration of the three indenyl rings in these zirconium and hafnium systems in terms of a rapid $\eta^5 \rightarrow \eta^3 \rightarrow \eta^1$ ligand interconversion process (*via* the intermediates **1.21** to **1.24**, Scheme 1.11), though no specific mechanistic details were provided. Indirect support for the viability of η^1 species was gained through the X-ray crystallographic

characterization of **1.24**, which was found to adopt an η^5-η^5-η^1 geometry in the crystal. Based on these crystallographic data, it is conceivable that the instantaneous structure in solution does not correspond to **1.19** and **1.20** as the authors suggest, but rather to that of the η^5-η^5-η^1 configuration possessed by **1.23** and **1.24**, in which rapid haptotropic shifts exchange η^5 and η^1 sites (leading to effective C_3 symmetry); at higher temperatures this dynamic process continues, and [1,5] metallotropic shifts become sufficiently rapid so as to equilibrate the two halves of the indenyl framework on the NMR timescale (leading to effective C_{3v} symmetry).

In separate publications, Alt and co-workers reported on the synthesis and characterization of **1.27**,[82] **1.28** and **1.29**,[83] three rare examples of η^1-1*H*-inden-2-yl transition metal complexes (Scheme 1.12); the structures of the zirconium and molybdenum compounds were confirmed by single crystal X-ray diffraction studies.

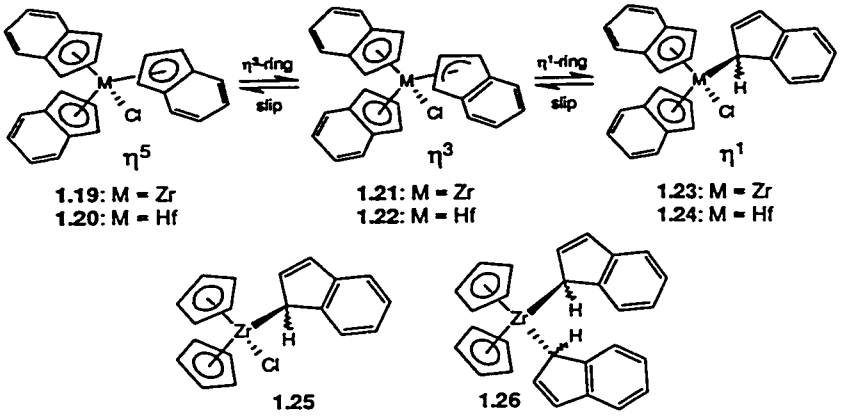

Scheme 1.11: *Some σ-indenyl derivatives of the heavier Group 4 elements.*

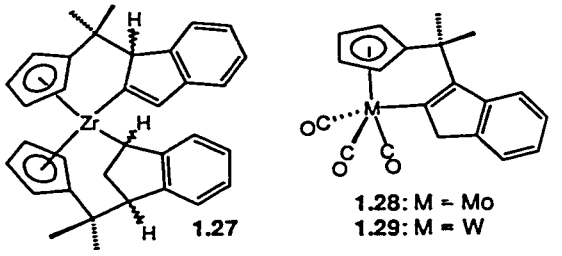

Scheme 1.12: *Rare examples of C(2)-bonded transition metal σ-indenyl complexes.*

1.4.3.3 Group 7

The successful conversion of η^5-C_9H_7 complexes into isolable η^1-C_9H_7 species *via* sequential ligand addition in an $\eta^5 \rightarrow \eta^3 \rightarrow \eta^1$ process, was first reported by Casey and O'Connor[84] in 1985 (Scheme 1.13). In attempting to prepare and examine the behavior of η^3-indenyl compounds, these workers noted that the addition of either trimethylphosphine or tri(*n*-butyl)phosphine to $(\eta^5$-$C_9H_7)Re(CO)_3$, **1.30**, instead resulted in the rapid generation of the double-addition, σ-indenyl complexes, **1.31** and **1.32**, respectively. In both cases only the facial isomer was generated, an assertion that was supported by comparison of spectroscopic data obtained from these samples with data acquired for *fac*-$(\eta^1$-$C_5H_5)Re(CO)_3(PMe_3)_2$, whose structure has been established by X-ray crystallography.[85]

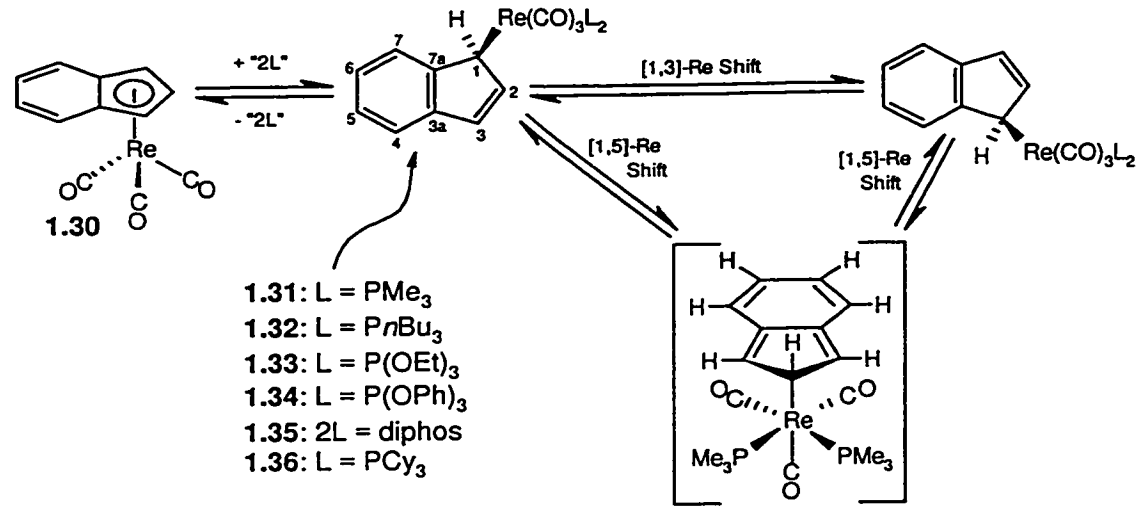

Scheme 1.13: *The synthesis and molecular rearrangements of* $(\eta^1$-$C_9H_7)Re(CO)_3L_2$ *complexes.*

The preparation of these rhenium complexes carries an additional significance, as they represent the first *bona fide* examples of dynamic η^1-indenyl species to be characterized; their stereochemically non-rigid character was documented *via* variable-temperature NMR studies. In the case of **1.31**, the low-temperature limiting ^{1}H NMR spectrum (-68 °C) is consistent with the "instantaneous" structure depicted in Scheme 1.13, and is characterized by the appearance of signals attributable to the diastereotopic (i.e. non-equivalent) trimethylphosphine ligands and an

η^1-indenyl framework. As the sample is warmed, the pairs of symmetry-related indenyl ring signals merge (H(1)/H(3), H(4)/H(7) and H(5)/H(6)), and at higher temperatures the diastereotopic phosphorus methyl signals similarly coalesce to a virtually coupled triplet, producing an overall "averaged" spectrum above 40 °C. Comparison of these experimentally obtained spectroscopic data with simulated NMR spectra yielded $\Delta G^{\ddagger} \sim 12.0 \pm 0.1$ kcal mol^{-1} for this dynamic process, a value which is significantly larger than that determined for the related cyclopentadienyl compound, $(\eta^1\text{-}C_5H_5)Re(CO)_3(PMe_3)_2$ ($\Delta G^{\ddagger} < 7$ kcal mol^{-1}).[84,85] The remarkable thermal stability of these η^1-compounds relative to $(\eta^5\text{-}C_5H_5)Fe(CO)_2(\eta^1\text{-}C_9H_7)$, **1.9**, was also brought to light during the variable-temperature ^{1}H NMR study of **1.31**, as the formation of neither dissociation nor substitution products was found, even after continuous heating at 65 °C for over an hour.

The virtual coupling involving the PMe_3 ligands of **1.31** in the fast exchange regime proved to be an important result, as it verified the non-dissociative nature of the dynamic process. Moreover, in the absence of restricted rotation about the indenyl-Re bond in the η^1-configuration at reduced temperatures, the exchanging phosphine methyl resonances confirmed the facial assignment, and suggests that the rearrangement proceeds with retention of configuration at the transition metal center. Casey and O'Connor skillfully recognized that these data, in consideration of the more rapid fluxional behavior of the cyclopentadienyl compound, are in agreement with a [1,5] sigmatropic shift mechanism; although they actually refer to a "1,2 shift" process without consideration of orbital symmetry requirements, the essence of their proposal is valid. However, based on the apparently rigid nature of Cotton's iron compound, **1.9**, the authors also propose that the required intermediacy of isoindenes in a "1,2" (=[1,5]) shift rearrangement pathway may be prohibitive, and that "*the observed fluxionality* ...of **1.31**... *may be due to a direct 1,3 shift*".[84]

Following the pioneering work of Casey and O'Connor, a detailed kinetic study was published by Bang, Lynch and Basolo,[86] in which reactions of **1.30** with a series of phosphines and phosphites were examined as a function of temperature and reactant concentration. In addition to detailing the preparation and characterization of four new η^1-indenyl rhenium

compounds, **1.33** to **1.36**, Basolo and co-workers identified the operation of both phosphine addition and carbonyl displacement reaction pathways, similar to that depicted in Scheme 1.10. For reactions involving triethylphosphite, reduced temperatures and high ligand concentrations favored the formation of the η^1-C_9H_7 complex, **1.33**; in contrast, under conditions of high temperature and low ligand concentration, the displacement product, $(\eta^5\text{-}C_9H_7)Re(CO)_2P(OEt)_3$, was preferentially formed. These workers noted that the nature of the entering phosphine plays a major role in partitioning between η^1 and η^5 products, with small and strongly basic nucleophiles favoring the formation of η^1-indenyl complexes. An additional facet of this work involved a kinetic study of the related compound, $(\eta^5$-trindenyl$)Re(CO)_3$; when reacted with triethylphosphite at 80 °C, the initially formed η^1-complex, **1.37**, is rapidly converted to the carbonyl displacement product, $(\eta^5$-trindenyl$)Re(CO)_2P(OEt)_3$ (Scheme 1.14). However, when the reaction temperature was lowered (40 °C), spectral changes corresponding to an $\eta^5 \rightarrow \eta^3 \rightarrow \eta^1$ conversion process were observed. The tributylphosphine complex, **1.38**, was also prepared and studied by these workers. [86]

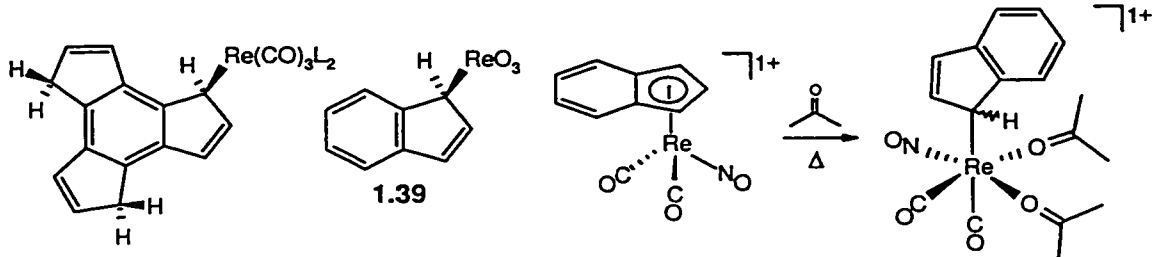

1.37: L = $P(OEt)_3$
1.38: L = $PnBu_3$

Scheme 1.14: *Selected rhenium-based η^1-indenyl compounds, including novel η^1-trindenyl species, an oxorhenium compound and a cationic complex containing a nitrosylrhenium center.*

Herrmann and co-workers[87] have demonstrated that tetrahedrally coordinated σ-indenyl rhenium complexes can also be prepared. The moisture and temperature-sensitive molecule, $(\eta^1\text{-}C_9H_7)ReO_3$, **1.39**, synthesized from Re_2O_7 and $(\eta^1\text{-}C_9H_7)Sn(n\text{Bu})_3$, was deemed stereochemically non-rigid based on data obtained from a variable-temperature spectroscopic study (Scheme 1.14). The ^{1}H NMR spectrum of **1.39** acquired at -50 °C is entirely consistent with

an η^1-C_9H_7 structural formulation; upon warming the sample to 0 °C, the H(1) and H(3) signals broaden significantly, and the aromatic protons approach coalescence. Presumably, the thermal instability of **1.39** (decomposition temperature ~ -30 °C) prevented the authors from acquiring sufficiently reliable spectroscopic data so as to allow for the accurate determination of the free energy associated with this rearrangement process. Even so, the qualitative description of the dynamic phenomenon provided by Hermann *et al.* is troublesome. In the abstract of their report, they state that "*a haptotropic structural rearrangement occurs > -25 °C in solution (1,3-shift mechanism)*", which implies that the rearrangement process is not operative below this temperature. Moreover, the description of a "haptotropic" process involving "1,3 shifts" clearly indicates that the potentially important role of orbital symmetry conservation has been overlooked.

In 1993, Zhou, Dewey and Gladysz[88] reported the inadvertent preparation of a novel cationic η^1-indenyl complex of rhenium. Starting from the tricarbonylrhenium compound, **1.30**, treatment with $NOBF_4$ in dichloromethane gave rise to what was the desired cationic π-complex, $[(\eta^5\text{-}C_9H_7)Re(CO)_2NO]^+BF_4^-$. However, when this product was dissolved in deuterated acetone to allow for an ambient-temperature NMR study, the observation of characteristic σ-indenyl resonances, including ReC*H* ^{1}H NMR signals, clearly revealed the formation of several η^1-complexes (Scheme 1.14); similar results were also obtained when acetonitrile was employed as the solvent. Ambient temperature ^{1}H and ^{13}C NMR spectral data acquired after heating the sample at 57 °C (0.5 h) verified the conversion of this mixture to a single product (> 95%), which was assigned as the facial-coordinated isomer, **1.40**. Unfortunately, attempts to isolate **1.40** were unsuccessful, and no comment is made about the operation of dynamic processes in this interesting molecule.

As an extension of the work of Casey and O'Connor, who studied the reactions of (η^5-C_9H_7)$Re(CO)_3$, **1.30**, with neutral, two-electron donor ligands, Richmond and Lee[89] examined associated reactions involving anionic reagents. Under ambient conditions, treatment of **1.30** with a hydride source was found to rapidly produce lithium indenide and the tetrametallic cluster,

$[H_6Re_4(CO)_{12}]^{2-}$ (Scheme 1.15). In rationalizing the formation of these products, Richmond proposed a set of reactions involving η^3- and η^1-anionic intermediates (**1.41** and **1.42**, respectively), which are ultimately converted to the observed "η^0" product (lithium indenide) and the tetrarhenium complex; neither of the purported intermediates were observed spectroscopically. Overall, the proposed reaction sequence represents an interesting example of an $\eta^5 \rightarrow \eta^3 \rightarrow \eta^1 \rightarrow \eta^0$ ring-slippage transformation process.

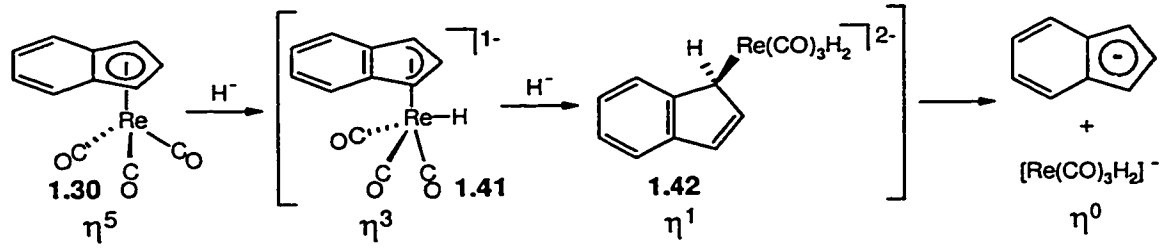

Scheme 1.15: *The successive transformation of the η^5-compound,* ***1.30****, into the "η^0" compound, lithium indenide, via the η^3 and η^1 intermediates,* ***1.41*** *and* ***1.42****.*

1.4.3.4 Group 8

Although the preparation and characterization of $(\eta^5\text{-}C_5H_5)Fe(CO)_2(\eta^1\text{-}C_9H_7)$, **1.9**, has already been presented in Section 1.3.3, given the considerable importance of this compound to the study of quasi-fluxional behavior in η^1-indenyl compounds, further discussion pertaining to the dynamics of this molecule is warranted. In contrast to the highly fluxional cyclopentadienyl compound, **1.3**, NMR spectroscopic data published by Cotton *et al.*[39] clearly indicate that any chemical exchange process involving **1.9** is slow on the NMR timescale. Indeed, these authors recognized that a [1,5] shift process involving **1.9** would proceed *via* the high-energy isoindene intermediate **1.10** (Scheme 1.5), and so similar migrations involving **1.3** should be much more facile. The apparently "non-fluxional" nature of **1.9** has since been put forward in support of a [1,5] shift mechanism for sigmatropic rearrangements in **1.3** and related cyclopentadienyl species, and continues to underpin our belief and understanding of η^1-indenyl complexes of the transition metals.

The subsequent discovery of quasi-fluxionality in bis(η^1-indenyl)mercury, **1.43**, (see Section 1.4.3.7, Scheme 1.27) prompted Cotton to rationalize the observed difference in dynamic behavior between this compound and the iron complex, **1.9**.[90] In doing so, Cotton and Marks proposed the formation of a migratory transition state (or intermediate) geometry for **1.43**, in which the mercury atom is positioned over the indenyl C_5 fragment, with bonding interactions between the metalloid center and three or more of the ring carbon atoms. Using this description of the transition state structure, Cotton and Marks suggest that while the mercury atom is capable of participating in such a bonding scheme *via* utilization of additional 6*p* valence orbitals, no such orbitals are available on the iron center in **1.9**, thus leading to the rigid characteristics of the latter compound. The paucity of characterized η^1-indenyl transition metal(loid) complexes at the time of publication (1969) restricted Cotton and Marks to a discussion centered on these two species alone, and this must be considered when evaluating the validity of their rationale. Nonetheless, it is evident that in light of the numerous main group (*vide infra*) and transition metal indenyl complexes which are now known to exhibit quasi-fluxional behavior, such a rudimentary valence orbital description does not accurately portray the transition state interactions of all dynamic η^1-indenyl species.

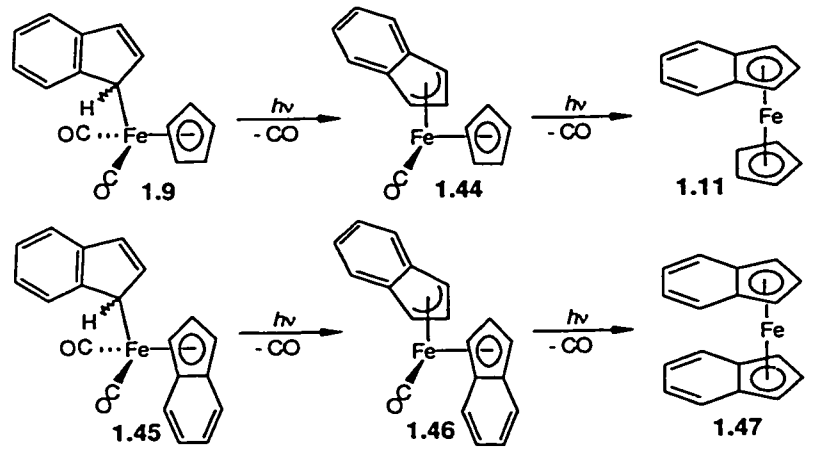

Scheme 1.16: *The photochemcially promoted decarbonylation reactions of the dicarbonyliron complexes,* ***1.9*** *and* ***1.45****.*

In 1986, Belmont and Wrighton[91] reported on the stepwise photochemical decarbonylation of Cotton's compound, **1.9**, and the related bis(indenyl) complex, (η^5-C_9H_7)Fe(CO)$_2$(η^1-C_9H_7), **1.45**. Irradiation with near-UV light at reduced temperatures allowed for the infrared detection of the corresponding monocarbonyl compounds, **1.44** and **1.46**, in which a formerly η^1-bonded ring has slipped to an η^3-configuration (Scheme 1.16); these monocarbonyl species were found to be thermally and photochemically labile, readily yielding the metallocenes, **1.11** and **1.47**.

Two intriguing examples of η^1-indenyl ruthenium compounds, **1.48** and **1.49**, have recently been published by Carty and co-workers[92] (Scheme 1.17). These crystallographically characterized complexes were generated in an unconventional manner, from reactions involving butadiynyl-Ru$_2$(CO)$_6$ complexes and the carbene derived from Ph_2CN_2. The authors rationalize the stability of these dimetallic η^1-complexes as arising due to the presence of an unsaturated fragment at the C(2) position, which allows for intramolecular coordination to the second ruthenium center.

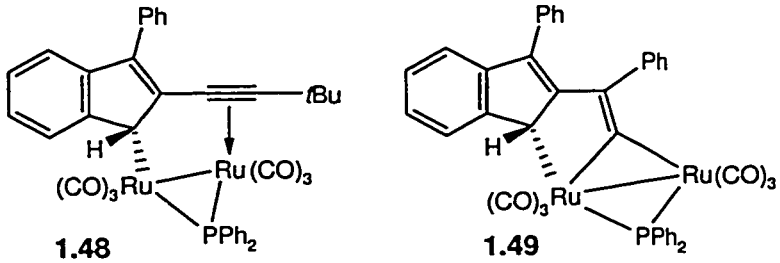

Scheme 1.17: *Rare examples of crystallographically characterized η^1-indenyl compounds of ruthenium.*

1.4.3.5 Group 9

Group 9 η^1-indenyl complexes were first observed spectroscopically by Green and co-workers[93] in 1977. In examining the reactivity of (η^5-C_9H_7)Rh(C_2H_4)$_2$, these workers noted that while treatment with two equivalents of *tert*-butyl isonitrile rapidly displaces ethylene to form **1.50**, the addition of excess *tert*-butyl isocyanide generates the σ-indenyl complex, **1.51** (Scheme 1.18). The formation of **1.51** was proposed based only on infrared spectroscopic data.

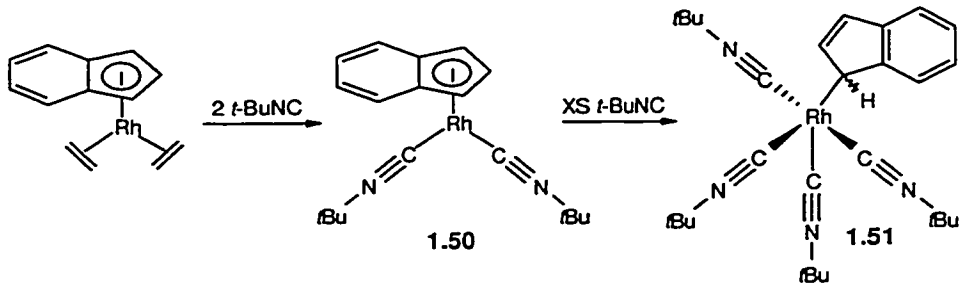

Scheme 1.18: *Generation of the first spectroscopically detected σ-indenyl complex of rhodium.*

In 1989, Merola and Kacmarcik[94] reported on the conversion of the η^5 iridium complex, **1.52**, to the crystallographically characterized η^0 species, **1.55** (Scheme 1.19). In studying the reactivity of **1.52** with nucleophiles, these workers observed that reaction with excess carbon monoxide displaces the 1,5-cyclooctadiene (COD) ligand, giving rise to $(\eta^5\text{-}C_9H_7)Ir(CO)_2$, **1.56**. In contrast, the addition of excess PMe_3 to **1.52** unexpectedly resulted in the quantitative formation of **1.55**, in which the indenyl fragment has formally been transferred from the iridium center to the cyclooctadiene moiety. Merola *et al.* propose an $\eta^5 \rightarrow \eta^3 \rightarrow \eta^1 \rightarrow \eta^0$ ring-slippage mechanism for the formation of **1.55** (Scheme 1.19), which parallels that put forth by Richmond for the reaction of **1.30** with hydride (Scheme 1.15).

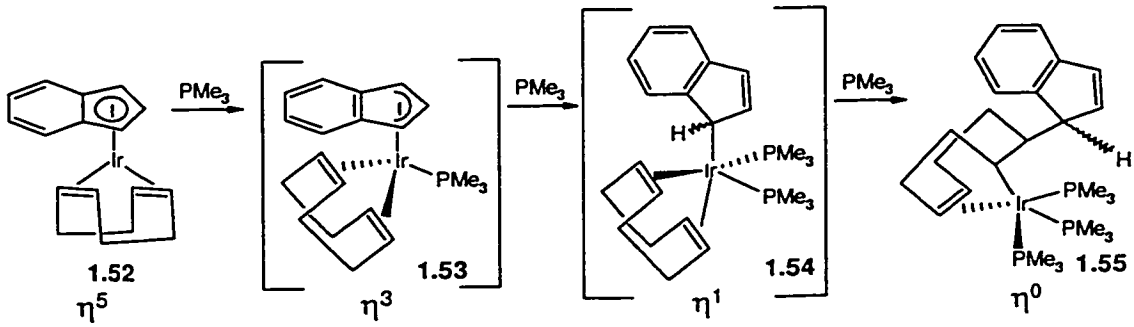

Scheme 1.19: *The proposed stepwise η^5 to η^1 conversion of the iridium complex,* ***1.52.***

In the same year, Crabtree and co-workers[95] reported on the formation of isolable η^1-indenyl compounds, derived from reactions of $[(\eta^5\text{-}C_9H_7)Ir(R)(PPh_3)_2]^+$ (R = H, Me) with donor ligands. Addition of *tert*-butyl isonitrile to the aforementioned hydride precursor at -73 °C, generates an η^3-intermediate, while above this temperature, low-yield conversion to the η^1 complex, **1.57**, is detected by NMR (< 20%) (Scheme 1.20); as the sample is warmed further, signals attributable to

free indene are observed, coinciding with an $\eta^5 \rightarrow \eta^3 \rightarrow \eta^1 \rightarrow \eta^0$ ring-slippage process. Comparable reactivity is found for the cationic methyl complex, $[(\eta^5\text{-}C_9H_7)Ir(Me)(PPh_3)_2]^+$, with the exception that the η^1 complex, **1.58**, is preferentially formed and can be isolated in ~ 90% yield. The *cis* orientation of the "R" (H, Me) and indenyl ligands in **1.57** and **1.58** was inferred by comparison with analogous derivatives whose structures are known. Interesting results were also obtained when $[(\eta^5\text{-}C_9H_7)Ir(H)(PPh_3)_2]^+$ was allowed to react with trimethylphosphine in dichloromethane under ambient conditions. During the early stages of the reaction (2-12 h), the authors noted the formation of **1.59**, in which the hydride and indenyl ligands are *cis* to one another; after 24 h, this kinetic product is transformed into the thermodynamic *trans*-disposed product, **1.60**, which was isolated as an analytically pure solid in 86% yield. The structures of these products were readily assigned based on the magnitude and multiplicity of the coupling (J_{PH}) between the Ir-*H* proton and the phosphine ligands. It is interesting to note that the hydrides **1.59** and **1.60** show no tendency to eliminate indene, in contrast to the behavior of **1.57**.

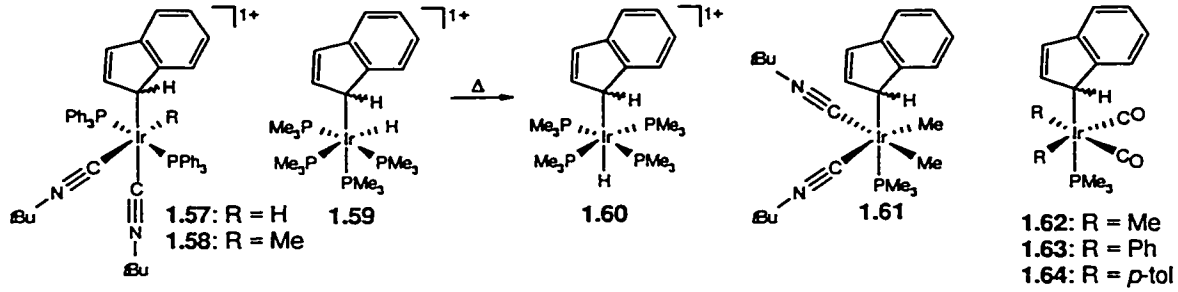

Scheme 1.20: *Some selected examples of η^1-indenyl iridium compounds bearing hydride and alkyl substituents.*

The library of isolable η^1-indenyl complexes of iridium was extended by Foo and Bergman[96] in 1992. Starting from $(\eta^5\text{-}C_9H_7)IrMe_2(PMe_3)$, the σ-indenyl complex, **1.61**, was rapidly generated *via* addition of excess *tert*-butyl isonitrile, and subsequently isolated in 97% yield as a white analytically pure solid. The dialkyl derivatives, $(\eta^5\text{-}C_9H_7)Ir(R)_2(PMe_3)$ (R = Me, Ph, *p*-tol), were similarly converted in high yield to the corresponding $(\eta^1\text{-}C_9H_7)Ir(R)_2(PMe_3)(CO)_2$ compounds, **1.62** to **1.64**, upon exposure to excess carbon monoxide. The relative orientation of the ligands in

compounds **1.61** to **1.64** was determined based on IR and NMR spectroscopic data. Especially informative was the diastereotopic nature of the isonitrile and methyl ligands in **1.61**, and the alkyl and carbonyl moieties in compounds **1.62** to **1.64**, which arises due to the stereogenic indenyl C(1) center in these species. Consistent with such an occurrence was the generation of diastereomeric mixtures of η^1-indenyl complexes when asymmetrical precursors (η^5-C_9H_7)Ir(R)(R')(PMe_3) (R ≠ R'; R and R' include Me, Ph, *p*-tol, H) were reacted in the presence of carbon monoxide. In the case of these hydrido-alkyl η^1-indenyl products, Foo and Bergman noted that the addition of excess carbon monoxide at ambient temperature eventually resulted in the reductive elimination of R-H, possibly leading to the formation of (η^1-C_9H_7)Ir(CO)(PMe_3)$_3$.

Ceccon and co-workers have published a series of papers pertaining to the synthesis and spectroscopic examination of η^3 and η^1-indenyl complexes of rhodium and iridium. Following the work of Merola and Kacmarcik[94] in 1989, Ceccon and co-workers[97] carefully reexamined the reaction between (η^5-C_9H_7)Ir(COD), **1.52**, and carbon monoxide, in the hopes of observing one or more of the intermediates along the associative substitution reaction pathway. In agreement with the findings of Merola *et al.*, Ceccon noted that under ambient conditions, solutions of **1.52** are rapidly converted to (η^5-C_9H_7)Ir(CO)$_2$, **1.56**, when treated with excess carbon monoxide (Scheme 1.21). However, when the reaction temperature was kept below -30 °C, these workers observed the quantitative formation of the σ-indenyl complex, **1.65**; this dicarbonyl species is directly comparable to the trimethylphosphine intermediate, **1.54**, proposed by Merola and co-workers. The presence of an η^1-bonded indenyl ligand in **1.65** is supported by the apparent magnetic non-equivalence of the carbonyl ligands and the appearance of characteristic σ-indenyl ^{1}H NMR resonances. The COD ligand also produces two well-resolved signals in the ^{1}H NMR spectrum of **1.65** at -40 °C, due to the diastereotopic effect of the chiral indenyl ligand; as the temperature is lowered, the rotation of the COD ligand is slow on the NMR time scale, giving rise to four distinct resonances at -100 °C. Furthermore, on raising the temperature to ~ 0 °C, broadening of the indenyl H(1) and H(3) signals and related pairs of C_6 ring proton signals is evident. Unfortunately,

attempts to monitor this dynamic process at higher temperatures were thwarted by the competitive decomposition of **1.65**, leading to **1.56**. In the absence of kinetic data, the authors qualitatively rationalized these NMR spectral changes in terms of "*a rapid 1,3-exchange through an* η^3*-species in which COD is monodentate and the Ir maintains its 18-electron shell*".[97] However, this mechanism appears to be unnecessarily convoluted, in light of the non-rigid nature of the indenyl complexes, **1.31**, **1.39** and **1.72** (*vide infra*), and the numerous other fluxional η^1-cyclopentadienyl transition metal complexes that do not possess multidentate ancillary ligands required for such a process. Alternatively, the observed spectroscopic features can be rationalized in terms of an *overall* shift of the iridium fragment from C(1) to C(3), involving [1,5] sigmatropic iridium shifts, *via* the metalloisoindene, **1.66**.

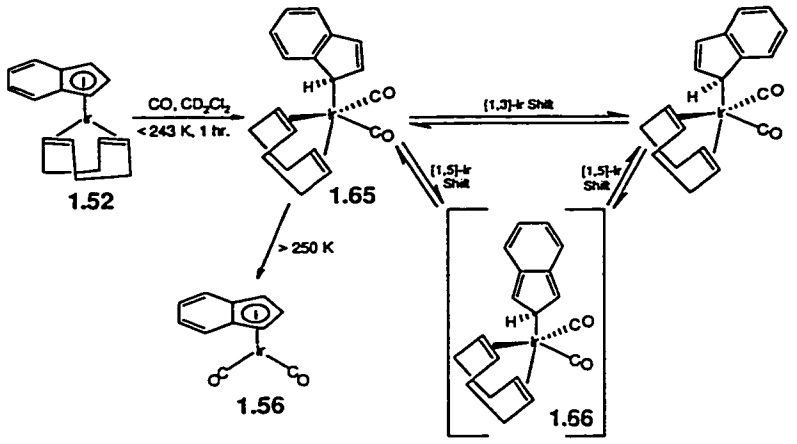

Scheme 1.21: *Synthesis, decomposition and possible molecular rearrangement pathways involving the dynamic iridium compound,* ***1.65****.*

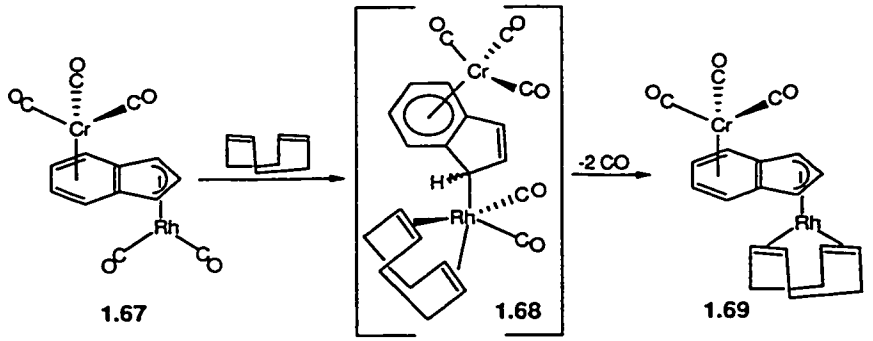

Scheme 1.22: *Conversion of the bimetallic pentacarbonyl complex,* ***1.67****, into* ***1.69****, via carbonyl displacement.*

In 1996, Ceccon and co-workers[98] examined the kinetics and mechanistic aspects of carbonyl substitution at rhodium in a bimetallic system. These studies involved the addition of either COD or norbornadiene (NBD) to the *anti*-coordinated chromium-rhodium complex, **1.67** (Scheme 1.22), and were monitored by use of UV-Vis spectroscopy. The rate of carbonyl substitution in **1.67** was found to be approximately 2000 times more rapid than in $(\eta^5\text{-}C_9H_7)Rh(CO)_2$, inspiring the authors to refer to this phenomenon as the "extra-indenyl effect". Based on the kinetic data obtained in these experiments, Ceccon *et al.* postulated that the rate determining step involves addition of the bidentate olefin to the pentacarbonyl complex, generating an η^1-intermediate such as **1.68** in the case of COD addition; the observed substitution product, **1.69**, is then generated *via* rapid loss of two molecules of carbon monoxide. Although no low hapticity species were spectroscopically detected in these studies, evidence for the existence of intermediates analogous to **1.68** was provided in a subsequent publication, in which related iridium complexes were examined.[99]

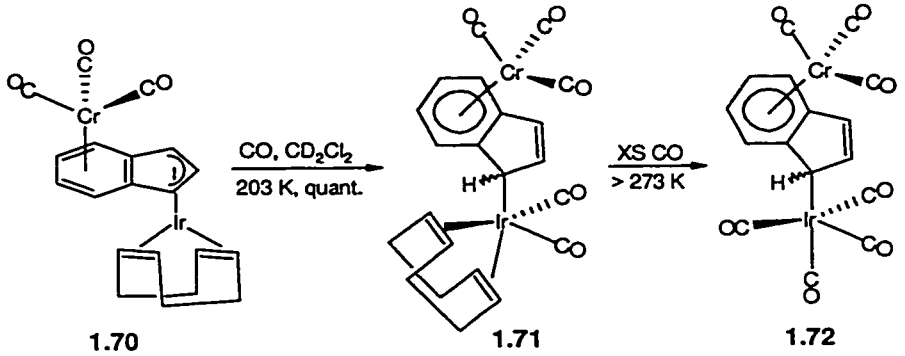

Scheme 1.23: *Addition of carbon monoxide to the bimetallic complex* ***1.70****, producing* ***1.71*** *and ultimately the heptacarbonyl complex,* ***1.72****.*

In 1998, Cecchetto, Ceccon and co-workers[99] logically extended the aforementioned studies to include *anti*-coordinated iridium-based bimetallic complexes (Scheme 1.23). The reaction of **1.70** with an excess of carbon monoxide at reduced temperature (-70 °C) led to the quantitative formation of the η^1-indenyl complex, **1.71**; this compound is directly comparable to the iridium complex, **1.65**, and the proposed rhodium bimetallic intermediate, **1.68**. However, unlike these species, **1.71** is cleanly converted (above 0 °C) to the heptacarbonyl η^1-complex, **1.72**. The

preferential formation of this latter compound is in striking contrast to the facile transformation of **1.65** into the η^5-complex, **1.56**; notably, the conversion of **1.72** into the chromium-complexed analogue of **1.56** requires forcing conditions. Indeed, the bimetallic η^1-indenyl complex, **1.72**, is remarkably stable, persisting in solution up to 40 °C. Analogous experiments carried out using tricarbonylchromium-complexed $(\eta^5\text{-}C_9H_7)Ir(COE)_2$ (COE = cyclooctene) also yielded **1.72**, presumably *via* an undetected pentacarbonyl intermediate similar to **1.71**.

The chemical reactions described above were readily monitored by use of IR and ^{1}H NMR spectroscopy; no ^{13}C NMR spectral data were supplied by the authors due to the low solubility of the products. Conversion of the η^5-compound, **1.70**, into the η^1-complex, **1.71**, was accompanied by the appearance of two IR bands attributable to an $Ir(CO)_2$ fragment, and the development of ^{1}H NMR signals indicative of a σ-indenyl complex. Subsequently, the generation of **1.72** was followed by a decrease in the intensity of the aforementioned IR absorptions, and the concomitant growing in of three new signals characteristic of an $Ir(CO)_4$ unit. The formation of **1.72** was also evinced by the considerable shift of the H(1) signal to higher frequency ($\Delta\delta$ ~ 1.5 ppm), an observation which is consonant with the replacement of olefinic ligands in **1.71** with carbonyl groups in **1.72**.

The molecular dynamics of **1.72** were qualitatively probed by Ceccon and co-workers through the acquisition of ^{1}H NMR spectra between -40 °C and 25 °C, though no quantitative rate data were provided. Slow warming of a dichloromethane solution containing **1.72** over this temperature range was accompanied by the collapse of the H(1) and H(3) signals, and the transformation of the H(2) signal from a doublet of doublets into a triplet. Similar spectral changes were observed for the signals associated with the indenyl C_6 unit. These workers interpreted the spectral changes in terms of "*the occurrence of a [1,3]-shift of the Ir(CO)$_4$ group*",[99] citing the similarity in dynamic behavior between **1.72** and the monometallic complex, **1.65**. However, orbital symmetry considerations would suggest that a mechanism involving [1,5] iridium shifts, as

depicted for **1.65** in Scheme 1.21, represents a more viable dynamic rearrangement pathway for **1.72.**

1.4.3.6 Groups 10 and 11

Zargarian and co-workers[100,101] have studied the chemistry of related nickel complexes. Using the synthetic methodology depicted in Scheme 1.24, σ-indenyl species such as **1.74** (R = H, Me) and the corresponding methylnickel compounds have been prepared and characterized. Starting from the indenyl anion derived from an appropriately substituted indene precursor, these authors propose that reaction with $(PPh_3)_2NiCl_2$ generates **1.74**, *via* the η^1-indenyl intermediate, **1.73.** Interestingly, vestiges of η^1-coordination in **1.73** are retained in **1.74**, as evidenced by crystallographic data obtained for the unsubstituted indenyl analog (R = H), which reveal asymmetrical bonding in the solid state (Ni-C(1) ~ 2.04 Å; Ni-C(3) ~ 2.09 Å), and solution ^1H NMR ($\Delta\delta_{H(1)-H(3)}$ > 2.9 ppm) and ^{13}C NMR ($\Delta\delta_{C(1)-C(3)}$ > 20 ppm) data which suggest that this asymmetry is retained in solution.[100]

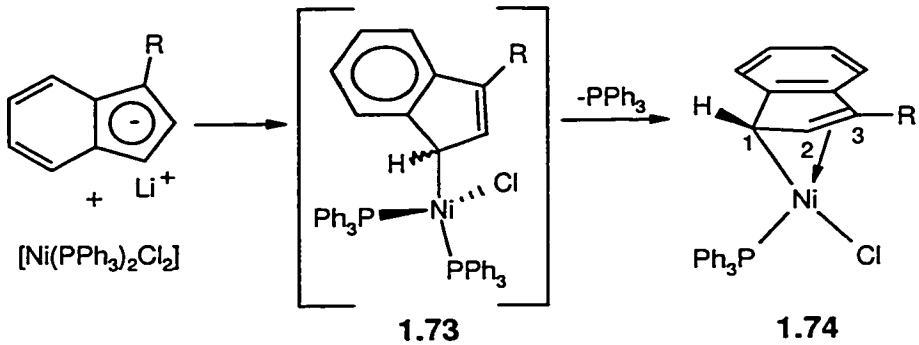

1.73 **1.74**

Scheme 1.24: *A proposed synthetic pathway to "η^1:η^{2}" indenyl nickel complexes,* ***1.74*** *(R = H or Me), via the η^1-intermediate,* ***1.73.***

The preparation of η^1-indenyl derivatives of platinum was examined by O'Hare in 1987.[102] Treatment of $Pt(COD)Cl_2$ with either 1.0 or 2.5 equivalent(s) of sodium indenide in tetrahydrofuran at room temperature produced compounds **1.75** and **1.76**, respectively, which were isolated as crystalline solids in approximately 70% yield (Scheme 1.25). The chloride, **1.75**, was found to exhibit remarkable stability in polar solvents, showing little tendency to isomerize to the

corresponding η^5-indenyl compound, in contrast to its η^1-C_5H_5 and η^1-C_5Me_5 counterparts. Although the bis(η^1-indenyl) compound, **1.76**, proved to be considerably less stable in solution, the ^1H and ^{13}C NMR data obtained for this compound were of sufficient quality so as to allow for the assignment of a 1:1 mixture of diastereomers, arising from the stereogenic nature of the indenyl C(1) centers. O'Hare was also able to demonstrate that the formation of the cationic complex, **1.77**, could be realized *via* treatment of either **1.75** with $AgBF_4$, or **1.76** with HBF_4.

In 1999, Ackermann *et al.*[103] presented what is only the fourth example of a simple η^1-1*H*-inden-2-yl complex, **1.78** (Scheme 1.26). Prepared *via* cyclization of an η^1-propargyl precursor, this interesting platinum species was isolated as an off-white solid in 76 % yield, and subsequently characterized by use of a variety of techniques, including X-ray crystallography. The structure of **1.78** can be compared with the two other crystallographically characterized compounds containing a metal-indenyl C(2) linkage, **1.27** and **1.29** (Scheme 1.12).

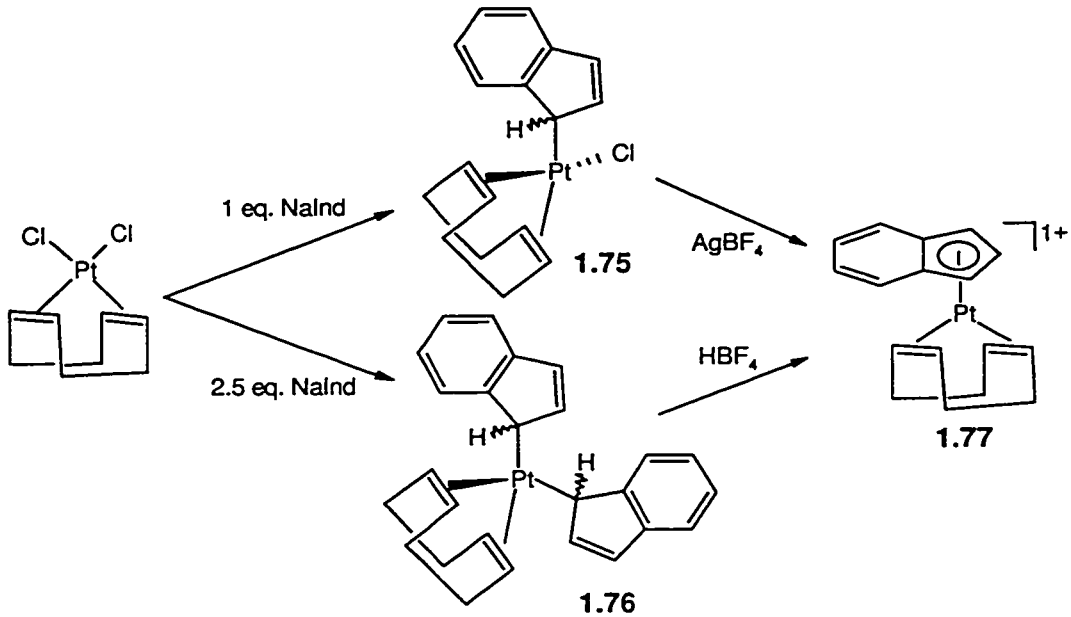

Scheme 1.25: *The preparation of mono(σ-indenyl) (**1.75**) and bis(σ-indenyl) (**1.76**) complexes of platinum, and their subsequent conversion to the cationic η^5-complex, **1.77**.*

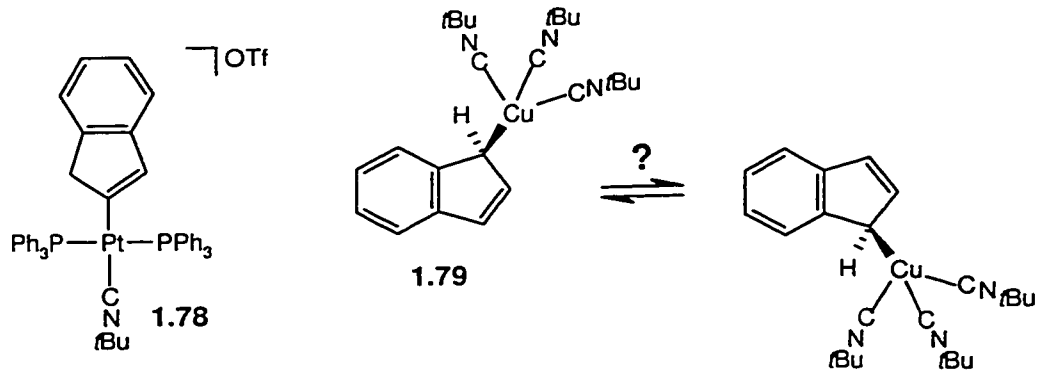

Scheme 1.26: *A novel η^1-indenyl complex of platinum,* ***1.78****, and the apparently dynamic σ-indenyl copper system,* ***1.79****.*

A report pertaining to the synthesis of an indenylcopper complex was published in 1971 by Segusa, Ito and Tomita.[104] From a mixture of indene, Cu_2O and *tert*-butyl isonitrile was isolated **1.79**, as a heat- and moisture-sensitive compound, in 30% yield. The ^{1}H NMR spectrum of this product at room temperature is comprised of an $A_2B_2X_2Y$ signal pattern, which was tentatively rationalized by the authors as arising due to the rapid interconversion of the carbon-metal bond between the C(1) and C(3) positions in an η^1-species, as depicted in Scheme 1.26. Support for this σ-bonding proposal, rather than one involving an η^5-bonded copper fragment, was based primarily on a comparison of the NMR spectral data acquired for **1.79** with those obtained for **1.43**.[90] Unfortunately, low-temperature NMR spectroscopic data for **1.79**, which may provide further insight into the instantaneous structure of this compound, were not provided in this report.

1.4.3.7 Group 12

As has been alluded to in the precursory sections, bis(η^1-indenyl)mercury, **1.43**, has played an important role in the early development of the field of dynamic σ-indenyl complexes. The synthesis of this metalloid compound was published by Cotton and Marks[90] in 1969, who noted that the addition of mercuric chloride to a solution of lithium indenide at reduced temperature, followed by purification, affords **1.43** as a colorless solid in 12% yield. In this report, these workers also presented ^{1}H NMR spectroscopic data acquired between -41 °C and 68 °C. The spectrum of **1.43** at the low temperature limit is entirely consistent with a σ-indenyl structural

formulation, as presented in Scheme 1.27; similar results have also been obtained for (η^1-C_9H_7)HgCl[105] and (η^1-C_9H_6Me)HgCl.[106] Curiously, although Cotton and Marks were astute in recognizing that **1.43** should exist as a mixture of racemic and meso isomers (as in **1.76**), they found no indication of such an isomeric mixture in the low-temperature limiting spectrum of **1.43.** Upon warming, several reversible spectral changes ensued, including the broadening, collapse, coalescence and sharpening of the signals assigned to the H(1) and H(3) protons. The concentration independence of these spectral changes allowed for the exclusion of second-order intermolecular phenomena, and led the authors to propose the operation of one or more temperature-dependent intramolecular exchange process(es), which permute the H(1) and H(3) indenyl ring environments in **1.43.** Careful analysis of these ^{1}H NMR data allowed for a determination of the activation energy (E_a = 12.9 ± 0.6 kcal mol^{-1}) for this system.[90] Insight into a possible rearrangement mechanism for **1.43** was provided in 1975, when Cotton *et al.* published a variable temperature ^{13}C NMR examination of **1.4**, **1.43**, and (η^1-C_5H_5)HgCl.[107] Data obtained in the course of these studies clearly pointed to the operation of a [1,5] shift mechanism involving (η^1-C_5H_5)HgCl (E_a = 7.7 ± 0.7 kcal mol^{-1}); by analogy, a [1,5] shift mechanism involving **1.43** may be equally viable.

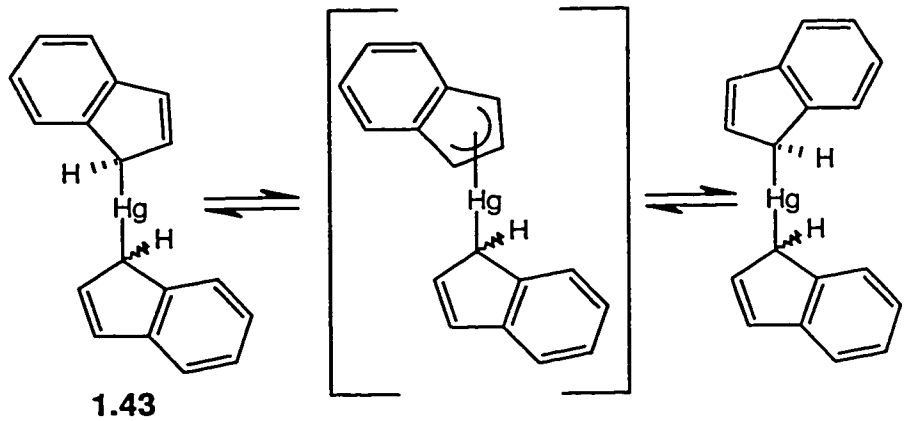

1.43

Scheme 1.27: *Quasi-fluxional behavior in bis(η^1-indenyl)mercury,* ***1.43.***

1.4.4 Main Group Complexes

Main group σ-indenyl complexes have been known for over four decades, and their historical relevance has been highlighted in the preceding sections. More recently, the increasingly important role of Group 13, 14 and 15 indenyl derivatives as ligands in the synthesis of chiral metallocene precatalysts has led to a renaissance in this field;[108,109] (1-indenyl)trimethylsilane, **1.109**, and bis(1-indenyl)dimethylsilane, **3.6**, have even become commercially available reagents (see Schemes 1.33 and 3.2, respectively). Such poly(1-indenyl) precursors, which have been extensively utilized in the preparation of chiral *ansa*-bridged precatalysts,[110] invariably exhibit diastereoisomerism due to the stereogenic nature of the C(1) carbon on indene; in many cases this phenomenon has been overlooked, leading to a proliferation of confusing and erroneous reports in the literature. Moreover, studies pertaining to the dynamics of σ-indenyl main group systems, unlike those involving the corresponding transition metal derivatives, are in some instances complicated by the propensity of these compounds to isomerize to the corresponding vinylic (sp^2) complexes; a similar situation was encountered in the analogous cyclopentadienyl series (Section 1.3.4).

1.4.4.1 Group 13

The earliest examples of indenylboranes were provided by Mikhailov and co-workers. In 1972, these researchers reported that treatment of indenyllithium with chlorodimethoxyborane at reduced temperatures produced the indenylborane, **1.80**, which was subsequently isolated in 33% yield by distillation.[111] The connectivity in **1.80** was identified based primarily on ^1H and ^{11}B NMR data, which clearly revealed the allylic structure shown in Scheme 1.28. Despite the moisture-sensitive nature of **1.80**, this compound was shown to be thermally stable up to ~ 120 °C.

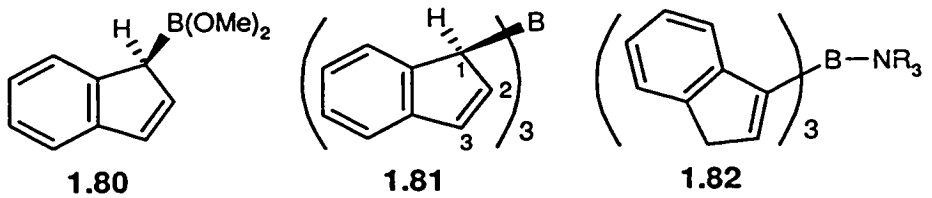

1.80 **1.81** **1.82**

Scheme 1.28: *Early examples of indenylboranes.*

In a subsequent publication, Mikhailov *et al.*[112] presented the synthesis and characterization of the tris(indenyl)borane, **1.81**. Prepared by the reaction of indenyllithium with BF_3, the spectroscopic features of this novel compound between 20 °C and 120 °C were found to depend reversibly on temperature. Below 20 °C, the ^1H NMR spectrum of **1.81** is comprised of signals attributable to a σ-indenyl system; as the sample is warmed the H(1) (~ 2.8 ppm) and H(3) (~ 6.8 ppm) signals slowly broaden, with full collapse observed near 104 °C. Simultaneously, the H(2) signal (~ 5.9 ppm) is transformed from a doublet of doublets into a triplet, behavior which parallels that described for the quasi-fluxional transition metal complexes, **1.31** and **1.72**, in Section 1.4.3. Evaluation of these dynamic NMR data using the Arrhenius methodology allowed for an estimation of the activation energy for this dynamic process (E_a = 13 ± 1 kcal mol^{-1}). Although the spectral assignments and kinetic data provided by the authors appear to be in order, their description of the dynamic phenomenon exhibited by **1.81** and several other features of their ensuing commentary are confusing. Mikhailov *et al.* refer to an "*allylic rearrangement*" process involving **1.81**, which appears to coincide with an overall C(1) to C(3) transfer of the boron fragment; the spectral data provided are in agreement with such a process, though orbital symmetry control may require a stepwise mechanism involving [1,5] boron shifts. However, the authors also state that "*if the signal at 6.83 ppm had belonged to the* ...H(2)... *proton, then a 1,2-shift would have occurred, and not* [an] *allyl rearrangement*". It is not clear what chemical exchange process involving the migration of the boron fragment alone could result in the permutation of the H(1) and H(2) sites. It appears that the authors have erroneously attempted to apply the methodology developed by Cotton and various co-workers[37] for the mechanistic evaluation of metal(loid) η^1-cyclopentadienyl complexes (Section 1.3.3), *directly* to the study of indenyl compounds. Moreover, the authors failed to recognize the potential for diastereoisomerism in **1.81**; this compound could, in principle, exist as a mixture of four isomers due to the stereogenicity of the indenyl C(1) center. The generation of such isomeric mixtures is

not a concern in the case of the tris(indenyl)borane Lewis adducts, **1.82**, which are prepared *via* reaction with amines.

In the twenty years following these studies by Mikhailov *et al.*, the field of indenylborane chemistry received little attention. However, the potential utility of these complexes as transition metal ligands has prompted several research groups to take up the study of these molecules; in fact, the vast majority of reports pertaining to indenylboranes have appeared only in the last three years. In 1997, Rufanov *et al.*[113] reported on the synthesis and dynamic behavior of silicon- and boron-functionalized indenes. The disubstituted compounds, **1.83** and **1.84**, were generated in high yield as a 1:1 mixture, *via* quenching of $[C_9H_6SiMe_3]Li$ with Ph_2BBr at room temperature (Scheme 1.29); the analogous BX_2 compounds (X = Cl, Br) were also prepared by mixing $C_9H_6(SiMe_3)_2$ with an appropriate BX_3 precursor, albeit in lower yield and as a complicated mixture of isomers. The claim made by the authors that the mixture of **1.83** and **1.84** "*seems to be fluxional in solution*", implies the interconversion of these species, though no variable-temperature NMR data were provided. The bis(σ-indenyl) compounds, **1.85** and **1.86**, similarly prepared *via* anion quenching with the appropriate dichloroalkylborane, also appear to be fluxional. In the case of **1.85**, elementotropic rearrangements are proposed based solely on the complexity of the ^1H NMR spectrum; for **1.86**, the authors claim that the observation of broadening in the H(1) region of the ^1H NMR spectrum "*indicates some fluxionality of the $(Me_3Si)_3CB$ moiety*".

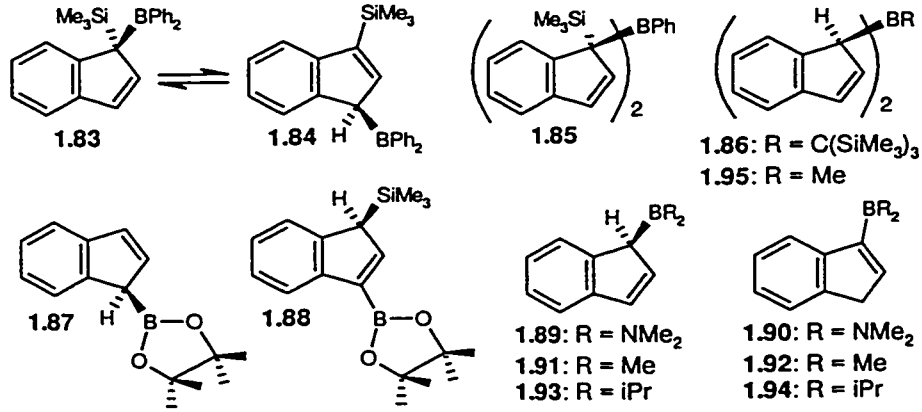

Scheme 1.29: *Some recently reported indenylboranes, containing carbon, nitrogen, oxygen and silicon based ligands.*

Herberich and various co-workers[114,115] have reported on the preparation of indenylboranes and their transition metal complexes. The 1,3,2-dioxaborolanyl- and dimethylamino-substituted indenes **1.87** and **1.89** were readily prepared *via* borylation of lithium indenide; **1.88** was also synthesized in ~ 80% yield by the reaction of the lithium indenide salt of **1.87** with chlorotrimethylsilane. In the case of **1.87**, only the sp^3-isomer depicted in Scheme 1.29 was observed, even after distillative workup. In contrast, warming of **1.89** to temperatures above 0 °C resulted in the rapid conversion of this kinetic product into the thermodynamically favored sp^2-isomer, **1.90**. Herberich and co-workers accurately recognized that while the conversion of **1.89** to **1.90** could be rationalized in terms of [1,5] hydrogen shifts *via* isoindene intermediates, a base catalyzed process is more likely, given the apparently low barrier associated with this isomerization and the observed difference in behavior between the dioxaborane, **1.87**, and the diamino compound, **1.89**.

Further studies by Herberich and co-workers involved an examination of the dialkylboranes, **1.91** and **1.93**. In keeping with the results detailed above, these sp^3-isomers were generated at low temperatures as the kinetic products, while treatment of **1.93** with triethylamine or pyridine gave rise to the sp^2-compound, **1.94**, evinced by data obtained during a ^1H, ^{11}B and ^{13}C NMR spectroscopic study of this system. Interestingly, during the synthesis of **1.91**, the bis(1-indenyl)borane, **1.95**, was also identified as a minor component of the reaction mixture. The ^1H and ^{13}C NMR spectra of this minor product were assigned based on an approximate 1:1 mixture of C_2 and C_s isomers, with further support for this structural formulation coming from two-dimensional NMR experiments, as well as mass spectrometric studies.

The utility of pentafluorophenyl-containing indenylboranes as ligands in preparation of "single-component" zwitterionic catalysts has been examined by Bochmann and co-workers.[116] Addition of the diethyl ether complex of bis(pentafluorophenyl)fluoroborane to a solution of either $[C_9H_7]Li$ or $[C_9H_6SiMe_3]Li$ produced mixtures containing **1.96** and **1.97** or **1.98** and **1.99**, respectively (Scheme 1.30). In the former reaction, fractional crystallization allowed for the

isolation of the expected C(3) product (**1.97**) and the unusual C(2) species (**1.96**), which were generated in a 5:2 ratio. Although no mechanistic rationalization for the formation of **1.96** was provided by the authors, there is little precedent for the generation of such a main group complex *via* direct attack at C(2). An alternative route leading to **1.96** may involve addition of the $B(C_6F_5)_2$ unit to the indenyl C(1) position in the usual manner, followed by a [1,5] shift of the boron fragment (giving a C(2)-substituted isoindene) and a subsequent [1,5] shift (possibly base-catalyzed) of the C(2) hydrogen in the isoindene. Furthermore, treatment of crude mixtures of **1.96** and **1.97** with *tert*-butylamine yielded a single crystalline product, which was identified as the Lewis adduct derived from **1.97**; analogous adducts of **1.96** were not identified. In contrast to **1.96** and **1.97**, crystalline material isolated from the reaction involving $[C_9H_6SiMe_3]Li$ was found to contain both of the silicon-substituted products, **1.98** and **1.99**, which were subsequently characterized as a mixture in solution by NMR spectroscopy. Although no direct evidence in support of fluxional behavior is provided by the authors, it is plausible that **1.98** and **1.99** exist in solution as an equilibrium mixture, with interconversions occurring *via* [1,5] silatropic shifts. The **1.98**-**1.99** system, in which silicon continually occupies an sp^3-hybridized position, can be contrasted with the analogous non-fluorinated arylboranes reported by Rufanov *et al.*, **1.83**-**1.84**, in which boron prefers allylic locations (Scheme 1.29).[113]

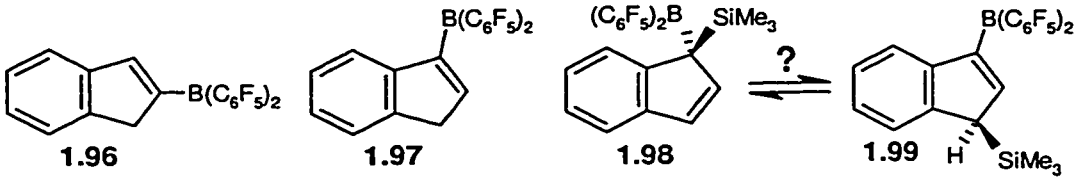

1.96 **1.97** **1.98** **1.99**

Scheme 1.30: *Indenylboranes containing pentafluorophenyl ligands.*

The chemistry and molecular rearrangements of indenyldiboranes were examined by Nöth and co-workers[117] in 1998. The monoindenyl complex, **1.100**, was prepared in the usual manner *via* quenching of lithium indenide with the appropriate dichlorodiborane (Scheme 1.31). During distillative purification, this product was transformed into the sp^2-isomer, **1.101**, a thermally promoted isomerization process that parallels the conversion of the simple aminoborane, **1.89**,

into the C(3) species, **1.90** (Scheme 1.29). The corresponding bis(σ-indenyl) complex, **1.102**, was prepared in an analogous manner by using half an equivalent of the dichlorodiborane. Although the B-C(1) connectivity in **1.102** is clearly indicated by the ^{1}H and ^{13}C NMR spectral data provided, the authors do not justify the complexity of these spectra, which are curiously assigned based on the presence of four unique indenyl rings in this product. In what may be interpreted as an attempt to rationalize the number of resonances in these spectra, the authors allude to the possibility of hindered B-C rotation in **1.102**, without acknowledging the potentially diastereomeric nature of the product. Indeed, the likely occurrence that **1.102** is actually generated as a mixture of C_s and C_2 isomers is completely overlooked, though the presence of such an isomeric mixture would not be expected to give rise to NMR spectra of such complexity. X-Ray crystallographic data provided for **1.102** correspond to the homochiral diastereomer, which is presumably comprised of *RR* and *SS* enantiomers, though it is not formally recognized as such by the authors.

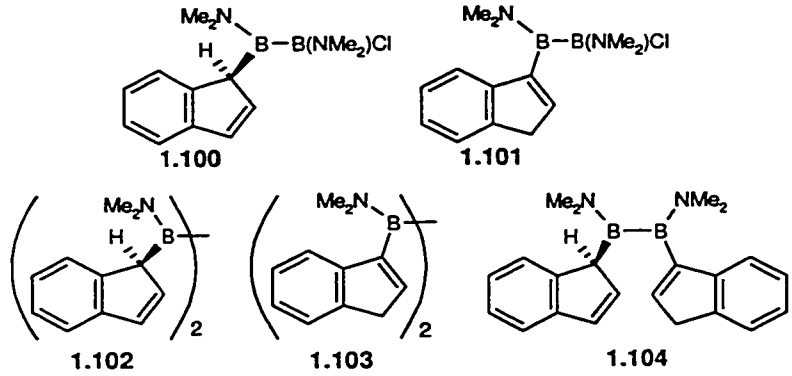

Scheme 1.31: *Mono(σ-indenyl) and bis(σ-indenyl) diborane derivatives.*

In the same report, Nöth and co-workers also discuss the thermal conversion of **1.102** into **1.103**, a process which proceeds *via* the spectroscopically and crystallographically characterized "mixed" intermediate, **1.104**. Finally, in commenting on the viability of other synthetic routes to bis(σ-indenyl)boranes, the authors state that the preparation of such complexes *via* substituent exchange involving $B_2(NMe_2)_4$ is "*prevented simply by the access to tri(indenyl)borane, an as yet unknown triorganylborane*", despite the fact that this precursor, **1.81**, was presented twenty-five years earlier by Mikhailov.[112]

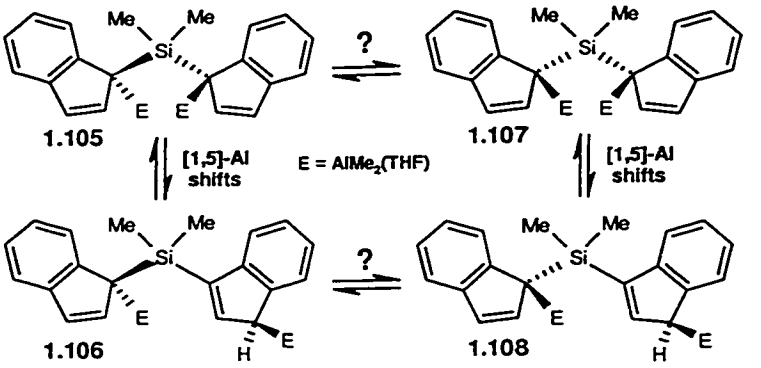

Scheme 1.32: *An isomeric mixture of silicon- and aluminum-functionalized indenes.*

Thiyagarajan, Jordan and Young[118] reported the synthesis, structure and dynamics of silicon- and aluminum-functionalized indenes in 1998. These authors noted that the addition of two equivalents of dimethylchloroalane to a solution containing $[Me_2Si(C_9H_6)_2]Li_2$ generated a mixture of air and moisture sensitive racemic diastereomeric products (**1.105** to **1.108**) (Scheme 1.32); recrystallization allowed for the isolation of **1.106**, which was characterized by X-ray crystallography. Based on temperature-dependent NMR data obtained from a mixture containing only **1.105** and **1.106**, Jordan and co-workers propose that the interconversion of these products occurs *via* suprafacial [1,5] aluminum shifts; at low temperatures (-60 °C) signals attributable to a 1:2 mixture of **1.105** and **1.106** are observed, while at room temperature, an averaged spectrum is found. It was also documented that after three days at room temperature, solutions containing these two compounds are transformed into a mixture of all four diastereomers (**1.105** to **1.108**). The presence of the newly formed complexes was rationalized by the authors in terms of the operation of a [1,5] hydrogen shift process, though it is unclear how such processes alone could transform **1.105** into **1.107** and **1.106** into **1.108**, given that no sp^3-hydrogen atoms are available for such migrations in either **1.105** or **1.106**; for example, a series of [1,5] aluminum shifts and [1,5] hydrogen shifts (*via* the enantiomer of **1.106**) are required to interconvert molecules **1.105** and **1.107**. Interestingly, Jordan and co-workers observed that these complexes also readily participate in aluminum-based ligand disproportionation reactions, under conditions in which isomerization occurs. As a result, the direct transformation of either **1.105** into **1.107** or **1.106** into

1.108 may actually proceed by a dissociative process, rather than by an intramolecular route requiring a complex series of elementotropic shifts.

1.4.4.2 Group 14

Given the many carbon-functionalized indenes that have been reported to date, and that the free energies associated with sigmatropic shifts of carbon fragments in these molecules are often too high to be detected by use of dynamic NMR techniques, the following summary of Group 14 σ-indenyls is restricted to the heavy element complexes. Moreover, since the majority of this thesis study pertains to the dynamic behavior of indenylsilanes, only an overview of important early work is presented in this section, with a more detailed synopsis of particularly relevant literature presented as introductory sections in Chapters Three and Four.

The study of indenylsilanes was initiated by Sommer and Marans[119] in 1951, who reported on the preparation and characterization of the mono(σ-indenyl)silanes, **1.109** to **1.112**, and the bis(σ-indenyl) complexes, **3.6** and **3.7** (Schemes 1.33 and 3.2). The methodology employed by these workers involved quenching of sodium or lithium indenide with an appropriate alkylhalosilane. The efficacy of this general synthetic approach has been abundantly demonstrated in the preceding sections; with some notable exceptions, this is by far the most common route to Group 14 derivatives of indene.

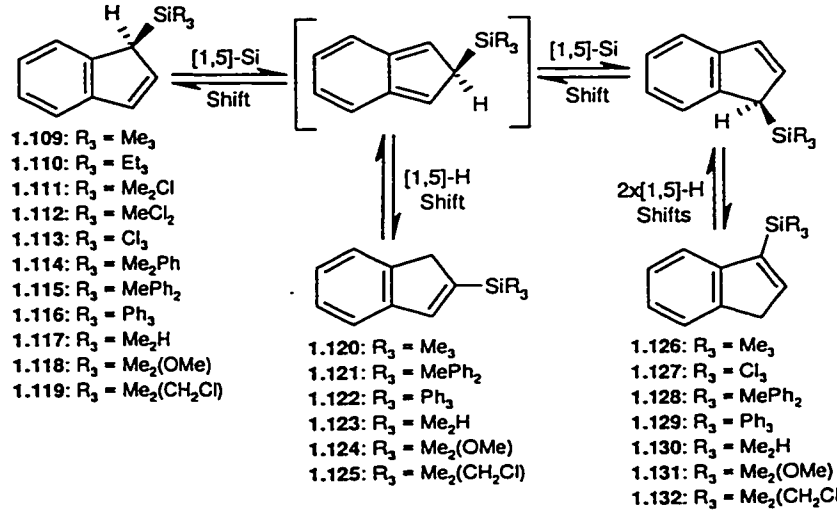

Scheme 1.33: *[1,5] Sigmatropic shifts rearrangements involving indenylsilanes.*

The dynamics of indenylsilanes were first probed by Rakita and Davison[120] by use of variable-temperature NMR techniques. Based on the partial collapse of the H(1) and H(3) signals in the ^{1}H NMR spectrum of **1.109** acquired at 180 °C, and in light of the apparent quasi-fluxional behavior of the corresponding germanium and tin complexes (*vide infra*), the aforementioned indenylsilane was deemed stereochemically non-rigid.

In 1970, Larrabee and Dowden[121] reported on their attempt to quantify the barrier to silicon migrations in **1.109**. Using the saturation transfer methodology developed by Forsén and Hoffman,[9] Larrabee *et al.* noted that for experiments carried out at 150 °C, saturation of the H(1) resonance of **1.109** resulted in a decrease in the intensity of the H(3) resonance, but not the H(2) signal. Due to the fact that relaxation processes in **1.109** were found to be fast in comparison to the exchange rate, these spectroscopic data allowed only for a maximum value of the activation energy of (~ 29 kcal mol^{-1}) to be calculated. These workers also noted that silicon shifts must be significantly more rapid than hydrogen shifts in **1.109**, since the generation of vinylic isomers (**1.120** and **1.126**) was observed to be slow relative to the observed rate of chemical exchange between H(1) and H(3).

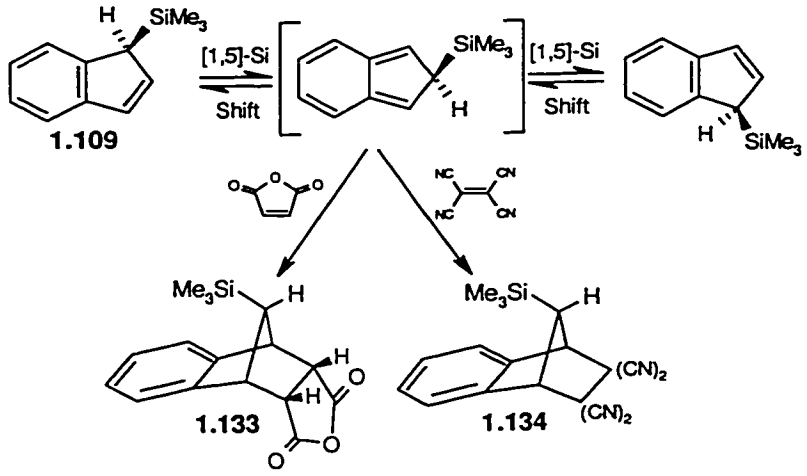

Scheme 1.34: *Diels-Alder trapping of trimethylsilylisoindene with maleic anhydride and tetracyanoethylene, yielding* ***1.133*** *and* ***1.134****, respectively.*

In the same report, Larrabee and Dowden[121] examined the mechanism of silicon shifts in **1.109** by use of Diels-Alder chemistry (Scheme 1.34). Given that the barrier to silicon shifts in this

compound was considerably greater that that found for the cyclopentadienyl analogue, **1.12** (E_a ~ 13 kcal mol^{-1}), these workers postulated that isoindenes may mediate the observed interconversion of H(1) and H(3) in **1.109**. In an attempt to probe for the presence of silicon-substituted isoindene intermediates in these migratory processes, an equimolar mixture of **1.109** and maleic anhydride was heated to 150 °C. The product obtained from this reaction, following sulfuric acid methanolysis workup, yielded NMR spectroscopic data which implied the generation of the cycloadduct, **1.133**, and thus, the operation of a concerted, suprafacial [1,5] silicon shift process, involving **1.109**.

Related Diels-Alder adducts derived from dicyanomaleimide and tetracyanoethylene (**1.134** in Scheme 1.34) were described by Ashe[122] in the same year. In addition to qualitatively alluding to the intermediacy of isoindenes, treatment of solutions of **1.109** with a large excess of dienophile allowed for the determination of temperature-dependent rate constants associated with [1,5] silicon migrations in **1.109**, by use of dilatometric techniques; analysis of these data permitted an estimation of the activation energy (E_a ~ 22.5 kcal mol^{-1}) for this migratory process. This value is in good agreement with the barrier (E_a ~ 22.4 kcal mol^{-1}) determined by Luzikov and co-workers by use of variable-temperature ^{13}C NMR techniques.[70]

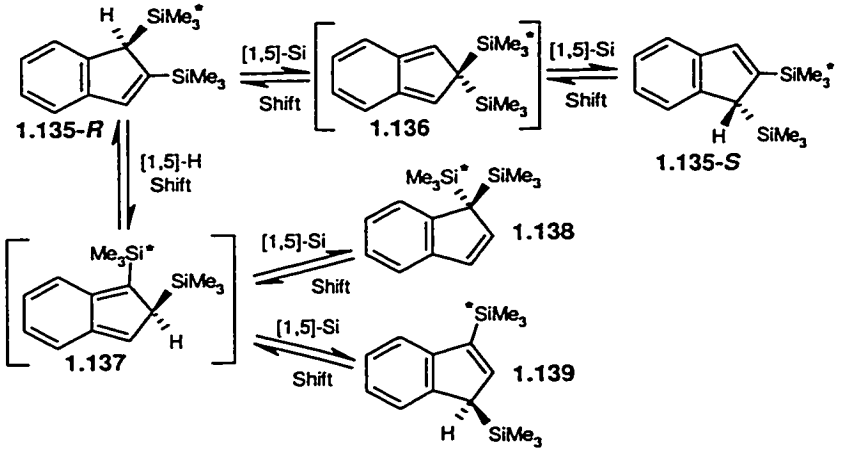

Scheme 1.35: *Scrambling of the trimethylsilyl groups in* ***1.135****, due to [1,5] silicon shifts; one silicon group is arbitrarily marked with an asterisk (*) to aid in monitoring its position throughout the various migratory processes.*

One of the most mechanistically insightful studies pertaining to indenylsilane dynamics was published by Davison and Rakita[123] in 1970. These workers cleverly realized that while suprafacial [1,3] silicon shifts in **1.135** would interconvert the *R* and *S* enantiomers of this compound (thus equilibrating the two halves of the indenyl framework), the trimethylsilyl groups in **1.135** would retain their chemical and magnetic non-equivalence. In contrast, a mechanism involving sequential [1,5] shifts would proceed *via* the symmetric isoindene intermediate, **1.136**, leading both to a permutation of the related indenyl environments and to chemical exchange of the trimethylsilyl groups. During the course of a variable-temperature NMR study, these authors noted that the silicon fragments in **1.135** were equilibrated on the NMR time scale with the same barrier (E_a ~ 26 kcal mol^{-1}) as that associated with exchange between the H(1) and H(3) protons. This observation provided compelling evidence for a [1,5] shift mechanism in which both silicon groups reside temporarily at C(2) (**1.136**), as depicted in Scheme 1.35.

Numerous other hetero-substituted indenylsilanes have been prepared, and many have been utilized as precursors to transition metal complexes. Recent examples of such molecules include **1.137**,[124] the nitrogen-functionalized silicon complexes, **1.138** and **1.139**, the methoxy-substituted indene, **1.140**,[125] 1,2-bis(σ-indenyl)tetramethyldisilane, **1.141**, and 1,3-bis(σ-indenyl)tetramethyldisiloxane, **1.142** (Scheme 1.36).[126]

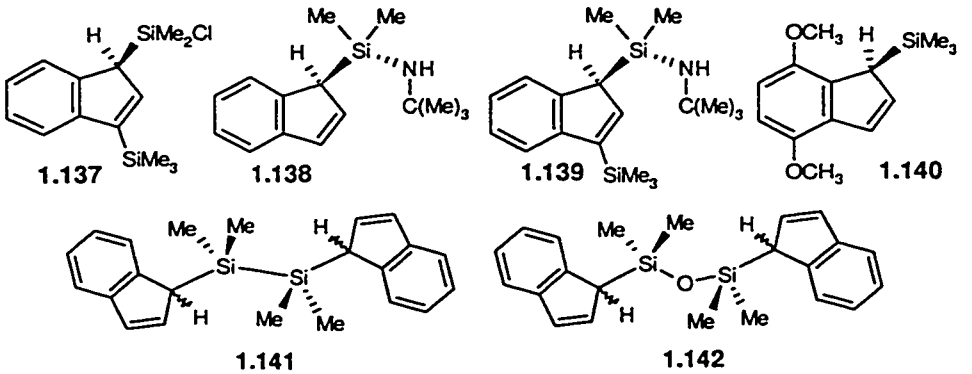

Scheme 1.36: *Some miscellaneous indenylsilanes bearing alkyl, alkoxy and amido substituents.*

Indenyl complexes of the heavier Group 14 elements have also been prepared and their dynamics examined. In 1969, Davison and Rakita[120] studied the behavior of trimethylgermyl- and

trimethylstannylindene, **1.143** and **1.145**, respectively, by use of variable-temperature NMR (Scheme 1.37). As alluded to in the foregoing discussion of indenylsilane dynamics, these germanium and tin complexes are stereochemically non-rigid, evidenced by the collapse of the H(1) and H(3) signals in the ^{1}H NMR spectra of these compounds at elevated temperatures; changes in the aromatic region are also indicative of an overall C(1) to C(3) migratory process. However, in keeping with the trend of diminishing migratory barriers upon descending the *p*-block, the ^{1}H NMR spectral features observed for **1.109** at 180 °C are evident for **1.143** between 134 °C and 149 °C, while for the tin complex, **1.145**, Davison and Rakita were able to observe the complete range of limiting low- to limiting high-temperature spectra. At temperatures below -37 °C, the ^{1}H NMR spectrum of **1.145** is consistent with a "static" σ-indenyl structure, as depicted in Scheme 1.37; as the sample is warmed, the H(1) and H(3) protons broaden in the usual manner, with complete collapse observed at 49 °C. Above 140 °C, the averaged "dynamic" ^{1}H NMR spectrum is observed for **1.145**. The persistence of tin-hydrogen coupling between the methyl hydrogen atoms and the tin center in **1.145** over the entire temperature range points to an intramolecular rearrangement process.

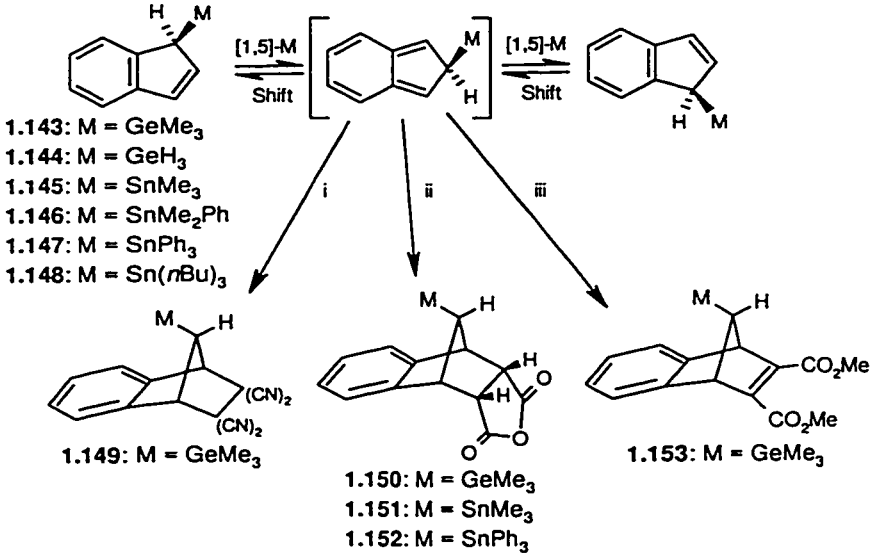

Scheme 1.37: *Sigmatropic migrations and Diels-Alder cycloaddition chemistry of germanium- and tin-substituted indenes (i = tetracyanoethylene; ii = maleic anhydride; iii = dimethylacetylenedicarboxylate).*

An additional facet of the aforementioned study published by Luzikov and co-workers,[70] involved an examination of the dynamics of **1.143** and **1.145** by use of variable-temperature ^{1}H and ^{13}C NMR techniques. In the case of the indenylgermane, **1.143**, spectroscopic information obtained from ^{13}C NMR experiments yielded a barrier to germanium shifts (E_a ~ 18.4 kcal mol^{-1}; $\Delta G^{\ddagger}_{300}$ ~ 21.8 kcal mol^{-1}) which is comparable to an earlier estimate of the activation energy (E_a ~ 22 kcal mol^{-1}) advanced by Larrabee and Dowden.[121] Similarly, ^{13}C NMR data were utilized in determining the barrier to tin migrations in the indenylstannane, **1.145** (E_a ~ 12.7 kcal mol^{-1}; $\Delta G^{\ddagger}_{300}$ ~ 15.2 kcal mol^{-1}).[70,127] The increased barrier to metallotropic shifts in these heavier Group 14 indenyl complexes, in comparison to their cyclopentadienyl analogues, was rationalized by Luzikov and co-workers in terms of the formation of an energetically unfavorable, short-lived metalloisoindenyl intermediate during the migratory process. In an effort to fortify this proposal, **1.143** was reacted with tetracyanoethylene, maleic anhydride and dimethylacetylenedicarboxylate, yielding the Diels-Alder cycloadducts, **1.149**, **1.150** and **1.153**, respectively (Scheme 1.37). In contrast, these workers noted that analogous reactions involving the indenylstannane, **1.145**, result in tin-indenyl bond cleavage, accompanied by the generation of products containing both the dienophile and the trimethyltin fragment. These latter results contradict findings published a year earlier by Rakita and Taylor,[128] who provided NMR spectroscopic and mass spectrometric evidence in support of the [4+2] cycloadduct, **1.151**, and who referred to a report[129] in which the generation of **1.152** is claimed. The isolation of such Diels-Alder adducts of germanium and tin supports the proposal of a [1,5] shift mechanism involving these heavier Group 14 compounds.

The synthesis, structure and dynamic behavior of indenylgermane, **1.144**, were examined by Angus and Stobart[130] in 1973. These authors noted that between 175 °C and 195 °C, ^{1}H NMR signals attributable to the indenyl C_5 hydrogen atoms in **1.144** partially coalesce, corresponding to the onset of chemical exchange on the ^{1}H NMR timescale. Further measurements at higher temperatures proved impossible due to instrumental limitations, and so no quantitative kinetic data were provided. In addition to these variable-temperature NMR studies, vibrational

spectroscopic as well as mass spectrometric studies involving **1.144** were carried out; ν[Ge-C(1)indenyl] was found to be near 370 cm^{-1}.

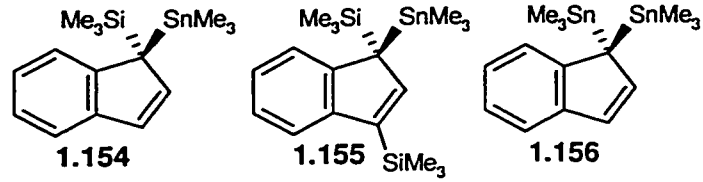

1.154 **1.155** **1.156**

Scheme 1.38: *Some polymetallic Group 14 σ-indenyl complexes.*

In 1975, Orrell and co-workers[131] reported on the synthesis and dynamic behavior of the polymetallated indenes, **1.154** to **1.156**. Variable-temperature ^1H NMR studies conducted between 0 °C and 170 °C revealed that these molecules exhibit dynamic behavior typical of this class of compounds (Scheme 1.38). Based on a comparison of experimentally derived and computed spectral data, the Arrhenius parameters for the metallotropic shift of the trimethylstannyl fragments in **1.154** (E_a ~ 13.4 kcal mol^{-1}), **1.155** (E_a ~ 16.1 kcal mol^{-1}) and **1.156** (E_a ~ 16.4 kcal mol^{-1}) were determined. Interestingly, the 1,1-isomer of **1.156**, depicted in Scheme 1.38, was found to predominate in solution over the corresponding 1,3-isomer (ratio > 20:1), an observation which is counterintuitive based on steric considerations and which contrasts the approximate 1:1 ratio observed for the bis(trimethylsilyl)indene isomers, **1.138** and **1.139** (Scheme 1.35);[123] it is possible that electronic factors strongly favor sp^3-bonded tin fragments in these indenyl complexes. In discussing these kinetic results, Orrell *et al.* noted that while the observed ^1H NMR line shape changes can be rationalized in terms of a [1,3] shift pathway, a [1,5] mechanism involving a short-lived isoindenyl intermediate cannot be ruled out.

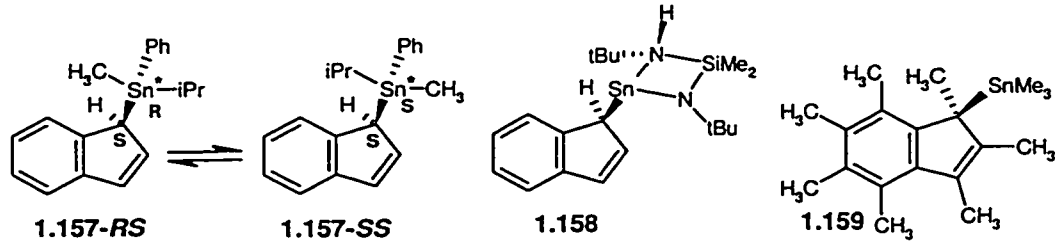

1.157-*RS* **1.157-*SS*** **1.158** **1.159**

Scheme 1.39: *The dynamics of the chiral-at-tin indenylstannanes,* ***1.157****, and the structures of the bis(amino)stannylene complex,* ***1.158****, and the heptamethylindenylstannane,* ***1.159****.*

Following reports by Kashin and various co-workers[132,133] on the synthesis and reactivity of optically active indenyl compounds of tin, McMaster and Stobart[134] published an important study regarding the dynamics of indenylstannanes bearing chiral tin fragments. Compound **1.157** was prepared as a four-component mixture *via* quenching of indenyllithium with (*i*Pr)(Me)(Ph)SnBr; the generation of these isomers is due to the racemic nature of the tin bromide precursor and the presence of the chiral C(1) center on indene. The two compounds possessing indenyl sp^3 carbon atoms with "S" absolute configurations are depicted in Scheme 1.39; enantiomers exist for each of these two molecules, but are not shown. This interesting molecular system provided McMaster and Stobart with a direct means of probing the effect of suprafacial metallotropic shifts on the stereochemistry at the migrating center. For example, the occurrence of [1,5] migrations involving **1.157-*RS***, in which the configuration at tin is retained, results in the formation of the enantiomer of **1.157-*SS*** (i.e. **1.157-*RR***). In contrast, if migrations were to proceed with inversion of configuration at the metal center, then diastereomeric interconversion would not occur; instead, **1.157-*RS*** would simply interconvert with its enantiomer **1.157-*SR***, a process which cannot be detected by use of NMR spectroscopy. At low temperature (- 60 °C) the ^1H and ^{13}C NMR spectra of **1.157** were interpreted by these workers in terms of an unequal population (~ 60:40) of diastereomers; unique sp^3-hydrogen atoms on indene and Sn-CH_3 groups were readily discernible. Upon warming to 60 °C, coalescence of the distinguishable NMR sub-spectra for the diastereomers was observed. Moreover, the hydrogen atoms of the isopropyl groups in the isomers of **1.157** initially appeared as a complex multiplet at - 60 °C, but collapsed to an A_3B_3X pattern in the fast exchange regime (> 60 °C). This latter result is especially significant as it demonstrates that even in the fast exchange limit, the isopropyl methyl groups remain magnetically non-equivalent, which is consistent with a process involving retention of configuration at tin.

Despite the long history of indenylstannane chemistry, the dynamic behavior of these compounds continues to intrigue chemists. In 1996, Veith and co-workers[135] demonstrated that nitrogen-functionalized stannylenes react with indene to give σ-bonded "adducts", such as **1.158**,

via attack by tin at the indene C(1) position, followed by migration of the hydrogen onto one of the nitrogen atoms (Scheme 1.39). In contrast to the analogous π-cyclopentadienyl adduct, the indenyl complex, **1.158**, was shown to contain a metal-indene σ-bond, based on data obtained from X-ray crystallographic experiments. Variable-temperature ^{1}H and ^{13}C NMR studies revealed that **1.158** is stereochemically non-rigid, yielding a value of approximately 14 kcal mol^{-1} for the activation enthalpy associated with this dynamic process.

The synthesis and dynamics of the heptamethylindenylstannane, **1.159**, was presented by Herrmann and co-workers[136] in 1997. This compound was prepared in 65% yield *via* alkylation of chlorotrimethyltin with $[C_9(CH_3)_7]Li$, and subsequently characterized by use of X-ray crystallographic and NMR spectroscopic techniques. Although no kinetic data were provided, it appears that **1.159** is quasi-fluxional, based on the claim by these authors that warming causes a "*hapticity change*" that is observable by NMR spectroscopy. In the same year, Nifant'ev and Ivchenko also reported on the preparation of indenylstannanes, which were subsequently used in the preparation of metallocene complexes.[137]

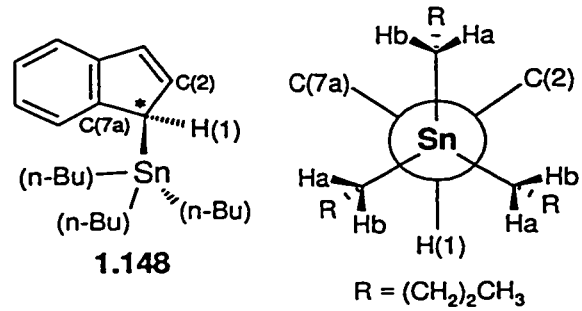

1.148

Scheme 1.40: *Newman projection along the Sn-C(1) bond of* ***1.148****, showing the local* C_s *symmetry which equilibrates only the Ha and only the Hb protons, but does not interconvert these sites*

Despite the overwhelming structural, mechanistic and reactivity data which have been put forth as evidence in support of the operation of a symmetry-allowed, suprafacial [1,5] sigmatropic shift mechanism involving σ-indenyl compounds of silicon, germanium and tin, misconceptions concerning the dynamic behavior of these complexes still persist — even in the current literature. In 1997, Morris and co-workers[138] reported the preparation and variable-temperature study of (η^1-

$C_9H_7)Sn(nBu)_3$, **1.148** (Scheme 1.40). In addition to incorrectly stating that all prior dynamic NMR studies of silicon and tin trialkyl(σ-indenyl) compounds involved only methyl-substituted species, these authors attributed the apparent signal averaging in the NMR spectra of **1.148** at 40 °C to *"a rapid 1,3 shift"*, rather than the successive [1,5] shifts predicted by the Woodward-Hoffmann rules; perhaps the authors are implying an *overall* C(1) to C(3) shift process, but this point is not made clear in the report in question. Even more curiously, whereas it is claimed that the broadening of the methylene ^{1}H NMR signals of the butyl chains in **1.148** indicates slowed rotation about the C(1)-Sn axis, the authors failed to recognize the diastereotopic character of these methylene protons when the Bu_3Sn group is attached to the stereogenic indenyl C(1) center (Scheme 1.40).

Although the vast majority of studies regarding quasi-degenerate rearrangements in σ-indenyl main group compounds have involved the Group 14 elements, these are certainly not unique in this regard, as evidenced by the Group 13 examples provided in Section 1.4.4.1. In fact, the dominance of Group 14 species in this field of study is likely more a result of the ease with which these molecules can be prepared, in addition to the inherent thermodynamic stability of the sp^3 isomers of these Group 14 compounds.

1.4.4.3 Group 15

The chemistry of indenylphosphines was examined by Schmutzler and co-workers[139] in 1989. Throughout the course of these studies, details of the synthesis and spectroscopic characterization of $(\eta^1$-$C_9H_7)PF_2$, **1.160**, the bis(σ-indenyl)phosphine, **1.163**, and the tris(σ-indenyl) compound, **1.164**, were provided (Schemes 1.41 and 1.42). For molecule **1.160**, the benzannulated derivative of **1.18** (Scheme 1.7), multinuclear NMR spectroscopic data revealed the PF_2-C(1) connectivity depicted in Scheme 1.41. Although no kinetic data pertaining to the dynamics of this compound were provided, the authors noted that upon reacting **1.160** with tetracyanoethylene, a 1:1 adduct is obtained. The product proposed by Schmutzler and co-workers, **1.161**, corresponds to a [4+2] cycloadduct involving the indene **1.160**. Although the non-equivalence of the fluorine atoms in the ^{19}F NMR of **1.160** concur with such a formulation, in the

absence of crystallographic data, ene or [2+2] addition products of **1.160**, and possibly even the Diels-Alder adduct, **1.162**, derived from the corresponding isoindene, remain possible alternatives.

The tris(σ-indenyl)phosphine, **1.164**, was prepared from lithium indenide and triphenylphosphite, and isolated as an analytically pure solid in 37% yield.[139] The simplicity of the NMR spectra obtained from samples of **1.164** is indicative of the tris(3-indenyl) structure depicted in Scheme 1.42, as no diastereotopic behavior is possible for this isomer. Similarly, the generation of the bis(σ-indenyl) complex, **1.163**, and isomers of this compound, were identified based on ^{1}H, ^{13}C, ^{19}F and ^{31}P NMR data. From a reaction which included **1.160** and isomers of bis(σ-indenyl)fluorophosphines, the platinum compound, **1.165**, was isolated and characterized by X-ray crystallography. In spite of the fact that the quality of these diffraction data is rather low, the connectivity in the sp^2-bonded $(C_9H_7)PF_2$ ligand in **1.165**, and the presence of both 1- and 3-indenyl groups in the unexpected tris(σ-indenyl)phosphine fragment is unmistakable.

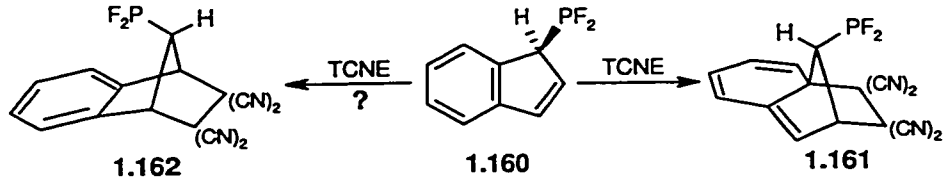

1.162 1.160 1.161

Scheme 1.41: *The reaction of the σ-indenylphosphine,* ***1.160****, with tetracyanoethylene, leading to the 1:1 adduct,* ***1.161****, as proposed by Schmutlzer and co-workers.*

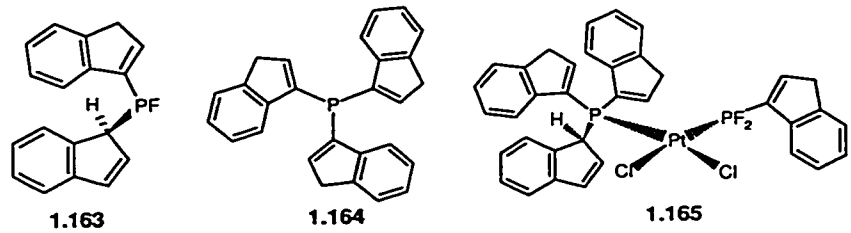

1.163 1.164 1.165

Scheme 1.42: *The poly(σ-indenyl)phosphines,* ***1.163*** *and* ***1.164****, and the platinum complex,* ***1.165.***

In 1992, Anderson and co-workers[140] examined the molecular rearrangements and reactivity of diphenylphosphino(indene)-based complexes. These workers noted that treatment of indenyllithium with chlorodiphenylphosphine yielded the sp^3-bonded kinetic product, **1.166**, which

was fully characterized by use of standard spectroscopic and physical techniques (Scheme 1.43); due to the stereogenic C(1) center on indene, the phenyl groups attached to phosphorus were observed to exhibit diastereotopism. On standing in solution at ambient temperature for several days, **1.166** was quantitatively converted into the thermodynamically favored C(3) isomer, **1.167**, which was characterized by use of ^{1}H, ^{13}C and ^{31}P NMR and X-ray crystallography. Based on the fact that the rate of this isomerization process is greatly enhanced by the interaction of solutions of **1.166** with alumina, the authors invoked an acid- or base-catalyzed protonation/deprotonation mechanism to account for the rapid conversion of **1.166** into **1.167**. Indeed, such a proposal seems rational as the rate of uncatalyzed [1,5] hydrogen migrations in indenes is rather low under ambient conditions. The corresponding phosphine sulfides, **1.168** and **1.169** were subsequently prepared from **1.166** and **1.167**, respectively; a similar transformation of **1.168** into **1.169** was noted.

Despite the tendency of **1.166** to isomerize to **1.167**, Anderson and co-workers demonstrated that freshly prepared samples of each of these compounds could be used as ligands in the preparation of novel platinum complexes. Reactions involving $PtCl_2(COD)$, PtMeCl(COD) and $PtMe_2(COD)$ all yielded products in which the stereochemical integrity of the indenylphosphine ligand was maintained. For example, the reaction **1.166** with $PtCl_2(COD)$ resulted in the formation of *cis*-$[PtCl_2(PPh_2(1\text{-}C_9H_7))_2]$, which was readily identified as a mixture of C_2 and C_s diastereomers based on ^{1}H, ^{13}C, and ^{31}P NMR spectral data.

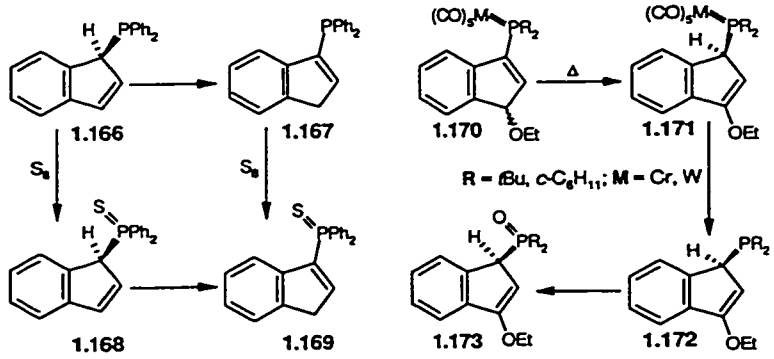

Scheme 1.43: *Chemical transformations involving the indenylphosphines,* ***1.166*** *to* ***1.173.***

A study describing (σ-indenyl)phosphines derived from the intramolecular cyclization of (arylcarbene)-Group 6 complexes has been published by Aumann *et al.*[141] According to these workers, the conversion of such a metal carbene into the corresponding phosphine, such as **1.172**, proceeds sequentially *via* the isolable intermediates, **1.170** and **1.171** (Scheme 1.43). Such observations are noteworthy, in that they represent rare examples of the thermally promoted conversion of an sp^2-bonded (σ-indenyl)phosphine into an sp^3-bonded complex. All of compounds **1.170** to **1.172** were fully characterized by use of NMR spectroscopy and other analytical techniques, and in the case of **1.171** (R = *t*Bu; M = Cr), by X-ray crystallography. The (σ-indenyl)phosphines, **1.172**, readily react with air to form the corresponding phosphine oxides, **1.173**, behavior which appears to be typical of this class of molecules. Unfortunately, no experimental data pertaining to the molecular dynamics of these interesting metal-complexed indenylphosphines were provided in this report.

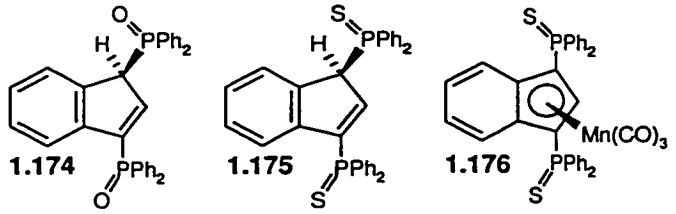

Scheme 1.44: *Three examples of crystallographically characterized indenylphosphine complexes.*

As an extension of the work of Anderson *et al.*, Stradiotto and co-workers[142] reported on the preparation, characterization and reactivity of indenyl-diphosphines. Lithiation of **1.166**, followed by quenching with chlorodiphenylphosphine and subsequent oxidation with an oxygen or sulfur source led to the formation of **1.174** and **1.175**, respectively; 1,3-disubstituted compounds were exclusively formed in these reactions (Scheme 1.44). Preparation of the manganese complex, **1.176**, established the utility of these compounds as transition metal ligands. The molecular structures of **1.174** to **1.176** in solution were elucidated based upon NMR spectroscopic

data; single-crystal X-ray diffraction studies provided data which confirmed the existence of these structures in the solid state.

The list of indenyl complexes of the heavier Group 15 elements which have been prepared and characterized is rather short; indeed, it is possible that a report published by Rufanov *et al.*[113] contains the only known examples of such compounds. The indenylarsanes, **1.177** to **1.182** were prepared in greater than 43% yield from arsenic halides and indenyllithium (Scheme 1.45). The structure of the simplest of these, **1.177**, was elucidated based on solution ^{1}H and ^{13}C NMR data; resonances attributable to the sp^3-bonded σ-indenyl framework were observed, as were signals assignable to the diastereotopic methyl groups. This compound served effectively as a precursor to the silane, **1.178** and the stannane, **1.180**. While upon warming **1.178** was converted into a mixture (~ 1:1) of this compound and the 1,3-substituted compound, **1.179**, a similar rearrangement was not observed for **1.180**. The NMR spectroscopic characterization of poly(σ-indenyl)arsanes was also detailed in this report.[113] The spectra of the product mixture derived from the quenching of lithium indenide with dichloro(*tert*-butyl)arsane indicated the presence of *meso* and *racemic* isomers; due to the asymmetry at the arsenic center, two *meso* isomers exist for **1.181**, leading to a three component mixture. Fractional crystallization of this mixture allowed for a sample containing about 85% of the *racemic* compound and 15% of one of the *meso* isomers to be isolated. The latter compound was characterized by use of X-ray diffraction techniques, which revealed sp^3-bonded indenyl groups consistent with the solution NMR data, and with the depiction of the molecule presented in Scheme 1.45.

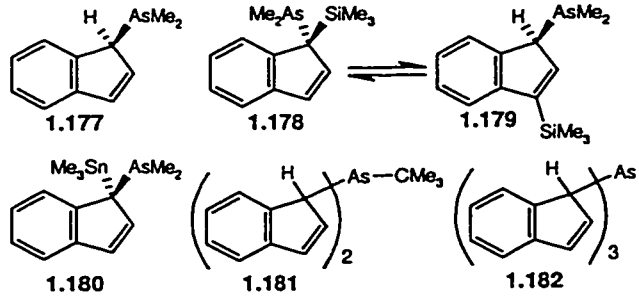

Scheme 1.45: *Indenylarsane and poly(σ-indenyl)arsane complexes.*

The description provided by these authors of the tris(η^1-indenyl)arsane system, **1.182**, is considerably more convoluted. Based on the observation of four unique indenyl environments in the ^{1}H and ^{13}C NMR spectra of the purified product mixture, Rufanov *et al.* propose that **1.182** exists as a mixture of four isomers in solution, the identities of which can be determined based on the introduction of a third indenyl group to the isomers of **1.181**. It is evident, though, that this rationale is seriously flawed; when one employs a group theory approach (see Chapter Three),[143] four unique indenyl environments are predicted for the tris(η^1-indenyl)arsane system, **1.182**. However, these arise due to the existence of a C_1 diastereomer, in which all three indenyl ring environments are magnetically non-equivalent, and a C_3 compound, which is one-third less abundant than the C_1 isomer, but for which all three indenyl environments are equivalent. The claim by Rufanov and co-workers that four isomers are present is correct, but not in the sense implied by these authors; each of the C_1 and C_3 isomers of **1.182** has an enantiomeric partner, the pairs of which cannot be distinguished by use of NMR techniques.

1.4.4.4 Groups 16 and 17

Main group η^1-indenyl complexes containing heavier elements from Groups 16 and 17 are neither as numerous nor as well documented as those bearing other *p*-block elements, and so only a few examples are provided in the following section for the sake of completion. In 1977, Kashin and co-workers[144] published a brief account of the electrophilic substitution reaction involving (3-methylindenyl)trimethylstannane and sulfur dioxide. Starting from a enantiomerically pure sample of the stannane, treatment with SO_2 produced **1.183**, which rapidly isomerized to the 1,3-disubstituted indene, **1.184** in the presence of excess SO_2 (Scheme 1.46). By monitoring each step of the reaction sequence by using ^{1}H NMR and IR spectroscopy, in addition to optical rotation studies, these workers concluded that the reaction involved backside electrophilic attack on the leaving group. Sulfur derivatives of indene have also been studied by Hartke and Schilling-Pindur.[145] For example, these authors noted that the reaction between dimethyl disulfide and lithium indenide produces 3-(methylthio)indene, **1.186**, presumably *via* the intermediacy of the

sp^3-isomer, **1.185**, while lithiation of **1.186** followed by quenching with methyl iodide produces the 1,1-disubstituted compound, **1.187**, exclusively. When **1.186** was instead treated with methyl fluorosulfonate in CCl_4, the interesting C(2) substituted compound, **1.188**, was generated in 26% yield.

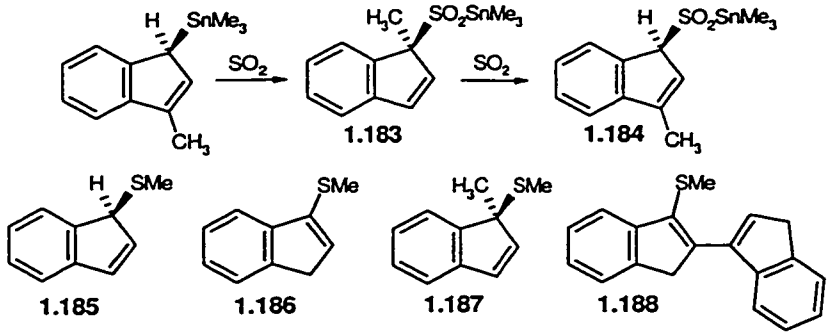

Scheme 1.46: *Selected examples of sulfur-functionalized indenes, including* ***1.184****, generated via electrophilic attack of SO_2 on an indenylstannane.*

In 1974, Feast and Preston[146] reported on the photochemically promoted isomerization of perfluoroindene, **1.189** (Scheme 1.47). Upon irradiation (λ = 253 nm), **1.189** is converted to the corresponding perfluoroisoindene, which can, remarkably, be trapped *in situ* with dienophiles as weak as ethylene. Moreover, when solutions of **1.189** are treated with ethylene without irradiation, the corresponding [2+2] adduct is obtained exclusively.

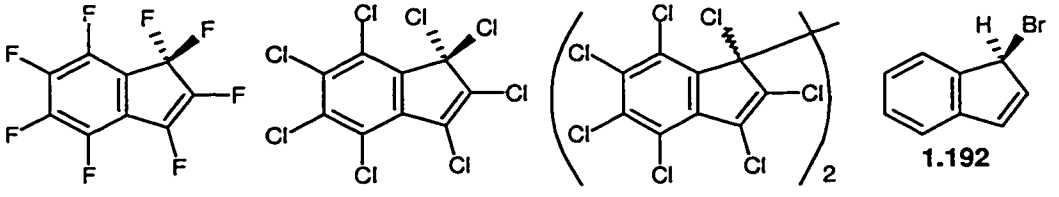

Scheme 1.47: *Examples of indenes bearing Group 17 elements.*

Castañer *et al.*[147] published a study pertaining to the reactivity of perchloroindene, **1.190.** These workers demonstrated that the perchlorinated 1-indenyl dimer, **1.191**, could be obtained as an analytically pure compound in approximately 77% yield, *via* treatment of **1.190** with pentacarbonyliron in benzene. Upon heating, both **1.190** and **1.191** gave rise to the corresponding perchloro(1-indenyl) radical, which was detected by EPR spectroscopy.

Bromoindenes are also known; a facile synthetic route to 1-bromoindene, **1.192**, was published by Woell and Boudjouk[148] in 1980.

1.5 Objectives of the Thesis

The survey of transition metal and main group η^1-indenyl compounds provided in Section 1.4 serves not only to highlight the important work in this field, but also to underscore the need for a more extensive examination of the molecular dynamics and reactivity of this class of molecules. Thus, the primary objectives of this thesis are to: (a) gain insight into the sequential nature of metal and metalloid migrations about the periphery of indenyl rings, including the provision of evidence for the symmetry-allowed [1,5] migratory pathway; (b) investigate the factors that influence these migrations and the generation of metalloisoindenes; (c) explore the reactivity of these molecules and their derivatives.

Over the more than three decades since Cotton and co-workers first probed the dynamic behavior of $(\eta^5\text{-}C_5H_5)Fe(CO)_2(\eta^1\text{-}C_9H_7)$, **1.9**, the "non-fluxional" nature of this compound has almost been granted an imprimatur. Indeed, acceptance of the apparently static nature of this important molecule continues to influence the way chemists interpret and rationalize the reactivity of η^1-indenyl transition metal complexes. In an attempt to test the validity of this belief, the potential for stereochemically non-rigid behavior involving **1.9** was reexamined by use of 2D-EXSY and single selective inversion NMR techniques. The results of these studies are presented in Chapter Two.

The utility of σ-indenyl main group compounds has been discussed in the foregoing sections. Although the dynamics of this class of compounds have been thoroughly examined and, in many cases, persuasive mechanistic arguments pertaining to the molecular rearrangement pathway provided, the stereochemical complexity of the related poly(σ-indenyl) systems continues to provide a source of confusion. In light of the misconceptions surrounding the spectroscopic features exhibited by tris(σ-indenyl) main group compounds, an important extension of the work in this field includes an examination of the hitherto unknown tris(σ-indenyl)silane series. The synthesis, characterization, molecular dynamics and reactivity of a series of tris(σ-indenyl)silanes are presented in Chapter Three.

Previous studies indicate that the nature of the alkyl substituents on silicon in trialkyl(σ-indenyl)silanes has little effect on the rate of [1,5] silicon migrations. In contrast, the strategic addition of hydrocarbon fragments onto the indenyl framework can serve either to raise or to lower the barrier to such silatropic rearrangements. Chapter Four includes an examination of the impact of organometallic complexation, either adjacent to silicon or on the indenyl C_6 ring, on the barrier to [1,5] silicon shifts in indenylsilanes.

Intramolecular Diels-Alder reactions have been widely used in the preparation of bridged polycyclic species, including many natural products. Although intermolecular [4+2] cycloaddition reactions involving dienophiles and silyl-isoindenes have been documented, the corresponding intramolecular reactions have not been examined. Chapter Five contains some preliminary studies directed toward assessing the utility of functionalized indenylsilanes as synthetic precursors to novel polycyclic organic architectures, *via* intramolecular Diels-Alder trapping of isoindenes.

CHAPTER TWO

The Quasi-Fluxional Nature of $(\eta^5\text{-}C_5H_5)Fe(CO)_2(\eta^1\text{-}C_9H_7)$

2.1 Introduction

Any historical perspective on stereochemical non-rigidity in σ-indenyl complexes must cite the now classic report authored by Cotton and co-workers, in which the dynamics of $(\eta^5\text{-}C_5H_5)Fe(CO)_2(\eta^1\text{-}C_9H_7)$, **1.9**, were probed by use of variable-temperature NMR techniques; the relevance of this work to fluxional σ-cyclopentadienyl compounds was delineated in Section 1.3.3, and further elaborated upon in Section 1.4.3.4. The lack of detectable ^1H NMR line broadening for **1.9** led these workers to describe this compound as "*nonfluxional*".[39] However, in a subsequent report, Cotton explicated this situation with more precision, noting that "*in the case of* $(\eta^5\text{-}C_5H_5)Fe(CO)_2(\eta^1\text{-}C_9H_7)$*, the 2-indenyl structure* ...**1.10**... *is so unfavorable that it does not serve as a suitable transition state or intermediate for the interconversion* ...of **1.9*R*** and **1.9*S***... *at a rate sufficient to cause broadening of the NMR spectrum even at +70 °C (above which temperature the compound undergoes rapid decomposition)*" (Scheme 1.5).[90] These authors did not state that the interconversion of the enantiomers of **1.9** could not occur, they merely placed limits on the rate!

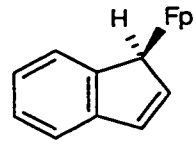

1.9

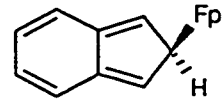

1.10

It is well documented that for the $(\sigma\text{-}C_5H_5)EMe_3$ and $(\sigma\text{-}C_9H_7)EMe_3$ series (E = Si, Ge, Sn), the $\Delta G^{\ddagger}$ values for the Group 14 element migrations in the indenyl systems are ~ 9 kcal mol^{-1} higher than in the corresponding cyclopentadienes.[70] The overall pattern which emerges from these data is that of a common [1,5] suprafacial shift mechanistic pathway for both classes of molecules; in the

case of indenyl compounds, the barriers are larger because of the decreased aromatic character of the isoindene intermediates, which can also be trapped as Diels-Alder adducts by suitably reactive dienophiles.[121,122] Analogously, if **1.9** were in fact stereochemically non-rigid, a migratory barrier in excess of 20 kcal mol^{-1} would be anticipated,[70] based on the value of the barrier associated with (η^5-C_5H_5)Fe(CO)$_2$(η^1-C_5H_5), **1.3** (~ 10.7 kcal mol^{-1}). Such a [1,5] shift process proceeding with a barrier in the 20 kcal mol^{-1} range would be extremely difficult to detect by use of techniques which require the observation of changes in the NMR line-shape, especially below the decomposition temperature of **1.9**. In contrast, the selective inversion and 2D-EXSY NMR techniques described in Sections 1.2.2 and 1.2.3 are readily amenable to the study of such chemical exchange phenomena. As such, the molecular dynamics of the purportedly "static" molecule, **1.9**, were reinvestigated by use of these slow exchange regime dynamic NMR techniques.[149]

2.2 Results and Discussion

2.2.1 NMR Studies

The compound of interest, **1.9**, was prepared from (η^5-C_5H_5)Fe(CO)$_2$I and indenyllithium, and readily identified by use of ^{1}H and ^{13}C NMR spectroscopic techniques. In the absence of published data acquired on a high-field NMR spectrometer, ^{1}H and ^{13}C NMR spectra were obtained for **1.9** (at 500 MHz and 125 MHz, respectively) and unequivocally assigned based on a combination of ^{1}H-^{1}H COSY (COrrelated SpectroscopY), ^{1}H-^{13}C HSQC (Heteronuclear Single Quantum Coherence) and ^{1}H-^{13}C HMBC (Heteronuclear Multiple Bond Correlation) two-dimensional NMR experiments. Gratifyingly, careful analysis of these spectroscopic data led to an assignment of the signals attributable to the vinylic hydrogens in **1.9** which concurs with that originally put forth by Cotton *et al.*;[39] H(3) resonates at a lower frequency than H(2).

With the availability of modern 2D-EXSY techniques, it is straightforward to demonstrate that **1.9** is indeed quasi-fluxional, even at temperatures where no line-broadening is evident. Figure 2.1 shows the results of a phase-sensitive ^{1}H-^{1}H EXSY experiment acquired at 45 °C with a mixing time

of 5 seconds; at this temperature, decarbonylation of **1.9** to yield benzoferrocene, **1.11**, is relatively slow. One can clearly observe off-diagonal correlations between H(1) and H(3), and also between the aromatic protons H(4) and H(7), which are indicative of chemical exchange arising from an *overall* C(1) to C(3) migratory process.

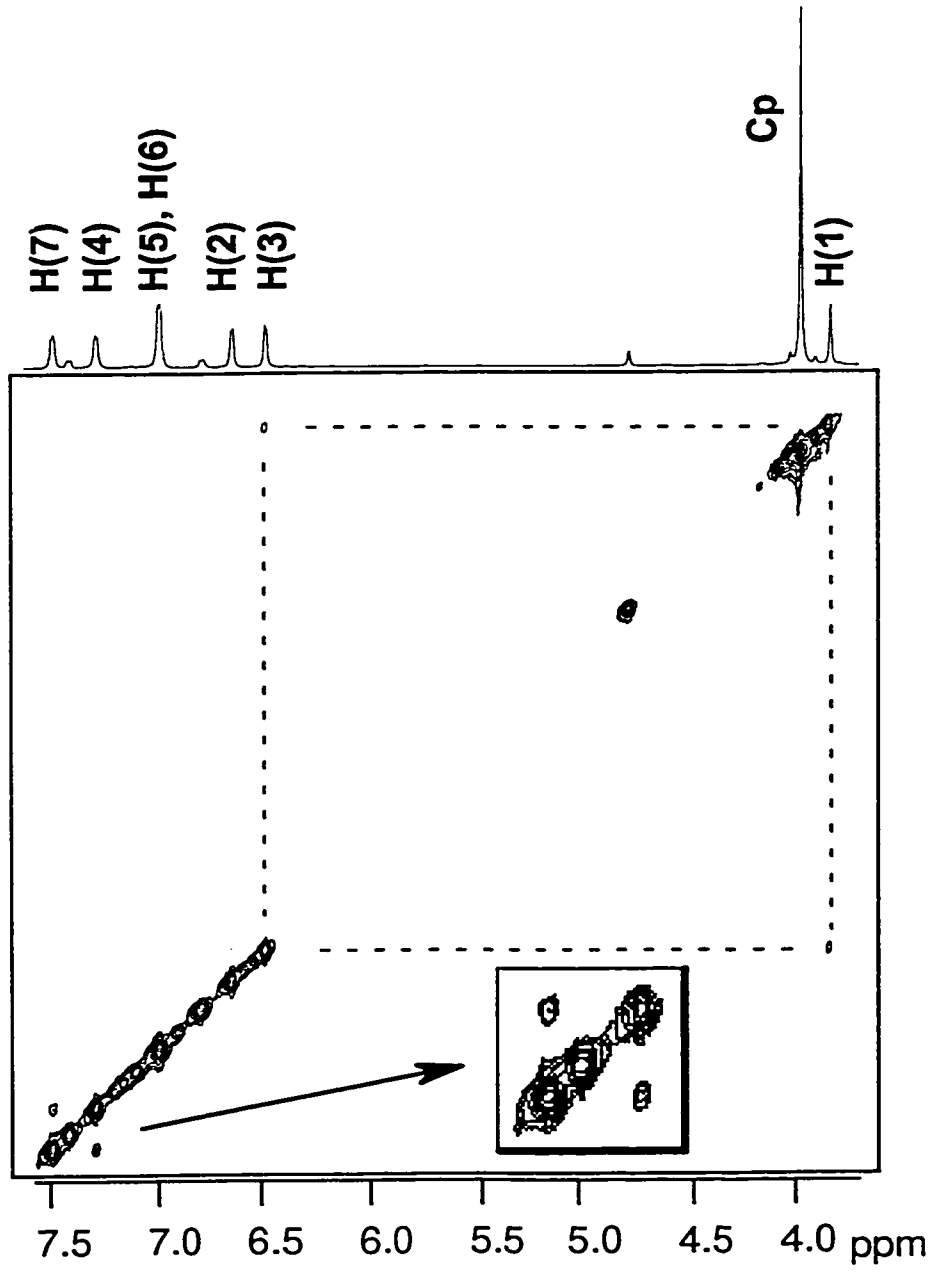

Figure 2.1: *^{1}H-^{1}H EXSY spectrum of **1.9** in C_6D_{12} at 45 °C, acquired with a mixing time of 5 seconds.*

From a given two-dimensional spectrum, one can readily extract a number of one-dimensional spectra in the form of perpendicular "slices". Figure 2.2 shows a stacked plot of such 1D slices, comprised of rows containing the H(3) diagonal peak and its off-diagonal correlation peak with H(1); these spectra were extracted from a series of ^{1}H-^{1}H EXSY spectra that were acquired by using various mixing times. From the stacked plot of 1D spectra it is evident that the magnitude of the off-diagonal cross-peak relating the H(3) and H(1) sites, relative to the H(3) diagonal peak, grows with increasing mixing time. Moreover, since the diagonal and off-diagonal resonances have the same phase, one can be sure that these correlations arise as the result of chemical exchange, not from nuclear Overhauser effect (nOe) interactions.

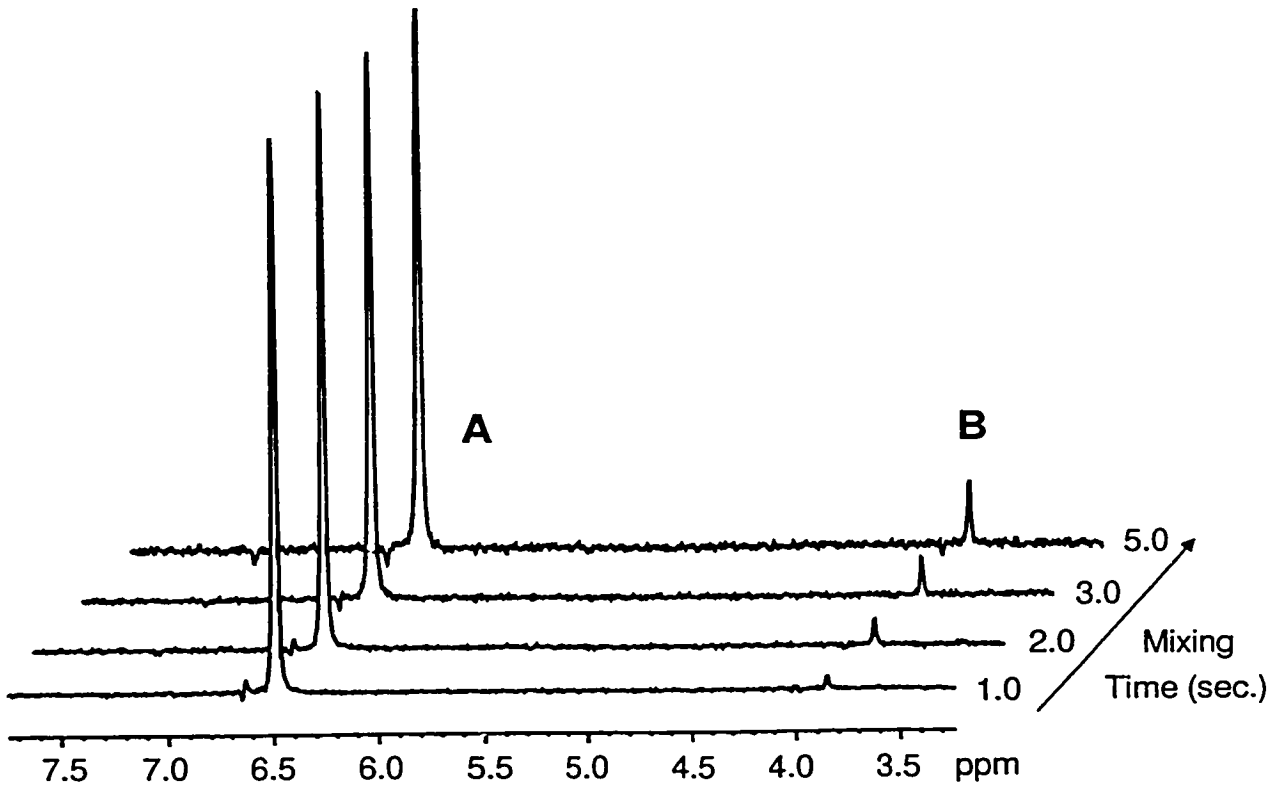

Figure 2.2: *Cross-sections from ^{1}H-^{1}H EXSY spectra of* ***1.9*** *acquired with different mixing times. In each case, signal* ***(A)*** *is the diagonal peak attributable to H(3); signal* ***(B)*** *is the off-diagonal peak arising from chemical exchange with H(1).*

Although 2D-EXSY experiments conveniently map out exchanging sites, for quantitative exchange measurements, one-dimensional NMR methods are often more efficient. In the present case, the problem of rapid sample decomposition at the elevated temperatures required to observe chemical exchange necessitates that the NMR measurements be carried out as rapidly as possible. For a given temperature, ^{1}H NMR selective inversion experiments utilizing single-scan acquisitions provided acceptable kinetic data in under fifteen minutes. In these experiments, the H(1) signal was selectively inverted and the intensity of the H(1) and H(3) signals subsequently monitored as a function of time; additional experimental details are provided in Chapter Seven. Analysis of such data collected over a range of temperatures (45 °C to 65 °C) yielded a $\Delta G^{\ddagger}$ value of 20 ± 2 kcal mol^{-1}, for this **1.9*R*** ⇔ **1.9*S*** enantiomerization process.[149]

2.2.2 Probing for the Intermediacy of Isoindenes

In 1996, Kerber *et al.*[150] reported that **1.9** participates in a [3+2] cycloaddition with maleic anhydride and TCNE, yielding the cycloadducts **2.1** and **2.2**, whose structures were assigned on the basis of their NMR spectra; the [3+2] cycloaddition reaction, as typified by the allyl-iron complex shown in Scheme 2.1, has been comprehensively reviewed by Welker.[151] However, in light of the stereochemically non-rigid nature of **1.9**, it is possible to envisage the generation of such products *via* Diels-Alder [4+2] additions to the isoindene **1.10** (Scheme 2.2), rather than by a [3+2] process involving the indene, **1.9**. As such, it was deemed necessary to establish unequivocally the stereochemistry of the products.

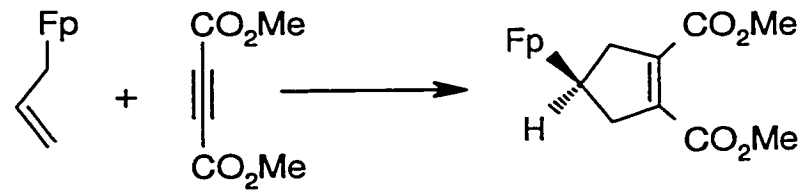

Fp = $Fe(CO)_2(\eta^5\text{-}C_5H_5)$

Scheme 2.1: *The [3+2] cycloaddition reaction of (η^1-allyl)$Fe(CO)_2Cp$ with dimethylacetylenedicarboxylate.*

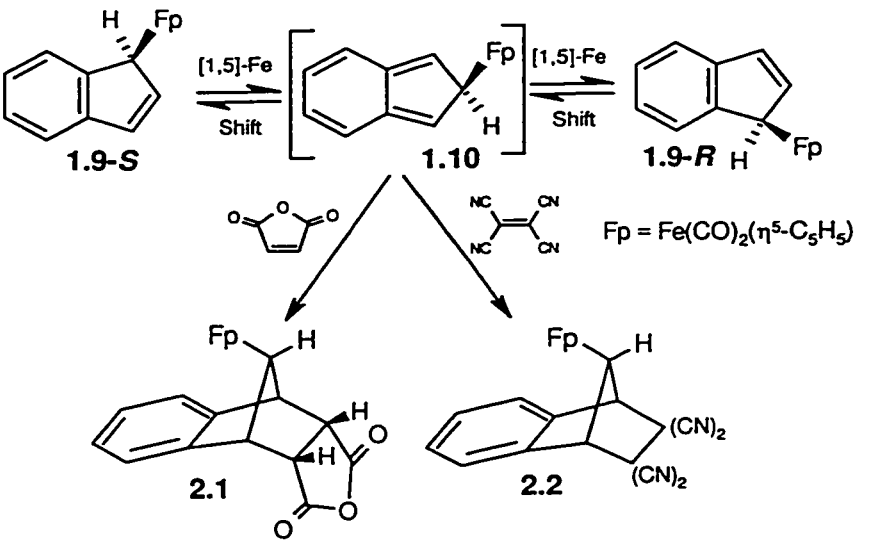

Scheme 2.2: *Diels-Alder trapping of the iron(isoindene),* ***1.10****, with maleic anhydride and tetracyanoethylene, yielding* ***2.1*** *and* ***2.2****, respectively.*

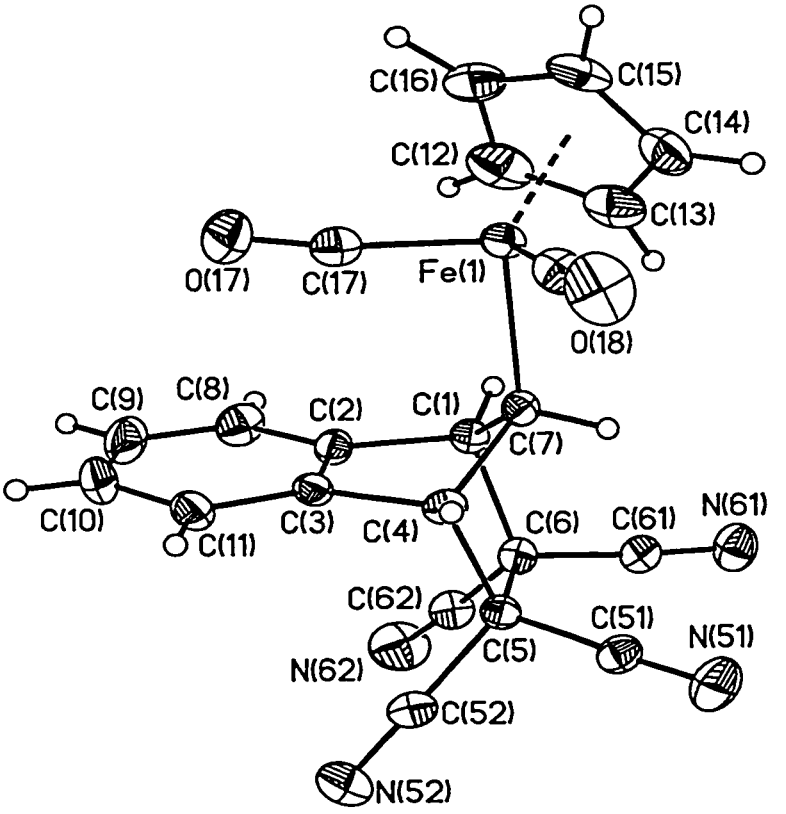

Figure 2.3: *The X-ray structure of* ***2.2****, showing the atomic numbering scheme. Thermal ellipsoids are shown at the 30% probability level and only one of the two independent molecules is shown.*

The X-ray crystal structure of the TCNE adduct, **2.2**, is presented in Figure 2.3, with the important crystallographic parameters and geometrical data provided in the Appendix. In the crystalline lattice, the adduct, **2.2**, packs with two crystallographically-independent, pseudo-enantiomorphic rotamers per asymmetric unit, between which no unusually close intermolecular contacts exist. Given the similarity between these two rotamers, commentary on specific geometric parameters in the following discussion is limited to only one of the independent molecules.

Perhaps the most striking structural feature is the *anti* orientation of the Fp and TCNE moieties in **2.2**, which parallels structural data obtained for **1.134** (see Chapter Three), the Diels-Alder adduct of trimethylsilyl-isoindene with TCNE, and also for **2.3**, the cycloaddition product of **1.3** with maleic anhydride (Scheme 2.3).[152] The steric demands of the $(\eta^5\text{-}C_5H_5)Fe(CO)_2$ unit in **2.2** are evident in the expansion of the Fe(1)-C(7)-C(1) and Fe(1)-C(7)-C(4) angles from ideal tetrahedral geometry, an effect which has been observed for other related transition metal complexes.[152,153] Overall, however, the geometric features of the $(\eta^5\text{-}C_5H_5)Fe(CO)_2$ fragment in **2.2** are generally quite similar to those previously reported for other $(\eta^5\text{-}C_5H_5)Fe(CO)_2(\eta^1\text{-alkyl})$ complexes.[152,154] With the exception of the observed lengthening in both the incipient Diels-Alder bonds, C(1)-C(6) and C(4)-C(5), and the formerly olefinic TCNE bond, C(5)-C(6), the carbocyclic framework in **2.2** exhibits no unusual features. Such an increase in $C(sp^3)$-$C(sp^3)$ distance has been rationalized in other cyclic structures as resulting from the electron withdrawing character of the cyano substituents.[154]

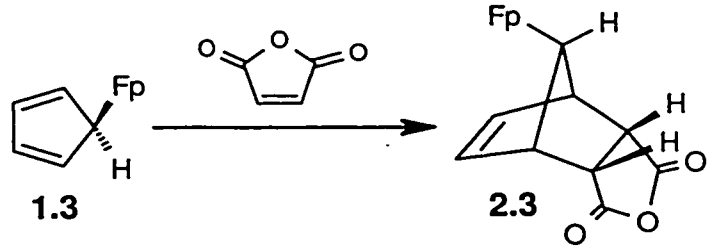

Scheme 2.3: *A Diels-Alder cycloaddition involving* $(\eta^5\text{-}C_5H_5)Fe(CO)_2(\eta^1\text{-}C_5H_5)$, ***1.3****, leading to* ***2.3****.*

2.2.3 Mechanistic Implications in Cycloaddition Chemistry

The detection of quasi-fluxional behavior involving **1.9** has considerable relevance to the cycloaddition chemistry of this compound. Prior to this work, the assumed stereochemically rigid nature of **1.9** precluded the involvement of the corresponding isoindene in cycloaddition reactions. In fact, Kerber *et al.*[150] went so far as to claim that **1.9** "*lacks a diene unit and is incapable of participating in a Diels-Alder [4+2] reaction, so that only [3+2] cycloadditions should be found*". Although it is apparent that these workers were referring to the absence of the isoindene intermediate, **1.10**, it is important to recognize that Diels-Alder reactions involving indene itself and reactive dienophiles are known.[155]

While the cycloaddition chemistry of $(\eta^1\text{-}C_5H_5)Fe(CO)_2(\eta^1\text{-allyl})$ can be understood in terms of [3+2] processes, studies carried out by both Glass and McConnell,[156] and by Kerber *et al.*,[150] strongly support a concerted [4+2] mechanistic pathway, rather than a metal-mediated [3+2] route, in the reactions of $(\eta^5\text{-}C_5H_5)Fe(CO)_2(\eta^1\text{-}C_5H_5)$, **1.3**, with electrophilic alkenes. With the viability of the isoindene, **1.10**, clearly demonstrated, it is no longer necessary to invoke a [3+2] mechanism in rationalizing the formation of adducts such as **2.1** and **2.2**. Whereas the suppressed reactivity of dienophiles towards **1.9**, relative to **1.3**, has previously been attributed to the fact that **1.9** could only avail itself of the slower [3+2] reaction pathway,[150] these observations can equally be interpreted in terms of the required generation of the reactive isoindene intermediate, **1.10**. Moreover, the fact that the *anti* disposition of the $(\eta^5\text{-}C_5H_5)Fe(CO)_2$ unit and the dienophilic fragment in **2.2** parallels that observed in the crystal structure of the metallocyclopentadiene-based Diels-Alder adduct **2.3**, can be taken as indirect support for a [4+2] mechanism involving **1.10**.

2.3 Conclusions

The present work[149] establishes unambiguously that $(\eta^5\text{-}C_5H_5)Fe(CO)_2(\eta^1\text{-}C_9H_7)$, **1.9**, is quasi-fluxional and, since sigmatropic shifts in metal-cyclopentadienyl or -indenyl complexes have

been shown to proceed *via* [1,5] shifts, the [3+2] reaction pathway is no longer the only viable mechanistic route to adducts such as **2.1** and **2.2**.

The possible intermediacy of isoindenes in the formation of the silicon-substituted adduct, **1.134** was initially investigated by Ashe in 1970.[122] He used a dilatometric method to measure the temperature dependence of the rate of formation of **1.134** from trimethylsilylindene, **1.109**, and TCNE, and obtained an activation energy of ~ 22.5 kcal mol^{-1}. The striking similarity of this value to that found for silatropic shifts leads one to conclude that these migrations occurred *via* successive [1,5] shifts, and that Ashe had trapped the short-lived isoindene intermediate. A similar kinetic study would be required in order to unequivocally demonstrate that prior isomerization to **1.10** is necessary for the formation of the adducts, **2.1** and **2.2**. Reaction of **1.9** with an efficient trapping agent, such as TCNE, would be first-order in substrate and zero-order in TCNE, and the activation energy for this process should be at least 20 kcal $mole^{-1}$, the energy required to achieve the initial isomerization of **1.9** to **1.10**; in contrast, a [3+2] mechanism should proceed with second-order kinetics.

CHAPTER THREE

The Molecular Dynamics and Reactivity of Tris(σ-indenyl)alkylsilanes

3.1 Introduction

3.1.1 The Synthesis and Dynamics of Poly(σ-indenyl) Complexes of Group 14

Twenty-five years after Gilman and Gist[157] first reported on the synthesis of the mono(η^1-indenyl) complex, **1.147**, and the bis(η^1-indenyl)stannane, **3.1**, McMaster and Stobart[143] qualitatively examined the dynamic behavior of the latter molecule and other poly(η^1-indenyl) complexes of germanium and tin (**3.2** to **3.5** in Scheme 3.1). The tris(η^1-indenyl)tin species were prepared in the usual manner from lithium indenide and the appropriate trichloroalkylstannane, in approximately 50% yield. Proton NMR spectroscopic data obtained at -60 °C from samples of these compounds consisted of signals attributable to the alkyl substituent (*n*Bu in **3.2**; Ph in **3.3**), a complex multiplet due to the aromatic/olefinic hydrogen atoms, and four distinct diastereotopic H(1) signals between 3.7 and 3.5 ppm. Warming to 60 °C caused these latter signals to merge into a single broad resonance which eventually collapsed, accompanied by the growing in of a well-resolved triplet near 6.2 ppm. Spectral data obtained from ^{13}C NMR experiments coincided with these results; at low temperature, four unique indenyl C(1) resonances were found for **3.2**, while for **3.3**, three signals of approximate intensity 1:2:1 were observed. Upon warming, these and the other geometrically related indenyl signals coalesced, which is entirely consistent with the operation of a metallotropic shift process which is rapid on the NMR time scale. Diastereotopic effects and coalescence behavior were also detected for the tetra(σ-indenyl) complexes, **3.4** and **3.5**. Interestingly, such effects were not found for bis(σ-indenyl)diphenylstannane, **3.1**, paralleling the situation described by Cotton and Marks[90] for the mercury analogue, **1.43**.

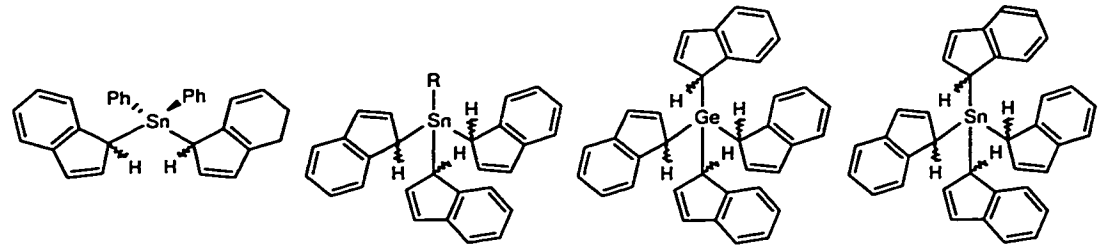

3.1 **3.2**: R = *n*Bu **3.3**: R = Ph **3.4** **3.5**

Scheme 3.1: *Poly(σ-indenyl) complexes of germanium and tin.*

In an attempt to rationalize the observed number of signals in the low temperature spectra of these poly(η^1-indenyl) complexes of germanium and tin, McMaster and Stobart[143] systematically evaluated the (σ-indenyl)$_n$MR$_{4-n}$ (R = achiral substituent) series by use of group theory. As previously described, (σ-indenyl)MR$_3$ compounds exist as a pair of enantiomers, which yield identical NMR spectral data, while for (σ-indenyl)$_2$MR$_2$ complexes, such as the silicon complexes **3.6** to **3.9** (Scheme 3.2), and the tin compound, **3.1**, *meso* and racemic (*d, l*) isomers are possible. For (σ-indenyl)$_3$MR complexes, the existence of two diastereomers is viable, one possessing C_3 symmetry, and another in which the absolute configurations of the C(1) carbon in the three indenyl rings are not identical (C_1 symmetry). McMaster and Stobart reasoned that while the C_1 isomer of (σ-indenyl)$_3$MR compounds gives rise to three magnetically non-equivalent indenyl ring environments, the indenyl environments of the C_3 isomer are identical. Such a scenario results in the expectation of four unique indenyl ^{1}H and ^{13}C NMR signals for this class of compounds. When statistical weighting is considered, the description provided by these workers provides a rationale for the observation of four equal intensity indenyl sp^3-CH signals in the ^{1}H and ^{13}C NMR spectra of **3.2**. In the case of the (σ-indenyl)$_4$M complexes, such as **3.4** and **3.5**, three isomers of D_2, C_1 and S_4 symmetry are predicted *a priori*; the experimentally observed peak multiplicities in these compounds were also rationalized by these workers, using a similar group theoretical approach. Although no Group 14 compounds of the type (σ-indenyl)$_3$MR have been

crystallographically characterized to date, single crystal X-ray data for the S_4-symmetric isomers of both **3.4** and **3.5** were provided in a subsequent publication by Stobart and co-workers.[158]

In 1993, Rausch and co-workers[159] reported the synthesis and characterization of the indenylsilanes, **1.113**, **1.127** (Scheme 1.33) and **3.13**, and the bis(σ-indenyl)silanes, **3.6** and **3.8** to **3.12** (Scheme 3.2). An important part of this study involved an examination of the molecular dynamics of bis(σ-indenyl)silanes, by use of variable temperature NMR spectroscopy. In the case of **3.6**, the *meso* isomer (C_s symmetry) contains two magnetically non-equivalent methyl groups, while the C_2 symmetry of the *d, l* compound renders the methyl groups magnetically equivalent; for each of these diastereomers an enantiomeric partner exists, for which the chemical shifts are isochronous. Additionally, though the pairs of indenyl ligands within each of these C_s and C_2 isomers are equivalent, each diastereomer exhibits unique indenyl ^{1}H and ^{13}C resonances.

The molecular dynamics of **3.6** (and similarly **3.8** and **3.9**) were probed by monitoring the conversion of a pure sample of the *d,l* (racemic) isomer (isolated by crystallization) into a mixture containing both diastereomers. At temperatures above 110 °C, the authors noted that the ^{1}H NMR methyl resonances attributable to the two diastereomers began to broaden; higher temperatures were not explored due to instrumental limitations. In an attempt to extract additional kinetic data below this temperature, an alternative methodology was employed in which a pure sample of the *d,l* isomer was maintained at a given temperature for approximately fifteen minutes, and the measured intensity ratio of the *d,l* to *meso* methyl resonances was taken as the equilibrium constant (K_{eq}) at that temperature. Based on the temperature-dependent K_{eq} data obtained from these experiments, Rausch and co-workers[159] proposed that the diastereomerization of **3.6** occurs by way of a concerted, intramolecular [1,3] silicon shift pathway below 110 °C, with some other "*fluxional process*" (presumably [1,5] silatropic shifts) being operative at higher temperatures.

Troubled by the claim of Rausch and co-workers[159] that the aforementioned bis(σ-indenyl)silanes are "*not fluxional up to 110 °C*", and concerned by the proposal of symmetry-

forbidden [1,3] silicon shifts involving **3.6** at low temperatures, Rigby *et al.*[160] reinvestigated the dynamics of this system in 1995. By use of ^{1}H-^{1}H EXSY and single selective inversion NMR techniques, Rigby and co-workers were able to monitor and obtain temperature-dependent rate constants, rather than equilibrium constants, for the interconversion of the *d,l* and *meso* isomers of **3.6**, even at temperatures below which this process is too slow to induce significant NMR line broadening. Moreover, these workers demonstrated that kinetic data obtained between 47 °C and 107 °C are fit by a single dynamic process, and yield a barrier ($\Delta G^{\ddagger}$ ~ 24 kcal mol^{-1}) associated with this migratory phenomenon that is in agreement with the value obtained for trimethylsilylindene, **1.109**.[70,122] Having demonstrated that **3.6** is indeed fluxional, even at reduced temperatures, Rigby and co-workers sought evidence in support of a symmetry-allowed [1,5] silicon shift mechanism. Using the approach of Ashe,[122] a solution of **3.6** treated with two equivalents of tetracyanoethylene yielded the double Diels-Alder adduct, **3.14** (Scheme 3.2), an observation which can be rationalized in terms of the sequential trapping of isoindene intermediates generating during a [1,5] silatropic shift process.

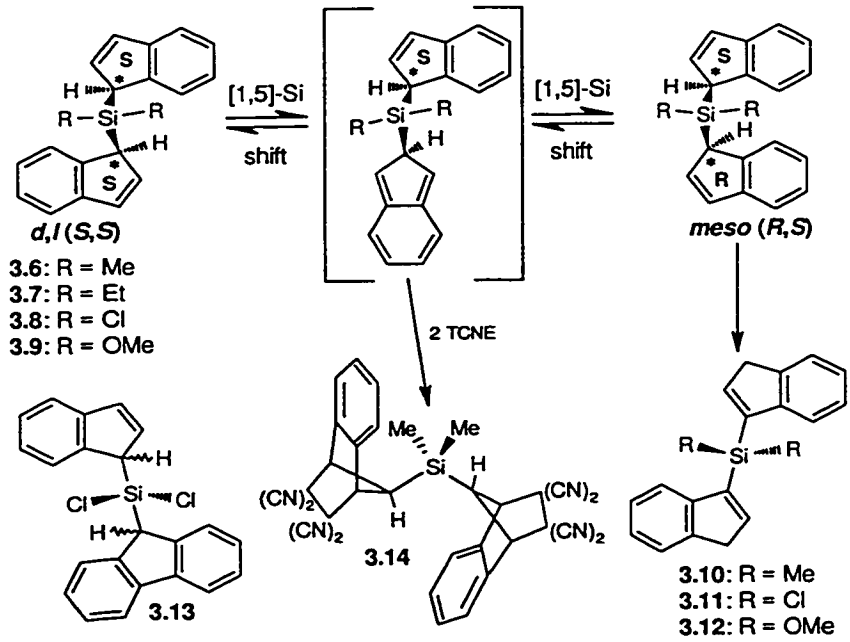

Scheme 3.2: *Sigmatropic shifts and cycloaddition chemistry, involving bis(σ-indenyl)silanes.*

Additional evidence for the intermediacy of isoindenes in dynamic processes involving **3.6** came from a subsequent report by Jordan and co-workers,[161] who described the synthesis and X-ray structure of a novel C_1-symmetric *ansa*-hafnocene [$Me_2Si(\eta^5$-1-indenyl)(η^3-2-indenyl)]$Hf(NMe_2)_2$, **3.17**, in which one of the indenyl moieties is bridged to the silicon center through the indenyl C(2) position (Scheme 3.3). Jordan *et al.* rationalized the formation of **3.17** as resulting from the intramolecular elimination of dimethylamine from the isoindene **3.16**, which is formed as a result of a single [1,5] silatropic shift of an $Me_2Si(\eta^5$-1-indenyl)$Hf(NMe_2)_3$ unit about the periphery of the uncoordinated indenyl ring in **3.15**. The intramolecular "trapping" of the isoindenyl fragment in **3.16** strongly supports the viability of intermolecular [4+2] cycloadditions involving thermally generated isoindenes and electron-deficient dienophiles.

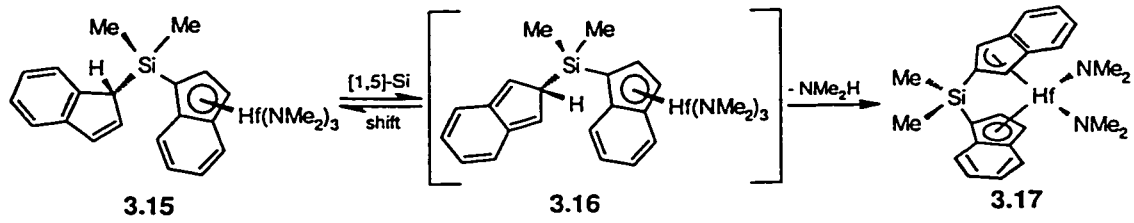

Scheme 3.3: *Intramolecular trapping of an isoindene at a hafnium center.*

3.1.2 Probing the Molecular Dynamics of Tris(σ-indenyl)silanes

The widespread use of poly(σ-indenyl) main group compounds as ligands in the preparation of chiral metallocene pre-catalysts continues to provide an impetus for the preparation of novel poly(σ-indenyl) frameworks, and for studies in which the molecular dynamics of this class of compounds are examined. As described in the previous section, for quasi-fluxional poly(σ-indenyl) compounds such as bis(1-indenyl)dimethylsilane, **3.6**, the stereogenic character of the C(1) carbons results in the formation of interconverting diastereomers (**3.6-*d,l*** and **3.6-*meso***) (Scheme 3.2), each of which, after incorporation of a Group 4 metal, for example, gives rise to an *ansa*-bridged catalyst possessing unique structure, molecular symmetry and polymerization activity. As such, the diastereoselective synthesis of an *ansa*-bridged catalyst necessitates that a diastereomerically pure poly(σ-indenyl) ligand be employed, and that the stereochemical integrity

of this precursor be maintained throughout the metallation procedure. Any process which leads to a change in configuration in these poly(σ-indenyl) compounds, including [1,5] sigmatropic shifts, is therefore worthy of examination at a rather fundamental level.

In light of the situation depicted above, a synthetic and mechanistic examination of tris(σ-indenyl)silanes is warranted. Despite the fact that such an investigation represents a direct extension of bis(σ-indenyl)silane chemistry, tris(σ-indenyl)silanes have yet to be reported. McMaster and Stobart[143] have put forth an eloquent theoretical rationale for the stereochemical subtleties of tris(σ-indenyl) complexes, by use of an approach rooted in group theory (Section 3.1.1); preliminary qualitative experimental support for these concepts were also provided by these workers through NMR spectroscopic studies involving tris(σ-indenyl)tin compounds. Nevertheless, a complete and unequivocal analysis of the NMR spectral features and molecular dynamics of a tris(σ-indenyl) system has not appeared in the literature thus far, and reports which have emerged, including the study of tris(1-indenyl)borane, **1.81**,[112] and tris(1-indenyl)arsine, **1.182**,[113] seem to require clarification. The current availability of high-field NMR spectrometers equipped with multiple pulse capability allows for the rich stereochemical complexities of poly(σ-indenyl)silanes to be examined, as demonstrated by the elegant reexamination of the bis(1-indenyl)dimethylsilane system, **3.6**, by Rigby *et al.*[160] Such a full analysis of the molecular dynamics of tris(σ-indenyl)silanes could, in turn, provide considerable insight into the sequential nature of elementotropic shifts in all poly(σ-indenyl) complexes.

3.2 Results and Discussion

3.2.1 Synthesis and Characterization of Tris(σ-indenyl)silanes

The targeted tris(σ-indenyl)silanes, **3.18** to **3.20**, were prepared in a straightforward manner by quenching of an appropriately substituted trichlorosilane with an excess of indenyllithium, followed by chromatographic purification on silica. Interestingly, the reaction involving trichlorosilane itself proved to be much more efficient (64% yield) than the corresponding reactions in which alkyltrichlorosilanes were

utilized (42% and 13% for **3.18** and **3.19**, respectively), likely owing to the reduced congestion in **3.20**. In addition to mass spectrometric, infrared spectroscopic and elemental analysis studies, all three tris(σ-indenyl)silanes were thoroughly characterized by use of ^{1}H, ^{13}C and ^{29}Si one- and two-dimensional NMR spectroscopic techniques.[162]

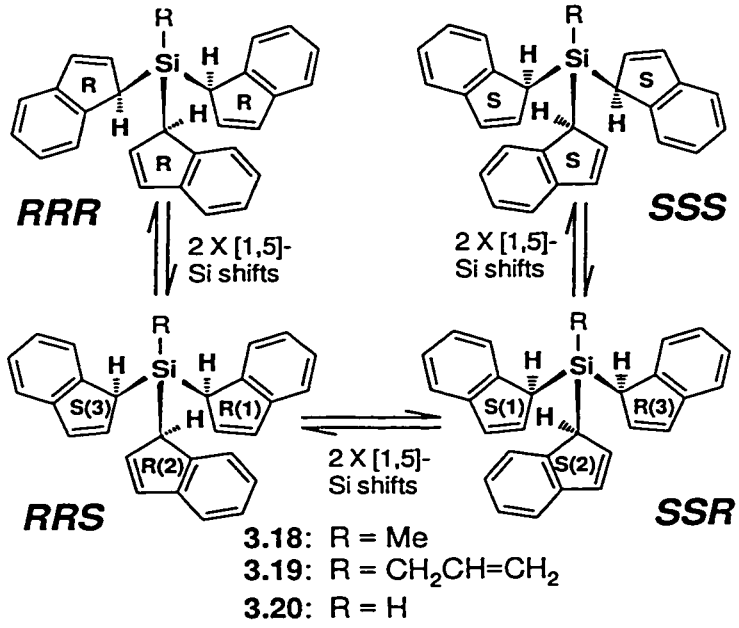

Scheme 3.4: *Interconversion of the eight different indenyl ring environments in the RRR, RRS, SSR and SSS isomers of tris(σ-indenyl)silanes.*

The synthetic protocol described above generates a given tris(σ-indenyl)silane as the anticipated statistical (1:3) mixture of interconverting *RRR/SSS* and *RRS/SSR* diastereomers (Scheme 3.4); the "*R*" and "*S*" labels refer to the absolute configurations of the C(1) carbons in these molecules. The formation of such an isomeric mixture is evidenced by the ^{29}Si NMR spectrum of tris(σ-indenyl)methylsilane, **3.18**, which contains two peaks in an approximate 1:3 intensity ratio. The 500 MHz ^{1}H NMR spectrum of this compound shows four clearly separated signals for each of the H(1), H(2) and H(3) sites. The connectivity of the three C_5 ring hydrogen atoms for each of the four individual types of indenyl fragments in **3.18** was easily ascertained by careful scrutiny of the ^{1}H-^{1}H COSY spectrum. With these ^{1}H NMR assignments in hand, the C(1), C(2) and C(3) carbon signals

within each indenyl environment in **3.18** were assigned based on data obtained from ^{1}H-^{13}C shift-correlated experiments (HSQC and HMBC).

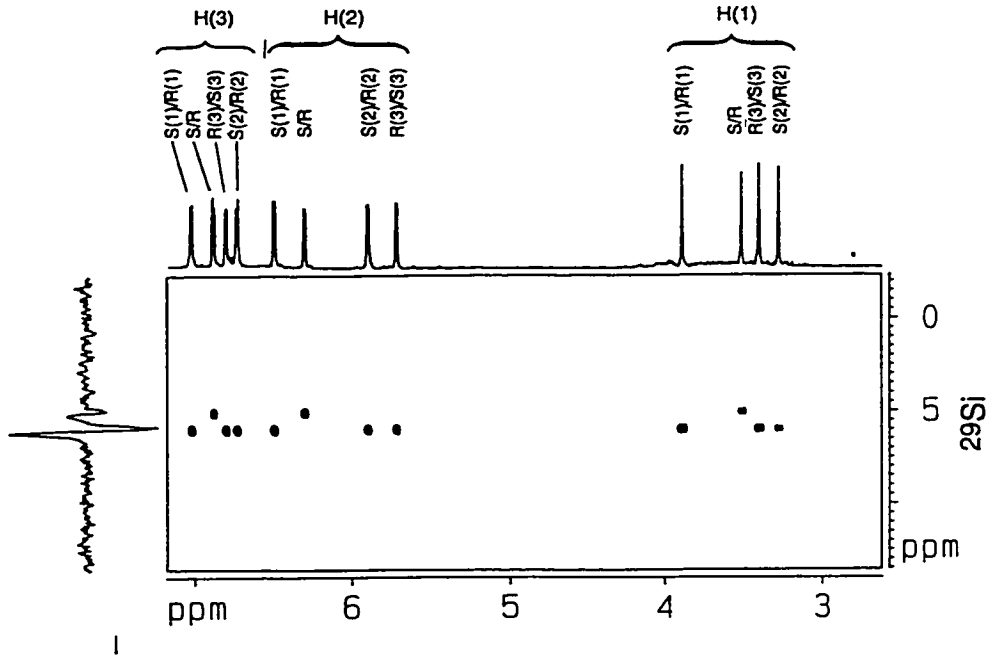

Figure 3.1: *^{1}H-^{29}Si shift-correlated NMR spectrum of tris(σ-indenyl)methylsilane,* ***3.18.***

At this point in the NMR spectroscopic analysis of **3.18**, it was necessary to identify the set of indenyl ^{1}H NMR resonances attributable to the *RRR/SSS* isomers, in addition to the three indenyl environments in the *RRS/SSR* molecules. This was readily accomplished *via* analysis of the data obtained from a ^{1}H-^{29}Si shift-correlated experiment, as illustrated in Figure 3.1; the ^{29}Si resonance at 5.04 ppm (intensity 1) couples to only one proton in each of the H(1), H(2) and H(3) environments, while its counterpart at 5.96 ppm (intensity 3) correlates to the other three hydrogens in each set. These data are entirely consistent with the stereochemical features of the $(\eta^{1}$-indenyl$)_3$SnR systems originally discussed by Stobart *et al.* In studying this class of complexes, these workers recognized that while the indenyl ring environments in the *RRR/SSS* isomers are homotopic, three unique ring environments are present in the *RRS/SSR* enantiomorphs. Qualitative experimental support for these ideas was obtained from studies involving *n*-butyltris(η^{1}-indenyl)tin, **3.2**, for which the expected 1:3 statistical ratio of *RRR/SSS* and *RRS/SSR* stereoisomers was observed. Ideally, **3.2** should exhibit

four equally intense ^{1}H and ^{13}C NMR resonances for each of the C(1), C(2) and C(3) positions; although four peaks are discernible for the C(1) and H(1) sites, with the limited magnetic fields accessible at that time, Stobart *et al.* were unable to provide detailed spectral assignments.

The other tris(σ-indenyl)silanes, **3.19** and **3.20**, exhibited ^{1}H ^{13}C and ^{29}Si NMR spectral features which paralleled those observed for the methyl-substituted compound, **3.18**, and were characterized in a similar way by use of a combination of multidimensional and multinuclear NMR techniques; a portion of the ^{1}H-^{29}Si shift correlated spectrum of **3.19** is presented as Figure 3.2.[163] Correlation between the ^{29}Si resonance at 2.1 ppm (**3.19-*RRR/SSS***) and a single proton in each of the H(1), H(2) and H(3) regions is readily observable, while the ^{29}Si resonance at 3.4 ppm (**3.19-*RRS/SSR***) shows coupling to the other hydrogens in each set.

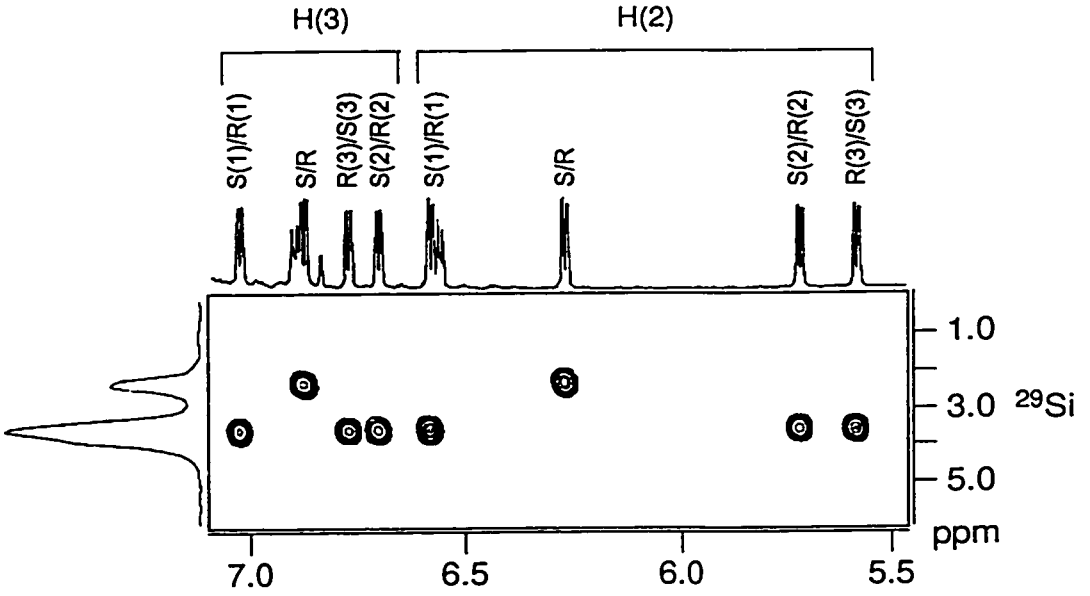

Figure 3.2: *^{1}H-^{29}Si shift-correlated NMR spectrum of tris(σ-indenyl)allylsilane,* ***3.19.***

To complement these NMR spectroscopic studies, a crystalline sample of **3.20** was also characterized by use of X-ray diffraction techniques. The molecular structure of **3.20-*SSR*** appears as Figure 3.3 and represents the first crystallographically characterized tris(σ-indenyl)silane; important crystallographic data and metrical parameters are provided in the Appendix. In the crystalline lattice, **3.20-*SSR*** and **3.20-*RRS*** pack as two crystallographically

independent molecules per asymmetric unit, between which no unusually close intermolecular contacts exist. Given the structural similarity between these two enantiomers, commentary on specific geometric details is provided for only one of the independent molecules (**3.20-*SSR***). The molecular geometry of **3.20-*SSR*** contains no unusual features and can be compared to other crystallographically-characterized sp^3-bonded main group indenyl complexes.[113,117,118,158,142] Importantly, the crystal structure of **3.20-*SSR*** is concordant with the NMR spectral data presented above, in that all three of the indenyl fragments are connected to the silicon center through sp^3-hybridized C(1) carbons. The silicon environment in this compound deviates only modestly from ideal tetrahedral geometry and is characterized by normal Si-C bond lengths, while the carbocyclic indenyl fragments are essentially planar and possess distinct allylic (C(1)-C(2)=C(3), etc.) linkages.

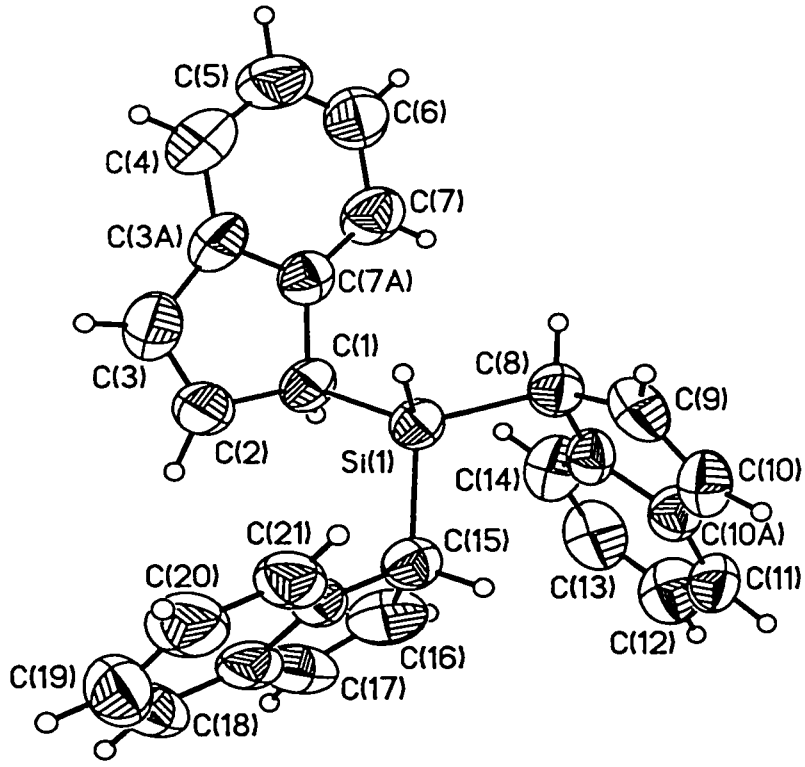

Figure 3.3: *The X-ray structure of one of the two independent molecules of* ***3.20****, showing the atomic numbering scheme. Thermal ellipsoids are shown at the 50% probability level. The absolute configurations at C(1), C(8) and C(15) are S, S and R, respectively.*

3.2.2 Stereochemical Considerations and Dynamic NMR Studies

Successive [1,5] suprafacial silatropic shifts interconvert the C(1) and C(3) positions within an indenyl moiety, while inverting the configuration of the stereocenter within the C_5 ring. As previously described in Section 3.1.1; this phenomenon accounts for the reported interconversion of the *meso*- and *d,l*-isomers of bis(σ-indenyl)dimethylsilane, **3.6** (Scheme 3.2). As pictorially represented in Scheme 3.4, successive [1,5] silicon shifts about the periphery of a single indenyl moiety in a given tris(σ-indenyl)silane would analogously invert the chirality of one indenyl ring and take a molecule of configuration *RRR* into its *RRS* stereoisomer. This rearrangement process takes the three equivalent H(2) protons of the *RRR* isomer (in which all three indenyl ring environments can be designated **R**) and moves them into three new indenyl ring environments, labeled **R(1)**, **R(2)** and **S(3)**. A second ring inversion interconverts the enantiomorphic *RRS* and *RSS* molecules; this takes the indenyl rings labeled **R(1)**, **R(2)** and **S(3)** into **R(3)**, **S(2)** and **S(1)** environments, respectively. Finally, the third step regenerates a homotopic molecule, *SSS*, in which all three indenyl rings environments are identically **S**. These labels (**R**, **S(2)**, etc.) correspond to the configuration of the C(1) stereocenter in the particular indenyl ring environment; *RRS* refers to one of four diastereomeric (1-indenyl)$_3$SiR molecules.

Figure 3.4 depicts a cube onto which can be mapped all the permitted exchange pathways for the H(2) environments in molecules **3.18**, **3.19** and **3.20**. Each exchange along a cube edge requires two successive [1,5] shifts of an R(indenyl)$_2$Si moiety across the surface of the remaining indenyl ring; the net result is equivalent to an *overall* [1,3] shift. It is noteworthy that (i) the **R(1)** to **S(1)** and **R(2)** to **S(2)** transformations are invisible since they involve isochronous sites, (ii) the **R(1)** to **R(2)** or **S(1)** to **S(2)** exchanges require that one traverse two adjacent edges of the cube (*i.e.* the configurational inversion of two indenyl rings), and (iii) the interconversion of the **R** and **S** environments (corresponding to transformation of *RRR* into *SSS*) inevitably must proceed *via* [1,5] silicon shifts about the periphery of all three indenyl fragments. A cube has previously been utilized

by Mislow[164] in depicting the stereochemical consequences of correlated rotation in propeller-shaped triarylboranes.

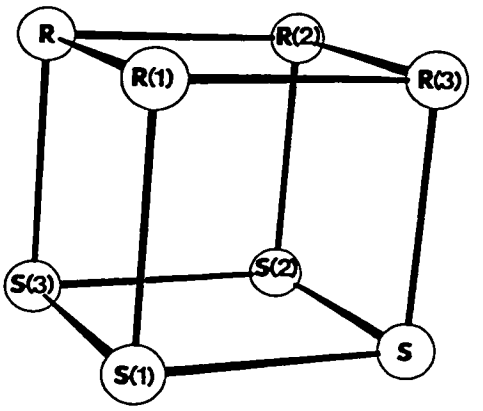

Figure 3.4: *Cube vertices represent the eight indenyl H(2) environments in a tris(σ-indenyl)silane, while the edges map out the exchange pathways.*

Unlike the previously studied tris(η^1-indenyl)tin system, **3.2**, where the barrier associated with tin migrations is rather low and peak coalescence is evident even at room temperature, the activation energies for [1,5] silicon shifts in tris(η^1-indenyl)silanes are sufficiently high that exchange pathways are most conveniently detected by 2D-EXSY experiments. Quasi-fluxional behavior in compounds **3.18** to **3.20** is readily detectable at temperatures in excess of 100 °C, and Figure 3.5 shows the exchange pattern for the indenyl protons at the H(2) position in **3.18**. In keeping with the mechanism depicted graphically in Figure 3.4, it is evident that the unique **R/S** environment (previously identified from the ^{1}H-^{29}Si spectrum, Figure 3.1) exchanges directly with the other three sites. Similarly, one other resonance shows off-diagonal correlations with the other three H(2) peaks; this can be assigned to the H(2) atom in the **R(3)/S(3)** indenyl environment. It is apparent that there is no direct interconversion of the two remaining H(2) sites, and these must be situated in the **R(1)/S(1)** and **R(2)/S(2)** indenyl rings. The 2D-EXSY spectrum shown in Figure 3.5 was acquired with a relatively long delay time of 1.5 s, at which point the development of small cross-peaks for the **R(1)** to **R(2)** interconversion in **3.18** becomes apparent. This corresponds to sequential configurational inversion of two indenyl rings (or traversal of two adjacent edges of the cube shown in Figure 3.4).

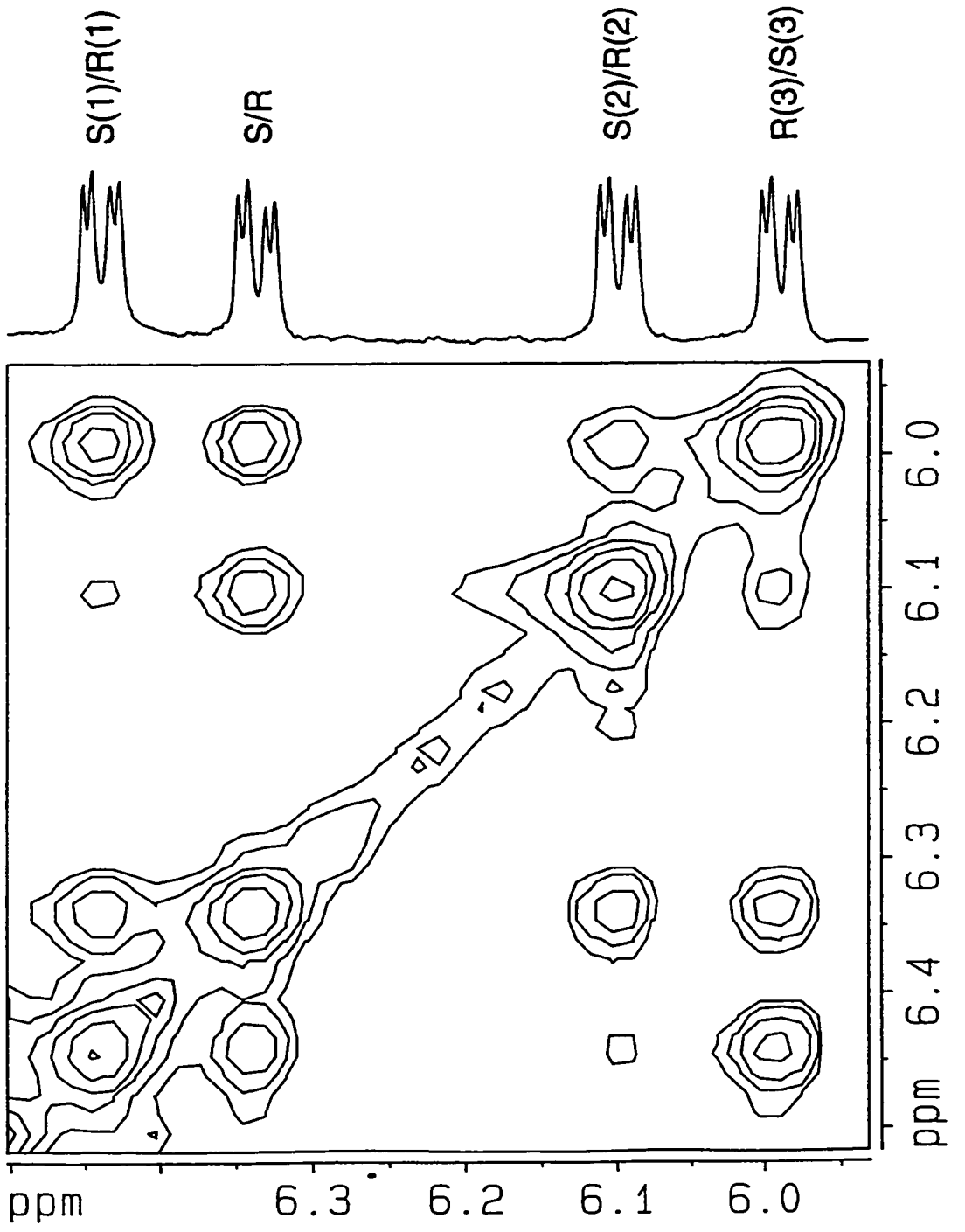

Figure 3.5: *A portion of the ^{1}H-^{1}H EXSY spectrum of* ***3.18*** *acquired at 105 °C. The large cross-peaks correlate the indenyl H(2) environments that undergo direct exchange.*

The scenario for the exchange between the various H(1) and H(3) environments is slightly more complicated. Two successive [1,5] silicon shifts within an indenyl moiety not only bring about inversion of the configuration at the C(1) center of the ring, but they also interconvert the H(1) and H(3) sites. Specifically, the three homotopic H(1)-**R** protons in the *RRR* isomer become H(1)-**R(1)**, H(1)-**R(2)**, and H(3)-**S(3')** in the *RRS* molecule. That is, two of the three sp^3-carbons retain their absolute configuration but now find themselves in magnetically different environments, as do their attached hydrogens; after the departure of the silyl group, the third carbon is now sp^2-hybridized and occupies the C(3) site *in an indenyl ring whose configuration has been inverted.* This set of exchange pathways is conveniently represented by a hypercube[165] (Figure 3.6) in which the *inner* cube corresponds to the eight sp^3-bonded H(1) environments (labeled **S**, **R(3)**, etc.); the vinylic H(3) protons are mapped onto the *outer* cube and are designated **R'**, **S(1')**, etc. The utility of the hypercube as a multi-dimensional graph was demonstrated by Gust and Patton[166] in their study of the dynamic stereochemistry of hexaarylbenzenes.

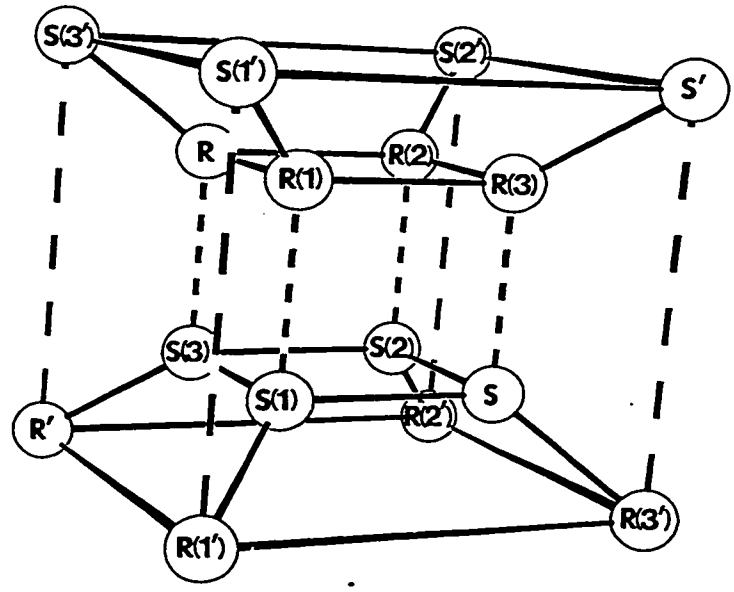

Figure 3.6: *The vertices of the inner cube represent the eight sp^3-bonded indenyl H(1) environments, while those of the outer cube correspond to the eight sp^2-bonded indenyl H(3) environments. Edges connected by solid lines represent observed exchange processes, while dashed lines connect sites that do not interconvert.*

It is evident that direct interchange between the inner and outer cubes in Figure 3.6 must occur with inversion of configuration of an indenyl ring environment. Moreover, the three-step interconversion of the *RRR* and *SSS* enantiomers requires that all three sp^3-bonded H(1) protons in the former molecule occupy vinylic H(3) environments in the latter isomer. The net result is that the **R** and **S'** cube vertices are connected, but the **R** to **R'** and **S** to **S'** transformations are not possible. The hypercube depicted in Figure 3.6 shows that there are two non-interconverting manifolds into which enantiomorphic environments are separated. In the tris(σ-indenyl)silanes, **3.18** to **3.20**, only four H(1) and four H(3) resonances are observed in each case. However, if the alkyl group in any one of these molecules were to be replaced by a chiral substituent, *e.g.* menthyl, then one should see a total of sixteen resonances for the H(1) and H(3) environments, but the 2D-EXSY spectrum should exhibit off-diagonal correlations only within the two groups of eight.

The experimental ^{1}H-^{1}H EXSY data for exchange between the H(1) and H(3) environments in the tris(σ-indenyl)silane, **3.18**, are shown in Figure 3.7 and confirm in all respects the mechanistic model represented graphically by the hypercube in Figure 3.6. Thus, each H(1) proton shows clear and unambiguous off-diagonal correlations with two other H(1) environments and with a single H(3) site. The central portion of Figure 3.7 (between 6.50 and 5.75 ppm) shows exchange only between H(2) sites; Figure 3.5 presents an enlarged view of this section.

The statistically expected 3:1 ratio of *RRS/RSS* to *RRR/SSS* molecules found for each of **3.18**, **3.19** and **3.20** suggests that the free energies of each of these pairs of enantiomers are essentially identical, but this does not provide data on the relative exchange rates between the four isomers. That is, the rate of interconversion between enantiomers (*RRS* to *RSS*) is not necessarily the same as between diastereomers (*RRR* to *RRS*, or *SSS* to *SSR*). However, it is evident from the foregoing mechanistic analysis that it is possible to monitor both processes simultaneously. For example, one could evaluate the rates of interconversion among the various H(2) environments in the study of these compounds; the transition **R(1)** to **R** probes the *RRS* to *RRR* process, while **R(1)** to **R(3)** measures the *RRS* to *RSS* isomerization.

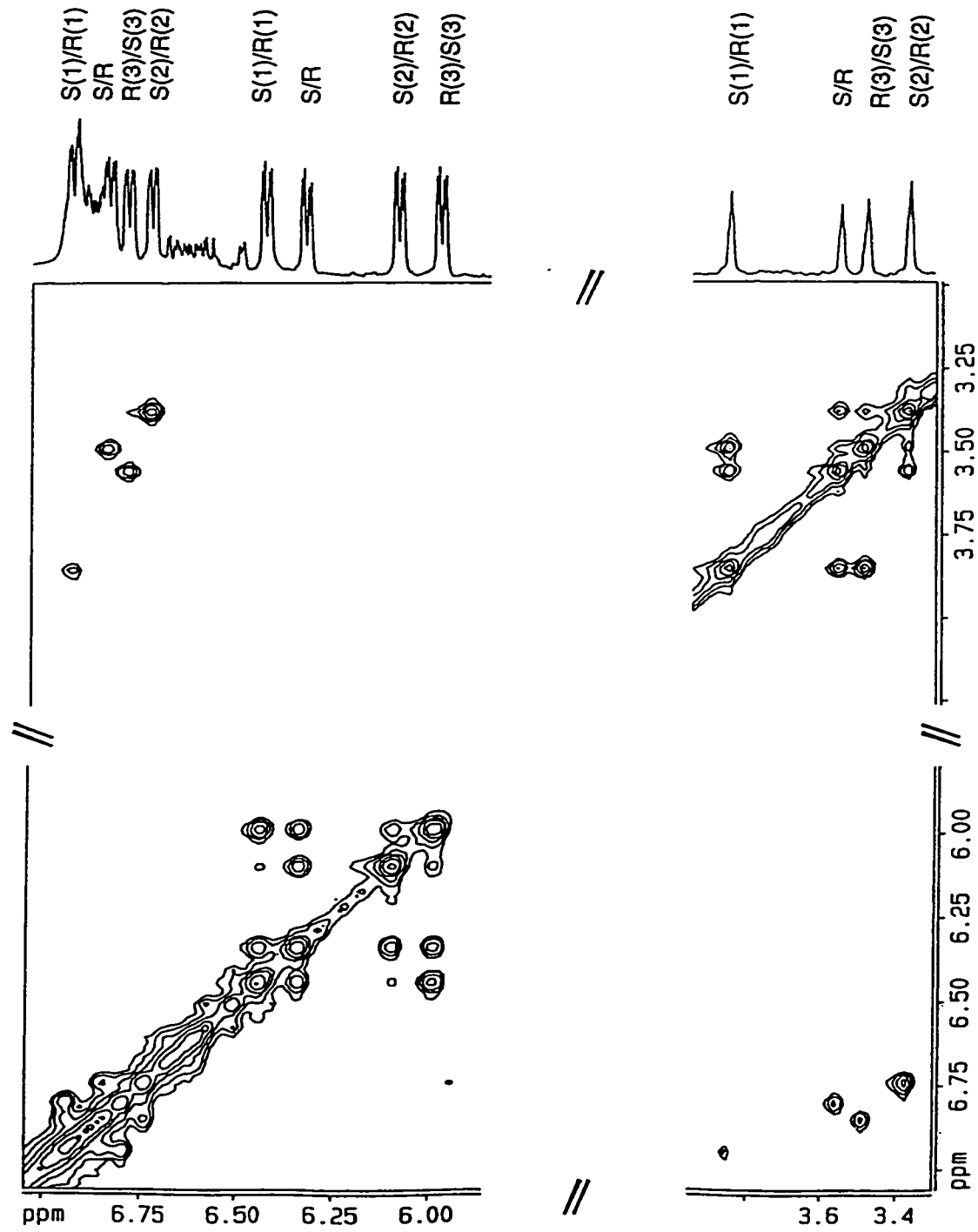

Figure 3.7: *Sections of the 2D-EXSY spectrum of tris(σ-indenyl)methylsilane,* ***3.18****, showing exchange within H(1) and H(3) environments, and also exchange between H(1) and H(3) sites. Note how H(2) peaks exchange only among themselves. Data were acquired at 105 °C in toluene-d_8.*

The efficacy of the single selective inversion NMR methodology in the acquisition of rate data for molecular processes which have relatively high activation energies was described in Section 1.2.2, and demonstrated for the iron complex, **1.9**, in Chapter Two. Indeed, although 2D-EXSY methods are excellent for qualitative mechanistic studies, selective inversions provide quantitative rate data much more efficiently. In separate experiments, the H(2)-**R(1)** resonance in **3.18**, **3.19** or **3.20** was selectively inverted, and the rates of recovery of this nucleus and the H(2)-**R** and H(2)-**R(3)** sites were monitored. For all three compounds, the temperature dependence of these rate constants yielded identical activation energies for each of the two isomerization pathways, suggesting that the configuration at the silicon atom has little influence on the migration process; the barriers ($\Delta G^{\ddagger}$) to silicon shifts in **3.18**, **3.19** and **3.20** were estimated to be 24 ± 0.5 kcal mol^{-1}, 25 ± 2 kcal mol^{-1} and 24 ± 1 kcal mol^{-1}, respectively. These free energies of activation are in excellent accord with values previously reported for [1,5] silicon shifts in simple indenylsilanes, showing that no unusual steric effects come into play in these poly(σ-indenyl) systems.

3.2.3 Probing for Isoindene Intermediates

Ashe[122] has claimed that the intermediate trimethylsilylisoindene can be trapped by tetracyanoethylene (TCNE) as its Diels-Alder adduct, **1.134**, for which spectroscopic data were reported (Section 1.4.4.2). However, since it is known that indene itself undergoes [2+2] cycloadditions and/or "ene" reactions with electron-poor double-bonded systems,[167,168] the identity of **1.134** as the Diels-Alder adduct was confirmed by means of a single crystal X-ray diffraction experiment. The product is indeed the Diels-Alder adduct described by Ashe and the resulting structure appears as Figure 3.8, while relevant crystallographic data and metrical parameters are provided in the Appendix. It is apparent that TCNE approaches the less hindered face of the silicon-substituted isoindene such that the bulky trimethylsilyl substituent lies directly over the aromatic ring in **1.134**; a similar *anti* geometry was also found in iron cycloadduct, **2.2**. In comparison with other structurally characterized benzannulated norbornene systems,[169,170] the C(1)-C(6) and C(4)-C(5) bonds (1.582(8) Å and 1.593(8) Å, respectively) are rather long; these linkages are the ones made in the Diels-Alder

reaction and their bond distances suggest that they are relatively weak. The even longer C(5)-C(6) bond (1.608(8) Å) is typical for such a TCNE Diels-Alder adduct,[171] and is identical to the distance found in the iron-functionalized benzonorbornyl compound, **2.2** (1.613(5) Å).[149]

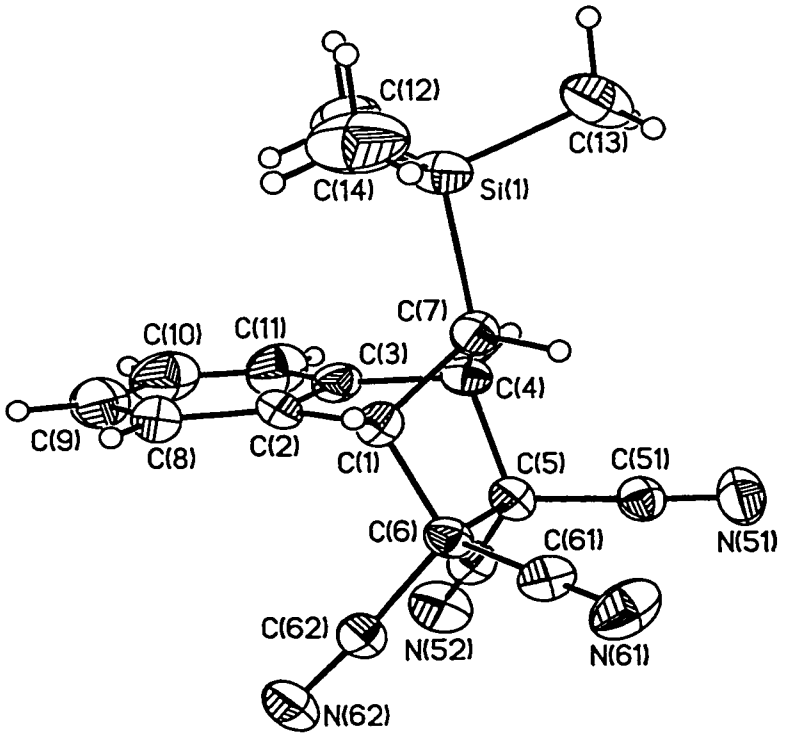

Figure 3.8: *The crystallographically determined structure of the cycloaddition product involving trimethylsilyl-substituted isoindene and TCNE,* ***1.134****, shown with 30% thermal ellipsoids.*

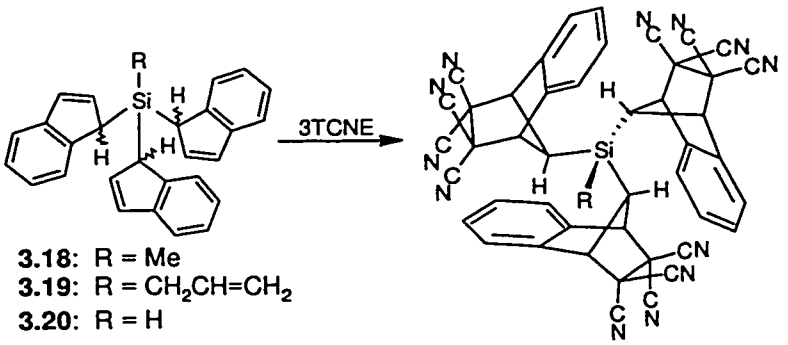

3.18: R = Me
3.19: R = $CH_2CH{=}CH_2$
3.20: R = H

3.21: R = Me
3.22: R = $CH_2CH{=}CH_2$
3.23: R = H

Scheme 3.5: *The triple Diels-Alder reactions of tris(σ-indenyl)silanes with tetracyanoethylene.*

With the authenticity of the cycloadduct, **1.134**, clearly established, attempts were made to demonstrate that the fluxional behavior of tris(σ-indenyl)silanes can be rationalized in terms of successive [1,5] silicon shifts, *via* the corresponding isoindene intermediates. Treatment of either **3.18**, **3.19** or **3.20** with three equivalents of TCNE allowed for the sequential interception of the transient isoindenes *in situ*. Gratifyingly, the products isolated in all three reactions yielded NMR spectroscopic and mass spectrometric data consistent with the formation of the corresponding triple Diels-Alder cycloadduct (**3.21** to **3.23**, respectively) as in Scheme 3.5.

In the absence of reported structural data for tris(benzonorbornyl)silanes, definitive crystallographic characterization was sought for this class of molecules. Upon cooling an acetonitrile solution of **3.22**, crystals suitable for single crystal X-ray studies were obtained; the crystal structure appears in Figure 3.9 and selected metrical parameters are collected in the Appendix. The X-ray structure of **3.22** serves to unequivocally confirm its identity as the desired triple cycloadduct, and reveals that in all three cases the dieneophilic attack by TCNE on the silicon-substituted isoindene occurs on the less-hindered face, opposite to that occupied by the $R_2Si(CH_2CH{=}CH_2)$ unit. Overall, the geometric features of the individual benzonorbornyl units found in the crystal structure of **3.22** are consistent with those observed for the monoadduct, **1.134**. So as to relieve unfavorable steric interactions, the bulky benzonorbornyl units in **3.22** rotate with respect to one another. Torsion angles of 156.4, 109.0, and 69.2 degrees (defined by H-C(*n*)-Si(1)-CH_2Si, where n = 7, 27, 47) are observed in this compound; for comparison, a structure possessing C_{3v} symmetry would exhibit torsion angles of either 0 or 180 degrees. It is also apparent from the structure of **3.22** that the orientation of the benzonorbornyl units places the allyl methylene group directly over an arene ring (containing C(8)-C(11)); such a scenario should bring about noticeable aromatic ring current effects on these allyl protons. This prediction is verified by the marked shielding of nearly 1.3 ppm for the methylene protons in **3.22**, relative to the tris(σ-indenyl) precursor, **3.19**; a similar result was also observed on converting **3.18** into the cycloadduct, **3.21**

($\Delta\delta$ ~ -1.9 ppm). In the case of this latter molecule, ring current calculations were carried out using the program *LARC*,[172] which employs the Waugh-Fessenden-Johnson-Bovey ring current model.[173-175] Assuming that the inherent chemical shift of the silicon methyl hydrogens in **3.21** is similar to that observed for tetramethylsilane, then the experimentally observed ^{1}H NMR resonance for the methyl group in **3.21** (-1.88 ppm) seems eminently reasonable, given the calculated incremental shielding of ~2.2 ppm for the methyl hydrogen atoms in **3.21**, due to the three adjacent benzonorbornyl arene fragments.

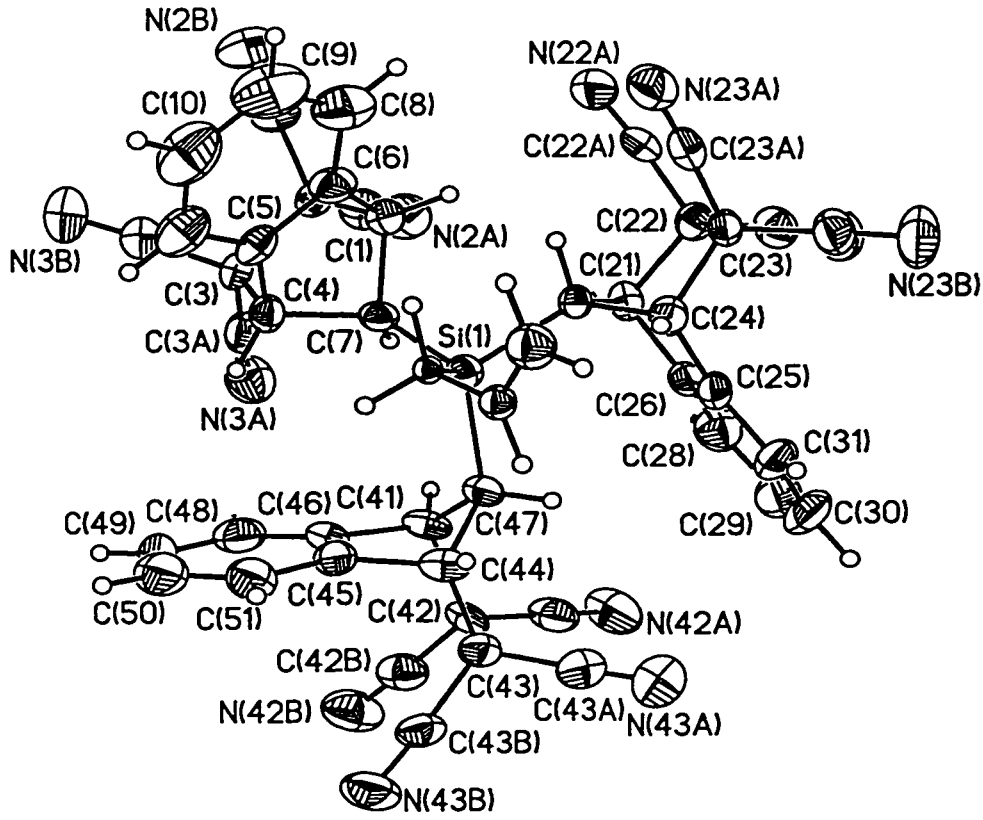

Figure 3.9: *The X-ray structure of **3.22**, showing the atomic numbering scheme. Thermal ellipsoids are shown at the 40% probability level.*

In combination, these spectroscopic and reactivity studies provide considerable insight into the mechanism of diastereomerization *via* silicon migrations in tris(σ-indenyl)silanes. Firstly, the suprafacial [1,5] shift character of the migrations has been abundantly demonstrated; the 2D-EXSY data reveal an *overall* C(1) to C(3) chemical exchange phenomenon, while the Diels-Alder trapping

of isoindenes supports the viability of such intermediates in a [1,5] shift process. Secondly, the sequential nature of the inversion of configuration of the indenyl rings mandates that the $(indenyl)_2SiR$ fragment in compounds such as **3.18** to **3.20**, retain its stereochemical integrity during the course of the migration; this result is in accord with Stobart's study involving the chiral indenylstannane, **1.157**.[134] Thirdly, [1,5] silatropic shifts over the three indenyl units are uncorrelated, since only those sites directly connected by edges of the cube in Figure 3.4 (or the hypercube in Figure 3.6) exhibit large cross-peaks in the 2D-EXSY spectra. If migrations were to occur over two or more rings simultaneously, one would see direct exchange across the cube diagonals.

3.2.4 Silicon-Based Reactivity Studies

In an effort to survey the utility of the tris(σ-indenyl)silanes and their related tris(benzonorbornyl) complexes as synthetic precursors to other novel organosilicon complexes, a preliminary study examining the reactivity of these species was undertaken. Indeed, it was postulated that the steric demands of the indenyl and benzonorbornyl groups may confer interesting chemical properties to these compounds. Although the presence of a third indenyl fragment in tris(σ-indenyl)silanes provides an opportunity for the preparation of polymetallic *ansa*-metallocene complexes, the study of such compounds falls outside of the scope of this thesis work (see Section 6.4).

3.2.4.1 Hydrolysis and Hydrosilylation Reactions

The hydrolytic conversion of a hydrosilane to the corresponding silanol, with concomitant loss of dihydrogen, is a well-defined reaction in organosilicon chemistry. Starting from the tris(benzonorbornyl)silane, **3.23**, an attempt was made to generate the silanol, **3.24**, by stirring the hydrosilane in wet acetone (Scheme 3.6). The transformation of **3.23** into the desired product was readily monitored by use of ^1H NMR. For **3.23**, the silicon hydride resonance appears as a quartet, due to coupling with the three equivalent H(7) methine protons, whereas the hydroxyl group in **3.24** gives rise to a singlet at higher frequency; after 24 h under ambient conditions, quantitative formation of the tris(benzonorbornyl)silanol was observed. The triple adduct, **3.24**, was also characterized in the solid state by use of single crystal X-ray diffraction techniques as the

double acetone solvate; the structure of **3.24** appears as Figure 3.10, while crystallographic data and metrical parameters are collected in the Appendix.

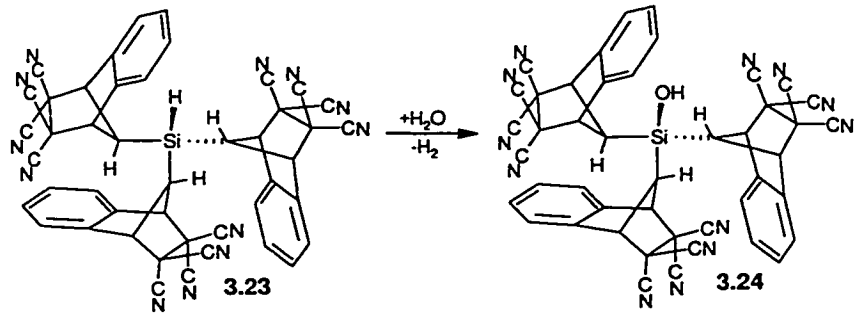

Scheme 3.6: *Conversion of the silane,* ***3.23****, into the tris(benzonorbornyl)silanol,* ***3.24****.*

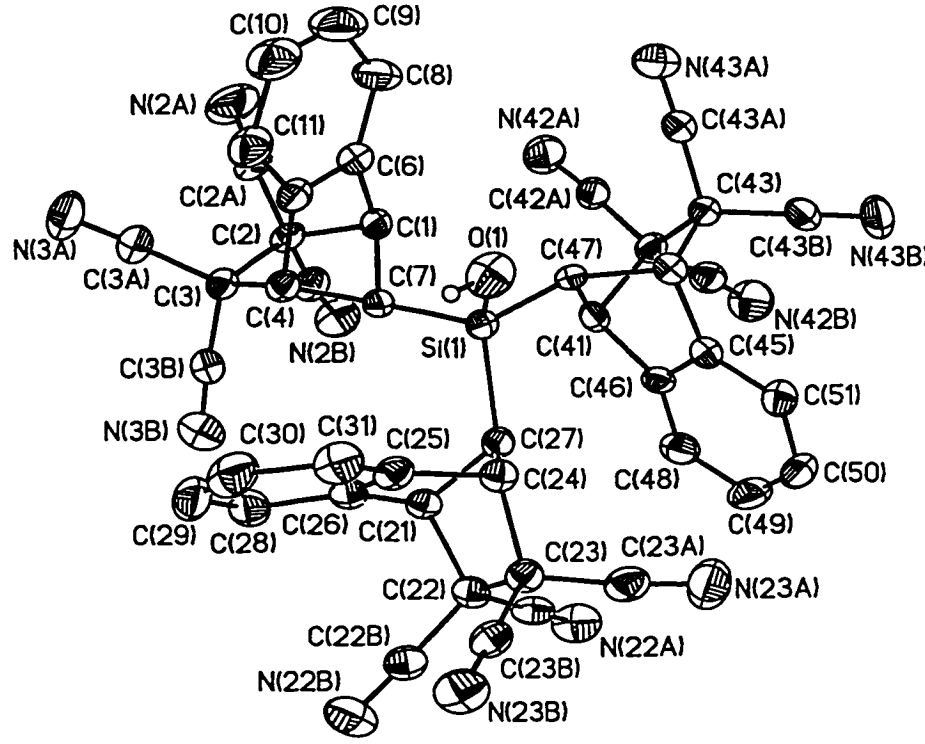

Figure 3.10: *X-ray structure of* ***3.24****, showing the atomic numbering scheme. Thermal ellipsoids are shown at the 40% probability level. The two solvated acetone molecules and all alkyl-hydrogen atoms have been omitted for clarity.*

The X-ray structure of **3.24** serves to unequivocally confirm its identity as the product derived from the hydrolysis of **3.23**. The silanol possesses structural features which mirror those observed for the allylsilane, **3.22** (Figure 3.9), including *anti*-oriented silyl and dienophilic

fragments. As noted previously for **3.22**, the non-uniform orientation of the benzonorbornyl units in **3.24** leads to the observation of C_1 molecular symmetry for this compound; if the position of the hydroxyl hydrogen atom is ignored, **3.24** could, in principle, adopt a geometry with C_3 or even C_{3v} symmetry. It is noteworthy that, despite the sterically demanding nature of the substituents in **3.22** and **3.24**, and the apparent preference for an asymmetric C_1 geometry in the solid state, negligible NMR line broadening is observed for these compounds, even at -80 °C. Indeed, the simplicity of the ^1H and ^{13}C NMR spectra obtained from samples of **3.22** and **3.24** suggests a time-averaged C_{3v} molecular geometry in solution, resulting from rapid rotation about the Si-C(benzonorbornyl) bond.

Comparison of the benzonorbornyl torsion angles (H-C(*n*)-Si(1)-O(1), where $n = 7, 27, 47$) in **3.24** to those found in **3.22** reveals that in the solid state, the orientation of the ligands in these two compounds are strikingly similar (Figure 3.11); torsion angles of 157.1, 111.8 and 71.1 degrees in **3.24** are essentially identical to those previously noted for **3.22** (156.4, 109.0, and 69.2 degrees). The apparent duplication of the geometric features in **3.22** and **3.24** strongly suggests that this C_1 structural motif represents the energy minimum for tris(benzonorbornyl)silanes.

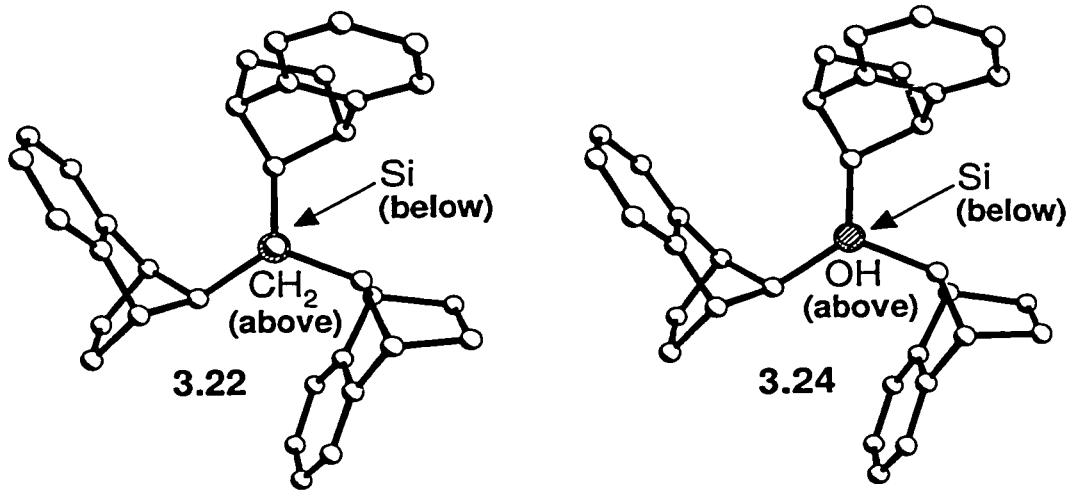

Figure 3.11: *Comparing the solid-state geometries of the crystallographically characterized tris(benzonorbornyl)silanes,* ***3.22*** *and* ***3.24****. Selected atoms have been omitted for clarity.*

In direct contrast to the successful conversion of **3.23** into **3.24**, when this methodology was employed using the indenylsilane, **3.20**, quantitative hydrolysis of the Si-C(1)indenyl bond, as opposed to the Si-H bond, was observed, evinced by the generation of indene (Scheme 3.7).

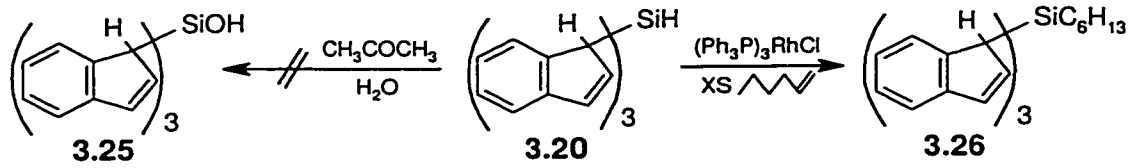

Scheme 3.7: *Hydrolysis and hydrosilylation reactions, involving* ***3.20.***

Alternatively, functionalization of tris(σ-indenyl)silane, **3.20**, and its triple Diels-Alder adduct, **3.23**, *via* hydrosilylation was also undertaken. In neat 1-hexene, and in the presence of Wilkinson's catalyst ($(Ph_3)_3RhCl$), **3.20** was converted to tris(1-indenyl)hexylsilane, **3.26**, in moderate yield (34%) (Scheme 3.7). Unfortunately, **3.23** did not participate in hydrosilylation reactions under similar experimental conditions, likely owing to unfavorable steric interactions between the bulky benzonorbornyl substituents and the ligands present on the rhodium catalyst.

3.2.4.2 Reactions Involving Electrophiles

Although *prima facie* the steric demands of the benzonorbornyl ligands in **3.22** and **3.24** would be expected to impede reactivity at the silicon center in these molecules, careful inspection of their crystal structures suggests that the allyl and hydroxyl moieties in these compounds should be accessible to incoming chemical reagents. As such, the reactivity of the tris(σ-indenyl)silanes, **3.19** and **3.20**, and the tris(benzonorbornyl)silanes, **3.22**, **3.23** and **3.24**, with electrophiles was examined. For the silanes and the silanol, such electrophilic reactions carried out in the presence of nucleophilic species are expected to proceed *via* direct abstraction of the hydride or the hydroxyl group, followed by rapid nucleophilic addition at the cationic silicon center. In the case of the allylsilanes, electrophilic attack initially occurs at the terminus of the allyl fragment, leading to a carbocationic intermediate which is stabilized by the presence of β-silyl group (Scheme 3.8). This intermediate is then prone to nucleophilic attack at silicon, leading to the generation of R_3SiNu and an olefinic compound, in an overall S_E2' process.

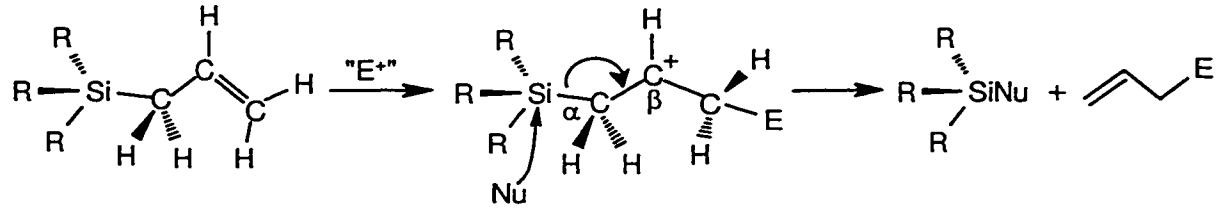

Scheme 3.8: *A generalized mechanistic representation of the reactions involving electrophiles and the allylsilanes* ***3.19*** *and* ***3.22.***

The NMR spectral data obtained immediately after adding either $HBF_4O(C_2H_5)_2$ or Ph_3CPF_6 to a CD_2Cl_2 solution of **3.19** or **3.20** suggested the formation of the anticipated product, tris(1-indenyl)fluorosilane, **3.27** (Scheme 3.9), based on the loss of ^{29}Si NMR signals attributable to the starting material and the appearance of two overlapping doublets at approximately 12.2 ppm ($^1J_{SiF}$ = 277 Hz, corresponding to the *RRR/SSS* and *RRS/SSR* isomers).[176,177] Due to the complexity of the ^1H and ^{13}C NMR spectra obtained from these mixtures, no conclusive chemical shift assignments could be made. Reexamination of these samples after approximately 24 h at -20 °C showed nearly complete deterioration of the ^{29}Si NMR peaks near 12 ppm, and the formation of a new, broad signal centered at -15.5 ppm. This new resonance was tentatively assigned to hexa(indenyl)disiloxane, **3.28**, which may have been generated by the presence of trace moisture in the NMR solvent; solutions of the fluorosilane, **3.27**, generated and stored under rigorously anhydrous conditions showed little decomposition, even after six weeks. Analogous reactions carried out using either **3.22**, **3.23** or **3.24** in CD_3CN similarly gave rise to the corresponding fluorosilane, **3.29**, which was unambiguously characterized by use of ^1H, ^{13}C, ^{19}F and ^{29}Si NMR spectroscopic techniques (Scheme 3.10).

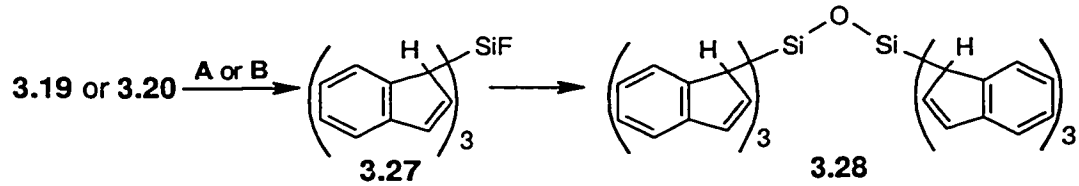

Scheme 3.9: *Reactions between tris(σ-indenyl)silanes (**3.19** or **3.20**) and electrophiles (H^+ or Ph_3C^+);* ***A*** *= HBF_4Et_2O and* ***B*** *= Ph_3CPF_6.*

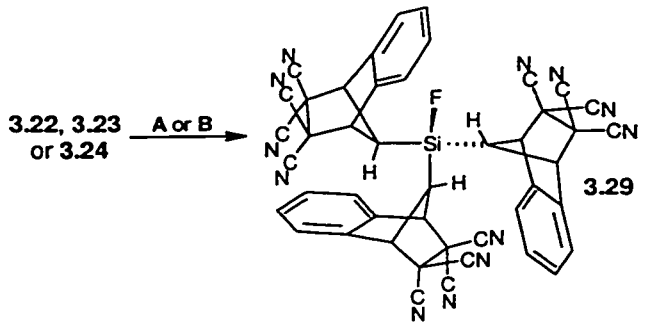

Scheme 3.10: *Reactions between tris(benzonorbornyl)silanes (**3.22**, **3.23** or **3.24**) and electrophiles (H^+ or Ph_3C^+); **A** = HBF_4Et_2O and **B** = Ph_3CPF_6.*

3.2.4.3 Precursors to Silylium Ions?

The generation of persistent carbocations, either in superacid media or as complexes with transition metals is a well-defined facet of the chemistry of carbon.[178,179] Conversely, the generation of long-lived "free" silicon cations, or silylium ions, in the condensed phase has eluded chemists for some time; the definitive characterization of such molecular species has been the source of considerable controversy.[180-182] Despite the fact that both gas-phase measurements and *ab initio* calculations show silylium ions to be more thermodynamically stable than their carbon counterparts, the kinetic accessibility of these three-coordinate cations make them difficult to generate in the condensed phase.

While a variety of experimental approaches have been employed in the attempt to generate persistent silylium ions in solution,[181] it is apparent that the use of a weakly nucleophilic combination of anion and solvent is required. Additionally, substituents on silicon must be judiciously chosen such that chemical transformations leading to the formation of the silicon cation are viable, while at the same time thwarting subsequent attack at the cationic center by nucleophiles. This invariably requires the use of a sterically loaded silane precursor, such as allyltrimesitylsilane, **3.30**, which was converted to the corresponding trimesitylsilylium cation, **3.31** by Lambert and Zhao[183] in 1997 (Scheme 3.11). Although no crystallographic data were provided, the ^{29}Si NMR chemical shift at ~ 225 ppm indicates that **3.31** possesses the most substantial silylium ion character of any known R_3Si^+ compound.

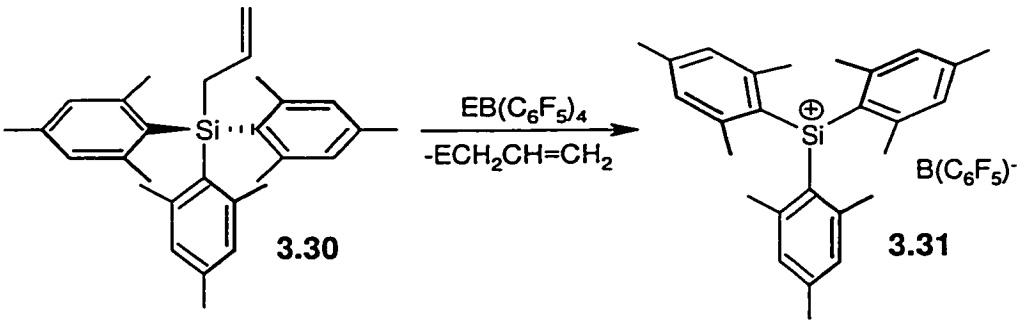

3.30 **3.31**

Scheme 3.11: *Generation of the "free" trimesitylsilylium cation,* ***3.31.***

Encouraged by the reactivity of **3.19**, **3.20** and **3.22** to **3.24** with HBF_4 and Ph_3CPF_6, the utility of these compounds as precursors to silylium ions was investigated. These reactions typically involved stirring stoichiometric amounts of the silane and the trityl salt of the "least-coordinating" anion, tetrakis(pentafluorophenyl)borate, in a minimally coordinating deuterated solvent at reduced temperature, followed by examination by use of ^{1}H, ^{13}C, and ^{29}Si NMR. Upon completion of these spectroscopic studies, the sample was then quenched with a hydride source and the resulting products evaluated by use of standard spectroscopic and analytical techniques. In all cases, addition of the electrophile to a solution containing the silane generated dark red mixtures, and in many cases, an insoluble precipitate. However, throughout the course of these experiments, no NMR spectroscopic evidence for the formation of either silylium ions or related carbocationic species, was obtained. Moreover, the resulting products generated after treatment with hydride exhibited broad NMR signals, and could not be identified with certainty. The deeply colored solutions and consumption of the starting materials in these reactions do imply that some reaction between the silane and the electrophile takes place. Given the severity of the conditions employed, it is plausible that electrophilic attack at the indenyl olefinic fragments (in **3.19** and **3.20**) or the nitrile units (in **3.22**, **3.23** and **3.24**) is preferred. Statistically, such a proposal is tenable in that the ratio of olefinic fragments or nitrile moieties to Si-*H* or Si-*CH_2=$CHCH_2$* units in these species is 3:1 and 12:1, respectively. Based on the poor quality of the NMR signals and the production of insoluble materials, it is possible that initial attack at the olefinic or nitrile moieties is

followed by either by decomposition or polymerization, leading to the complicated and ill-defined mixtures described herein.

3.3 Conclusions

A series of hitherto unknown tris(σ-indenyl)silanes was prepared and unambiguously characterized by use of a variety of techniques, including NMR spectroscopy and X-ray crystallography.[162,163] The quasi-fluxional nature of these compounds was qualitatively probed by use of 2D-EXSY NMR, and quantitatively evaluated by using single selective inversion NMR techniques. The barrier ($\Delta G^{\ddagger}$) to [1,5] silicon shifts in these compounds is approximately 24 kcal mol^{-1}, which is in agreement with values previously reported for similar silicon shifts in other indenylsilanes. Evidence for the intermediacy of isoindenes generated during these migratory processes was gained through Diels-Alder trapping reactions involving tetracyanoethylene. For each of the tris(σ-indenyl)silanes examined, the corresponding triple Diels-Alder adduct was isolated and characterized by use of standard physical and spectroscopic techniques; in the case of the adducts derived from tris(σ-indenyl)allylsilane, and the isoindene generated from trimethylsilylindene, data obtained from X-ray crystallographic studies verified the identity of the products. Although these tris(σ-indenyl)silanes and tris(benzonorbornyl)silanes proved not to be suitable precursors to silylium ions, preliminary reactivity studies suggest that, despite the bulky nature of the substituents in these molecules, the silicon center can still participate in chemical transformations.

CHAPTER FOUR

Probing the Factors Which Affect Silicon Migrations in Indenylsilanes

4.1 Introduction

Notwithstanding the variety of *ortho*-xylylene complexes that have been generated, trapped and characterized spectroscopically,[184] the analogous isoindenes have proven much more difficult to isolate and characterize. The very limited reports of "free" isoindenes often describe species that are generated photochemically, and which incorporate tetra-substitution designed to suppress any potential [1,5] sigmatropic migrations.[185-187] Inasmuch as isoindenes are synthetically attractive species, their propensity to isomerize to the corresponding indene presents a formidable obstacle to their use as reagents under standard experimental conditions. As a result, the formation and stabilization of isoindenes under thermally controlled conditions remains an important synthetic goal.

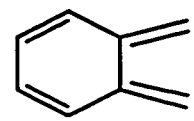

***o*-xylylene**

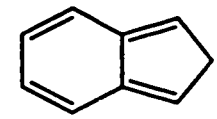

isoindene

Given that the thermally promoted isomerization of metalloindenes to the corresponding metalloisoindenes is facile, it is possible that careful modification of the indenyl framework may provide a route to stabilized isoindenes, under synthetically mild conditions. With the ultimate objective of enhancing the stability of metalloisoindenes so as to allow for their use in synthetic applications, attempts were made to examine the effect of incorporating carbon, silicon and transition metal substituents into the indenylsilane architecture, on the rate of [1,5] silicon migrations in these molecules. As a prelude to a discussion of this thesis work, an overview of the few published reports pertaining to such substituent effects in the heavier Group 14 indenyl complexes is provided.

Kinetic data obtained for [1,5] silicon shifts in a variety of simple (σ-indenyl)trialkylsilanes suggest that the nature of the alkyl substituents on silicon has little effect on the barrier to [1,5] silicon shifts ($\Delta G^{\ddagger}$ ~ 24 kcal mol^{-1}, see Table 4.1), a trend that has also been noted for related (σ-cyclopentadienyl)silanes (Section 1.3.4).[46] Indeed, this phenomenon was observed by Davison and Rakita,[123] who provided an early examination of substituent effects in indenyl compounds of silicon and tin. Variable-temperature NMR data acquired for (σ-C_9H_7)$SiMe_2Ph$, **1.114**, clearly indicated chemical exchange of the diastereotopic methyl groups at silicon; comparison of these data to calculated spectra permitted an estimation of the barrier for this process (E_a ~ 23 kcal mol^{-1}) which reveals that the incorporation of silyl-phenyl groups has little impact on the rate of [1,5] silicon shifts (Scheme 1.33). Permutation of the magnetically non-equivalent diastereotopic methyl environments in the related tin complex, **1.146**, was established by a series of ^{1}H NMR spectra obtained between -23 and 52 °C (Scheme 1.37). Kinetic data obtained from these spectroscopic studies provided an estimate of the activation energy associated with this quasi-fluxional process (~ 14 kcal mol^{-1}).

In the same report, Davison and Rakita also noted that the ^{1}H NMR spectrum of the methyl-substituted organosilicon compound, **4.1**, acquired at 160 °C, contained no significant amount of the related isomers, **4.3** and **4.5** (Scheme 4.1). The latter compound is the anticipated product of a [1,5] silicon shift process, and should be observable by use of NMR techniques, assuming that **4.1** and **4.5** are comparable in terms of thermodynamic stability. Attempts to study the dynamics of the symmetrically substituted species, **4.7**, were impeded due to difficulties in preparing this compound. In the related indenyltin series, compound **4.2** also showed no sign of isomerization to the corresponding *gem*-disubstituted isomer, **4.6**, or any other species. However, these workers were successful in preparing the dimethylindenylstannane, **4.8**, which was subsequently studied by use of dynamic NMR techniques. Compound **4.8** gave rise to ^{1}H NMR spectral features at -41 °C which were readily attributable to a σ-bonded dimethylindenyl group. As the temperature was raised, spectral changes typically associated with quasi-degenerate dynamic behavior ensued, which

included broadening and coalescence of the indenyl methyl resonances. The fast-exchange limiting spectrum for **4.8** was obtained at 84 °C, and included one sharp singlet in the indenyl methyl region, with appropriate tin satellites. The activation energy associated with tin migrations in this system (~ 14 kcal mol^{-1}) cannot be distinguished from the barriers obtained for unsubstituted indenylstannanes, suggesting that the incorporation of methyl groups at C(1) and C(3) does little to perturb the indene-isoindene equilibrium in this compound.

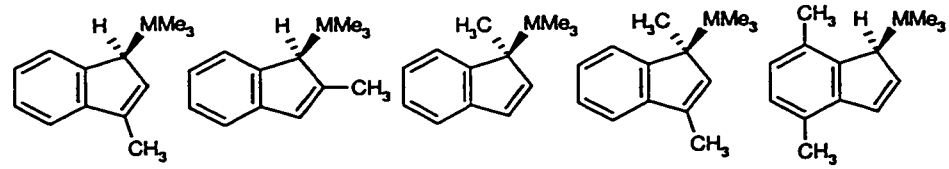

4.1: M = Si
4.2: M = Sn

4.3: M = Si
4.4: M = Sn

4.5: M = Si
4.6: M = Sn

4.7: M = Si
4.8: M = Sn

4.9: M = Si
4.10: M = Sn

Scheme 4.1: *Some alkyl-substituted indenylsilanes and indenylstannanes.*

The thermal isomerization of indenylsilanes has been examined in considerable detail. Davison and Rakita[123] reported that prolonged heating (180 °C) of solutions of the C(1) and C(2) disubstituted bis(trimethylsilyl)indene, **1.135**, led to the formation of a mixture containing **1.135**, and the 1,1- and 1,3-disubstituted species, **1.138** and **1.139**, presumably *via* [1,5] hydrogen shifts and the isoindene, **1.137** (Scheme 1.35). Spectroscopic identification of **1.138** and **1.139** was made possible by comparison with data obtained from a mixture (~ 1:1) of these compounds, rationally prepared *via* silylation of trimethylsilylindene, **1.109**. The kinetics of this class of rearrangements were subsequently examined in a series of publications authored by Rakita and Taylor.[128,188,189] Throughout the course of their studies, these workers prepared and characterized numerous new indenylsilanes (including **1.115** to **1.126** and **1.128** to **1.132**, Scheme 1.33), and found that the equilibrium distribution of C(1), C(2) and C(3) isomers, but not the activation parameters, were sensitive to the nature of the substituents at silicon.

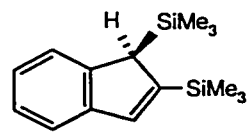

1.135

1.138

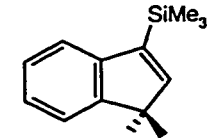

1.139

Andrews, Rakita and Taylor[190,191] examined the effect of methyl substitution at the indenyl C(2), C(4) and C(7) positions on the rate of [1,5] metallotropic shifts in indenylsilanes and indenylstannanes. Calculations (EHMO) carried out by these workers suggested that while the smallest π-electron density occurs at C(4) and C(7) of the indenyl radical, the electron density reaches a maximum at C(2); thus, alkyl substitution at C(4) and C(7) should stabilize the transition state species, whereas substitution at C(2) would have a destabilizing effect. In an attempt to test the validity of these results, the dynamics of the indenylsilanes, **4.3** and **4.9**, were studied by use of variable-temperature NMR spectroscopy. Using the coalescence temperature approximation method, the free energy of activation associated with [1,5] silicon shifts in **4.3** ($\Delta G^{\ddagger}$ ~ 26.5 kcal mol^{-1}) was found to be larger than for trimethylsilylindene, **1.109** ($\Delta G^{\ddagger}$ ~ 23.8 kcal mol^{-1}), while for **4.9** ($\Delta G^{\ddagger}$ ~ 21.8 kcal mol^{-1}) a lower barrier was calculated. Although there appears to be a real difference between the barriers associated with **4.3** and **4.9** ($\Delta\Delta G^{\ddagger}$ ~ 5 kcal mol^{-1}), it is unclear whether or not there is a statistically significant difference between **1.109** and either **4.3** or **4.9**. Analogously, variable-temperature NMR data obtained from samples of the indenylstannanes, **4.4** and **4.10** demonstrated that methyl substitution at C(2) results in a heightened barrier to metallotropic shifts ($\Delta G^{\ddagger}$ ~ 18.6 kcal mol^{-1}), while the introduction of C(4) and C(7) methyl groups has no statistically significant effect on this barrier ($\Delta G^{\ddagger}$ ~ 14.0 kcal mol^{-1}), relative to trimethylstannylindene, **1.145**. The authors recognize that steric factors, in addition to electronic stabilization, may contribute significantly to the observed free energy differential within each of the two sets of molecules.

In a series of papers spanning over twenty years, Jones and co-workers[192-194] have examined the factors that affect the migration of alkyl groups in substituted indenes. In addition to studying simple alkyl-substituted compounds, the dibenz[*e*,*g*]indene system (**4.11**) has been employed in order to reduce the barrier to alkyl group shifts by enhancing the aromatic character of the isoindene intermediate (Scheme 4.2). The capacity of the two fused benzo fragments in **4.11** to stabilize the corresponding isoindene is exemplified by the parent compound, cyclopenta[*l*]phenanthrene, **4.13**; a recent report by McGlinchey and co-workers included the NMR

spectroscopic and X-ray crystallographic characterization of the Diels-Alder adduct, **4.14**, a rare example of a thermally generated isoindene, **4.15**, trapped *in situ* by its progenitor, **4.13** (Scheme 4.3).[195]

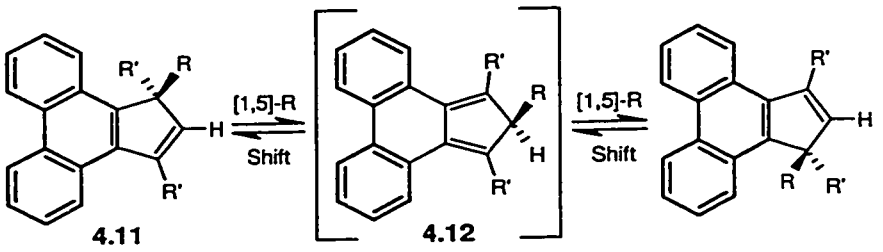

Scheme 4.2: *Suprafacial, sigmatropic alkyl group shifts in the substituted dibenz[e,g]indene system, **4.11**; " R' " is typically methyl or phenyl.*

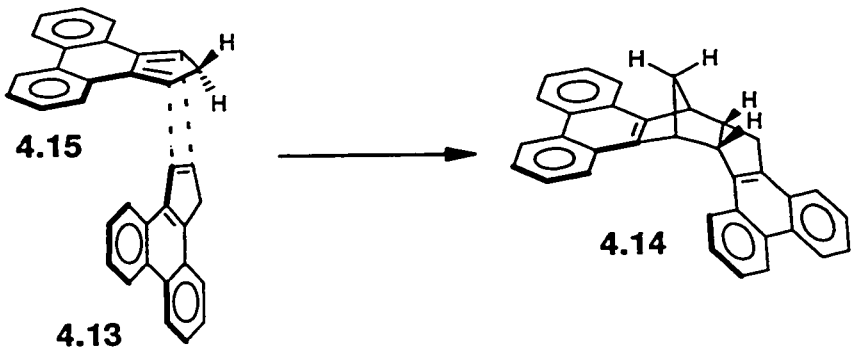

Scheme 4.3: *Diels-Alder cycloaddition involving **4.15** and **4.13**, leading to the adduct, **4.14**.*

In light of the seemingly insignificant effect that silicon substituents have on the rate of [1,5] silicon migrations in indenylsilanes, McGlinchey and co-workers[196,197] endeavored to utilize the approach of Jones and co-workers as a means of disturbing the indene-isoindene equilibrium. Computational studies carried out by these researchers at the semi-empirical level of theory suggested that the strategic incorporation of fused aromatic rings, as in **4.16** to **4.19**, should lead to a reduced barrier to [1,5] silatropic shifts in these systems, presumably attributable to the enhanced aromatic character of the transition state and/or intermediate species (Scheme 4.4). These predictions were validated by kinetic data obtained from ^{1}H-^{1}H EXSY and single selective inversion NMR experiments involving these compounds. The interconversion of **4.17** and **4.18** was found to

proceed with a $\Delta G^{\ddagger}$ value of approximately 21.9 kcal mol^{-1}, while the incorporation of two fused benzo rings onto the indenyl framework, as in **4.19**, lowered the barrier even further (17.6 kcal mol^{-1}).

Table 4.1. Experimentally Determined Activation Parameters for [1,5] Metallotropic Shifts in Group 14 η^1-Indenyl Complexes.

Migrating Element	Compound Number	E_a (kcal mol^{-1})	$\Delta G^{\ddagger}$ (kcal mol^{-1})	Reference
Si	**1.109**	< 29	—	121
	1.109	22.5	—	122
	1.109	22.4 ± 1.0	23.8 ± 0.1	70
	1.109	—	23.8	190
	1.114	23.0 ± 1.6	—	123
	1.135	26.1 ± 1.4	—	123
	3.6	—	24.2 ± 0.5	160
	4.3	—	26.5	190
	4.9	—	21.8	190
	4.17-4.18	—	21.9 ± 0.5	197
	4.19	—	17.6 ± 0.2	197
Ge	**1.143**	22	—	121
	1.143	18.2 ± 0.5	21.6 ± 0.1	70
	1.143	18.4 ± 0.4	21.8 ± 0.1	70
Sn	**1.145**	—	15.0	190
	1.145	12.0 ± 0.3	15.3 ± 0.1	70
	1.145	12.1 ± 0.2	15.1 ± 0.1	70
	1.145	12.7 ± 0.4	15.2 ± 0.1	70
	1.145	13.8 ± 0.8	—	127
	1.146	14.1 ± 0.4	—	123
	1.148	—	15.4	138
	1.154	13.4 ± 0.1	17.1	131
	1.155	16.1 ± 0.3	17.6 ± 0.3	131
	1.156	16.4 ± 0.2	17.1	131
	4.4	—	18.6	190
	4.8	14.2 ± 0.7	—	123
	4.10	—	14.0	190

The barrier to [1,5] silicon shifts in **4.19** was reduced so significantly that the ^{1}H and ^{13}C NMR spectra obtained exhibited normal peak coalescence behavior between 30 °C and 90 °C; as such, spectral simulation methods were employed and the estimated temperature-dependent rates used in the determination of the Gibbs free energy for this migratory process. Further

support for the occurrence of [1,5] silicon shifts in these systems was provided by these authors through Diels-Alder trapping of the isoindene intermediates with tetracyanoethylene, yielding **4.20** and **4.21**.

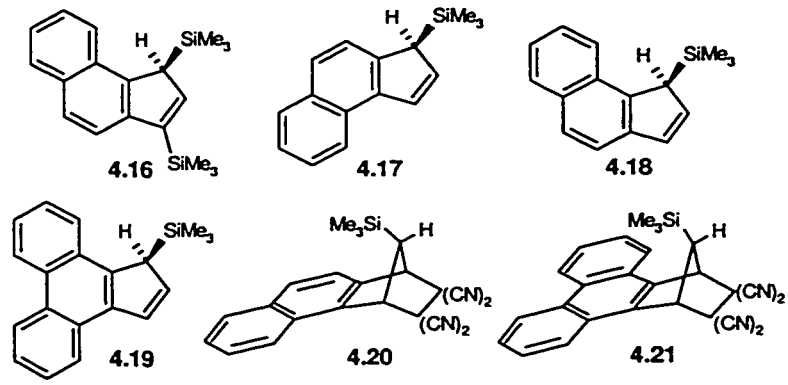

Scheme 4.4: *Benzannulated indenylsilanes and the corresponding tetracyanoethylene cycloadducts.*

4.2 Results and Discussion

4.2.1 In Search of the Sterically Loaded Isoindene: Tris(trimethylsilyl)isoindene

In continuation of the direction taken by Andrews, Rakita and Taylor, metalloindenes comprising sterically demanding functionalities at the C(1) and C(3) positions, rather than at the C(4) and C(7) sites, were sought. An initial approach in this regard was to create a system in which the bulky C(1) and C(3) substituents were identical to the migrating fragment, so as to facilitate the generation of sterically loaded isoindenes, while avoiding complications arising due to the generation of complex isomeric mixtures. Toward this end, 1,1,3-tris(trimethylsilyl)indene, **4.22**, was identified as an attractive synthetic target, in which steric interactions between the trimethylsilyl groups on C(1) could facilitate isomerization to the corresponding 1,2,3-tris(trimethylsilyl)isoindene, **4.23** (Scheme 4.5). The choice of **4.22** appeared especially judicious in light of the fact that synthetic precursors were known (**1.138** and **1.139**), and because the exchanging trimethylsilyl environments in **4.23**, arising due to [1,5] silatropic shifts, could be readily monitored by use of 2D-EXSY NMR.

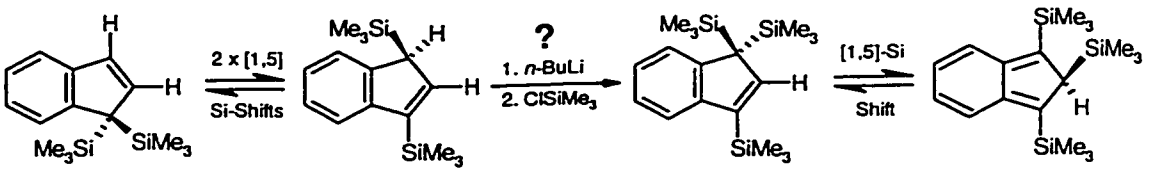

1.138 **1.139** **4.22** **4.23**

Scheme 4.5: *Synthetic route to 1,1,3-tris(trimethylsilyl)indene,* ***4.22****, and its isomerization to the corresponding isoindene,* ***4.23****.*

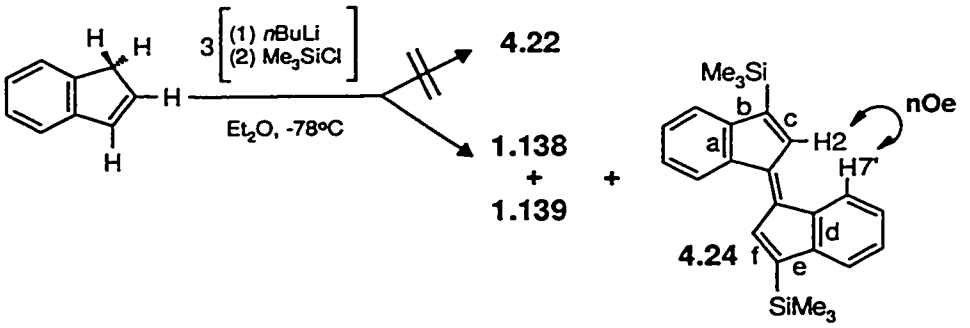

Scheme 4.6: *The unexpected generation of* ***4.24*** *during the attempted preparation of* ***4.22****; dibenzofulvalenes are named according to the bonds that are benzannulated.*

In an attempt to prepare the target compound, **4.22**, the standard synthetic approach involving the reaction of a carbanion with an appropriate chlorosilane was employed. Unfortunately, all attempts, either *via* three consecutive additions of base each followed by quenching with chlorotrimethylsilane (Scheme 4.6), or directly from a mixture of 1,1- and 1,3-bis(trimethylsilyl)indene, (**1.138** and **1.139**) produced neither the desired product, **4.22**, nor the isoindene, **4.23**, nor any other dimerization product derived from these species. However, careful chromatographic separation of the products in these reactions consistently yielded a bright red solid product, **4.24**, in low yield. Although the simplicity of the ^{1}H, ^{13}C and ^{29}Si NMR spectral data suggested the presence of one indene and one silicon environment in this compound, mass spectrometric data for **4.24** indicated a dimeric structure, comprised of two $(SiMe_3)C_9H_5$ fragments. This inference was further substantiated by the nOe enhancement of the H(7) signal when the H(2) signal was irradiated, an observation that cannot be rationalized for a compound containing only one indenyl unit. The connectivity in **4.24**, initially ascertained based on these data, was subsequently verified by data obtained during a single crystal X-ray diffraction study; the

structure appears as Figure 4.1. Although the crystal structure is seriously disordered (preventing a satisfactory anisotropic refinement), all of the heavy atoms were found and the location of the trimethylsilyl groups at the C(3) positions of the bis(trimethylsilyl)dibenzo[*a*,*d*]fulvalene is evident. The X-ray crystal structure of the corresponding hydrocarbon, *trans*-1,1'-bis(indenylidene) has recently been reported, and reveals an overall molecular structure which is qualitatively similar to that of the silylated complex, **4.24**.[198]

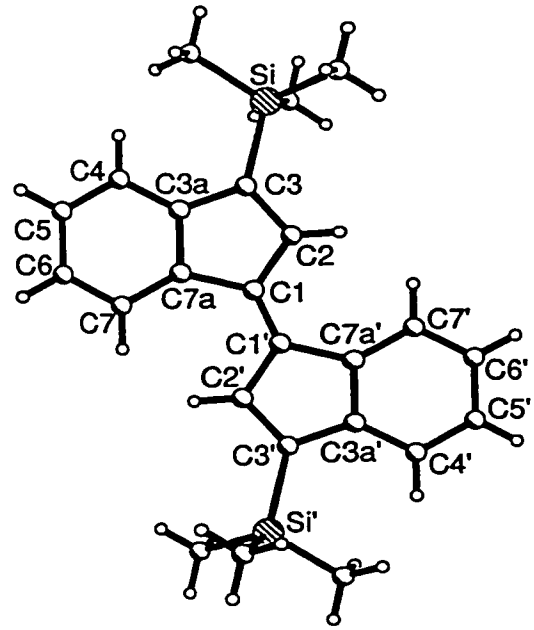

Figure 4.1: *The structure of* ***4.24****, determined by X-ray crystallography.*

Although the formation of the dibenzofulvalene, **4.24**, is surprising, precedent for the generation of dimeric indene species from isoindenes does exist. Warrener and co-workers report that, in addition to the well-known cycloaddition chemistry exhibited by molecules which contain the *ortho*-xylylene moiety, the dimerization of isoindenes *via* ene-type mechanisms can occur if a hydrogen atom is present at the C(2) position.[199-201] It is also noteworthy that dimeric compounds closely related to **4.24** have received recent attention in the literature. Olmstead and co-workers[202] have discussed the unexpected isolation of **4.25** in their attempt to generate an *ansa*-titanocene, while Youngs and co-workers[203,204] demonstrated that geometrically constrained

bis(trimethylsilyl)dibenzo[*a*,*f*]fulvalenes, such as **4.26**, can be readily prepared *via* oxidative coupling using Group 13 metal halides (Scheme 4.7).

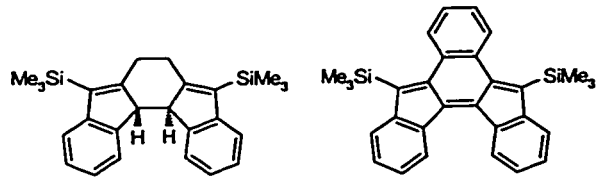

4.25 **4.26**

Scheme 4.7: *Some recently reported compounds,* ***4.25*** *and* ***4.26****, which possess molecular structures analogous to* ***4.24****.*

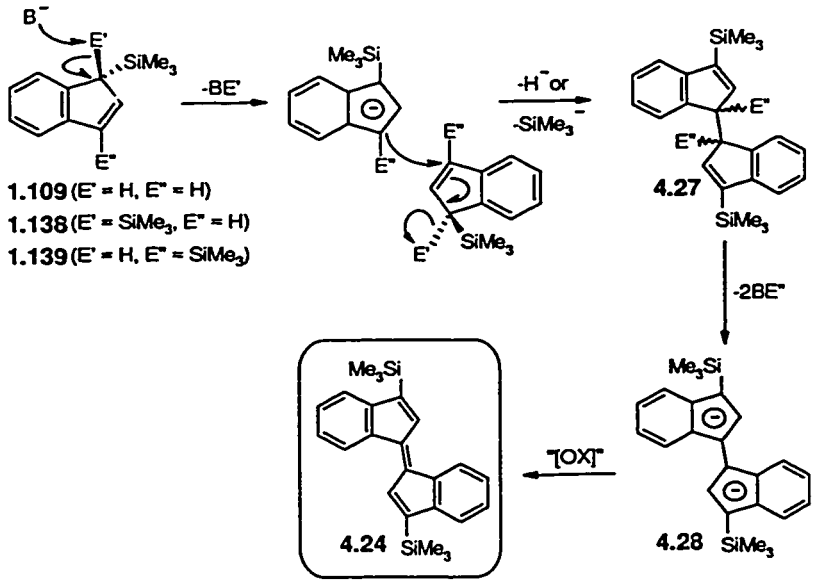

1.109 (E' = H, E" = H)
1.138 (E' = $SiMe_3$, E" = H)
1.139 (E' = H, E" = $SiMe_3$)

Scheme 4.8: *A generalized mechanistic rationale for the formation of* ***4.24****.*

In the absence of conclusive experimental data, decisive commentary on the mechanistic pathway leading to the formation of **4.24** cannot be provided. Nevertheless, given the paucity of evidence for either **4.22** or **4.23**, and in consideration of the highly basic experimental conditions employed, it is possible to rationalize the generation of **4.24** based on synthetic methodologies that have appeared in the literature.[205,206] In the presence of excess base, abstraction of either a trimethylsilylium ($SiMe_3^+$) fragment (in **1.138**) or a proton (in **1.109** or **1.139**) would generate the aromatic anion, as depicted in Scheme 4.8. Formation of a substituted 1,1'-biindene, **4.27**, followed by attack by base would lead to the generation of the dianion, **4.28**. Subsequent

oxidative coupling of the tethered anions in **4.28** produces the dibenzofulvalene, **4.24**. Although the origin of the oxidant is not certain, such a process would be greatly facilitated by the eventual formation of the highly conjugated, 18-electron system in **4.24**. Indeed, molecular oxygen itself has proven effective in the formation of related conjugated organic structures.[207]

Extended planar aromatic systems are of considerable interest, both as ligands in the preparation of organometallic complexes[208] and as precursors to materials with novel electronic, magnetic and conductive properties.[209] Given the potential utility of compound **4.24**, its rational preparation was undertaken, using the approach summarized in Scheme 4.9. Starting from 3,3'-biindene, **4.29**, and/or 1-(indanylidene)-1-indene, **4.30**, treatment with base followed by quenching with chlorotrimethylsilane yielded **4.31** as a *meso/d,l* mixture. Subsequent double deprotonation of **4.31** generated the previously invoked dianion, **4.28**, which was efficiently oxidized, by use of iodine, to the dibenzofulvalene, **4.24**.

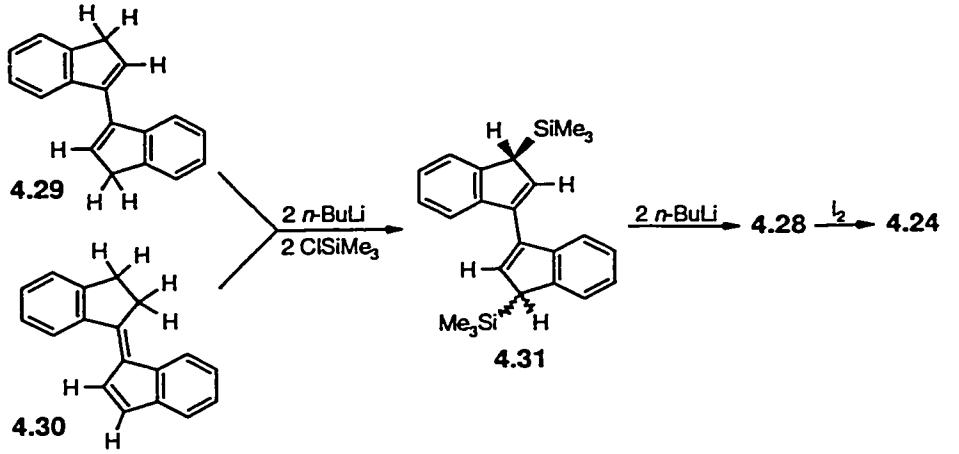

Scheme 4.9: *The rational synthesis of* ***4.24****, via* ***4.31****, the dimer of* ***1.109****.*

To summarize, in an attempt to prepare the sterically protected isoindene, **4.23**, the silicon-substituted dibenzofulvalene, **4.24**, was serendipitously generated; this latter compound was subsequently prepared in a rational manner from the dimer of trimethylsilylindene, **4.31**, *via* oxidation of the corresponding dianion, **4.28**. Although the generation of **4.24** represents a chemically interesting result, the fact that the desired compound, **4.22**, could not be synthesized is

perplexing. In contrast to the methyl-substituted indenylsilane, **4.1**, for which no *gem*-disubstituted isomer is observed, the corresponding bis(trimethylsilyl)indenes, **1.138** and **1.139** are readily prepared as a ~ 1:1 mixture of interconverting isomers. It is evident that the Si-C(1)indenyl bonds in these latter species are sufficiently long so as to accommodate two trimethylsilyl groups (**1.138**). Additional evidence in support of the viability of **4.22** comes from the existence of the corresponding tris(trimethylsilyl)cyclopentadiene series, **4.32**, which is prepared *via* deprotonation of the cyclopentadienyl analogue of **1.138**, followed by quenching with chlorotrimethylsilane (Scheme 4.10).[210,211] The isomerization of **4.32** (the counterpart of **4.22**) has been the focus of variable-temperature ^{1}H and ^{13}C NMR studies, which indicated the operation of a [1,5] silicon shift rearrangement process.

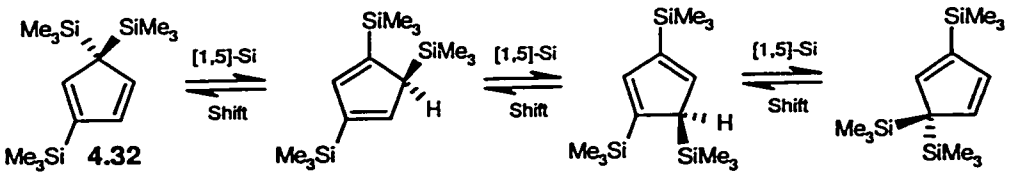

Scheme 4.10: *Quasi-degenerate molecular rearrangements involving the tris(trimethylsilyl)cyclopentadiene,* ***4.32.***

Given that unfavorable steric requirements in **4.22** can be ruled out as a significant factor preventing the generation of this compound, and without a persuasive argument based on electronic effects, one is left to consider the experimental conditions employed. Based on the mechanism depicted in Scheme 4.8, a critical step leading to the formation of **4.24** may involve the attack of an indenyl anion on a substituted indene, giving rise to **4.27**. In a typical experiment, indene precursor concentrations of ~ 0.3 M were employed; perhaps more dilute conditions would lead to the preferential addition of a third trimethylsilyl group to the anion derived from **1.138** and **1.139**.

4.2.2 Studying the Effects of σ-Methyl and π-Cr(CO)$_3$ Substitution

4.2.2.1 The Synthesis and Dynamics of a Dimethylindenylsilane

In 1970, Davison and Rakita[123] noted that the introduction of methyl groups at the indenyl C(1) and C(3) positions, as in **4.8**, does little to lower the barrier to tin migrations, relative to the

parent compound, trimethylstannylindene, **1.145** (Section 4.1); a comparative study involving the silane, **4.7**, proved impossible, since this compound could not be synthesized. Data obtained from dynamic NMR studies involving **4.7** would, however, be instructive given that the contracted metal-indene distance in this molecule, relative to **4.8**, would be expected to lead to an increased ground state energy for the indene structure, and possibly to a reduced barrier to [1,5] silicon shifts. In contrast to the indenylsilane, **4.9**, which possesses C(4) and C(7) methyl substituents, any reduction in the barrier to silicon migrations involving **4.7** (relative to trimethylsilylindene, **1.109**) is best rationalized not in terms of electronic stabilization, but rather as arising due to the alleviation of unfavorable steric interactions between the indene methyl groups and the methyl substituents on the silicon fragment. The considerable appeal of **4.7** prompted a reinvestigation of the synthesis of this compound.

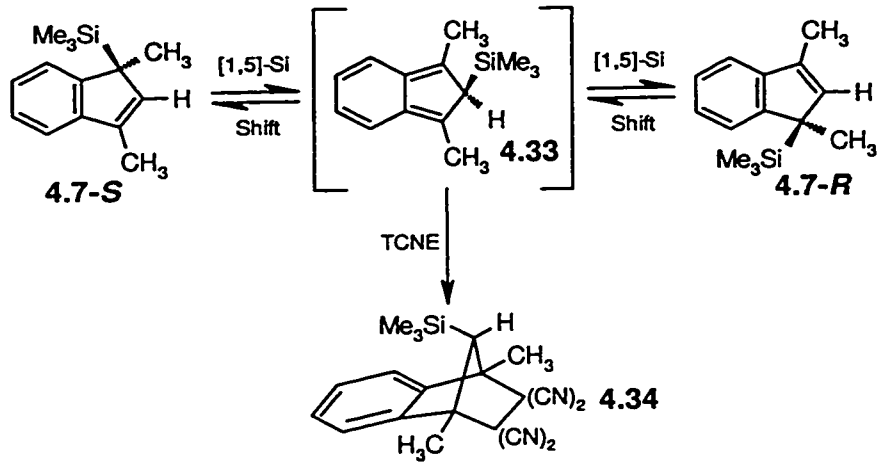

Scheme 4.11: *Molecular rearrangements involving **4.7**, and Diels-Alder trapping of the isoindene, **4.33**, with tetracyanoethylene.*

In attempting to prepare 1,3-dimethyl-1-trimethylsilylindene, **4.7**, Davison and Rakita utilized a classical synthetic protocol, which involved quenching of dimethylindenyllithium with chlorotrimethylsilane in hexane, followed by workup with deuterium oxide (D_2O). The formation of the isolated product, 1-deutero-1,3-dimethylindene, can be rationalized either in terms of the quenching of the unreacted lithium indenide or as arising due to the hydrolytic cleavage of the

silicon-indene bond in the desired product, **4.7**. Interestingly, this workup step was omitted in the successful synthesis of the indenylstannane, **4.8**.

Based on the fruitful preparation of **4.8**, 1,3-dimethylindenyllithium was quenched with chlorotrimethylsilane in tetrahydrofuran, *without aqueous workup*. Following purification *via* flash chromatography on silica, 1,3-dimethyl-1-trimethylsilylindene, **4.7**, was isolated as an analytically pure solid in 89% yield. It is noteworthy that substitution of diethyl ether for tetrahydrofuran as the reaction solvent resulted in a dramatic reduction in the yield (< 20%).

Having successfully prepared the desired dimethylindenylsilane, **4.7**, the molecular dynamics of this compound were probed in the usual manner by use of 2D-EXSY and single selective inversion NMR techniques (Scheme 4.11). The ^{1}H-^{1}H EXSY spectra obtained for **4.7** clearly indicate the operation of an exchange process which permutes the C(1)-C*H*$_3$ and C(3)-C*H*$_3$ chemical environments; similar off-diagonal peaks linking the aromatic hydrogen atom resonances are much more difficult to discern, owing to the extensive overlap of these signals. Moreover, as the mixing time is increased, the off-diagonal peaks linking the C(1)-C*H*$_3$ and the C(3)-C*H*$_3$ sites grow in intensity, and are consistently of the same phase as the diagonal signals. This phenomenon parallels that which was depicted graphically in Figure 2.2 for the iron compound, **1.9**, and serves to identify the origin of these off-diagonal signals as arising from chemical exchange, not nOe interactions. Data obtained from single selective inversion NMR experiments allowed for the barrier to [1,5] silicon shifts in **4.7** to be estimated ($\Delta G^{\ddagger}$ = 23 ± 1 kcal mol^{-1}); this value does not deviate significantly from those found for trimethylsilylindene, **1.109** (~ 24 kcal mol^{-1}), and the C(4) and C(7) methylated indenylsilane, **4.9** (~ 22 kcal mol^{-1}). As such, it is apparent that methyl substitution at the C(1) and C(3) positions on indene does not contribute in any significant way to a reduction in the barrier to silicon migrations in these systems, an observation which parallels the findings of Davison and Rakita, who examined the dynamics of the indenylstannane analogue, **4.8**. If sterically promoted rearrangements of indenylsilanes are to be realized, it is evident that the introduction of even bulkier molecular fragments will be required in order to perturb indene ground-state structure.

Although the introduction of the indenyl methyl substituents in **4.7** does not lead to an increased rate of [1,5] silicon shifts, the fact that these migrations continue to occur is important in and of itself. Indeed, **4.7** serves as a model compound in the development of systems which have the capacity to undergo intramolecular Diels-Alder reactions (Chapter Five). With the quasi-fluxional nature of this compound ascertained, the propensity of the corresponding isoindene, **4.33**, for [4+2] cycloadditions was examined by stirring a solution of **4.7** with tetracyanoethylene (Scheme 4.11).

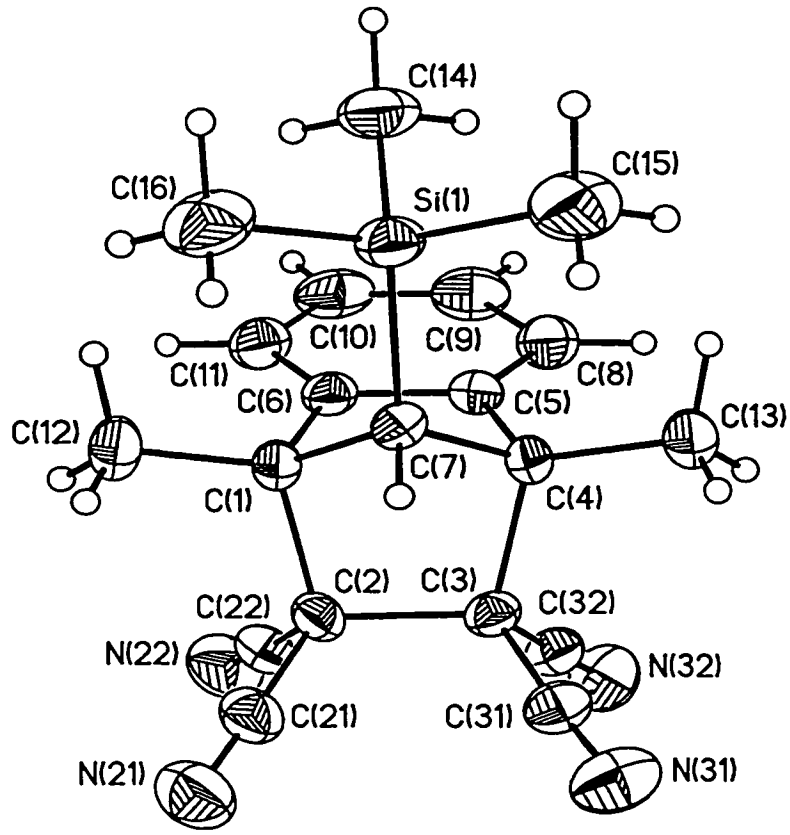

Figure 4.2: *The crystallographically determined structure of* ***4.34*** *(shown with 30% thermal displacement ellipsoids).*

The expected Diels-Alder cycloaddition product, **4.34**, was isolated in 83% yield and fully characterized by use of standard spectroscopic techniques and also by a single crystal X-ray diffraction study; the structure of **4.34** appears as Figure 4.2, while crystallographic data and metrical

parameters are collected in the Appendix. In the crystal, **4.34** possesses an effective σ-plane defined by Si(1) and C(7) and bisecting the C(2)-C(3) bond, giving rise to identical bond lengths and angles (within experimental error) for all fragments related by this mirror plane. Moreover, despite the presence of the methyl substituents at the bridgehead positions in **4.34**, the geometric characteristics of this molecule in the solid state parallel those found in other crystallographically characterized metalloisoindene cycloadducts of TCNE, including: (a) *anti*-oriented trimethylsilyl and TCNE fragments, (b) elongated incipient Diels-Alder (C(1)-C(2) and C(3)-C(4)) and formerly olefinic (C(2)-C(3)) bonds, and (c) expanded Si(1)-C(7)-C(1) and Si(1)-C(7)-C(4) angles (ave. ~ 119°).

4.2.2.2 Assessing the Impact of π-Cr(CO)$_3$ Complexation

Butenschön and co-workers[212-215] have demonstrated that the coordination of an η^6-tricarbonylchromium moiety to the six-membered ring in heteroatom-substituted benzocyclobutenes, **4.35**, increases the rate of ring opening to the corresponding *ortho*-xylylene, the latter of which has been trapped by a series of reactive dienophiles (Scheme 4.12).

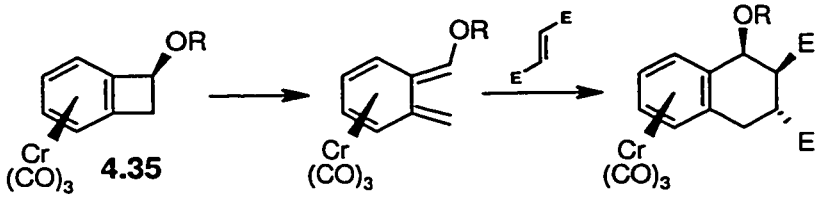

Scheme 4.12: *Chromium-facilitated ring opening of the benzocyclobutene, **4.35**, to the ortho-xylylene, and subsequent Diels-Alder trapping.*

In light of the similarity between this ring-opening process and the isomerization of indenes to the corresponding isoindenes, the effect of chromium complexation on the rate of [1,5] silicon shifts in indenylsilanes was examined. The tricarbonylchromium complex of (1-indenyl)trimethylsilane, **4.36**, was initially identified as a candidate for such dynamic NMR studies, and its synthesis was undertaken. Using the method described by Fischer and Kriebitzsch[216] for the preparation of the indenetricarbonylchromium, (1-indenyl)trimethylsilane, **1.109**, and excess $Cr(CO)_6$ were heated to reflux in dibutyl ether (~ 140 °C) for 72 h (Scheme 4.13). However, the

indenylchromium product isolated from this reaction, following chromatographic purification, was not the desired complex, **4.36**, but rather the corresponding 3-indenyl isomer, **4.37**, for which [1,5] silicon migrations are not possible; the ^{1}H and ^{13}C NMR signals attributable to the methylene group and the single vinylic methine unit were diagnostic of the structure depicted in Scheme 4.13. The generation of **4.37**, formally the tricarbonylchromium complex of **1.126** (Scheme 1.33), can be rationalized in terms of two consecutive [1,5] hydrogen shifts that become possible at the high temperatures employed in the synthesis. It is not known whether these hydrogen migrations occur in the precursor, **1.109**, in the complex, **4.36**, or *via* some bimolecular chromium-mediated reaction pathway. The possibility of the latter is supported by a report from Ceccon and co-workers,[217] who noted that the rearrangement of 1-phenylindene to 3-phenylindene is accelerated by the addition of $(CH_3CN)_3Cr(CO)_3$ in tetrahydrofuran.

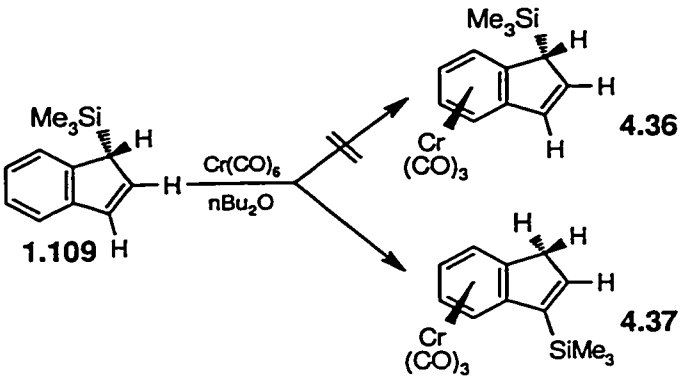

Scheme 4.13: *Attempted preparation of the η^6-Cr(CO)$_3$ complexed (1-indenyl)silane,* ***4.36.***

Although low temperature metallation of **1.109** using $(CH_3CN)_3Cr(CO)_3$ could provide a route to **4.36**,[218] complexation of the dimethylindenylsilane, **4.7**, was selected as an alternative means of generating a chromium-containing 1-indenylsilane. Since the barrier to [1,5] methyl shifts is considerably higher than that associated with hydrogen migrations, it was anticipated that the use of **4.7** as a precursor would circumvent the isomerization pathways which eventually lead to the formation of sp^2-bonded silicon complexes. Using the aforementioned synthetic approach, **4.7** and excess $Cr(CO)_6$ were allowed to react in refluxing dibutyl ether for 96 h; the single product isolated from this reaction yielded spectroscopic data consistent with the formation of a single

complex containing the required C(1)-bonded trimethylsilyl unit. However, these data provided no insight into the stereochemistry of the addition; in principle, the $Cr(CO)_3$ fragment could bind *exo* or *endo* to the trimethylsilyl group. The *exo* geometry of the product, depicted in Scheme 4.14, was ascertained by use of X-ray crystallographic techniques; the structure of **4.38** appears as Figure 4.3, while crystallographic data and metrical parameters are collected in the Appendix.

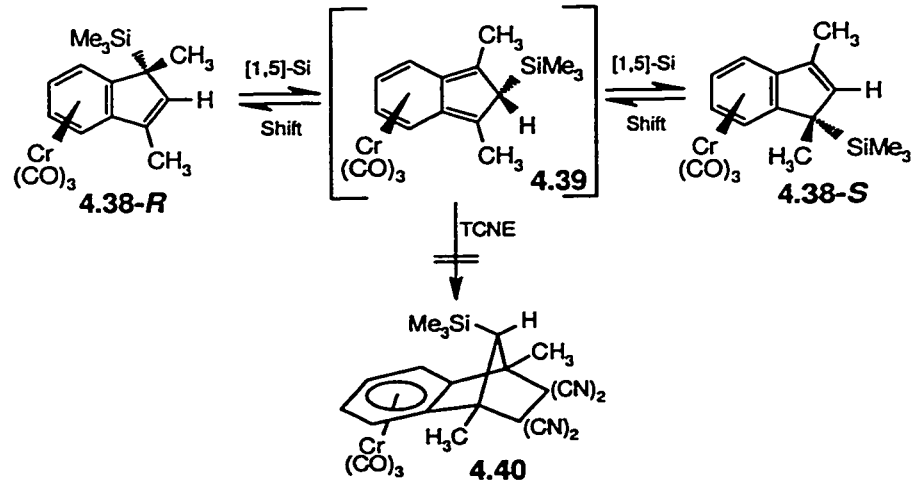

Scheme 4.14: *Molecular rearrangements involving **4.38**, and the attempted Diels-Alder trapping of the isoindene, **4.39**, with tetracyanoethylene.*

Congestion at the quaternary C(1) center in **4.38** results in an elongated C(1)-silicon bond (C(1)-Si(1) = 1.938(7) Å) relative to tris(1-indenyl)silane, **3.20** (C-Si(1) = 1.896(5) Å, 1.889(4) Å and 1.895(5) Å), although statistically significant lengthening of the C(1)-Me bond in **4.38** (C(1)-C(11) = 1.540(8) Å), in comparison to the other carbon-methyl distance in this compound (C(3)-C(33) = 1.508(9) Å) and those found in the cycloadduct, **4.34** ($C\text{-}CH_3$ = 1.519(4) Å, 1.505(4) Å), is not observed. Moreover, while the C_5 and C_6 rings in **4.34** deviate only modestly from planarity (0.0217 Å and 0.0128 Å, respectively), the plane defined by the allylic unit (C(1)-C(2)=C(3)) intersects the C_6 plane (C(3a), C(4), C(5), C(6), C(7) and C(7a)) at an angle of approximately 3.2°, possibly due to unfavorable steric interactions between the C(1)-methyl group and the chromium fragment. Such a phenomenon may also be responsible for the asymmetric bonding between the chromium group and the arene ring. On traversing the C_6 unit from the annulated edge (Cr(1)-

C(3a) = 2.280(7) Å, Cr(1)-C(7a) = 2.293(6) Å), through the centroid of the ring (Cr(1)-C(4) = 2.217(6) Å, Cr(1)-C(7) = 2.237(8) Å), to the rear edge (Cr(1)-C(5) = 2.172(8) Å, Cr(1)-C(6) = 2.205(9) Å), the distances between the chromium unit and the arene ring gradually contract. While this differential bonding pattern seems to be slightly more pronounced than in related complexes reported by Kerber and Waldbaum,[219] and Ustynyuk and co-workers,[220] such distortions in **4.38** are apparently less than those found in the crystal structure of the η^6-$Cr(CO)_3$ complex of naphthalene. The approximate staggered-*exo* orientation of the tricarbonylchromium unit in **4.38** is typical of such polycyclic chromium complexes (Figure 4.3, inset).[221]

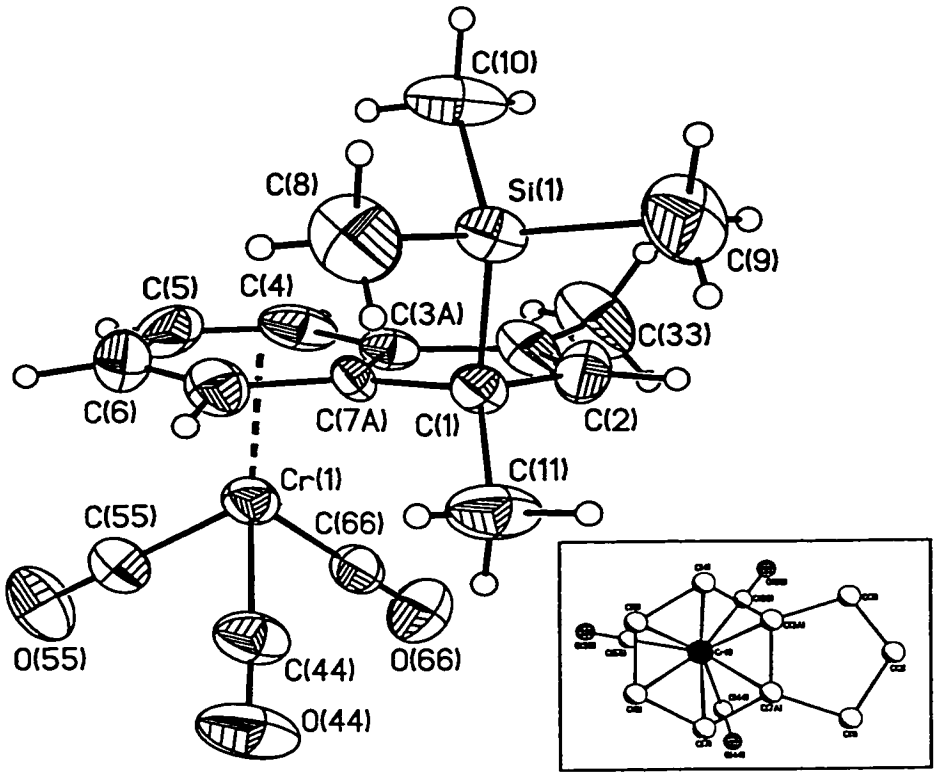

Figure 4.3: *The crystallographically determined structure of* ***4.38*** *(shown with 30% thermal displacement ellipsoids); the inset figure shows the staggered-exo orientation of the tricarbonylchromium fragment.*

Having synthesized and fully characterized the required tricarbonylchromium complex, **4.38**, the resilience of the suprafacial [1,5] silatropic shift process was probed. Based on the findings of Butenschön and co-workers (Scheme 4.12), it is reasonable to suggest, *a priori*, that the

presence of the chromium fragment in **4.38** would facilitate the generation of isoindenes. However, it is also evident that the conversion of the indenylsilane, **4.38**, into the isoindene, **4.39**, gives rise to what can formally be considered a 16-electron chromium center in **4.39** (Scheme 4.14). If geometric constraints exist in the isoindene that are not present in the *ortho*-xylylene (perhaps arising as a result of the methylene unit in the former), then possible long-range coordination to the C_5 diene fragment may be prohibited in the isoindene, leading to a destabilization of the 16-electron intermediate, **4.39**. Such a scenario could, in principle, lead to a reduction in the rate of [1,5] silicon shifts in **4.38**, relative to the uncomplexed compound, **4.7**.

The molecular dynamics of **4.38** were qualitatively examined by use of 2D-EXSY NMR techniques; a portion of a ^{1}H-^{1}H EXSY spectrum acquired from a sample of this complex is presented as Figure 4.4. The off-diagonal peaks linking the C(1)-C*H*$_3$ and C(3)-C*H*$_3$ sites verify that [1,5] silicon migrations continue to occur in **4.38**. The low-frequency shift of the arene ^{1}H NMR resonances following complexation by a $Cr(CO)_3$ fragment is a well-defined phenomenon.[24] This process is particularly fortuitous in the present case, as the heavily overlapped H(4) to H(7) ^{1}H NMR resonances in **4.7** are converted into well-resolved multiplets in **4.38**, allowing for the observation of distinct 2D-EXSY off-diagonal signals, which correlate the exchanging arene ring environments in this chromium complex.

Given that silatropic shifts are operative in **4.38**, single selective inversion NMR experiments were conducted in order to quantify the effect of chromium complexation on the rate of [1,5] silicon shifts; an analysis of the temperature-dependent rate data obtained during these dynamic NMR experiments revealed the barrier to silicon shifts in **4.38** ($\Delta G^{\ddagger}$ = 24 ± 1 kcal mol^{-1}) to be indistinguishable from the uncomplexed silane, **4.7** ($\Delta G^{\ddagger}$ ~ 23 kcal mol^{-1}). That fact that the presence of the chromium fragment served neither to increase nor diminish the rate of [1,5] silicon shifts was unexpected, and as such, the behavior of the $Cr(CO)_3$ unit throughout the migratory process was reexamined.

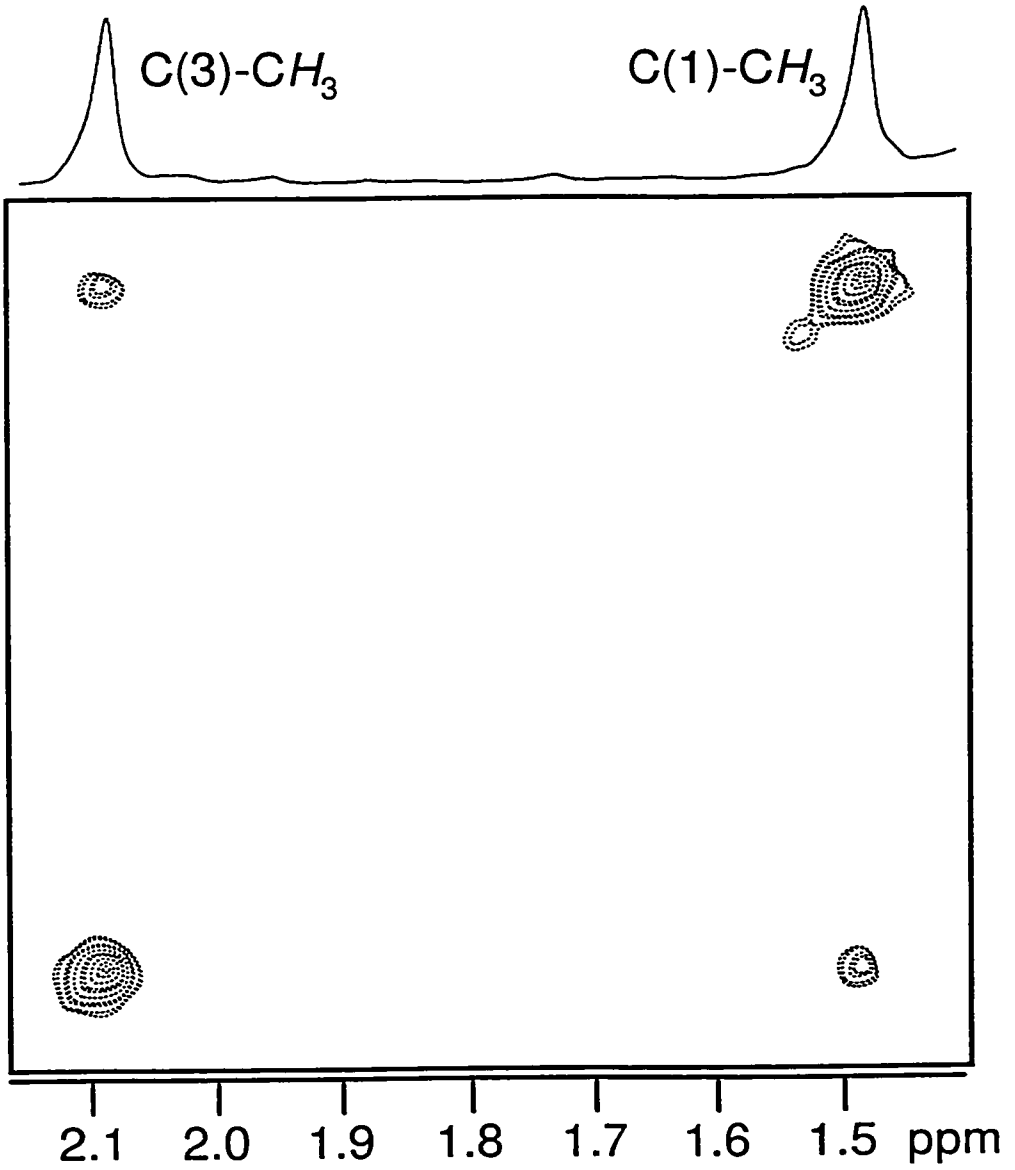

Figure 4.4: *The indene-CH_3 region of the ^1H-^1H EXSY spectrum of* ***4.38****, acquired in tetrachloroethane-d_2 at 105 °C with a mixing time of 1.0 second.*

During the course of this investigation, a report was published by Ustynyuk and co-workers[222] which is of considerable relevance to the molecular dynamics of **4.38**. These workers noted that upon warming, σ-methyl-(η^5-indenyl)tricarbonylchromium, **4.41**, is quantitatively converted into η^6-(1-*endo*-methylindene)tricarbonylchromium, **4.42**, and ultimately the thermodynamically favored C(3)-methyl isomer, **4.44** (Scheme 4.15). Mechanistic aspects of these rearrangements

were examined by use of density functional theory (DFT) calculations, which revealed that the conversion of **4.42** into **4.44**, occurs *via* the isoindene intermediate, **4.43**, and that during the entire migratory process, the chromium fragment remains bound to the C_6 ring of the indene skeleton; once the chromium-bonded methyl fragment in **4.41** is delivered to the indene, the $Cr(CO)_3$ group migrates to the C_6 ring rapidly and irreversibly. The isomerization of **4.42** into **4.44** is qualitatively similar to the conversion of the 1-indenylsilane, **4.36**, into the 3-indenylsilane, **4.37** (Scheme 4.13). Moreover, the energy-minimized structure provided for **4.43** contains bond lengths (Table 4.2) which are indicative of an "η^4-$Cr(CO)_3$" fragment in **4.43**, especially when compared to the metrical parameters associated with the crystallographically characterized η^6-bonded indenylsilane, **4.38**; short distances are observed between the chromium center and C(4), C(5), C(6) and C(7) in **4.43**, while the bonds to C(3a) and C(7a) are considerably longer. Experimental support for the viability of complexes possessing "slipped" η^4-geometries has also been presented by Ceccon and various co-workers, who have provided crystallographic data for a series of bimetallic indenyl complexes, including **4.45**, **4.46** and **4.47** (Scheme 4.16).[223,224] In these compounds, the chromium and rhodium fragments share the same face of the indenyl ligand, which forces these fragments toward the periphery of the C_6 and C_5 rings, respectively (Table 4.2). In fact, the solid state structures of these stable molecules exhibit approximate "η^4-η^3" configurations, despite the fact that the chromium and rhodium metal fragments in these molecules would preferentially coordinate to indene *via* η^6 and η^5 bonding modes, respectively, in the absence of the second organometallic unit (see **4.48** and **4.49** in Scheme 4.16).

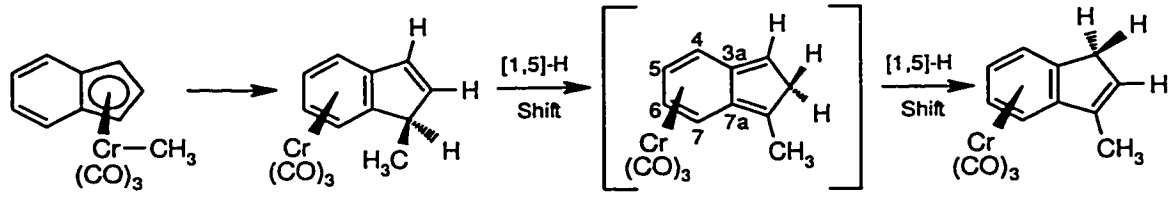

4.41 **4.42** **4.43** **4.44**

Scheme 4.15: *The "ricochet" inter-ring haptotropic rearrangement of **4.41** into **4.42**, followed by isomerization to **4.44**; numbering in the isoindene, **4.43**, is carried over from **4.42**.*

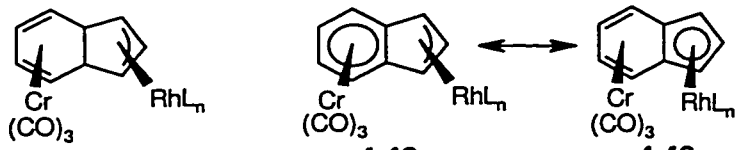

4.45: $L_n = (CO)_2$
4.46: L_n = NBD
4.47: L_n = COD

4.48 **4.49**

Scheme 4.16: *The chromium-rhodium bimetallic indenyl complexes, **4.45**, **4.46** and **4.47** (NBD = norbornadiene; COD = 1, 5-cyclooctadiene), and a pictorial representation of the electron sharing in these compounds.*

Table 4.2. Computationally and Experimentally Determined Bond Lengths (Å) For Some Indenylchromium Complexes.

	4.43[a]	**4.45**[b]	**4.46**[b]	**4.47**[c]
Cr-C(3a)	2.440	2.375(4)	2.448(3)	2.434(7)
Cr-C(7a)	2.417	2.401(4)	2.448(3)	2.464(6)
Cr-C(4)	2.247	2.239(4)	2.258(3)	2.255(7)
Cr-C(7)	2.230	2.257(4)	2.271(3)	2.267(5)
Cr-C(5)	2.209	2.181(5)	2.208(4)	2.194(6)
Cr-C(6)	2.206	2.188(4)	2.197(5)	2.189(5)

(a) DFT calculations (ref. 222). (b) X-ray diffraction data (ref. 223). (c) X-ray diffraction data (ref. 224).

In light of the computational and crystallographic results presented above, it appears that although a 16-electron chromium intermediate (**4.39**) can formally be invoked during the interconversion of the 18-electron complexes, **4.38-*S*** and **4.38-*R*** (Scheme 4.14), the energy cost associated with this process is not sufficiently large as to lead to a statistically significant increase in the barrier to [1,5] silicon shifts, relative to the unmetallated compound, **4.7**. In actuality, the chromium fragment is this system can be described as a spectator group, with respect to the operation of suprafacial [1,5] silicon shifts. As such, the dynamic behavior of the η^6-$Cr(CO)_3$-containing η^1-indenyl complex of iridium, **1.72** (Scheme 1.23), need not be rationalized in terms of symmetry-forbidden [1,3] shifts.[99] It is possible that such a process was suggested by the researchers who examined the dynamics of this compound, so as to avoid invoking the intermediacy of a high-energy η^4-$Cr(CO)_3$-complexed metalloisoindene, and because of the

presumed static nature of $(\eta^5\text{-}C_5H_5)Fe(CO)_2(\eta^1\text{-}C_9H_7)$, **1.9** (Chapter Two). Indeed, the operation of an allowed [1,5] iridium shift process is viable for **1.72**.

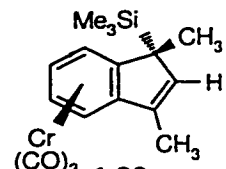

4.38

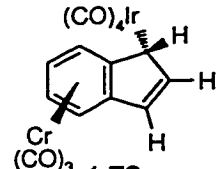

1.72

The assertion that the $Cr(CO)_3$ unit remains fixed to the C_6 ring during the interconversion of **4.38-*S*** and **4.38-*R*** suggests that the C_5 diene unit in the purported intermediate, **4.39**, should be available to participate in cycloaddition reactions. In an attempt to intercept **4.39**, pale yellow solutions of **4.38** and tetracyanoethylene were combined, which generated a dark blue mixture typically observed during these reactions. However, in contrast to the successful Diels-Alder trapping of **4.33**, the reaction involving **4.38** yielded a dark solid, from which only a small amount (approximately 10%, based on **4.38**) of the uncomplexed cycloadduct, **4.34**, could be extracted. The deeply colored solution formed upon addition of TCNE to a solution containing a metalloindene is consistent with the formation of a charge-transfer (CT) complex; arene[225] and even arenetricarbonylchromium[226,227] CT complexes with TCNE are well-documented. Although the significance of these CT complexes as precursor to the isolated isoindene cycloadducts is unclear, it is possible that in the case of the chromium complexes **4.38** and **4.39**, CT makes available reaction pathways which result in decomposition. Kündig and co-workers[228] have recently reported that the addition of an olefinic compound capable of η^4-coordination, such as methyl acrylate, to benzenetricarbonylchromium leads to rapid cleavage of the arene-metal linkage under mild conditions. Since arenetricarbonylchromium compounds are known to react with nitriles,[229,230] it is feasible that TCNE may also serve to promote demetallation of the indenyl ligand in **4.39**, *via* addition to what can be described as a coordinatively and electronically unsaturated chromium center in this molecule. The isolation of **4.34** as a side product in reactions involving **4.38** is in keeping with the occurrence of such a decomplexation event. Finally, it is also possible to argue that

the formation of **4.40** is disfavored on steric grounds alone, since the generation of such a cycloadduct possessing *anti* disposed silyl and dienophilic fragments would require that TCNE add to the isoindene, **4.39**, on the face occupied by the bulky $Cr(CO)_3$ unit. Although chromium complexes similar to the desired adduct, **4.40**, have been prepared[231,232] and crystallographically characterized,[233] the generation of these species typically involves the introduction of a chromium fragment to a pre-formed benzonorbornene.

4.2.3 Can an Adjacent Dicobalt Cluster Electronically Facilitate Silicon Shifts?

Metal cluster stabilized cations of the type $[(R'C{\equiv}C\text{-}ER_2)(ML_n)_2]^+$, **4.50** ($ML_n$ = $Co(CO)_3$ or $Mo(CO)_2(\eta^5\text{-}C_5H_5)$; E = C or Si), have been the focus of considerable research effort in recent years (Scheme 4.17).[234,235] In these systems, experimental data and theoretical considerations both indicate that the positive charge on "E" is alleviated through direct overlap of the vacant *p* orbital on carbon or silicon with a filled metal *d* orbital on the cluster. However, charge delocalization onto the metal appears to be much less favorable for silylium ions than for carbocations.[176,236]

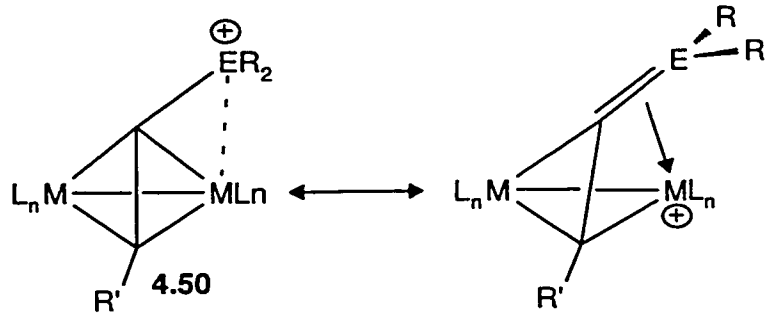

Scheme 4.17: *Cation stabilization in **4.50**, via charge delocalization onto an adjacent metal cluster (M = Co, Mo; E = C, Si).*

In the course of suprafacial [1,5] silicon shifts in σ-cyclopentadienyl or σ-indenylsilanes, it is plausible to envisage the development of positive charge at the migrating silicon center, given the potential for the cyclopentadienyl and indenyl groups to behave as "intrinsic acceptors" by generating transition states with 6π and 10π aromatic character (Scheme 4.18). This is also supported by the fact that for σ-cyclopentadienylsilanes, a reduction in the rate of [1,5] metallotropic shifts is observed as the electronegativity of the substituents attached to the silicon atoms increases.[51] In contrast, the

cycloheptatrienyl ring functions as an "intrinsic donor", and migrations in $(\sigma\text{-}C_7H_7)SiR_3$ systems are favored only when the seven-membered ring acquires some degree of positive charge, thus producing a 6π (tropylium-like) transition state.[237]

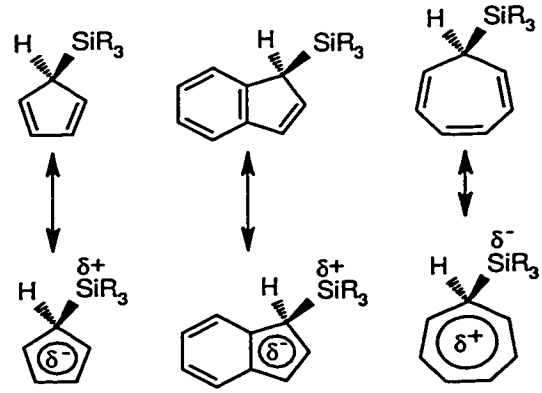

Scheme 4.18: *The donor-acceptor properties of a series of silicon-functionalized organopolyene compounds.*

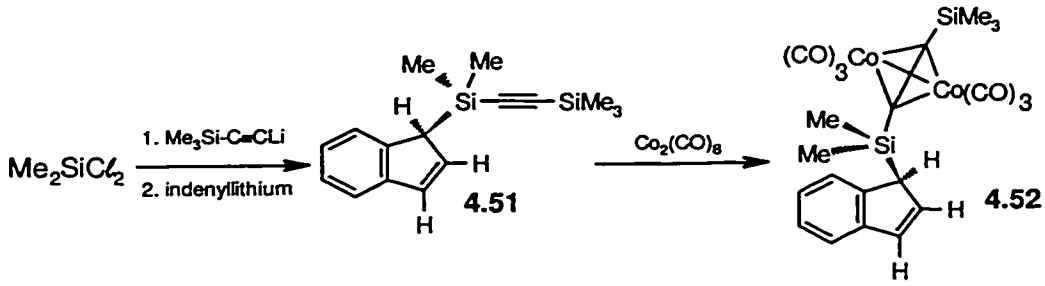

Scheme 4.19: *The synthetic route to compounds* ***4.51*** *and* ***4.52.***

In light of the situation depicted above, an indenylsilane with the capacity to alleviate any positive charge (*via* delocalization onto a neighboring metal cluster fragment) that might develop on the silicon center during its migration was sought. If silicon does in fact develop appreciable positive charge in its migratory transition state, it is reasonable to expect that anchimeric assistance from an adjacent metal cluster fragment would be reflected in a somewhat reduced barrier for the [1,5] silatropic shift. To this end, the alkynyl-silane, **4.51**, was prepared by successive treatment of Me_2SiCl_2 with the trimethylsilylethynyl and indenyl anions. As shown in Scheme 4.19, subsequent addition of $Co_2(CO)_8$ yield the dimetallic cluster, **4.52**.

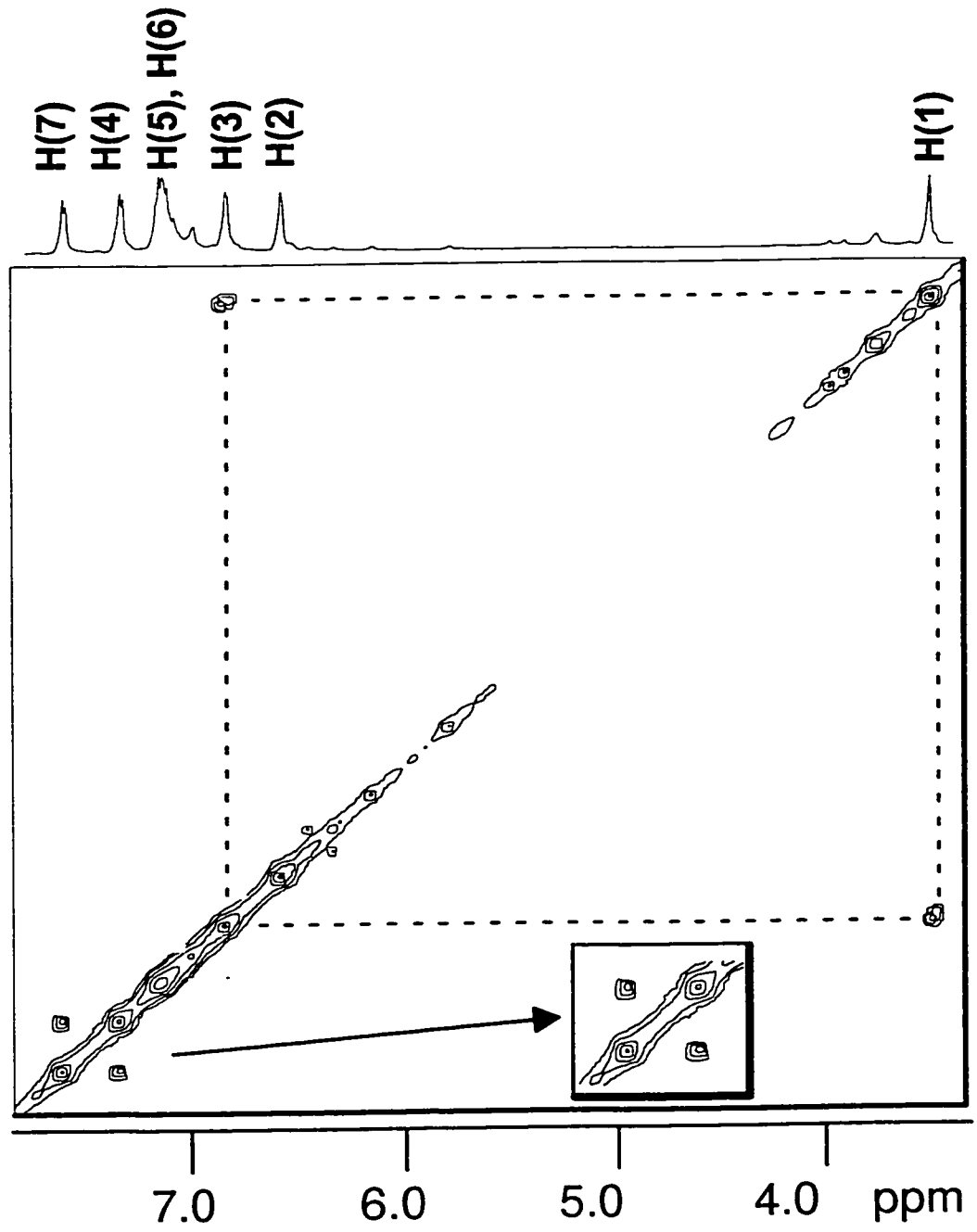

Figure 4.5: *The ^{1}H-^{1}H EXSY spectrum of **4.51** in toluene-d_8 at 72 °C, acquired with a mixing time of 5 seconds.*

The ^{1}H-^{1}H EXSY spectrum of (1-indenyl)$SiMe_2(C{\equiv}C\text{-}SiMe_3)$, **4.51**, is shown in Figure 4.5, and the off-diagonal correlations between the equilibrating sites are evident. Single selective inversion measurements yielded a $\Delta G^{\ddagger}$ value of 24 ± 2 kcal mol^{-1} for the migratory process in this compound. Moreover, to establish unequivocally that this rearrangement proceeds *via* successive [1,5] silicon shifts, the isoindene intermediate was successfully intercepted by tetracyanoethylene as the Diels-Alder adduct, **4.53** (Scheme 4.20).

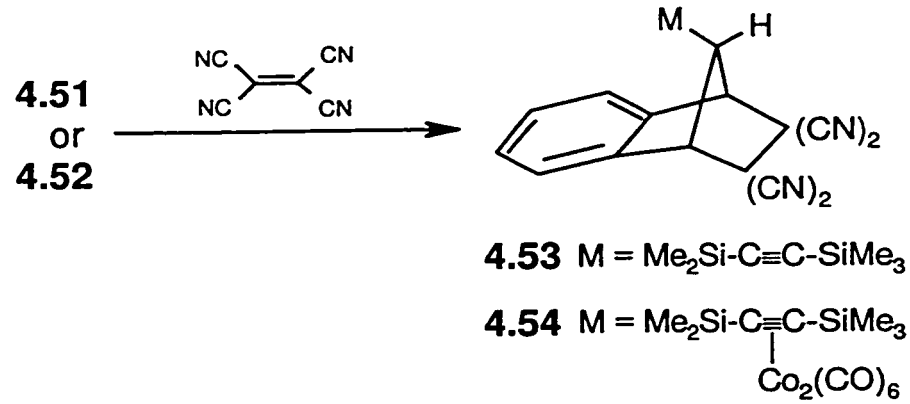

Scheme 4.20: *Generation of the cycloadducts,* ***4.53*** *and* ***4.54****, from the reaction of TCNE with* ***4.51*** *and* ***4.52****, respectively.*

The cobalt cluster, **4.52**, also exhibits fluxional behavior and the ^{1}H-^{1}H EXSY spectrum again reveals equilibration of the H(1) and H(3) protons within the five-membered ring, as well as between the aromatic proton pair, H(4) and H(7), and the diastereotopic methyl groups on silicon. At the elevated temperatures required for the single selective experiments (95 °C to 110 °C), the dimetallic compound, **4.52**, showed extensive decomposition and so a reliable value for $\Delta G^{\ddagger}$ cannot be quoted. However, under similar experimental conditions, the relative intensities of the off-diagonal signals in a series of ^{1}H-^{1}H EXSY spectra obtained for both **4.51** and **4.52** over a range of temperatures are remarkably similar, suggesting that the exchange rates, and thus the barriers to [1,5] silicon shifts, are essentially identical for these two systems. Assuming that the silicon center does in fact develop positive charge in the transition state, it is possible to conclude that the cobalt-mediated stabilization of this charge is rather small.[236]

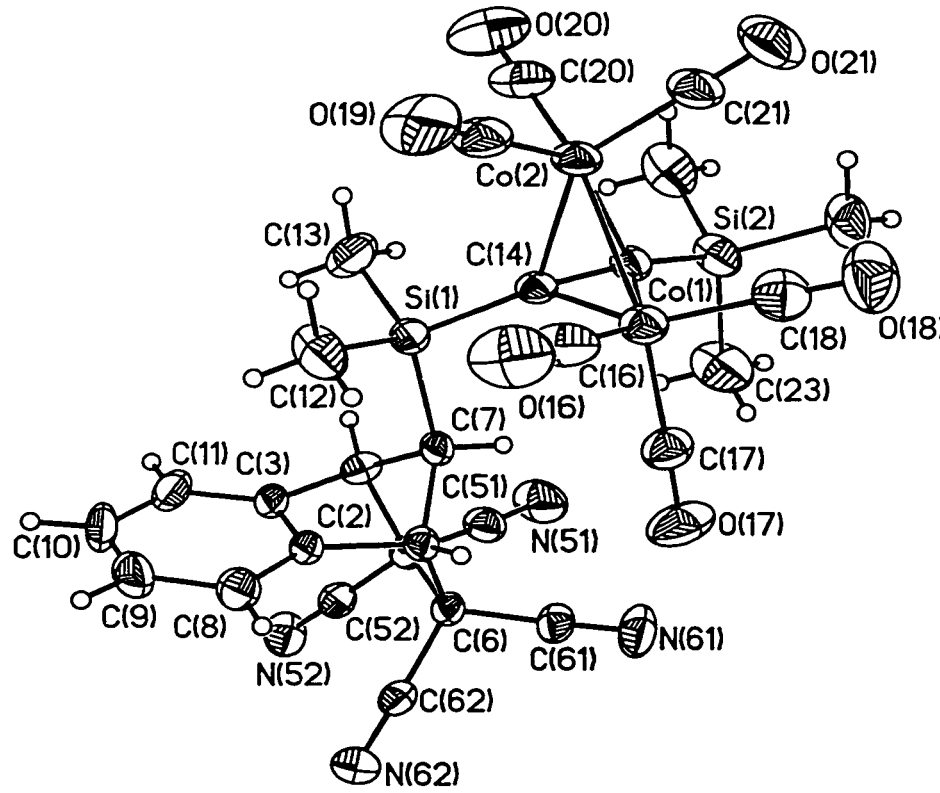

Figure 4.6: *The crystallographically determined structure of* ***4.54****, shown with 30% thermal ellipsoids.*

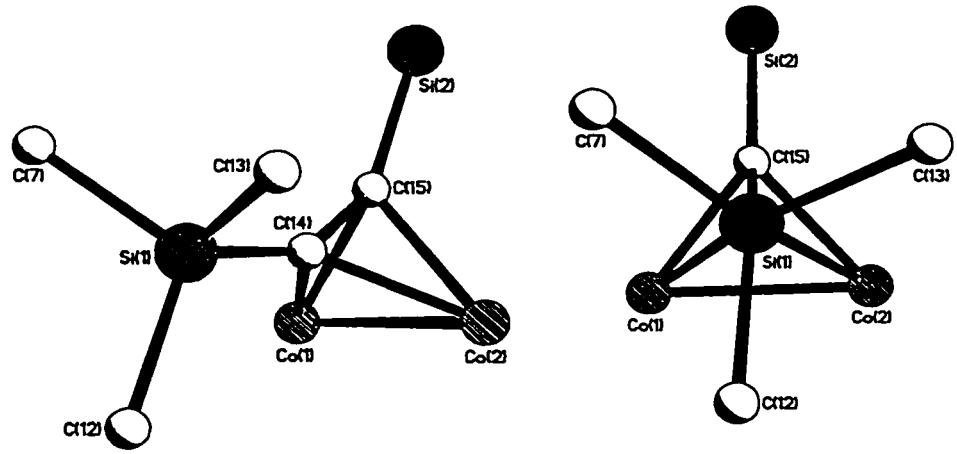

Figure 4.7: *Views of the* $SiMe_3[C_2Co_2]Si$ *core in* ***4.54****.*

As proof that the cobalt cluster complexed alkynyl-silane, **4.52**, does indeed undergo [1,5] silicon shifts *via* the corresponding isoindene, it was treated with TCNE and yielded the Diels-Alder adduct **4.54**, that was fully characterized spectroscopically and also by a single crystal X-ray diffraction study. The structure of **4.54** appears as Figure 4.6, and reveals that the dieneophile attacked the face opposite to that occupied by the Si_2Co_2 fragment, in the usual manner. Interestingly, the $Me_2Si(C{\equiv}C\text{-}SiMe_3)[Co_2(CO)_6]$ unit in **4.54** is oriented such that the molecule has no plane of symmetry, at least in the solid state. The geometric features of the benzonorbornyl fragment in this compound are generally quite similar to those previously found in related metalloisoindene-TCNE adducts, such as the trimethylsilylisoindene complex, **1.134**, and the iron cycloadduct, **2.2**. Figure 4.7 contains alternative views of the pseudo-tetrahedral dimetallic core in **4.54**; from these perspectives it is evident that the silyl cluster adopts a conformation which is comparable to that of a staggered ethane, such that unfavorable steric interactions between the trimethylsilyl substituent and the benzonorbornene framework are minimized.

The present data do not unambiguously demonstrate the delocalization of any positive charge built up on silicon during the migration process.[238] Based on the enhanced capacity of molybdenum clusters to alleviate positive charges, it is possible that the use of $(\eta^5\text{-}C_5H_5)Mo(CO)_2$ rather than $Co(CO)_3$ as the stabilizing center could lead to a reduced barrier to [1,5] silicon shifts. Moreover, to lower the migration barriers (and temperatures at which NMR measurements need to be made), it may be profitable to incorporate additional aromatic rings onto the indenyl skeleton, in a manner analogous to that previously described by McGlinchey and co-workers[196,197] for 1-trimethylsilylcyclopenta[*l*]phenanthrene, **4.19**.

4.3 Conclusions

In comparison to complexes comprising Group 13 or Group 15 elements, the role of substituents in determining the rate of [1,5] metalloid shifts in Group 14 cyclopentadienyls is considerably less important;[46] a similar scenario has been observed for the indenylsilane series. Indeed, the suprafacial [1,5] silicon shift process in these compounds has demonstrated

remarkable tolerance to derivatization, both on the indenyl skeleton and at the migrating silicon center.

During the pursuit of a sterically loaded indene, **4.22**, the conjugated dimeric compound, **4.24**, was unexpectedly generated; while a mechanism has been proposed in an attempt to rationalize the formation of this compound, conclusive experimental evidence is still lacking. Although the processes leading to **4.24**, and the ensuing chemistry of this compound are of considerable interest, such studies provide little insight into the factors affecting silicon migrations in indenylsilanes.

In continuation of work initiated over two decades ago, the impact of methyl substitution at indene on the rate of [1,5] silicon shifts was examined. Though the desired compound, **4.7**, had previously evaded isolation,[123] modest, yet important modifications to the synthetic protocol allowed for this synthesis of this compound to be realized. Additionally, the preparation of the crystallographically characterized η^6-$Cr(CO)_3$ derivative this compound, **4.38**, allowed the effect of complexing the indene C_6 ring to be examined. The dicobalt fragment in **4.52** was introduced adjacent to silicon in an attempt to reduce the barrier to [1,5] silicon shifts, *via* charge delocalization onto the dimetallic cluster. Collectively, these structural modifications provided a means of probing the consequences of sterically and electronically perturbing the indenylsilane system.

All of the aforemented complexes were found to exhibit quasi-fluxional behavior, as evidenced by 2D-EXSY experiments. With the exception of the dimetallic complex, **4.52**, single selective inversion NMR experiments provided a means of quantifying the barriers associated with these dynamic processes. In the majority of cases, successful Diels-Alder trapping with tetracyanoethylene yielded experimental evidence in support of the intermediacy of isoindenes in these rearrangements; crystallographic data was obtained for the cycloadducts, **4.34** and **4.54**, which are derived from the indenes, **4.7** and **4.52**, respectively.

Table 4.3. Summary of the Experimentally Determined Barriers to [1,5] Silicon Shifts for the 1-Indenylsilanes Examined in this Thesis

Compound Number	Migrating Fragment	Migratory Barrier $\Delta G^{\ddagger}$ (kcal mol^{-1})
3.18	$(\sigma\text{-}C_9H_7)_2SiMe$	24 ± 0.5
3.19	$(\sigma\text{-}C_9H_7)_2SiC_3H_5$	25 ± 2
3.20	$(\sigma\text{-}C_9H_7)_2SiH$	24 ± 1
4.7	$SiMe_3$	23 ± 1
4.38	$SiMe_3$	24 ± 1
4.51	$SiMe_3C{\equiv}CSiMe_2$	24 ± 2

Remarkably, the steric and electronic demands of the organic and organometallic fragments incorporated into these indenysilanes proved to be inconsequential with respect to the [1,5] silicon shift processes in these complexes; Table 4.3 summarizes the experimentally determined migration barriers associated with the indenylsilanes examined as part of this thesis study. These thermodynamic data clearly indicate that none of the aforementioned structural modifications leads to a statistically significant reduction in the barrier to silicon shifts in indenylsilanes. Athough these results are surprising, they underscore the remarkable flexibility of the indenylsilane system, and imply that the [1,5] silicon shift process in such compounds can be advantageously utilized, even in highly functionalized organometallic systems.

CHAPTER FIVE

Towards Metalloisoindene-Mediated Intramolecular Diels-Alder Reactions

5.1 Introduction

The Diels-Alder [4+2] cycloaddition is truly one of the most synthetically useful reactions available to organic chemists. In the case of the intramolecular Diels-Alder (IMDA) reaction, in which the dienophile is tethered to the diene unit, two new ring structures are formed upon cyclization; of the two possible regiochemical modes of addition, the one leading to the fused product usually predominates over the alternative pathway in which a bridged species is generated (Scheme 5.1). The ability to construct two rings in a single synthetic step has led to the use of IMDA reactions in the preparation of polycyclic compounds, including many natural products.[239]

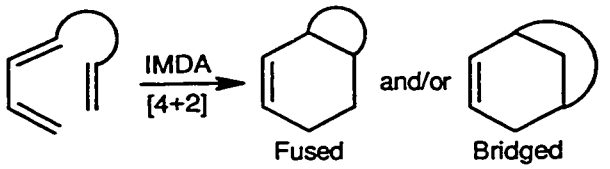

Scheme 5.1: *The intramolecular Diels-Alder (IMDA) reaction.*

Transition metal-mediated cyclization reactions have also gained considerable attention in recent years, since these methods often allow for several carbon-carbon connections to be formed under synthetically mild conditions and with high selectivity.[240] Pioneering studies in this area were conducted by Funk and Vollhardt,[241] who exploited $(\eta^5\text{-}C_5H_5)Co(CO)_2$-catalyzed alkyne cyclizations in the total synthesis of a series of racemic steroids, including *dl*-estrone. The key step in these cobalt-mediated processes involves the generation of an appropriately functionalized *ortho*-xylylene intermediate, such as **5.1**, which can then react *via* an IMDA reaction to give the desired polycyclic product; a typical example is provided in Scheme 5.2. More recently, Malacria and co-workers[242] presented a metal-mediated cyclization reaction in which six carbon-carbon

bonds and four rings were stereoselectively formed in a one-pot sequence. The inclusion of elements such as silicon[243] and boron[244] into the dienophilic tether in such IMDA reactions has recently provided a means of generating novel heteroatom-containing polycyclic compounds.

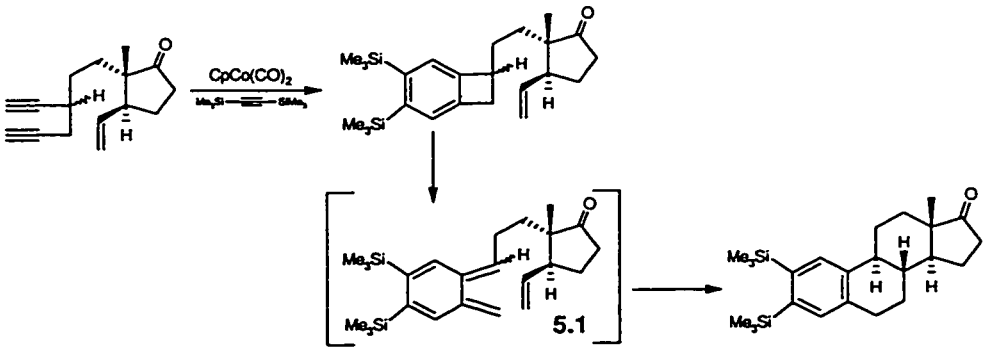

Scheme 5.2: *The cobalt-mediated generation and IMDA trapping of the ortho-xylylene,* ***5.1****.*

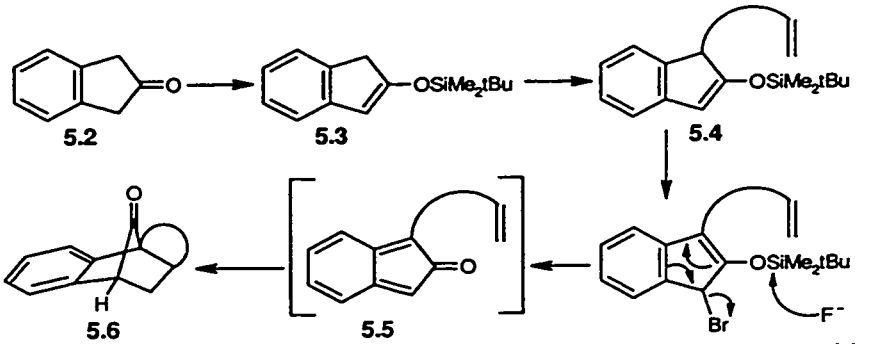

Scheme 5.3: *Intramolecular trapping of an isoindenone, leading to the adduct,* ***5.6****.*

Whereas the *ortho*-xylylene synthon has been extensively employed in organic synthesis, the corresponding isoindene has received considerably less attention; the inherent difficulty in utilizing isoindenes in synthetic applications was described in Section 4.1. Nonetheless, Padwa *et al.*[245] have successfully exploited the photosensitized triplet reactions of 1-allylindenes as a means of preparing benzotricyclo[3.3.0.$0^{2,7}$]octanes by way of an intramolecular [2+2] cycloaddition pathway. More recently, Jones and Ryder[246] published a report in which the generation and intramolecular trapping of isoindenones was examined (Scheme 5.3). Starting from 2-indanone, **5.2**, treatment with base followed by quenching with ^{t}BuMe$_2$SiCl generates the silyl enol ether, **5.3**, to which was introduced a tethered olefin, as in **5.4**; bromination, followed by desilylation with CsF presumably generates the intermediate isoindenone, **5.5**, which was subsequently trapped in an

IMDA reaction, producing **5.6**. While the synthetic utility of an isoindenone generated *in situ* is appealing, the low-yield conversion (< 25%) of **5.2** into **5.6** suggests that this is not an efficient route to such complexes.

5.2 Results and Discussion

Given the ease with which metalloisoindene intermediates participate in intermolecular cycloadditions, the preparation of indenylsilanes possessing the capacity for intramolecular cyclizations was undertaken. The required dienophilic chain can be built into the indenylsilane architecture in numerous ways; three approaches are depicted in Scheme 5.4. Precursors similar to **5.7** are comprised of a C(1) alkylated indene, to which a migrating metal(loid) fragment has been added; **5.8** is identical to **5.7**, with the exception that the tethered dienophile is attached at the C(2) position. In **5.9**, the dienophile is instead linked to the migrating center itself, such that the [1,5] metallotropic shift is followed by an IMDA reaction involving one of the metalloid substituents. These three classes of reactions are complementary, as each leads to a unique benzonorbornene product upon cyclization. Preliminary synthetic efforts were directed at the development of silicon analogues of **5.7**.

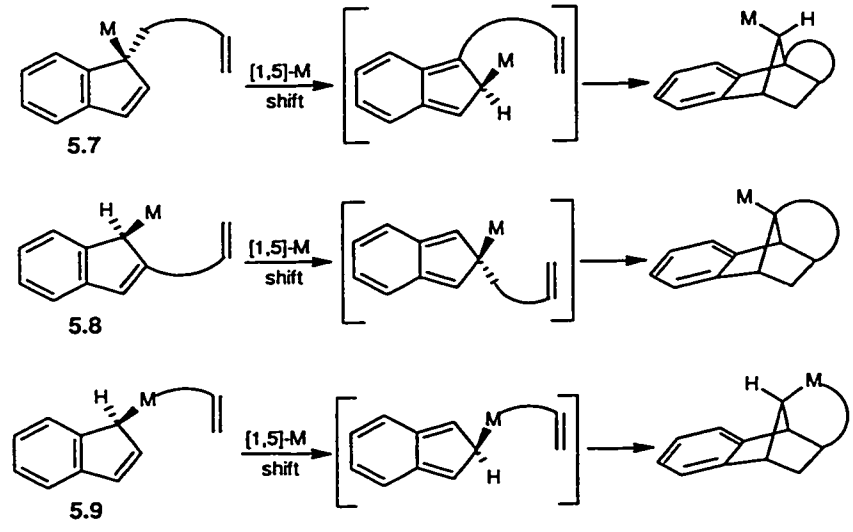

Scheme 5.4: *Some possible options for incorporating a tethered dienophile into a metalloindene framework.*

Starting from 1-trimethylsilylindene, the C_5 dienophilic tether in **5.10** was introduced *via* addition of base, followed by quenching with 5-bromopent-1-ene. The identity of the purified compound was ascertained in the usual manner by use of standard physical and spectroscopic techniques, and revealed an sp^3-bonded C(1)-silicon group and a C(3)-bound tether, as depicted in Scheme 5.5; isomers derived from **5.10** (including **5.12**) were not observed during these studies, suggesting that the 1,3-disubstituted indene predominates in this system. These findings parallel observations made by Davison and Rakita, who noted that (3-methylindenyl)trimethylsilane, **4.1**, shows no tendency to isomerize to the corresponding 1,1-isomer, **4.5** (Scheme 4.1).[123] It is anticipated that the facile interconversion of such 1,1- and 1,3-disubstituted isomers (**5.10** and **5.12**, respectively) would be mandatory in order to make available the required isoindene intermediate, **5.11**, for the desired intramolecular cyclization. Even after heating **5.10** for 5 days at 180 °C, neither cyclization nor isomerization products were detected.

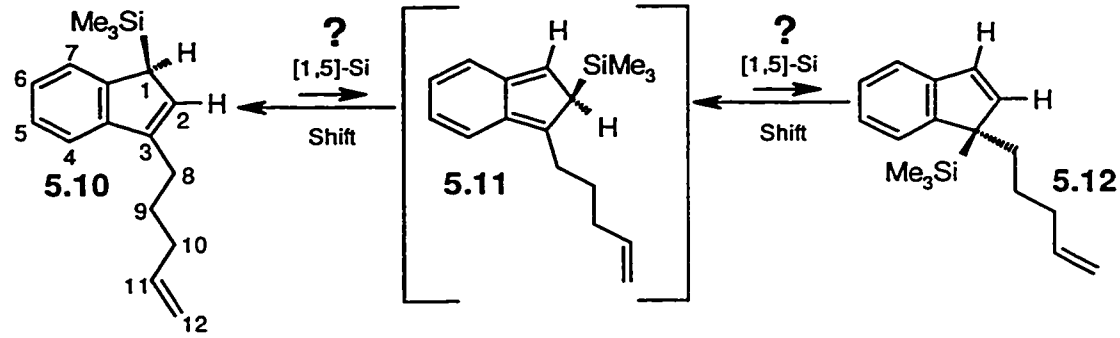

Scheme 5.5: *Preferential formation of the 1,3-disubstituted isomer,* ***5.10****.*

It is evident from the examination of **5.10** that the successful preparation of a quasi-fluxional indenylsilane, analogous to **5.7**, requires that the steric character of the C(1) and C(3) sites in these molecules be similar. Encouraged by the dynamic behavior of the dimethylindenylsilane, **4.7**, and its propensity for intermolecular cycloadditions with tetracyanoethylene (leading to **4.34**), the preparation of a C(1)-methylated derivative of **5.10**, was undertaken (Scheme 5.6). Treatment of 3-methyl-1-indanone, **5.13**, with the Grignard reagent derived from 6-bromopent-1-ene, followed by sulfuric acid workup yielded the dialkylindene, **5.14**,

which was purified and characterized. Subsequent lithiation of **5.14**, followed by the addition of chlorotrimethylsilane generated a mixture of **5.15** and **5.17** (~ 2:1); this latter mixture was extensively examined by use of ^{1}H, ^{13}C and ^{29}Si multidimensional NMR techniques.

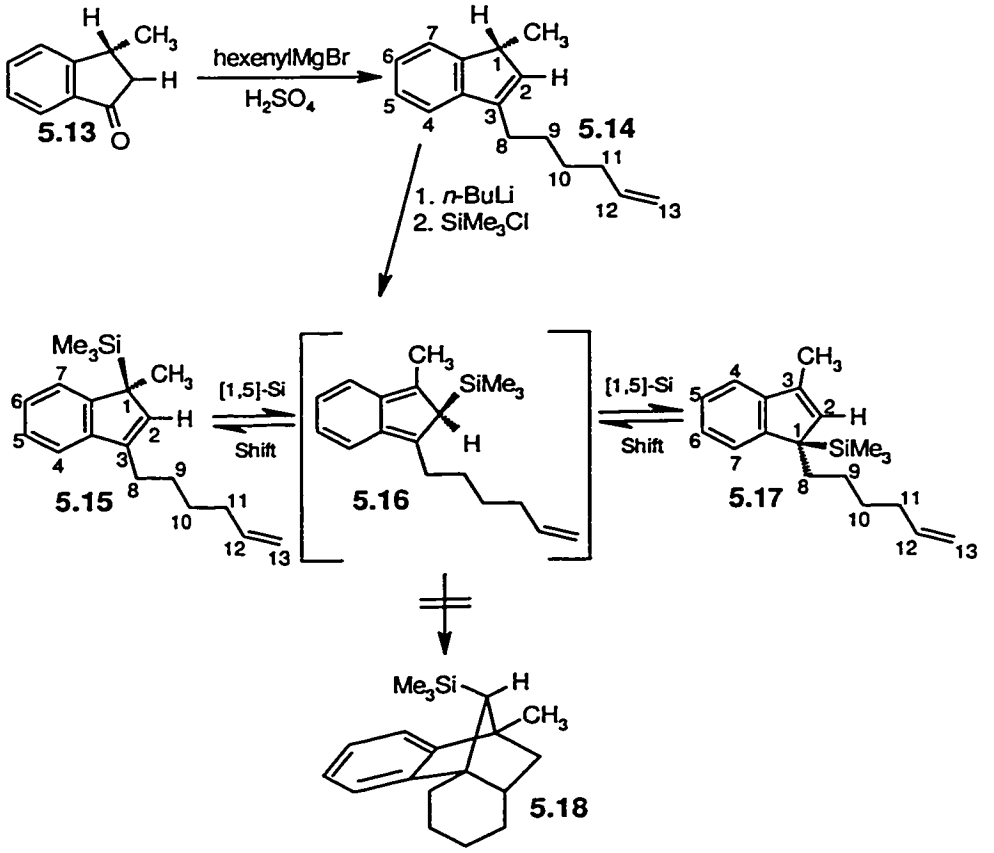

Scheme 5.6: *The synthesis and molecular dynamics of **5.15** and **5.17**.*

The observation that both **5.15** and **5.17** are generated during this synthetic process suggests that they are of comparable stability, assuming that the reaction is carried out under thermodynamically controlled conditions. As such, the interconversion of **5.15** and **5.17** *via* the isoindene, **5.16**, appeared likely, and the operation of such a rearrangement process was probed by use of 2D-EXSY techniques; a portion of the ^{1}H-^{1}H EXSY spectrum obtained from a mixture of these indenylsilanes dissolved in toluene-d_8 is provided in Figure 5.1. Off-diagonal peaks correlating the C(1)-CH_3 hydrogen atoms in **5.15** ($\delta^{1}H$ ~ 1.25 ppm; ~ 1.42 ppm in $CDCl_3$) with those of the C(3)-CH_3 group in **5.17** ($\delta^{1}H$ ~ 2.00 ppm; ~ 2.18 ppm in $CDCl_3$) are consistent with an

overall C(1) to C(3) transition of the trimethylsilyl fragment; similar correlations are observed between the C(11)H_2 sites **5.15** (δ^1H ~ 1.93 ppm; ~ 2.10 ppm in $CDCl_3$) and **5.17** (δ^1H ~ 1.71 ppm; ~ 1.87 ppm in $CDCl_3$).

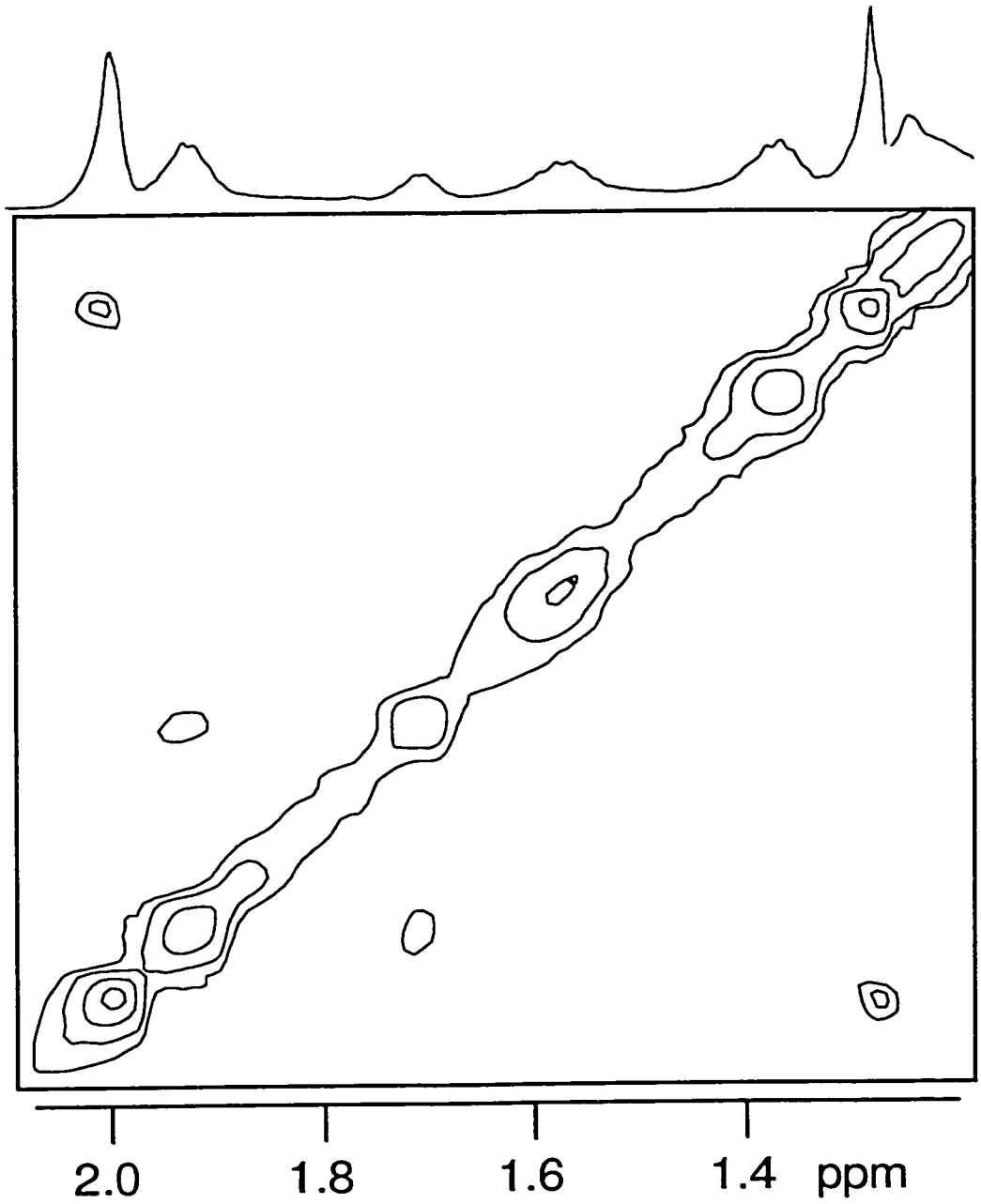

Figure 5.1: *A portion of the ^1H-^1H EXSY spectrum obtained from a mixture of **5.15** and **5.17** dissolved in toluene-d_8, showing the interconversion of these isomers.*

Having unequivocally established that mixtures of **5.15** and **5.17** are quasi-fluxional, the thermal conversion of these complexes into the desired cyclization product, **5.18**, was attempted. After heating sealed tetrachloroethane-d_2 solutions of **5.15** and **5.17**, and even **5.14**, for extended periods of time (180 °C, 3 weeks), the generation of cyclization products, such as **5.18**, could not be detected by use of NMR spectroscopy. Since the interconversion of **5.15** and **5.17**, can best be rationalized as proceeding *via* the isoindene, **5.16**, the absence of cycloaddition products can be attributed to the failure of the dienophilic fragment to intramolecularly capture this isoindene intermediate. In the case of the isoindenone, **5.5**, a simple olefin is successful in trapping this species. However, in contrast to the isoindene, **5.16**, no efficient isomerization pathway exists for **5.5**, and so it persists for a sufficiently long time so as to be trapped by the unactivated dienophile. In the case of **4.33** (Scheme 4.11), the dimethylisoindene analogue of **5.16**, it was demonstrated that an electron-poor olefin (TCNE) is capable of intercepting **4.33** before it has the opportunity to isomerize to the corresponding indenylsilane, **4.7**.

5.3 Conclusions

The preliminary reactivity studies presented herein reveal that while a quasi-fluxional indenylsilane system containing a tethered olefinic fragment can be synthesized, the incorporation of an unactivated dienophile in these systems does not lead to the generation of intramolecular cycloaddition products. It is apparent that in order to facilitate such a silicon-mediated IMDA cyclization, the **5.15**-**5.17** molecular system may require the introduction of electron-withdrawing groups to the termini of the olefinic tethers in these compounds, in keeping with the "inverse electron demand" principle;[247] this concept is depicted in Scheme 5.7. Two reaction pathways are available to a given olefin-tethered metalloisoindene (**5.19**) – isomerization to the corresponding indene, **5.20**, and IMDA cyclization to yield **5.21**; the path chosen will depend on the relative magnitudes of the barriers associated with each of these processes. In the case of an isoindene bearing an unreactive tethered olefin (L = electron-donating group), the barrier to the IMDA

cyclization process (**A**) is large in comparison to the barrier required for isomerization to the indene (**B**). In contrast, when electron-withdrawing substituents are present on the linked dienophile (for example, L = CN) the activation energy associated with the IMDA pathway (**C**) may be decreased to such an extent (**C** < **B**) that the intramolecular cycloaddition is favored, leading to the adduct, **5.21**.

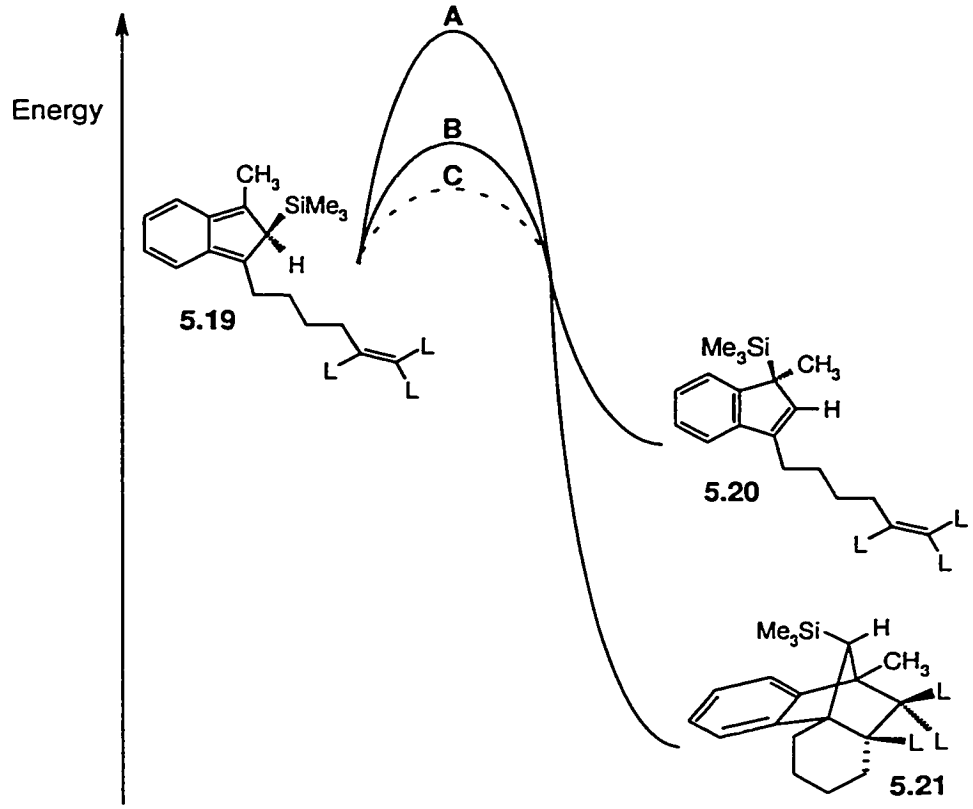

Scheme 5.7: *A qualitative reaction coordinate diagram, in which the isoindene,* ***5.19****, can either isomerize to the indene,* ***5.20****, or undergo an IMDA cyclization, leading to* ***5.21****.*

CHAPTER SIX

Future Work

6.1 Reexamining the Molecular Dynamics of σ-Indenyl Transition Metal Complexes

With the quasi-fluxional nature of $(\eta^5\text{-}C_5H_5)Fe(CO)_2(\eta^1\text{-}C_9H_7)$, **1.9**, revealed, a number of other reports of stereochemically non-rigid σ-indenyl transition metal complexes, including those pertaining to the indenylrhenium complexes, **1.31** and **1.39**,[84,87] merit further study; these were assumed to involve [1,3] shifts, and no attempts were made to intercept metalloisoindene intermediates (Scheme 6.1). Moreover, the molecular dynamics and cycloaddition chemistry of the higher poly(η^1-indenyl) transition metal complexes are also worthy of investigation. In addition to providing insight into the [1,5] metallotropic shift process, the corresponding metal-centered multiple Diels-Alder cycloadducts could exhibit interesting reactivity, due to the steric demands of the ancillary benzonorbornyl ligands.

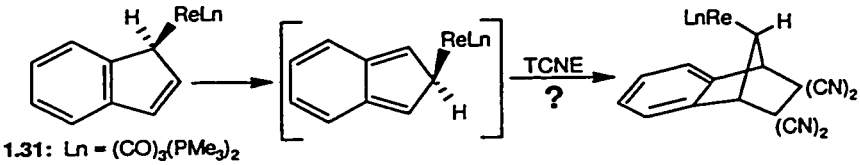

1.31: Ln = $(CO)_3(PMe_3)_2$
1.39: Ln = O_3

Scheme 6.1: *Diels-Alder trapping of metalloisoindenes.*

6.2 Tetracyanoethylene Cycloadditions: Probing for Indenylsilane Radicals

The trapping of metalloisoindenes as the corresponding [4+2] cycloadducts has provided support for the operation of [1,5] shifts in transition metal and main group σ-indenyl complexes;[121,122] tetracyanoethylene has proved to be an extremely effective dienophile in this regard. However, despite the fact that the deeply colored solutions observed upon treatment of a metalloindene with tetracyanoethylene can be interpreted in terms of the formation of a charge-transfer complex, no study of these intermediate species has been undertaken. In light of the fact

that these charge-transfer complexes may serve as important intermediates along the Diels-Alder cycloaddition reaction pathway, an examination of these species is warranted. Initial work in this area could include efforts to characterize the metalloindenyl radical cation, by use of electron paramagnetic resonance (EPR) spectroscopy (Scheme 6.2). The tetracyanoethylene radical anion is well-documented and its signals could readily be subtracted from the EPR spectrum of the complex, making the spectral peaks attributable to the indenyl species more easily discernible.

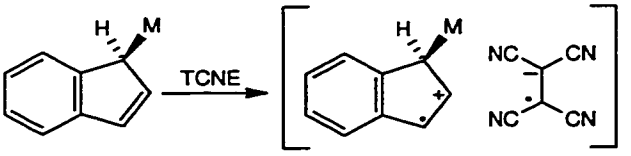

Scheme 6.2: *The generation of a metalloindene-TCNE charge-transfer complex.*

6.3 Promoting the Formation of Isoindene Intermediates

The few studies pertaining to the preparation and characterization of boron and phosphorus σ-indenyl complexes reveal that these often prefer vinylic, rather than allylic coordination, a tendency which may prove useful in the pursuit of stabilized isoindenes. The introduction of two such substituents to the indenyl framework would invariably lead to the generation of a C(1) and C(3) disubstituted indene, in which one fragment unfavorably resides at an sp^3-position. The subsequent introduction of a trialkylsilyl group, which exhibits a propensity to coordinate to the C(1) center on indene, could lead to a system which, after a [1,5] silicon shift, produces an isoindene that is stabilized by the sp^3 to sp^2 hybridization change at the formerly C(1) carbon.

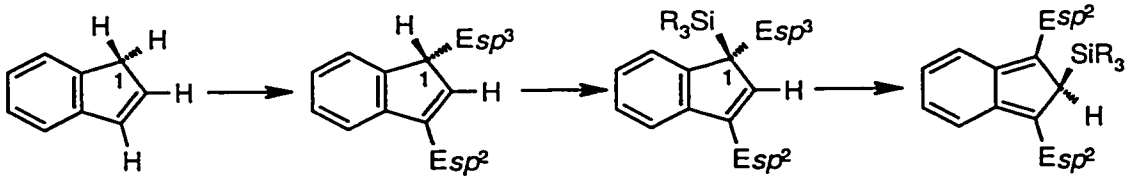

Scheme 6.3: *The generation of a stabilized metalloisoindene; "E" is a Group 13 or Group 15 based fragment.*

6.4 Extending the Chemistry of Tris(σ-indenyl)silanes and Their Cycloadducts

Although organometallic derivatives of mono- and bis-indenyl complexes have been examined, the metallation of tris(σ-indenyl) species remains unexplored. As alluded to in the forgoing sections, trifunctional indenyl compounds of this type could provide a facile route to polymetallic *ansa*-metallocene catalyst precursors. The main group center may also provide a point of attachment to a transition metal fragment, as in the tris(σ-indenyl)phosphine complex depicted in Scheme 6.4. Such polymetallic complexes, in which the metal centers possess markedly different electron counts, are thought to be attractive synthetic targets in that the metals have the potential to interact in a simultaneous and cooperative fashion in the activation of organic substrates.[248]

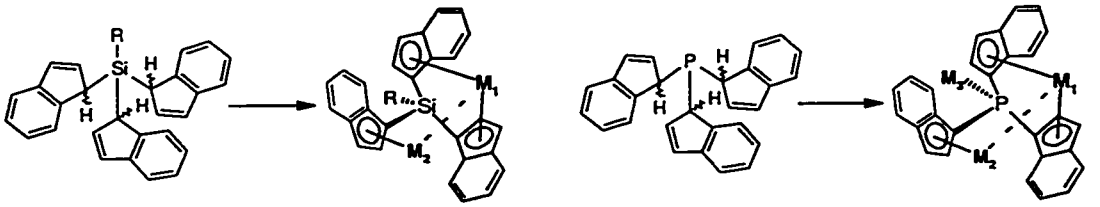

Scheme 6.4: *The preparation of polymetallic complexes derived from tris(σ-indenyl) main group compounds.*

The preliminary reactivity studies presented herein have demonstrated that the silicon center in tris(benzonorbornyl)silanes can be functionalized under suitably chosen reaction conditions. As such, it would be intriguing to examine the reactivity of such compounds with alcohols, and with ketones possessing enolizable protons (Scheme 6.5). Indeed, the steric demands of the polycyclic ligands in this class of compounds may allow for their use as protecting groups in organic chemistry.

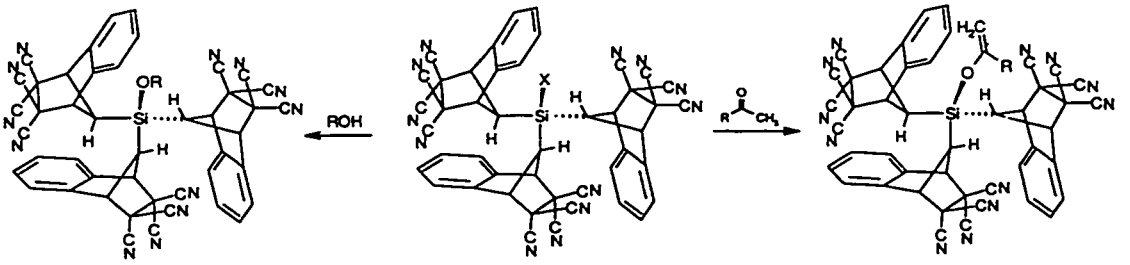

Scheme 6.5: *Tris(benzonorbornyl)silanes functioning as organic protecting groups.*

6.5 Developing Systems Capable of Intramolecular Cyclizations

The synthesis of polycyclic organic architectures *via* intramolecular Diels-Alder trapping of an isoindene remains an appealing goal. Although the synthesis of a quasi-fluxional metalloindene equipped with a tethered olefin has been realized (**5.15-5.17**), the failure of the latter fragment to participate as a dienophile in intramolecular [4+2] cycloadditions can likely be attributed to the absence of activating substituents on this olefin. As such, the incorporation of a tethered dienophile bearing electron-withdrawing cyano groups represents a logical progression in this work, one which may be brought about by using the synthetic approach depicted in Scheme 6.6. Starting from an ethylene glycol-protected bromopentanone, introduction of the indenyl skeleton could be carried out by use of standard Grignard chemistry involving 3-methylindan-1-one. Subsequent conversion of the deprotected ketone to the dicyanoethylene, followed by the addition of a migratory group ("M"), such as $SiMe_3$ or $(\eta^5\text{-}C_5H_5)Fe(CO)_2$, completes the synthesis of the indenyl precursor; a [1,5] metallotropic shift then uncovers the masked isoindene synthon, which is intramolecularly trapped by the dienophile.

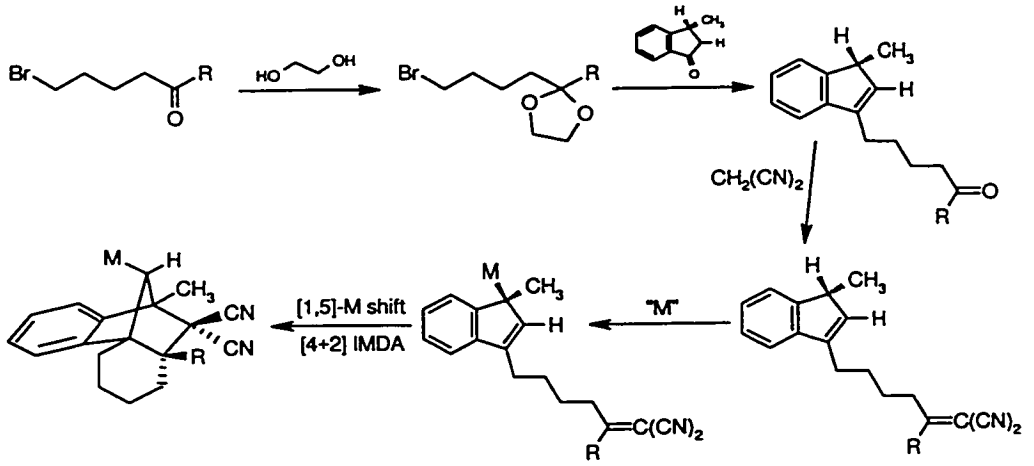

Scheme 6.6: *Proposed synthetic route to polycyclic organic compounds via metalloindenes.*

CHAPTER SEVEN

Experimental Work

7.1 General

All reactions were carried out under an atmosphere of dry nitrogen in oven-dried glassware, using freshly distilled solvents that were purified according to standard procedures. Unless otherwise stated, reagents were obtained from the Aldrich Chemical Company, Inc. and used as received; hexacarbonylchromium and octacarbonyldicobalt were purchased from Strem Chemical, Inc., and deuterated NMR solvents were obtained from Cambridge Isotope Laboratories, Inc. and used as received. Mass spectrometric data were obtained by use of a VG Analytical ZAB-SE spectrometer. Infrared spectra were obtained from liquid samples on a Bio-Rad FTS-40 FT-IR spectrometer using 0.1 mm NaCl windows. Melting points were measured in open glass capillaries using a Thomas Hoover Unimelt capillary melting point apparatus. Microanalyses were performed by Guelph Chemical Laboratories (Guelph, Ontario, Canada).

7.2 NMR Spectroscopy

One-dimensional NMR spectroscopic data were recorded using either a Bruker AC-200, Bruker AC-300 or Bruker Avance DRX-500 spectrometer. In all cases, NMR spectra were obtained from samples dissolved in deuterated solvents, with NMR signals referenced internally to tetramethylsilane (^{1}H, ^{13}C and ^{29}Si NMR spectra) or externally to trichlorofluoromethane (^{19}F NMR spectra). Except where noted, two-dimensional NMR experiments were conducted on the DRX-500 instrument, equipped with an 11.74 T superconducting magnet, a Bruker B-VT 2000 temperature controller, and a 5 mm multinuclear inverse probe possessing 3-axis gradient capabilities. These experiments consisted of ^{1}H-^{1}H COSY, ^{1}H-^{13}C HSQC, ^{1}H-^{13}C HMBC, ^{1}H-^{1}H EXSY and ^{1}H-^{29}Si HMBC experiments, the latter two are described in the following sections.

Sample temperatures were set and maintained throughout the course of these studies by use of the temperature controller, and externally calibrated by placing a copper-constantan thermocouple, contained within an NMR tube, into the probe. Using this procedure, absolute temperatures were measured and maintained within ± 1 °C.

7.2.1 ^{1}H-^{29}Si Multiple-Bond Correlation (^{1}H-^{29}Si HMBC) Experiments

In a typical ^{1}H-^{29}Si HMBC experiment, the ^{29}Si spectral width was 5531.0 Hz with 2048 data points, zero filled to 4096. The ^{1}H spectral width was 5952.4 Hz with 256 time increments and 64 scans per increment. A relaxation delay of 2 s between scans was employed. Values of $^{1}J_{Si\text{-}H}$ = 224 Hz, and $^{2}J_{Si\text{-}H}$ = 6.7 Hz, were used to calculate Δ_1 and Δ_2 [$\Delta_1 = 1/[2(^{1}J_{Si\text{-}H})]$ and $\Delta_2 = 1/[2(^{2}J_{Si\text{-}H})]$.

7.2.2 ^{1}H-^{1}H EXSY (EXchange SpectroscopY) Experiments

Two-dimensional ^{1}H-^{1}H EXSY spectra[8] were recorded in the phase-sensitive mode, using the 90° - t_1 - 90° - t_m - 90° - ACQ pulse sequence. In a typical experiment, 512 FID's were recorded in the f_2 dimension, with each FID acquired in 16 scans. These FID data were subsequently Fourier transformed using Gaussian window functions in both f_1 and f_2, with line broadening set to 3.0 Hz.

For the tris(σ-indenyl)silanes, **3.18**, **3.19** and **3.20**, ^{1}H-^{1}H EXSY data were obtained on a Bruker AC-300 spectrometer equipped with a 7.65 T superconducting magnet and a 5 mm QNP probe. All experiments were carried out in perdeuterated toluene between 102 °C and 108 °C, with mixing times ranging from 0.5 s to 2.7 s and the initial value of the 2D evolution set to 10 μs.; for tris(σ-indenyl)methylsilane, **3.18**, and tris(σ-indenyl)silane, **3.20**, the relaxation delay was set to 2.7 s, while for tris(σ-indenyl)allylsilane, **3.19**, a value of 1.0 s was employed.

Two-dimensional ^{1}H-^{1}H EXSY spectra for $(\eta^5\text{-}C_5H_5)Fe(CO)_2(\eta^1\text{-}C_9H_7)$, **1.9**, the dimethylindenylsilane, **4.7**, the chromium complex, **4.38**, the alkynylsilane, **4.51**, the dimetallic silane, **4.52**, and the **5.15-5.17** system were acquired on a Bruker Avance DRX-500 spectrometer. For **1.9**, spectral data were obtained from samples dissolved in perdeuterocyclohexane at 45 °C, using mixing times between 1.0 and 5.0 s, while for **4.7** and **4.38**, tetrachloroethane-d_2 was

employed as the solvent, and experiments were conducted at 105 °C, with mixing times ranging from 0.3 s to 1.5 s. For **4.51** and **4.52**, toluene-d_8 solutions were examined at 72 °C, using mixing times between 2.0 and 5.0 s, while for **5.15-5.17** the same solvent was employed and data were acquired at 90 °C, using mixing times between 3.0 and 5.0 s. In all of these 2D-EXSY experiments, the relaxation delay and the initial value for the 2D evolution, were set to 1.0 s and 10 μs, respectively.

7.2.3 Single Selective Inversion NMR Experiments

All kinetic data were obtained in the slow exchange regime by use of ^{1}H selective inversion NMR experiments,[14,15] in which one signal in the spectrum was perturbed using a 90 - τ - 90 pulse sequence, and then the return to equilibrium of this and the other signals involved in the chemical exchange process were monitored as a function of time, as in an inversion-recovery T_1 experiment. These experiments were conducted on a Bruker AC-300 spectrometer, equipped with a 7.65 T superconducting magnet, a Bruker B-VT 2000 temperature controller and a 5 mm QNP probe. Spectral data were obtained between 95 °C and 110 °C, with the exception of (η^5-C_5H_5)Fe(CO)$_2$(η^1-C_9H_7), **1.9**, for which data were collected at temperatures ranging from 45 °C to 65 °C. Non-linear least-squares fitting of the experimental data was performed using a C programming language version of the SIFIT program provided by McClung, and permitted the extraction of rate data. Analysis of these temperature-dependent rates using Eyring theory allowed for an estimate of the free energy of activation, $\Delta G^{\ddagger}$, associated with the dynamic process (Section 1.2.5); in all cases $\Delta G^{\ddagger}$ is reported at 303 K.

7.3 X-Ray Crystallography

X-Ray crystallographic data were collected from single crystal samples, which were mounted on a glass fiber. For **1.134**, diffraction data were collected on a Rigaku AFC6R diffractometer, equipped with a rotating anode and using graphite-monochromated Cu Kα radiation (λ = 1.54178 Å). Three standard reflections that were measured after every 97 reflections showed

neither instrument instability nor crystal decay; an empirical ψ-scan absorption correction was applied to these diffraction data. For all other compounds, single crystal diffraction experiments were carried out by use of a P4 Siemens diffractometer, equipped with a Siemens SMART 1K Charge-Coupled Device (CCD) Area Detector (using the program SMART) and a rotating anode using graphite-monochromated Mo-Kα radiation (λ = 0.71073 Å). The crystal-to-detector distance was 3.991 cm, and the data collection was carried out in 512 x 512 pixel mode, utilizing 2 x 2 pixel binning. The initial unit cell parameters were determined by a least-squares fit of the angular settings of the strong reflections, collected by a 4.5 degree scan in 15 frames over three different parts of reciprocal space (45 frames total). One complete hemisphere of data was collected, to better than 0.8 Å resolution. Upon completion of the data collection, the first 50 frames were recollected in order to improve the decay corrections analysis (if required). Processing was carried out by use of the program SAINT, which applied Lorentz and polarization corrections to three-dimensionally integrated diffraction spots. The program SADABS was utilized for the scaling of diffraction data, the application of a decay correction, and an empirical absorption correction based on redundant reflections. All structures were solved by using the direct methods procedure in the Siemens SHELXTL program library. Refinement was carried out by using full-matrix least squares methods with anisotropic thermal parameters for all non-hydrogen atoms. Unless stated, hydrogen atoms were added at calculated positions and refined using a riding model with isotropic displacement parameters equal to 1.2 times the equivalent isotropic displacement parameter of the attached carbon.[249-252]

In the case of $(\eta^5\text{-}C_5H_5)Fe(CO)_2(\eta^1\text{-}C_9H_7)$, **1.9**, two independent molecules were found in the asymmetric unit; two independent molecules (of absolute configuration *RRS* and *SSR*) were also located in the asymmetric unit of **3.20**. That the two enantiomers of **3.20** were truly independent and not related by a crystallographic inversion centre was verified externally by sending the crystallographic information file (CIF) through the automated checking program, CHECKCIF, made available by Acta Crystallographica (The International Union of

Crystallography), which failed to detect any missing crystallographic inversion centre. The final refined value of the absolute structure parameter (0.2) supported the absolute configurations chosen. The hydrogen atoms bound directly to silicon were found in the electron difference map and refined isotropically.

The final refined structure of **3.22** was based on a disordered model in which the allyl group could exist in one of two conformations. From the observed thermal displacement ellipsoids it was apparent that only the positions of the three allyl carbon atoms were affected by this disorder. The occupancy of the two conformations was allowed to refine as a free variable (final ratio of approximately 60:40) and then hydrogen atoms for each unique component of the disorder were added at calculated positions, and allowed to refine based on the carbon atoms to which they were attached. In the case of **3.24(CH_3COCH_3)$_2$**, no unusually close contacts exist between the primary complex and the two solvated acetone molecules were found in the asymmetric unit.

7.4 Syntheses and Characterization of Compounds

(η^5-C_5H_5)Fe(CO)$_2$(η^1-C_9H_7), 1.9. This compound was prepared following the approach initially described by Cotton and co-workers.[39] ^{1}H NMR (C_6D_{12}, 500 MHz): δ 7.49 (m, 1H, H(7)), 7.28 (m, 1H, H(4)), 6.98 (m, 1H, H(6)), 6.97 (m, 1H, H(5)), 6.64 (m, 1H, H(2)), 6.49 (m, 1H, H(3)), 3.98 (s, 5H, Cp), 3.85 (m, 1H, H(1)); ^{13}C NMR (C_6D_{12}, 125 MHz): δ 217.4 (C≡O), 216.6 (C≡O), 157.6 (C(3a)), 148.2 (C(2)), 141.8 (C(7a)), 124.1 (C(7)), 123.9 (C(6)), 123.6 (C(5)), 121.7 (C(4)), 120.8 (C(3)), 87.1 (Cp), 26.8 (C(1)).

Trapping of (trimethylsilyl)isoindene with tetracyanoethylene, 1.134. This compound was prepared using methods described by Ashe.[122] Complete assignments of the high field ^{1}H, ^{13}C and ^{29}Si NMR spectra of this compound had not been published prior to this study. ^{1}H NMR ($CDCl_3$, 300 MHz): δ 7.53-7.48 (m, 2H, H(8) and H(11)), 7.47-7.42 (m, 2H, H(9) and H(10)), 4.29 (d,

^3J = 1.05 Hz, 2H, H(1) and H(4)), 2.09 (t, ^3J = 1.05 Hz, 1H, H(7)), -0.21 (s, 9H, $SiMe_3$); ^{13}C NMR ($CDCl_3$, 125 MHz): δ 138.4 (C(2) and C(3)), 130.6 (C(9) and C(10)), 124.9 (C(8) and C(11)), 110.2, 112.3 (*exo* and *endo* nitriles), 60.5 (C(1) and C(4)), 50.3 (C(5) and C(6)), 49.8 (C(7), -2.0 ($SiMe_3$); ^{29}Si NMR (CH_2Cl_2, 99.35 MHz): δ 1.9; IR ($CDCl_3$, cm^{-1}): 3085 w, 3032 m, 2959 vs, 2901 m, 2860 sh, 1984 m, 1943 m; Mass spectra: (DEI, *m/z* (%)): 301 (11, $[M\text{-}CH_3]^+$), 188 (20, $[C_{12}H_{16}Si]^+$), 173 (13, $[C_{11}H_{15}Si]^+$), 115 (17, $[C_9H_7]^+$), 73 (100, $[Si(CH_3)_3]^+$); (high resolution, DEI): calculated for mass $^{12}C_{17}H_{13}SiN_4$ ($[M\text{-}CH_3]^+$), 301.0909 amu; observed, 301.0926 amu. A sample suitable for structural determination by single-crystal X-ray diffraction (0.2 x 0.2 x 0.2 mm^3) was obtained by crystallization from dichloromethane.

1, 1- and 1, 3-Bis(trimethylsilyl)indene, 1.138 and 1.139. These compounds, which exist as a set of interconverting isomers, were prepared using previously reported methods.[123] However, within these reports are presented only IR and somewhat ambiguous low-field ^1H NMR spectral data. Data for **1.138**: ^1H NMR ($CDCl_3$, 500 MHz): δ 7.12 (d, ^3J = 5.2 Hz, 1H, H(2)), 6.81 (d, ^3J = 5.2 Hz, 1H, H(3)), 0.04 (s, 18H, $Si(CH_3)_3$); ^{13}C NMR ($CDCl_3$, 125 MHz): δ 47.1 (C(1)), -0.8 (CH_3); ^{29}Si NMR ($CDCl_3$, 99.35 MHz): δ 0.5; Data for **1.139**: ^1H NMR ($CDCl_3$, 500 MHz): δ 6.97 (d, ^3J = 1.7 Hz, 1H, H(2)), 3.68 (d, ^3J = 5.2 Hz, 1H, H(1)), 0.44 (s, 9H, $Si(CH_3)_3$ at C(3)), 0.03 (s, 9H, $Si(CH_3)_3$ at C(1)); ^{13}C NMR ($CDCl_3$, 125 MHz): δ 49.2 (C(1)), -0.5 ($Si(CH_3)_3$ at C(1)), -2.3 ($Si(CH_3)_3$ at C(3)); ^{29}Si NMR ($CDCl_3$, 99.35 MHz): δ 1.6, -9.7; Data for (**1.138** and **1.139**): ^1H NMR ($CDCl_3$, 500 MHz): δ 7.67-7.24 (m, 8H, aromatic); ^{13}C NMR ($CDCl_3$, 125 MHz): δ 147.9, 146.9, 146.1, 145.8, 145.1, 141.8, 138.5, 136.3, 128.6, 125.0, 123.8, 123.6, 123.3, 122.5, 121.5, 121.3 (vinyl and aromatic). Mass spectra: (DEI, *m/z* (%)): 260 (21, $[M]^+$), 245 (38, $[M\text{-}CH_3]^+$), 73 (100, $[Si(CH_3)_3]^+$); (high resolution, DEI): calculated mass for $^{12}C_{15}H_{24}Si_2$ $(M)^+$, 260.1417 amu; observed mass: 260.1430 amu.

Trapping of (η^5-C_5H_5)Fe(CO)$_2$-Isoindene with Tetracyanoethylene, 2.2. This compound was prepared using methods described by Kerber and co-workers.[150] A complete assignment of the ^{13}C NMR spectrum of this compound had not been published prior to this study. ^{1}H NMR ($CDCl_3$, 500 MHz): δ 7.54-7.49 (m, 2H, H(8) and H(11)), 7.48-7.43 (m, 2H, H(9) and H(10)), 4.82 (s, 5H, Cp), 4.05 (s, 2H, H(1) and H(4)), 3.15 (s, 1H, H(7)); ^{13}C NMR ($CDCl_3$, 125 MHz): δ 215.4 (C≡O), 139.7 (C(2) and C(3)), 130.2 (C(9) and C(10)), 125.6 (C(8) and C(11)), 113.3 (C≡N, pseudo equatorial), 110.6 (C≡N, pseudo axial), 86.0 (Cp), 68.3 (C(1) and C(4)), 48.7 (C(5) and C(6)), 39.6 (C(7)). A sample suitable for structural determination by single-crystal X-ray diffraction (0.02 x 0.10 x 0.12 mm^3) was obtained by recrystallization from dichloromethane.

Tris(1-indenyl)methylsilane, 3.18. Indene (4.5 g, 38.8 mmol) in freshly distilled ether (100 mL) was cooled to -78 °C, and *n*-butyllithium (24.24 mL of a 1.6 M hexane solution, 39 mmol) was added dropwise over 1 h. The solution was stirred at -78 °C for an additional 2 h after which time methyltrichlorosilane (1.3g, 8.70 mmol) was added dropwise over 2 h. When the addition was complete, the mixture was allowed to warm to room temperature and stirred for an additional 18 h. The product was extracted by using water (3 x 100 mL), and the organic phase was dried over anhydrous $MgSO_4$. The residue obtained after removal of the ether was subjected to flash chromatography on silica gel. Elution with a mixture of hexanes and CH_2Cl_2 (70:30) gave **3.18** as a yellow waxy solid (1.41g, 3.63 mmol, 42%). ^{1}H NMR ($CDCl_3$, 500 MHz): δ 7.61-7.14 (m, 48H, aromatic), 7.02 (d of d, J = 5.4 Hz and 1.8 Hz, 3H, H(3) in S(1)/R(1)), 6.88 (d of d, J = 5.4 Hz and 1.8 Hz, 3H, H(3) in S/R), 6.80 (d of d, J = 5.4 Hz and 1.8 Hz, 3H, H(3) in R(3)/S(3)), 6.73 (d of d, J = 5.4 Hz and 1.8 Hz, 3H, H(3) in S(2)/R(2)), 6.49 (d of d, J = 5.4 Hz and 1.8 Hz, 3H, H(2) in S(1)/R(1)), 6.30 (d of d, J = 5.4 Hz and 1.8 Hz, 3H, H(2) in S/R), 5.90 (d of d, J = 5.4 Hz and 1.8 Hz, 3H, H(2) in S(2)/R(2)), 5.72 (d of d, J = 5.4 Hz and 1.8 Hz, 3H, H(2) in R(3)/S(3)), 3.89 (d, J = 1.8 Hz, 3H, H(1) in S(1)/R(1)), 3.51 (d, J = 1.8 Hz, 3H, H(1) in S/R), 3.40 (d, J = 1.8 Hz, 3H, H(1)

in R(3)/S(3)), 3.27 (d, J = 1.8 Hz, 3H, H(1) in S(2)/R(2)), -0.20 (s, 3H, $SiCH_3$ in 5-*RRR and* 5-*SSS*), -0.22 (s, 9H, $SiCH_3$ in 5-*RRS* and 5-*SSR*); ^{13}C NMR ($CDCl_3$, 125 MHz): δ 144.6-144.2 (C(3a), C(7a)), 134.9 (C(2) in R(3)/S(3)), 134.9 (C(2) in S(1)/R(1)), 134.8 (C(2) in S/R), 134.6 (C(2) in S(2)/R(2)), 130.4 (C(3) in S(1)/R(1)), 130.1 (C(3) in S/R), 129.7 (C(3) in R(3)/S(3)), 129.6 (C(3) in S(2)/R(2)), 125.7-121.3 (C(4), C(5), C(6) and C(7)), 44.1 (C(1) in S(1)/R(1)), 43.1 (C(1) in S/R), 42.7 (C(1) in R(3)/S(3)), 41.9 (C(1) in S(2)/R(2)), -7.5 ($SiCH_3$ in 5-*RRR* and 5-*SSS*), -7.5 ($SiCH_3$ in 5-*RRS* and 5-*SSR*); ^{29}Si NMR ($CDCl_3$, 99.35 MHz): δ 5.96 (5-*RRS* and 5-*SSR*), 5.04 (5-*RRR* and 5-*SSS*); IR ($CDCl_3$, cm^{-1}): 3068 m, 2960 s, 2927 m, 2873 w, 1452 s, 1257 s; Mass spectra: (DEI, *m/z* (%)): 388 (9, $[M]^+$), 273 (34, $[M-C_9H_7]^+$), 143 (27, $[M-2(C_9H_7)-CH_3]^+$), 115 (100, $[C_9H_7]^+$); (high resolution, DEI): calculated for mass $^{12}C_{28}H_{24}Si$, 388.1648 amu; observed, 388.1650 amu.

Tris(1-indenyl)allylsilane, 3.19. Indene (4.0 g, 34.5 mmol) in freshly distilled ether (100 mL) was cooled to -78 °C, and *n*-butyllithium (21.6 mL of a 1.6 M hexane solution, 35 mmol) was added dropwise over 1 h. The solution was stirred at -78 °C for 2 h after which time allyltrichlorosilane (1.2 g, 6.90 mmol) was added dropwise over 2 h. When the addition was complete, the mixture was allowed to warm to room temperature and stirred for an additional 18 h. The product was extracted by using water (3 x 100 mL), and the organic phase was dried over anhydrous $MgSO_4$. The residue obtained after removal of the ether was subjected to flash chromatography on silica gel. Elution with a mixture of hexanes and CH_2Cl_2 (80:20) gave **3.19** as a viscous yellow oil (0.36 g, 0.88 mmol, 13%). ^1H NMR ($CDCl_3$, 500 MHz): δ 7.64-7.11 (m, 48H, aromatic), 7.02 (d of d, J = 5.4 Hz and 1.9 Hz, 3H, H(3) in S(1)/R(1)), 6.86 (d of d, J = 5.4 Hz and 1.9 Hz, 3H, H(3) in S/R), 6.76 (d of d, J = 5.4 Hz and 1.9 Hz, 3H, H(3) in R(3)/S(3)), 6.69 (d of d, J = 5.4 Hz and 1.9 Hz, 3H, H(3) in S(2)/R(2)), 6.57 (d of d, J = 5.4 Hz and 1.9 Hz, 3H, H(2) in S(1)/R(1)), 6.26 (d of d, J = 5.4 Hz and 1.9 Hz, 3H, H(2) in S/R), 5.70 (d of d, J = 5.4 Hz and 1.9 Hz, 3H, H(2) in S(2)/R(2)), 5.57 (d of d, J = 5.4 Hz and 1.9 Hz, 3H, H(2) in R(3)/S(3)), 4.77-4.59 (m, 12H, $SiCH_2CHCH_2$), 4.00 (d, J

= 1.9 Hz, 3H, H(1) in S(1)/R(1)), 3.61 (d, J = 1.9 Hz, 3H, H(1) in S/R), 3.40 (d, J = 1.9 Hz, 3H, H(1) in R(3)/S(3)), 3.38 (d, J = 1.9 Hz, 3H, H(1) in S(2)/R(2)), 1.49 (m, 6H, $SiCH_2$ in 5-*RRS and* 5-*SSR*), 1.39 (m, 2H, $SiCH_2$ in 5-*RRR* and 5-*SSS*); ^{13}C NMR ($CDCl_3$, 125 MHz): δ 144.0-143.6 (C(3a), C(7a)), 134.9 (C(2) in R(3)/S(3)), 134.7 (C(2) in S(1)/R(1)), 134.4 (C(2) in S/R), 134.3 (C(2) in S(2)/R(2)), 133.3 ($SiCH_2CHCH_2$ in 5-*RRR* and 5-*SSS*), 133.2 ($SiCH_2CHCH_2$ in 5-*RRS* and 5-*SSR*), 130.6 (C(3) in S(1)/R(1)), 130.4 (C(3) in S/R), 129.9 (C(3) in S(2)/R(2)), 129.9 (C(3) in R(3)/S(3)), 126.2-120.9 (C(4), C(5), C(6) and C(7)), 42.3 (C(1) in S(1)/R(1)), 42.1 (C(1) in S/R), 41.8 (C(1) in R(3)/S(3)), 41.7 (C(1) in S(2)/R(2)), 19.8 ($SiCH_2$ in 5-*RRR* and 5-*SSS*), 18.9 ($SiCH_2$ in 5-*RRS* and 5-*SSR*); ^{29}Si NMR ($CDCl_3$, 99.35 MHz): δ 3.41 (5-*RRS* and 5-*SSR*), 2.11 (5-*RRR* and 5-*SSS*); IR ($CDCl_3$, cm^{-1}): 3048 m, 2952 s, 2929 m, 1448 s, 1259 s; Mass spectra: (DEI, *m/z* (%)): 414 (4, $[M]^+$), 299 (36, $[M-C_9H_7]^+$), 256 (100, $[M-(C_9H_7)-C_3H_5]^+$), 115 (95, $[C_9H_7]^+$); (high resolution, DEI): calculated for mass $^{12}C_{30}H_{26}Si$ (M^+), 414.1804 amu; observed, 414.1801 amu.

Tris(1-indenyl)silane, 3.20. Indene (4.0 g, 34.5 mmol) in freshly distilled diethyl ether (100 mL) was cooled to -78 °C, and *n*-butyllithium (21.6 mL of a 1.6 M hexane solution, 35 mmol) was added dropwise over 1 h. The mixture was stirred for an additional 2 h at -78 °C, and then trichlorosilane (1.6 g, 11.5 mmol) was added dropwise over 2 h. When the addition was complete, the mixture was allowed to warm to room temperature and stirred for an additional 18 h. The product was then extracted with water (3 x 100 mL), and the organic phase dried over anhydrous $MgSO_4$. The residue obtained after removal of the solvent was subjected to flash chromatography on silica gel. Elution with a mixture of hexanes and CH_2Cl_2 (80:20) yielded a viscous yellow oil, which solidified after several hours under vacuum at ambient temperature. Recrystallization from hexanes yielded **3.20** as a yellow powder, m.p. 91-92 °C (2.75 g, 7.36 mmol, 64%). ^1H NMR ($CDCl_3$, 500 MHz): δ 7.36-7.07 (m, 48H, aromatic), 6.77 (m, 3H, H(3) in S/R), 6.71 (m, 3H, H(3) in R(3)/S(3)), 6.62 (m, 3H, H(3) in S(2)/R(2)), 6.60 (m, 3H, H(3) in S(1)/R(1)), 6.57 (m, 3H, H(2) in R(3)/S(3)), 6.18 (m, 3H, H(2) in S/R), 5.87 (m, 3H, H(2) in

S(1)/R(1)), 5.60 (m, 3H, H(2) in S(2)/R(2)), 4.24 (m, 1H, Si*H* in 11-*SSS*/*RRR*), 3.83 (m, 3H, Si*H* in 11-*SSR*/*RRS*), 3.36 (m, 3H, H(1) in R(3)/S(3)), 3.14 (m, 3H, H(1) in S(2)/R(2)), 3.06 (m, 3H, H(1) in S/R), 2.91 (m, 3H, H(1) in S(1)/R(1)); ^{13}C NMR ($CDCl_3$, 125 MHz): δ 144.9-143.7 (C(3a), C(7a)), 135.2 (C(2) in S(1)/R(1)), 134.9 (C(2) in R(3)/S(3)), 134.7 (C(2) in S(1)/R(1)), 134.7 (C(2) in S(2)/R(2)), 130.9 (C(3) in R(3)/S(3)), 130.3 (C(3) in S(1)/R(1)), 130.2 (C(3) in S(2)/R(2)), 130.0 (C(3) in S/R), 126.5-121.2 (C(4), C(5), C(6) and C(7)), 42.4 (C(1) in R(3)/S(3)), 40.8 (C(1) in S/R), 40.8 (C(1) in S(2)/R(2)), 39.9 (C(1) in S(1)/R(1)); ^{29}Si NMR ($CDCl_3$, 99.35 MHz): δ -2.2 (11-*RRR* and 11-*SSS*), -3.4 (11-*RRS* and 11-*SSR*); IR ($CDCl_3$): υ_{Si-H} 2120 cm^{-1}; Mass spectra: (DEI, *m/z* (%)): 374 (17, $[M]^+$), 259 (42, $[M-C_9H_7]^+$), 143 (46, $[M-2(C_9H_7)]^+$), 115 (100, $[C_9H_7]^+$); (high resolution, DEI): calculated for mass $^{12}C_{27}H_{22}Si_1$, 374.1491 amu; observed, 374.1497 amu; Anal.: Calcd. for $C_{27}H_{22}Si_1$: C 86.58; H 5.92. Found: C 86.64; H 5.85. A sample suitable for structural determination by single-crystal X-ray diffraction (0.3 x 0.3 x 0.1 mm^3) was obtained by recrystallization from a mixture of dichloromethane and hexanes (1:1).

Tris(5,6-benzo-2,2,3,3-tetracyanobicyclo-(2.2.1)heptan-7-yl)methylsilane, 3.21. Upon addition of tetracyanoethylene (0.093 g, 0.73 mmol) to a solution of tris(1-indenyl)methylsilane, **3.18**, (0.08 g, 0.21 mmol) in ethyl acetate (75 mL), the solution turned dark blue; the dark coloration subsided after 72 h. After removal of the ethyl acetate, the residue was subjected to flash chromatography on silica gel. Elution with a mixture of diethyl ether and hexanes (30:70) gave **3.21** as a white powder (59 mg, 0.076 mmol, 33%). ^{1}H NMR (CD_3CN, 500 MHz): δ 7.52 (apparent d (5.6 Hz) of d (3.2 Hz), 6H, H(9) and H(10)), 7.47 (apparent d (5.6 Hz) of d (3.2 Hz), 6H, H(8) and H(11)), 4.26 (d, ^{3}J = 1.0 Hz, 6H, H(1) and H(4)), 2.28 (t, ^{3}J = 1.0 Hz, 3H, H(7)), -1.88 (s, 3H, $SiCH_3$); ^{13}C NMR (CD_3CN, 125 MHz): δ 139.6 (C(5) and C(6)), 131.7 (C(9) and C(10)), 126.6 (C(8) and C(11)), 113.5 (pseudo-equatorial nitriles), 111.9 (pseudo-axial nitriles), 60.2 (C(1) and C(4)), 50.8 (C(2) and C(3)), 48.5 (C(7)), -4.4 ($SiCH_3$); ^{29}Si NMR (CD_3CN, 99.35 MHz): δ 1.3. Mass spectrum: (DEI, *m/z* (%)): 644

(3, [M-(TCNE)]$^{+}$), 516 (8, [M-2(TCNE)]$^{+}$), 388 (12, [M-3(TCNE)]$^{+}$), 273 (100, [$C_{19}H_{17}Si$]$^{+}$), 143 (22, [C_9H_7Si]$^{+}$), 115 (45, [C_9H_7]$^{+}$).

Tris(5,6-benzo-2,2,3,3-tetracyanobicyclo-(2.2.1)heptan-7-yl)allylsilane, 3.22. Upon addition of tetracyanoethylene (0.216 g, 1.69 mmol) to a solution of tris(1-indenyl)allylsilane, **3.19** (0.200 g, 0.483 mmol) in ethyl acetate (75 mL) the solution turned dark blue; the dark coloration subsided after 72 h. Removal of the ethyl acetate left a solid residue, which was washed with hexanes to remove any residual **3.19**, and then dissolved in boiling diethyl ether (30 mL). Upon cooling, the desired compound, **3.22**, precipitated as a white powder (162 mg, 0.203 mmol, 42%). ^{1}H NMR (CD_3CN, 500 MHz): δ 7.62 (m, 6H, H(9) and H(10)), 7.56 (m, 6H, H(8) and H(11)), 4.77 (m, 2H, $SiCH_2CHCH_2$), 4.21 (d, ^{3}J = 1.0 Hz, 6H, H(1) and H(4)), 4.18 (m, 1H, $SiCH_2CHCH_2$), 1.97 (t, ^{3}J = 1.0 Hz, 3H, H(7)), 0.10 (m, 2H, $SiCH_2CHCH_2$); ^{13}C NMR (CD_3CN, 125 MHz): δ 139.5 (C(5) and C(6)), 132.2 (C(9) and C(10)), 130.1 ($SiCH_2CHCH_2$), 127.1 (C(8) and C(11)), 119.8 ($SiCH_2CHCH_2$), 113.4 (pseudo-equatorial nitriles), 111.8 (pseudo-axial nitriles), 59.7 (C(1) and C(4)), 50.6 (C(2) and C(3)), 48.2 (C(7)), 19.4 ($SiCH_2CHCH_2$); ^{29}Si NMR (CD_3CN, 99.35 MHz): δ -3.6; Mass spectrum: (DEI, *m/z* (%)): 670 (4, [M-(TCNE)]$^{+}$), 542 (6, [M-2(TCNE)]$^{+}$), 299 (100, [$(C_9H_7)_2SiCH_2CHCH_2$]$^{+}$), 143 (55, [C_9H_7Si]$^{+}$), 115 (14, [C_9H_7]$^{+}$). (CI, NH_3, *m/z* (%)): 799 (5, [M+1]$^{+}$), 688 (6, [M-(TCNE)+18]$^{+}$), 560 (100, [M-(2TCNE)+18]$^{+}$), 432 (57, [M-(3TCNE)+18]$^{+}$). A crystalline sample (0.36 mm x 0.06 mm x 0.03 mm) suitable for structural determination by single-crystal X-ray diffraction was grown from acetonitrile.

Tris(5,6-benzo-2,2,3,3-tetracyanobicyclo-(2.2.1)heptan-7-yl)silane, 3.23. Upon addition of tetracyanoethylene (2.8 g, 22 mmol) to a solution of tris(1-indenyl)silane, **3.20**, (2.8 g, 7.5 mmol) in ethyl acetate (100 mL) the solution turned dark blue; the dark coloration subsided after 72 h. The residual solid obtained after removal of the solvent was washed with hexanes (2 X 50 mL), and then purified by recrystallization from dichloromethane, yielding **3.23** as a beige powder m.p. (with

decomposition) 217-219 °C (2.7 g, 3.6 mmol, 47%). ^{1}H NMR (acetone-d_6, 99.35 MHz): δ 7.64 (apparent d (5.4 Hz) of d (3.1 Hz), 6H, H(8) and H(11)), 7.52 (apparent d (5.4 Hz) of d (3.1 Hz), 6H, H(9) and H(10)), 4.35 (d, ^{3}J = 1.1 Hz, 6H, H(1) and H(4)), 2.54 (d ($^{3}J_{Si-H}$ = 3.1 Hz) of t (^{3}J = 1.1 Hz), 3H, H(7)), 2.12 (quart., 1H, SiH); ^{13}C NMR (CD_3CN, 125 MHz): δ 139.4 (C(5) and C(6)), 131.3 (C(9) and C(10)), 126.7 (C(8) and C(11)), 113.4 (pseudo-equatorial nitriles), 111.5 (pseudo-axial nitriles), 60.5 (C(1) and C(4)), 50.5 (C(2) and C(3)), 49.6 (C(7)); ^{29}Si NMR (CD_3CN, 99.35 MHz): δ -10.3; IR (cm^{-1}): 2256, 2221, 2112, 1937; Mass spectrum: (CI, NH_3, *m/z* (%)): 724 (7, [M-2(CN)+18]$^{+}$), 648 (61, [M-(TCNE)+18]$^{+}$), 520 (100, [M-2(TCNE)+18]$^{+}$), 392 (92, [M-3(TCNE)+18]$^{+}$); Anal.: Calcd. for $C_{45}H_{22}N_{12}Si_1$: C 71.22; H 2.92; N 22.16. Found: 70.84; H 3.02; N 21.91.

Tris(5,6-benzo-2,2,3,3-tetracyanobicyclo-(2.2.1)heptan-7-yl)silanol, 3.24. A sample of **3.23** in wet acetone (approximately 3% water added) was quantitatively converted to the corresponding silanol, **3.24**, after stirring for 24 hours at room temperature. Slow evaporation of the solvent yielded **3.24(CH_3COCH_3)$_2$** as a white powder. ^{1}H NMR (acetone-d_6, 99.35 MHz): δ 7.59 (apparent d (5.4 Hz) of d (3.1 Hz), 6H, H(8) and H(11)), 7.48 (apparent d (5.4 Hz) of d (3.1 Hz), 6H, H(9) and H(10)), 5.16 (s, 1H, SiO*H*), 4.39 (d, ^{3}J = 1.1 Hz, 6H, H(1) and H(4)), 2.39 (t, ^{3}J = 1.1 Hz, 3H, H(7)); ^{13}C NMR (acetone-d_6, 125 MHz): δ 139.5 (C(5) and C(6)), 131.0 (C(9) and C(10)), 126.4 (C(8) and C(11)), 113.5 (pseudo-equatorial nitriles), 111.6 (pseudo-axial nitriles), 60.0 (C(1) and C(4)), 50.6 (C(2) and C(3)), 49.5 (C(7)); ^{29}Si NMR (acetone-d_6, 99.35 MHz): δ -4.7. The presence of the SiOH functionality was verified by a D_2O exchange experiment, and by data obtained from a ^{1}H-^{29}Si HMBC shift-correlated NMR experiment. A single crystal of **3.24(CH_3COCH_3)$_2$** (0.16 mm x 0.15 mm x 0.12 mm) grown from acetone was studied by X-ray crystallography, which verified the presence of two molecules of acetone per asymmetric unit, initially suggested by the elemental analyses data. Anal.: Calcd. for $C_{51}H_{34}N_{12}O_3Si_1$: C 68.75; H 3.85; N 18.86. Found: 68.62; H 3.77; N 19.03.

Tris(1-indenyl)hexylsilane, 3.26. Based on synthetic methods previously described in the literature,[253,254] tris(1-indenyl)silane, **3.20**, (210 mg, 0.56 mmol), 1-hexene (300 mg, 3.6 mmol) and a catalytic amount of Wilkinson's catalyst ($(Ph_3P)_3RhCl$) were sealed in an evacuated tube and kept at 60 °C for 7 d. The resulting solid obtained after removal of the residual olefin *in vacuo* was subjected to flash chromatography on silica gel. Elution with a mixture of hexanes and CH_2Cl_2 (90:10) yielded **3.26**, as a viscous oil (88 mg, 0.19 mmol, 34%). ^1H NMR ($CDCl_3$, 500 MHz): δ 7.56-6.99 (m, 48H, aromatic), 6.96 (d of d, J = 5.4 Hz and 1.9 Hz, 3H, H(3) in S(1)/R(1)), 6.83 (d of d, J = 5.4 Hz and 1.9 Hz, 3H, H(3) in S/R), 6.75 (d of d, J = 5.4 Hz and 1.9 Hz, 3H, H(3) in R(3)/S(3)), 6.67 (d of d, J = 5.4 Hz and 1.9 Hz, 3H, H(3) in S(2)/R(2)), 6.51 (d of d, J = 5.4 Hz and 1.9 Hz, 3H, H(2) in S(1)/R(1)), 6.26 (d of d, J = 5.4 Hz and 1.9 Hz, 3H, H(2) in S/R), 5.79 (d of d, J = 5.4 Hz and 1.9 Hz, 3H, H(2) in S(2)/R(2)), 5.62 (d of d, J = 5.4 Hz and 1.9 Hz, 3H, H(2) in R(3)/S(3)), 3.98 (d, J = 1.9 Hz, 3H, H(1) in S(1)/R(1)), 3.56 (d, J = 1.9 Hz, 3H, H(1) in S/R), 3.40 (d, J = 1.9 Hz, 3H, H(1) in R(3)/S(3)), 3.25 (d, J = 1.9 Hz, 3H, H(1) in S(2)/R(2)), 1.51-0.84 (m, 52H, hexyl); ^{13}C NMR ($CDCl_3$, 125 MHz): δ 144.7-143.4 (C(3a), C(7a)), 135.3 (C(2) in S(1)/R(1)), 135.0 (C(2) in S/R), 134.9 (C(2) in S(2)/R(2)), 134.9 (C(2) in R(3)/S(3)), 130.4 (C(3) in S(1)/R(1)), 130.1 (C(3) in S/R), 129.6 (C(3) in R(3)/S(3)), 129.5 (C(3) in S(2)/R(2)), 126.0-121.3 (C(4), C(5), C(6) and C(7)), 42.7 (C(1) in S(1)/R(1)), 42.4 (C(1) in S/R), 42.2 (C(1) in R(3)/S(3)), 41.9 (C(1) in S(2)/R(2)), 34.6-11.4 (hexyl). Some ^1H and ^{13}C NMR signal assignments were made by comparison to data obtained for tris(1-indenyl)methylsilane, **3.18**. Mass spectra: (DEI, *m/z* (%)): 458 (8, $[M]^+$), 401 (7, $[M-C_4H_9]^+$), 343 (74, $[M-C_9H_7]^+$), 258 (86, $[Si(C_9H_7)_2]^+$), 143 (100, $[Si(C_9H_7)]^+$), 115 (22, $[C_9H_7]^+$); (high resolution, DEI): calculated for mass $^{12}C_{33}H_{34}Si_1$, 458.2430 amu; observed, 458.2426 amu.

Reactions involving HBF_4 or Ph_3CPF_6. To a solution of the silane (0.05 mmol) in CD_2Cl_2 (**3.19** or **3.20**) or CD_3CN (**3.22**, **3.23** or **3.24**) was added either $HBF_4O(C_2H_5)_2$ or Ph_3CPF_6, (~ 0.07

mmol) at -78 °C under nitrogen in an NMR sample tube. In the case of **3.19** or **3.20**, the products (**3.27** and **3.28**) were inferred based on multidimensional NMR spectral data obtained from the mixture (at -50 °C) immediately thereafter. For **3.22**, **3.23** or **3.24**, the sample was allowed to warm to -30 °C, and the quantitative formation of the corresponding tris(5,6-benzo-2,2,3,3-tetracyanobicyclo-(2.2.1)heptan-7-yl)fluorosilane, **3.29**, verified *in situ* by use of NMR spectroscopy. Numerous attempts to isolate an analytically pure sample of **3.27**, **3.28** or **3.29** were unsuccessful.

Tris(5,6-benzo-2,2,3,3-tetracyanobicyclo-(2.2.1)heptan-7-yl)fluorosilane, 3.29. ^{1}H NMR (CD_3CN, 500 MHz): δ 7.65 (apparent d (5.7 Hz) of d (3.4 Hz), 6H, H-8,11), 7.56 (apparent d (5.7 Hz) of d (3.4 Hz), 6H, H(9) and H(10)), 3.95 (d, ^{3}J = 1.0 Hz, 6H, H(1) and H(4)), 2.11(d ($^{3}J_{HF}$ = 4.5 Hz) of t ($^{3}J_{HH}$ = 1.1 Hz), 3H, H(7)); ^{13}C NMR (CD_3CN, 125 MHz): δ 139.0 (C(5) and C(6)), 131.7 (C(9) and C(10)), 126.3 (C(8) and C(11)), 113.2 (pseudo-equatorial nitriles), 111.7 (pseudo-axial nitriles), 58.9 (C(1) and C(4)), 50.1 (C(2) and C(3)), 48.9 (d, $^{2}J_{FC}$ = 12 Hz, C(7)); ^{19}F NMR (CD_3CN, 282.4 MHz,): δ -148.4 (quart., $^{3}J_{HF}$ = 4.5 Hz); ^{29}Si NMR (CD_3CN, 99.35 MHz): δ -8.89 (d, $^{1}J_{SiF}$ = 278 Hz).

1,3-Dimethyl-1-trimethylsilylindene, 4.7. 1,3-Dimethylindene (3.3 g, 22.9 mmol) in freshly distilled tetrahydrofuran (150 mL) was cooled to -78 °C, and *n*-butyllithium (15 mL of a 1.6 M hexane solution, 24 mmol) was added dropwise over 1 h, after which the mixture was stirred and allowed to warm to ambient temperature over 2 h. Chlorotrimethylsilane (3.8 g, 35.2 mmol) was then added dropwise at -78 °C over 2 h, and the mixture warmed to room temperature over 18 h followed by refluxing for an additional 6 h. The solvent was then removed and the residue extracted using diethyl ether (3 X 75 mL). Subsequent purification of the extracted material by flash chromatography on silica gel using hexanes yielded **4.7** as a viscous yellow oil (4.4 g, 20.3 mmol, 89%); anal.: calcd. for $C_{14}H_{20}Si$: C 77.73, H 9.33, found: C 77.68, H 9.03; ^{1}H NMR ($CDCl_3$, 500 MHz): δ 7.44-7.27 (m, 4H, H(4),

H(5), H(6) and H(7)), 6.26 (s, 1H, H(2)), 2.28 (s, 3H, C(3)-CH_3), 1.53 (s, 3H, C(1)-CH_3), -0.06 (s, 9H, Si(CH_3)$_3$); ^{1}H NMR ($Cl_2DCCDCl_2$, 500 MHz): δ 7.33-7.21 (m, 4H, H(4), H(5), H(6) and H(7)), 6.13 (s, 1H, H(2)), 2.16 (s, 3H, C(3)-CH_3), 1.41 (s, 3H, C(1)-CH_3), -0.19 (s, 9H, Si(CH_3)$_3$); ^{13}C NMR ($CDCl_3$, 125 MHz): δ 151.0 (C(3a) or C(7a)), 144.6 (C(7a) or C(3a)), 137.7 (C(2)), 135.8 (C(3)), 124.7, 123.7, 121.7, 118.9 (C(4), C(5), C(6) and C(7)), 46.5 (C(1)), 16.0 (C(1)-CH_3), 12.7 (C(3)-CH_3), -3.56 Si(CH_3)$_3$; ^{29}Si NMR ($CDCl_3$, 99.35 MHz): δ -0.1; MS (DEI, *m/z* (%)): 216 (61, $[M]^+$), 201 (48, $[M-CH_3]^+$), 143 (32, $[M-Si(CH_3)_3]^+$), 73 (100, $[Si(CH_3)_3]^+$); MS (CI, NH_3, *m/z* (%)): 217 (100, $[MH]^+$).

Bis(trimethylsilyl)dibenzo[*a,d*]fulvalene, 4.24. In an effort to synthesize 1,1,3-tris(trimethylsilyl)indene, **4.22**, *n*-butyllithium (43.1 mL of a 1.6 M hexane solution, 68 mmol) was added dropwise over a 1 h period to a solution of indene (4.0 g, 34 mmol) in freshly distilled diethyl ether (100 mL) at -78 °C. After the addition of chlorotrimethylsilane (7.5 g, 68 mmol), the solution was stirred for 1 h and additional *n*-butyllithium (21.5 mL, 34 mmol) and chlorotrimethylsilane (3.8 g, 34 mmol) were added. The mixture was then allowed to warm to room temperature, and stirred for an additional 18 h. Extraction of the resulting opaque milky solution with water (3 x 100 mL) gave rise to a clear, bright red organic phase, which was dried over anhydrous $MgSO_4$. After removal of diethyl ether, the organic residue was subjected to flash chromatography on silica gel. Elution with hexanes gave 1,1- and 1,3-bis(trimethylsilyl)indene (identified by comparison to an authentic sample; see **1.138** and **1.139**) as a yellow oil (4.12 g, 15.9 mmol, 46%, *based on indene*). Subsequent elution with hexanes/dichloromethane (5:1) yielded **4.24** as a bright red powder, m.p. 129-130 °C (0.38 g, 1.0 mmol, approximately 6% *isolated yield based on indene*). ^{1}H NMR ($CDCl_3$, 500 MHz): δ 7.93 (d, ^{3}J = 7.4 Hz, 2H, H(4)), 7.54 (s, 2H, H(2)), 7.36 (d, ^{3}J = 7.3 Hz, 2H, H(7)), 7.24 (m, 2H, H(6)), 7.19 (m, 2H, H(5)), 0.36 (s, 18H, Si(CH_3)$_3$); ^{13}C NMR ($CDCl_3$, 125 MHz): δ 150.7 (C(1)), 147.2 (C(7a)), 141.1 (C(3)), 136.1 (C(2)), 138.0 (C(3a)), 128.3 (C(6)), 125.4 (C(5)), 125.2 (C(4)), 122.7 (C(7)), -1.1 (Si(CH_3)$_3$); ^{29}Si

NMR ($CDCl_3$, 99.35 MHz): δ -9.0; IR ($CDCl_3$, cm^{-1}): 3155.7 s, 1469.7 m, 1382.3 m; Mass spectra: (DEI, *m/z* (%)): 372 (35, $[M]^+$), 357 (17, $[M\text{-}CH_3]^+$), 299 (14, $[M\text{-}Si(CH_3)_3]^+$), 73 (100, $[Si(CH_3)_3]^+$); (high resolution, DEI): calculated mass for $^{12}C_{24}H_{28}Si_2$ $(M)^+$, 372.1729 amu; observed mass: 372.1736 amu. A crystalline sample of this material, produced by slow growth from a mixture of dichloromethane/acetone (1:1), was mounted on a glass fiber and studied by single-crystal X-ray diffraction. The following unit cell parameters were determined: a = 7.080(1) Å, b = 17.678(4) Å, c = 8.955(2) Å, α = 90.000 β = 90.090(3), and γ = 90.000. Subsequent refinement in a monoclinic space group ($P2_1/c$) revealed the existence of two independent half-molecules per asymmetric unit. However, in the latter stages of refinement, a disorder problem prevented the structure from being refined to an acceptable level (R1 > 35%). As a result, a discussion of the metrical parameters associated with **4.24** is not presented. Some of the difficulties in refining the structure (including the appearance of non-positive definite atoms) may be a consequence of a pseudo-orthorhombic twinning process; attempts to solve and refine the structure of **4.24** based on an orthorhombic unit cell were also unsuccessful. Such a disorder does appear plausible, in that a decrease in the β angle of only 0.1 degrees would give rise to an orthorhombic cell of higher crystallographic symmetry.

3,3'-Bis(1-trimethylsilyl)indene, 4.31. A solution of 3,3'-biindene, **4.29**,[255] and/or 1-(indanylidene)-1-indene, **4.30**,[256] (0.300 g, 1.3 mmol) in freshly distilled tetrahydrofuran (30 mL) was cooled to -78 °C, and *n*-butyllithium (2.2 mL of a 1.3 M hexane solution, 2.9 mmol) was added dropwise over a 1 h period. After stirring for an additional 3 h at ambient temperature, chlorotrimethylsilane (0.45 g, 4 mmol) was added at -78 °C, and the mixture stirred while slowly warming to ambient temperature over 18 h. The residue obtained after removal of the solvent was extracted with hexanes and the insoluble lithium salts separated by filtration. The filtrate was then concentrated and the residue subjected to flash chromatography on silica gel using hexanes, yielding **4.31** (a *meso* and *d,l* mixture) as a viscous yellow oil (0.200 g, 0.53 mmol, 41%). Based

on the intensities of the observed NMR signals, it is evident that one isomer (either *meso* or *d,l*) predominates (~ 1:1.3). Major isomer: ^{1}H NMR ($CDCl_3$, 500 MHz): δ 7.62 (d, J = 7.5 Hz, 2H, H(4)), 7.51 (d, J = 7.5 Hz, 2H, H(7)), 7.30-7.22 (m, 4H, H(5) and H(6)), 6.85 (d, J = 1.8 Hz, 2H, H(2)), 3.69 (d, J = 1.8 Hz, 2H, H(1)), 0.02 (s, 18H, $Si(CH_3)_3$); ^{13}C NMR ($CDCl_3$, 125 MHz): δ 146.0 (C(7a)), 143.3 (C(3a)), 136.3 (C(3)), 132.7 (C(2)), 124.7 (C(6)), 123.9 (C(5)), 122.9 (C(7)), 120.5 (C(4)), 45.9 (C(1)), -2.4 ($Si(CH_3)_3$); ^{29}Si NMR ($CDCl_3$, 99.35 MHz): δ 4.7. Minor isomer: ^{1}H NMR ($CDCl_3$, 500 MHz): δ 7.54 (d, J = 7.1 Hz, 2H, H(4)), 7.49-7.26 (m, 6H, H(5), H(6), and H(7)), 6.80 (d, J = 1.8 Hz, 2H, H(2)), 3.66 (d, J = 1.8 Hz, 2H, H(1)), 0.03 (s, 18H, $Si(CH_3)_3$); ^{13}C NMR ($CDCl_3$, 125 MHz): δ 146.1 (C(7a)), 143.6 (C(3a)), 136.8 (C(3)), 132.8 (C(2)), 124.7 (C(6)), 123.9 (C(5)), 122.8 (C(7)), 120.7 (C(4)), 45.8 (C(1)), -2.3 ($Si(CH_3)_3$); ^{29}Si NMR ($CDCl_3$, 99.35 MHz): δ 4.5; Mass spectra: (DEI, *m/z* (%)): 374 (12, $[M]^+$), 359 (16, $[M\text{-}Si(CH_3)_3]^+$), 73 (100, $[Si(CH_3)_3]^+$); (high resolution, DEI): calculated mass for $^{12}C_{24}H_{30}Si_2$ $(M)^+$, 374.1886 amu; observed mass: 374.1884 amu.

Oxidation of 16. Based on methods previously described in the literature,[205] a solution of 3,3'-bis(1-trimethylsilyl)indene, **4.31**, (0.082 g, 0.22 mmol) in freshly distilled tetrahydrofuran (30 mL) was cooled to -78 °C, and *n*-butyllithium (0.4 mL of a 1.3 M hexane solution, 0.5 mmol) was added dropwise over a 1 h period. After stirring for an additional 3 h at ambient temperature, iodine (0.110 g, 0.4 mmol) was added at -78 °C, and the mixture stirred while slowly warming to ambient temperature over 18 h. After removal of the tetrahydrofuran solvent, the residue was subjected to flash chromatography on silica gel using pentane, yielding **4.24** (0.055 g, 0.51 mmol, 68%).

(5,6-Benzo-2,2,3,3-tetracyano-1,4-dimethylbicyclo-(2.2.1)heptan-7-yl)trimethylsilane, 4.34. The addition of tetracyanoethylene (0.64 g, 5.0 mmol) to a solution of **4.7** (1.0 g, 4.6 mmol) in acetonitrile (50 mL) produced a dark blue solution; the dark coloration subsided after 72 h. The residue obtained after removal of the solvent was washed with hexane (1 x 25 mL), diethyl ether (3 x

15 mL), and then dried to give **4.34** as a beige powder (1.32 g, 3.8 mmol, 83%); m.p. 214-215 °C (with decomposition); anal.: calcd. for $C_{20}H_{20}N_4Si$: C 69.74, H 5.86, N 16.28, found: C 69.56, H 5.91, N 16.31; ^{1}H NMR (CD_3CN, 500 MHz): δ 7.51-7.48 (m, 2H, H(8), H(11)), 7.47-7.44 (m, 2H, H(9), H(10)), 2.01 (s, 1H, H(7)), 1.96 (s, 6H, C-C*H*$_3$), -0.23 (s, 9H, Si(C*H*$_3$)$_3$); ^{1}H NMR ($CDCl_3$, 500 MHz): δ 7.50-7.44 (m, 2H, H(8), H(11)), 7.41-7.35 (m, 2H, H(9), H(10)), 1.90 (s, 1H, H(7)), 1.96 (s, 6H, C-C*H*$_3$), -0.20 (s, 9H, Si(C*H*$_3$)$_3$); ^{13}C NMR (CD_3CN, 125 MHz): δ 143.2 (C(5), C(6)), 130.5 (C(9), C(10)), 123.6 (C(8), C(11)), 113.3 (pseudo-equatorial nitriles), 111.9 (pseudo-axial nitriles), 65.9 (C(1), C(4)), 57.6 (C(2), C(3) and C(7)), 15.5 (C-*C*H$_3$), -0.93 (Si(*C*H$_3$)$_3$); ^{13}C NMR ($CDCl_3$, 125 MHz): δ 141.6 (C(5), C(6)), 130.2 (C(9), C(10)), 122.5 (C(8), C(11)), 111.9 (pseudo-equatorial nitriles), 110.3 (pseudo-axial nitriles), 65.3 (C(1), C(4)), 57.0 (C(2) and C(3) or C(7)), 55.5 (C(7) or C(2) and C(3)), 15.2 (C-*C*H$_3$), -0.87 (Si(*C*H$_3$)$_3$); ^{29}Si NMR (CH_2Cl_2, 99.36 MHz): δ 2.4; Mass Spectrum (DEI, *m/z* (%)): 343 (6, $[M-H]^+$), 329 (3, $[M-CH_3]^+$), 270 (11, $[M-Si(CH_3)_3]^+$), 216 (23, $[M-C_6N_4]^+$), 128 (17, $[C_6N_4]^+$), 73 (100, $[Si(CH_3)_3]^+$); MS (CI, NH_3, *m/z* (%)): 362 (16, $[M+NH_4]^+$), 90 (42, $[Si(CH_3)_3+NH_4]^+$). A sample suitable for structural determination (0.38 x 0.25 x 0.20 mm^3) by single-crystal X-ray diffraction was obtained by recrystallization from acetonitrile.

η^6-(3-Trimethylsilylindene)tricarbonylchromium, 4.37. To a solution of 1-trimethylsilylindene, **1.109**, (1.5 g, 7.98 mmol) in *n*-butyl ether (100 mL) was added freshly distilled tetrahydrofuran (20 mL) and hexacarbonylchromium (3.51 g, 15.95 mmol) under nitrogen. The mixture was then heated at reflux for 72 h and the solvents removed under vacuum. The residue obtained was subjected to flash chromatography on silica gel using hexanes, yielding **4.37** as a bright yellow solid (1.71 g, 5.28 mmol, 66%); m.p. 94-95 °C; anal.: calcd. for $C_{15}H_{16}SiCrO_3$: C 55.55; H 4.98, found: C 55.63; H 4.83; IR (KBr, cm^{-1}) ν_{CO} 1959.1, 1876.1; ^{1}H NMR ($CDCl_3$, 500 MHz): δ 6.66 (m, 1H, H(2)), 5.29-5.13 (m, 2H, H(4), H(7)), 5.80-5.71 (m, 2H, H(5),H(6)), 3.49 (m, 2H, C*H*$_2$), 0.19 (s, 9H, Si(C*H*$_3$)$_3$); ^{13}C NMR ($CDCl_3$, 125 MHz): δ 228.4 (CO), 146.5 (C(2)), 137.4 (C(3)), 91.0, 90.1, 89.5, 88.4 (C(4), C(5), C(6) and C(7)), 42.4 (C(1)), -1.6 (Si(*C*H$_3$)$_3$); ^{29}Si NMR (CH_2Cl_2, 99.35 MHz):

δ -8.34; MS: (DEI, *m/z* (%)): 324 (22, $[M]^+$), 268 (17, $[M-2(CO)]^+$), 240 (82, $[M-3(CO)]^+$), 73 (100, $[Si(CH_3)_3]^+$); HRMS (DEI): calcd. for mass $^{12}C_{15}H_{16}Si_1Cr_1O_3$ ($[M]^+$), 324.0274 amu; found, 324.0279 amu.

η^6-(1,3-Dimethyl-1-*exo*-trimethylsilylindene)tricarbonylchromium, 4.38. To a solution **4.7** (1.3 g, 6.0 mmol) in *n*-butyl ether (50 mL) was added freshly distilled tetrahydrofuran (10 mL) and hexacarbonylchromium (2.5 g, 11.4). The mixture was heated at reflux for 96 h, the solvent removed under vacuum and the residue subjected to flash chromatography on silica gel. Elution using a mixture of hexanes and dichloromethane (5:1) yielded **4.38** as a bright yellow solid (0.66 g, 1.9 mmol, 32%); m.p. 128-130 °C; anal.: calcd. for $C_{17}H_{20}SiCrO_3$: C 57.94, H 5.73, found: C 58.02, H 5.61; IR (KBr, cm^{-1}) ν_{CO} 1956.6, 1879.3; ^{1}H NMR ($CDCl_3$, 500 MHz): δ 6.23 (s, 1H, H(2)), 5.78 (d, J = 6.0 Hz, 1H, H(4) or H(7)), 5.48 (d, J = 5.8 Hz, 1H, H(7) or H(4)), 5.42 (m, 1H, H(5) or H(6)), 5.01 (m, 1H, H(6) or H(5)), 2.06 (s, 3H, C(3)-C*H*$_3$), 1.43 (s, 3H, C(1)-C*H*$_3$), -0.11 (s, 9H, Si(C*H*$_3$)$_3$); ^{1}H NMR ($Cl_2DCCDCl_2$, 500 MHz): δ 6.24 (s, 1H, H(2)), 5.76 (d, J = 6.0 Hz, 1H, H(4) or H(7)), 5.51 (d, J = 5.8 Hz, 1H, H(7) or H(4)), 5.38 (m, 1H, H(5) or H(6)), 5.03 (m, 1H, H(6) or H(5)), 2.08 (s, 3H, C(3)-C*H*$_3$), 1.47 (s, 3H, C(1)-C*H*$_3$), -0.07 (s, 9H, Si(C*H*$_3$)$_3$); ^{13}C NMR ($CDCl_3$, 125 MHz): δ 238.1 (CO), 143.2 (C(2)), 135.0 (C(3)), 122.6 (C(3a) or C(7a)), 117.6 (C(7a) or C(3a)), 93.8, 90.2, 86.5, 83.2 (C(4), C(5), C(6) and C(7)), 46.3 (C(1)), 18.7 (C(1)-*C*H$_3$), 12.1 (C(3)-*C*H$_3$), -3.68 Si(*C*H$_3$)$_3$; ^{29}Si NMR ($CDCl_3$, 99.36 MHz): δ 9.7; MS (DEI, *m/z* (%)): 352 (7, $[M]^+$), 296 (11, $[M-2CO]^+$), 268 (19, $[M-3CO]^+$), 73 (100, $[Si(CH_3)_3]^+$). A sample suitable for structural determination (0.20 x 0.15 x 0.05 mm^3) by single-crystal X-ray diffraction was obtained by recrystallization from dichloromethane.

(1-Indenyl)SiMe$_2$(C≡C-SiMe$_3$), 4.51. Trimethylsilyl-acetylene (1.14 g, 11.6 mmol) in freshly distilled diethyl ether (100 mL) was cooled to -78 °C, and *n*-butyllithium (7.4 mL of a 1.6 M hexane solution, 12 mmol) was added dropwise over a 1 h period. After stirring at -78 °C for an additional

2 h, this solution was transferred *via* cannula into a flask containing dichlorodimethylsilane (1.5 g, 11.6 mmol) in freshly distilled ether (100 mL) at -78 °C. After allowing the mixture react at room temperature for 6 h, stirring was stopped in order to allow for the precipitated LiCl to settle. The resulting solution was then transferred *via* cannula into a flask containing a mixture of indene (1.35 g, 11.6 mmol) and *n*-butyllithium (7.4 mL of a 1.6 M hexane solution, 12 mmol) in freshly distilled ether (100 mL) at -78 °C. When the addition was complete, the mixture was allowed to warm to room temperature and stirred for an additional 18 h. The product was then extracted by using water (2 x 50 mL), and the organic phase dried over anhydrous Na_2SO_4. After removal of ether, the orange oily residue was subjected to column chromatography on silica gel. Elution with hexanes/CH_2Cl_2 (80:20) gave **4.51** as a pale yellow oil (2.73 g, 10.1 mmol, 87%). ^{1}H NMR ($CDCl_3$, 500 MHz): δ 7.59 (d, J = 7.5 Hz, 1H, H(7)), 7.43 (d, J = 7.5 Hz, 1H, H(4)), 7.24 (t, J = 7.4 Hz, 1H, H(5)), 7.17 (t, J = 7.4 Hz, 1H, H(6)), 6.93 (d of d, J = 5.3 Hz and J = 1.9 Hz, 1H, H(3)), 6.64 (d of d, J = 5.3 Hz and J = 1.9 Hz, 1H, H(2)), 3.64 (t, J = 1.9 Hz, 1H, H(1)), 0.20 (s, 9H, $SiMe_3$), -0.04 (s, 3H, Si(*Me*)(Me′)C≡CSiMe$_3$), -0.08 (s, 3H, Si(Me)(*Me′*)C≡CSiMe$_3$); ^{13}C NMR ($CDCl_3$, 125 MHz): δ 144.4 (C(3a)), 144.3 (C(7a)), 135.1 (C(2)), 130.0 (C(3)), 125.3 (C(5)), 123.9 (C(6)), 123.3 (C(7)), 121.1 (C(4)), 115.4 (SiMe$_2$C≡*C*SiMe$_3$), 111.8 (SiMe$_2$*C*≡CSiMe$_3$), 45.3 (C(1)), -0.08 ($SiMe_3$), -3.12 (Si(Me)(*Me′*)C≡CSiMe$_3$), -3.83 (Si(*Me*)(Me′)C≡CSiMe$_3$); ^{29}Si NMR (CH_2Cl_2, 99.35 MHz): δ 0.42 ($SiMe_2$), -0.23 ($SiMe_3$); Mass spectra: (DEI, *m/z* (%)): 270 (12, $[M]^+$), 255 (5, $[M-(Me)]^+$), 173 (56, $[(C_9H_7)SiMe_2]^+$), 155 (100, $[SiMe_2C{\equiv}CSiMe_3]^+$) 115 (70, $[C_9H_7]^+$), 73 (76, $[SiMe_3]^+$); Anal.: Calcd. for $C_{16}H_{22}Si_2$: C 71.04; H 8.21. Found: C 70.46; H 8.02.

(1-Indenyl)SiMe$_2$(C≡C-SiMe$_3$)[Co$_2$(CO)$_6$], 4.52. Octacarbonyldicobalt (0.65 g, 1.91 mmol) and **4.51** (0.50 g, 1.85 mmol) were allowed to react in freshly distilled tetrahydrofuran (50 mL) at room temperature for 18 h. After removal of solvent, the residue was subjected to flash chromatography on silica gel. Elution with hexanes gave **4.52** as a red viscous oil (0.86 g, 1.6 mmol, 84%). ^{1}H NMR ($CDCl_3$, 500 MHz): δ 7.57 (d, J = 7.4 Hz, 1H, H(7)), 7.47 (d, J = 7.4 Hz, 1H,

H(4)), 7.26 (t, J = 7.4 Hz, 1H, H(5)), 7.21 (t, J = 7.4 Hz, 1H, H(6)), 6.98 (d of d, J = 5.6 Hz and J = 1.7 Hz, 1H, H(3)), 6.73 (d of d, J = 5.6 Hz and J = 1.7 Hz, 1H, H(2)), 3.78 (t, J = 1.7 Hz, 1H, H(1)), 0.59 (s, 3H, Si(*Me*)(Me′)C≡CSiMe$_3$), 0.31 (s, 9H, SiMe$_3$), -0.17 (s, 3H, Si(Me)(*Me′*)C≡CSiMe$_3$); ^{13}C NMR ($CDCl_3$, 125 MHz): δ 145.3 (C(3a)), 144.9 (C(7a)), 136.4 (C(2)), 130.8 (C(3)), 126.4 (C(5)), 125.0 (C(6)), 124.4 (C(7)), 122.3 (C(4)), 94.42 (SiMe$_2$C≡*C*SiMe$_3$), 90.13 (SiMe$_2$*C*≡CSiMe$_3$), 47.4 (C(1)), 1.79 (Si(*Me*)(Me′)C≡C-SiMe$_3$), 1.40 (SiMe$_3$), -2.82 (Si(Me)(*Me′*)C≡CSiMe$_3$); ^{29}Si NMR (CH_2Cl_2, 99.36 MHz): δ -3.01 (SiMe$_3$), -3.24 (SiMe$_2$); Mass spectra: (DEI, *m/z* (%)): 556 (6, [M]$^+$), 528 (4, [M-(CO)]$^+$), 500 (10, [M-2(CO)]$^+$), 472 (32, [M-3(CO)]$^+$), 444 (16, [M-4(CO)]$^+$), 416 (37, [M-5(CO)]$^+$), 388 (74, [M-6(CO)]$^+$), 73 (100, [SiMe$_3$]$^+$).

(1-Indenyl)SiMe$_2$(C≡C-SiMe$_3$)TCNE, 4.53. Tetracyanoethylene (0.094 g, 0.73 mmol) was added to a solution of **4.51** (0.182 g, 0.67 mmol) in ethyl acetate (75 mL) and stirred at ambient temperature for 72 h. The residue obtained after removal of the solvent was washed with hexanes (3 x 25 mL) and then dried to give **4.53** as a pale beige powder, m.p. (with decomposition) 163-165 °C (0.243 g, 0.61 mmol, 91%). ^{1}H NMR (CD_3CN, 500 MHz): δ 7.58-7.52 (m, 2H, H(8) and H(11)), 7.50-7.44 (m, 2H, H(9) and H(10)), 4.66 (d, ^{3}J = 1.7 Hz, 2H, H(1) and H(4)), 2.11 (t, ^{3}J = 1.7 Hz, 1H, H(7)), 0.14 (s, 9H, SiMe$_3$), -0.12 (s, 6H, SiMe$_2$); ^{13}C NMR (CD_2Cl_2, 125 MHz): δ 140.4 (C(2) and C(3)), 130.9 (C(9) and C(10)), 126.4 (C(8) and C(11)), 118.4 (SiMe$_2$C≡*C*SiMe$_3$), 113.9, 112.2 (*exo* and *endo* nitriles), 109.7 (SiMe$_2$*C*≡CSiMe$_3$), 61.1 (C(1) and C(4)), 51.2 (C(5) and C(6)), 50.2 (C(7)), -0.26 (SiMe$_2$), -1.94 (Si(Me)$_3$); ^{29}Si NMR (CH_2Cl_2, 99.35 MHz): δ -17.9 (SiMe$_3$),-18.7 (SiMe$_2$); Mass spectra: (DEI, *m/z* (%)): 383 (14, [M-Me]$^+$), 270 (22, [M-(C_6N_4)]$^+$), 155 (100, [SiMe$_2$C≡CSiMe$_3$]$^+$); (CI, NH_3, *m/z* (%)): 416 (22, [M+18]$^+$); Anal.: Calcd. for $C_{22}H_{22}Si_2N_4$: C 66.29; H 5.56; N 14.06. Found: C 65.91; H 5.37; N 14.24.

(1-Indenyl)SiMe$_2$(C≡C-SiMe$_3$)[Co$_2$(CO)$_6$]TCNE, 4.54. Tetracyanoethylene (0.035 g, 0.27 mmol) was added to a solution of **4.52** (0.10 g, 0.18 mmol) in ethyl acetate (50 mL) and stirred at

ambient temperature for 72 h. The residue obtained after removal of the solvent was subjected to flash chromatography on silica gel. Elution with a mixture of CH_2Cl_2 and ethyl acetate (1:1) yielded **4.54** as a red crystalline solid (0.10 g, 0.15 mmol, 83%), which darkens considerably above 140 °C, but does not melt below 290 °C. ^{1}H NMR (CD_2Cl_2, 500 MHz): δ 7.65-7.61 (m, 2H, H(8) and H(11)), 7.53-7.48 (m, 2H, H(9) and H(10)), 4.73 (d, ^3J = 1.2 Hz, 2H, H(1) and H(4)), 2.22 (t, ^3J = 1.2 Hz, 1H, H(7)), 0.35 (s, 9H, $SiMe_3$), -0.08 (s, 6H, $SiMe_2$); ^{13}C NMR (CD_2Cl_2, 125 MHz): δ 200.8 (C≡O), 138.4 (C(2) and C(3)), 131.2 (C(9) and C(10)), 125.7 (C(8) and C(11)), 112.5, 110.8 (*exo* and *endo* nitriles), 94.3 ($SiMe_2C{\equiv}CSiMe_3$), 86.7 ($SiMe_2C{\equiv}CSiMe_3$), 60.8 (C(1) and C(4)), 50.8 (C(7)), 50.27 (C(5) and C(6)), 1.352 ($SiMe_3$), -0.33 ($SiMe_2$); ^{29}Si NMR ($CHCl_3$, 99.36 MHz): δ 1.1 ($SiMe_3$), -0.9 ($SiMe_2$); IR (CD_2Cl_2, cm^{-1}): 2226.3, 2070.9, 2035.8, 2017.2; Mass spectra: (DEI, *m/z* (%)): 684 (12, $[M]^+$), 628 (17, $[M\text{-}2(CO)]^+$), 572 (14, $[M\text{-}4(CO)]^+$), 544 (21, $[M\text{-}5(CO)]^+$), 516 (24, $[M\text{-}6(CO)]^+$), 457 (12, $[M\text{-}4(CO)\text{-}Co]^+$), 155 (100, $[SiMe_2C{\equiv}CSiMe_3]^+$) 115 (42, $[C_9H_7]^+$), 73 (52, $[SiMe_3]^+$); Anal.: Calcd. for $C_{28}H_{22}Co_2Si_2O_6N_4$: C 49.12; H 3.24; N 8.19. Found: C 49.41; H 3.12; N 8.09. A single red prism (0.35 mm X 0.12 mm X 0.08 mm) suitable for structural determination by single-crystal X-ray diffraction was obtained by recrystallization from a mixture of CH_2Cl_2 and diethyl ether (1:1).

3-Pentenyl-1-trimethylsilylindene, 5.10. A solution of 1-trimethylsilylindene, **1.109** (2.1 g, 11.2 mmol) in freshly distilled diethyl ether (100 mL) was cooled to -78 °C, and *n*-butyllithium (7.5 mL of a 1.6 M hexane solution, 12 mmol) was added dropwise over 1 h. After stirring the solution at room temperature for an additional 6 h, 6-bromopent-1-ene (1.7 g, 11.4 mmol) was added dropwise at -78 °C over a 1 h period. When the addition was complete, the mixture was allowed to warm to room temperature over 18 h, after which the solvent was evaporated and the residue extracted using diethyl ether (3 X 60 mL) and water (3 X 50 mL). The isolated organic residue was then subjected to flash chromatography on silica gel. Elution with hexanes yielded **5.10** as a yellow oil (1.66 g, 6.5 mmol, 58%). ^{1}H NMR ($CDCl_3$, 200 MHz): δ 7.29-6.98 (m, 4H, H(4), H(5),

H(6) and H(7)), 6.16 (d, 1.7 Hz, 1H, H(2)), 5.73 (m, 1H, C*H*=CH_2), 4.84 (m, 2H, CH=CH_2), 3.17 (d, 1.7 Hz, 1H, H(1)), 2.48 (m, 2H, H(8)), 2.15 (m, 2H, H(10)), 1.65 (m, 2H, H(9)), -0.20 ($Si(CH_3)_3$); ^{13}C NMR ($CDCl_3$, 50 MHz): δ 146.0 (C(7a)), 144.3 (C(3a)), 141.5 (C(3)), 138.5 (C(11)), 129.7 (C(2)), 124.5 (C(5)), 123.5 (C(6)), 122.5 (C(7)), 118.9 (C(4)), 114.7 (C(12)), 44.3 (C(1)), 33.7 (C(10)), 28.1 (C(9)), 27.0 (C(8)), -2.60 ($Si(CH_3)_3$); ^{29}Si NMR ($CHCl_3$, 99.36 MHz): δ 4.6; Mass spectra: (DEI, *m/z* (%)): 256 (56, $[M]^+$), 183 (32, $[M-(Si(CH_3)_3)]^+$), 73 (100, $[Si(CH_3)_3]^+$); (high resolution, DEI): calculated mass for $^{12}C_{17}H_{24}Si$ $[M]^+$, 256.1647 amu; observed mass: 256.1655 amu.

3-Hexenyl-1-methylindene, 5.14. To a suspension of magnesium turnings (190 mg, 7.8 mmol) and a catalytic amount of iodine in freshly distilled diethyl ether (100 mL) was added 6-bromohex-1-ene (1.0 g, 6.1 mmol) at 0 °C under an atmosphere of dry nitrogen. After allowing the mixture to warm to room temperature over 18 h, a solution of 3-methylindan-1-one (0.90 g, 6.1 mmol) in freshly distilled diethyl ether (20 mL) was added dropwise over a 1 h period and stirred for an additional 24 h. The precipitated magnesium salts were then filtered and the filtrate extracted with water (3 X 75 mL). To the residual diethyl ether solution was added glacial acetic acid (10 mL) and concentrated sulphuric acid (1 mL), followed by gentle heating for 5 h at 45 °C. The crude mixture was then cooled and the desired product extracted into diethyl ether, followed by drying over anhydrous $MgSO_4$. The residue obtained after removal of the solvent was subjected to column chromatography on silica gel. Elution with hexanes produced **5.14** as a pale yellow oil (1.06 g, 5.0 mmol, 82%). ^1H NMR ($CDCl_3$, 500 MHz): δ 7.30 (m, 1H, H(7)), 7.20 (m, 1H, H(4)), 7.17 (m, 1H, H(5)), 7.10 (m, 1H, H(6)), 6.03 (d, J = 1.6 Hz, 1H, H(2)), 5.73 (m, 1H, C*H*=CH_2), 4.88 (m, 2H, CH=CH_2), 3.31 (d (J = 1.8 Hz) of quart (J = 7.6 Hz), 1H, H(1)), 2.42 (t, J = 5.4 Hz, 2H, H(8)), 2.01 (m, 2H, H(11)), 1.60 (m, 2H, H(9)), 1.42 (m, 2H, H(10)), 1.18 (d, J = 7.6 Hz, 3H, CH_3); ^{13}C NMR ($CDCl_3$, 125 MHz): δ 150.0 (C(7a)), 144.6 (C(3a)), 142.6 (C(3)), 138.9 (C(12)), 135.0 (C(2)), 126.1 (C(5)), 124.6 (C(6)), 122.5 (C(7)), 118.9 (C(4)), 114.3 (C(13)), 43.7 (C(1)), 33.6

(C(11)), 28.8 (C(10)), 27.4 (C(9)), 27.3 (C(8)), 16.3 (CH_3).; Mass spectra: (DEI, *m/z* (%)): 212 (41, $[M]^+$), 197 (8, $[M-(CH_3)]^+$), 157 (45, $[M-(C_4H_7)]^+$), 143 (98, $[M-(C_5H_9)]^+$), 129 (100, $[M-(C_6H_{11})]^+$), 115 (55, $[C_9H_7]^+$); (high resolution, DEI): calculated mass for $^{12}C_{16}H_{22}$ $[M]^+$, 212.1565 amu; observed mass: 212.1563 amu; Anal.: Calcd. for $C_{16}H_{20}$: C 90.51; H 9.49. Found: C 90.44; H 9.56.

3-Hexenyl-1-methyl-1-trimethylsilylindene, 5.15, and 1-Hexenyl-3-methyl-1-trimethylsilylindene, 5.17. A solution of **5.14** (0.34 g, 1.6 mmol) in freshly distilled tetrahydrofuran (70 mL) was cooled to -78 °C, and *n*-butyllithium (1.6 mL of a 1.4 M hexane solution, 2.3 mmol) was added dropwise over 1 h under an atmosphere of dry nitrogen. After stirring the solution at room temperature for an additional 6 h, chlorotrimethylsilane (0.5 g, 4.6 mmol) was added dropwise at -78 °C over a 1 h period. When the addition was complete, the mixture was allowed to warm to room temperature over 18 h, and then refluxed for an additional 5 h, after which the solvent was evaporated and the residue extracted with cold diethyl ether (100 mL). After filtration of the lithium salts and removal of diethyl ether, the residue was subjected to flash chromatography on silica gel. Elution with a mixture of hexanes and CH_2Cl_2 (~1:1) yielded a mixture of **5.15** and **5.17** (in a ratio of ~ 2:1) as a yellow oil (0.35 g, 1.2 mmol, 75%). **5.15:** ^{1}H NMR ($CDCl_3$, 500 MHz): δ 7.35-7.16 (m, 4H, H(4), H(5), H(6) and H(7)), 6.15 (m, 1H, H(2)), 5.82 (m, 1H, C*H*=CH_2), 4.96 (m, 2H, CH=C*H*$_2$), 2.57 (m, 2H, H(8)), 2.10 (m, 2H, H(11)), 1.68 (m, 2H, H(9)), 1.53 (m, 2H, H(10)), 1.42 (s, 3H, CCH_3), -0.17 ($Si(CH_3)_3$); ^{13}C NMR ($CDCl_3$, 125 MHz): δ 151.2 (C(7a)), 144.0 (C(3a)), 140.6 (C(3)), 139.0 (C(12)), 136.8 (C(2)), 124.6 (C(5)), 123.7 (C(6)), 121.8 (C(7)), 119.0 (C(4)), 114.3 (C(13)), 46.0 (C(1)), 33.6 (C(11)), 29.0 (C(10)), 28.2 (C(9)), 27.4 (C(8)), 16.1 (CH_3), -3.52 ($Si(CH_3)_3$); ^{29}Si NMR ($CHCl_3$, 99.36 MHz): δ 6.9. **5.17:** ^{1}H NMR ($CDCl_3$, 500 MHz): δ 7.35-7.16 (m, 4H, H(4), H(5), H(6) and H(7)), 6.11 (quart., J = 1.4 Hz, 1H, H(2)), 5.68 (m, 1H, C*H*=CH_2), 4.87 (m, 2H, CH=C*H*$_2$), 2.18 (d, J = 1.4, 3H, CCH_3), 1.87 (m, 2H, H(11)), 1.29-1.26 (m, 4H, H(9) and H(10)), 0.87 (m, 2H, H(8)), -0.21 ($Si(CH_3)_3$); ^{13}C NMR ($CDCl_3$, 125 MHz): δ 148.9 (C(7a)),

145.4 (C(3a)), 141.2 (C(3)), 139.1 (C(12)), 135.6 (C(2)), 124.5 (C(5)), 123.5 (C(6)), 121.6 (C(7)), 118.8 (C(4)), 114.0 (C(13)), 51.8 (C(1)), 33.5 (C(11)), 31.6 (C(10)), 30.4 (C(9)), 29.7 (C(8)), 12.8 (CH_3), -3.39 ($Si(CH_3)_3$); ^{29}Si NMR ($CHCl_3$, 99.36 MHz): δ 6.2; Mass spectra: (DEI, *m/z* (%)): 284 (5, $[M]^+$), 269 (12, $[M-(CH_3)]^+$), 211 (14, $[M-(Si(CH_3)_3)]^+$), 73 (100, $[Si(CH_3)_3]^+$); (high resolution, DEI): calculated mass for $^{12}C_{19}H_{28}Si$ $[M]^+$, 284.1960 amu; observed mass: 284.1945 amu. Anal.: Calcd. for $C_{19}H_{28}Si$: C 80.21; H 9.92. Found: C 80.33; H 9.87.

REFERENCES

1. Muetterties, E. L. *Inorg. Chem.* **1965**, *4*, 769.
2. Doering, W. v. E.; Roth, W. R. *Angew. Chem. Int. Ed. Engl.* **1963**, *2*, 115.
3. Berry, R. W. *J. Chem. Phys.* **1960**, *32*, 933.
4. Schröder, G.; Oth, J. F. M.; Merényi, R. *Angew. Chem. Internat. Edit:* **1965**, *4*, 752.
5. Saunders, M. *Tetrahedron Lett.* **1963**, *25*, 1699.
6. Sanders, J. K. M.; Hunter, B. K. *Modern NMR Spectroscopy*; Oxford University Press: Toronto, 1987, p. 208.
7. Sandström, J. *Dynamic NMR Spectroscopy;* Academic Press: Toronto, 1982.
8. Perrin, C. L.; Dwyer, T. J. *Chem. Rev.* **1990**, *90*, 935.
9. Forsén, S.; Hoffman, R. A. *J. Chem. Phys.* **1963**, *39*, 2892.
10. Dahlquist, F. W.; Longmuir, K. J.; DuVernet, R. B. *J. Magn. Reson.* **1975**, *17*, 406.
11. Led, J. J.; Gesmar, H. *J. Magn. Reson.* **1982**, *49*, 444.
12. Grassi, M.; Mann, B. M.; Pickup B. T.; Spencer C. M. *J. Magn. Reson.* **1986**, *69*, 92.
13. Muhandiram, D. R.; McClung, R. E. D. *J. Magn. Reson.* **1987**, *71*, 187.
14. Bain, A. D.; Cramer, J. A. *J. Magn. Reson.* **1993**, *A 103*, 217.
15. Bain, A. D.; Cramer, J. A. *J. Phys. Chem.* **1993**, *97*, 2884.
16. Jeener, J.; Meier, B. H.; Bachmann, P.; Ernst, R. R. *J. Chem. Phys.* **1979**, *71*, 4546.
17. Abel, E. W.; Coston, T. P. J.; Orrell, K. G.; Šik, V.; Stephenson, D. *J. Magn. Reson.* **1986**, *70*, 34.
18. Detellier, C. In *Modern NMR Techniques and Their Application in Chemistry*; Popov, A. I., Hallenga, K., Eds.; Marcel Dekker: New York, 1991; Chapter 9.
19. Farrugia, L. J.; Rae, S. E. *Organometallics* **1992**, *11*, 196.
20. Perrin, C. L. *J. Magn. Reson.* **1989**, *82*, 619.
21. Cotton, F. A. *Acc. Chem. Res.* **1968**, *1*, 257.
22. Cotton, F. A. *J. Organometal. Chem.* **1975**, *100*, 29.

23. Cotton, F. A. In *Dynamic Nuclear Magnetic Resonance Spectroscopy*; Jackman, L. M., Cotton, F. A., Eds.; Academic Press: New York, 1975; p. 377.

24. Mingos, D. M. P. In *Comprehensive Organometallic Chemistry*; Wilkinson, G., Stone, F. G. A., Abel, E. W., Eds.; Pergamon Press: Toronto, 1982; Vol. 3, p. 1.

25. Mann, B. E. In *Comprehensive Organometallic Chemistry*; Wilkinson, G., Stone, F. G. A., Abel, E. W., Eds.; Pergamon Press: Toronto, 1982; Vol. 3, p. 89.

26. Mann, B. E. *Chem. Soc. Rev.* **1986**, *15*, 167.

27. Hoffmann, R.; Woodward, R. B. *Acc. Chem. Res.* **1968**, *1*, 17.

28. Woodward, R. B.; Hoffmann, R. *The Conservation of Orbital Symmetry*; Academic Press: New York, 1970.

29. Spangler, C. W. *Chem. Rev.* **1976**, *76*, 187.

30. Miller, S. I. *Adv. Phys. Org. Chem.* **1968**, *6*, 185.

31. Berson, J. A. *Acc. Chem. Res.* **1972**, *5*, 406.

32. McKinney, M. A.; Haworth, D. T. *J. Chem. Ed.* **1980**, *57*, 110.

33. Zimmerman, H. E.; Crumrine, D. S.; Dopp, D.; Huyffer, P. S. *J. Am. Chem. Soc.* **1969**, *91*, 434.

34. Hallam, B. F.; Pauson, P. L. *Chem. Ind.* **1955**, *23*, 653.

35. Wilkinson, G.; Piper, T. S. *J. Inorg. Nucl. Chem.* **1956**, *2*, 32.

36. Wilkinson, G.; Piper, T. S. *J. Inorg. Nucl. Chem.* **1956**, *3*, 104.

37. Bennett, M. J.; Cotton, F. A.; Davison, A.; Faller, J. W.; Lippard, S. J.; Morehouse, S. M. *J. Am. Chem. Soc.* **1966**, *88*, 4371.

38. Gutowsky, H. S.; Saika, A. *J. Chem. Phys.* **1953**, *21*, 1688.

39. Cotton, F. A.; Musco, A.; Yagupsky, G. *J. Am. Chem. Soc.* **1967**, *89*, 6136.

40. Cotton, F. A.; Marks, T. J. *J. Am. Chem. Soc.* **1969**, *91*, 7523.

41. Ciappenelli, D. J.; Cotton, F. A.; Kruczynski, L. *J. Organometal. Chem.* **1972**, *42*, 159.

42. Campbell, C. H.; Green, M. L. H. *J. Chem. Soc. A* **1970**, 1318.

43. Whitesides, G. M.; Fleming, J. S. *J. Am. Chem. Soc.* **1967**, *89*, 2855.

44. West, P.; Woodville, M. C.; Rausch, M. D. *J. Am. Chem. Soc.* **1969**, *91*, 5649.

45. Calderon, J. L.; Cotton, F. A.; Takats, J. *J. Am. Chem. Soc.* **1971**, *93*, 3587.

46. Jutzi, P. *Chem. Rev.* **1986**, *86*, 983.

47. Jutzi, P. *J. Organometal. Chem.* **1990**, *400*, 1.

48. Childs, R. F. *Tetrahedron* **1982**, *38*, 567.

49. Fritz, H. P.; Kreiter, C. G. *J. Organometal. Chem.* **1965**, *4*, 313.

50. Davison, A.; Rakita, P. E. *J. Am. Chem. Soc.* **1968**, *90*, 4479.

51. Abel, E. W.; Dunster, M. O.; Waters, A. *J. Organometal. Chem.* **1973**, *49*, 287.

52. Sergeyev, N. M.; Avramenko, G. I.; Ustynyuk, Y. A. *J. Organometal. Chem.* **1970**, *22*, 79.

53. Cotton, F. A.; Marks, T. J. *Inorg. Chem.* **1970**, *9*, 2802.

54. Davison, A.; Rakita, P. E. *Inorg. Chem.* **1970**, *9*, 289.

55. Bonny, A.; Holmes-Smith, R. D.; Hunter, G.; Stobart, S. R. *J. Am. Chem. Soc.* **1982**, *104*, 1855.

56. Johnson, H. D.; Hartford, T. W.; Spangler, C. W. *J. Chem. Soc., Chem. Commun.* **1978**, 242.

57. Schoeller, W. W. *J. Chem. Soc. Dalton Trans.* **1984**, 2233.

58. Mikhailov, B. M.; Baryshnikova, T. K.; Bogdanov, V. S. *Dokl. Akad. Nauk. SSSR.* **1972**, *202*, 358.

59. Kroll, W. R.; Naegele, W. *J. Chem. Soc., Chem. Commun.* **1969**, 246.

60. Fisher, J. D.; Budzelaar, P. H. M.; Shapiro, P. J.; Staples, R. J.; Yap, G. P. A.; Rheingold, A. L. *Organometallics* **1997**, *16*, 871.

61. Beachley, O. T., Jr.; Getman, T. D.; Kirss, R. U.; Hallock, R. B.; Hunter, W. E.; Atwood, J. L. *Organometallics* **1985**, *4*, 751.

62. Einstein, F. W. B.; Gilbert, M. M.; Tuck, D. G. *Inorg. Chem.* **1972**, *11*, 2832.

63. Jutzi, P.; Saleske, H. *Chem. Ber.* **1984**, *117*, 222.

64. Jutzi, P.; Kuhn, M. *Chem. Ber.* **1974**, *107*, 1228.

65. Bentham, J. E.; Ebsworth, E. A. V.; Moretto, H.; Rankin, D. W. H. *Angew. Chem. Int. Ed. Engl.* **1972**, *11*, 640.

66. Schoeller, W. W. *Z. Naturforsch.* **1984**, *39b*, 1767.

67. Deubzer, B; Elian, M.; Fischer, E. O.; Fritz, H. P. *Chem. Ber.* **1970**, *103*, 799.

68. Schoeller, W. W. *Z. Naturforsch.* **1983**, *38b*, 1636.

69. Field, D. J.; Jones, D. W. *J. Chem. Soc., Perkin Trans. I.* **1980**, 1909.

70. Luzikov, Yu. N.; Sergeyev, N. M.; Ustynyuk, Yu. A. *J. Organometal. Chem.* **1974**, *65*, 303.

71. Lobanova, I. A.; Zdanovich, V. I. *Russian Chem. Rev.* **1988**, *57*, 967.

72. Hart-Davis, A. J.; Mawby, R. J. *J. Chem. Soc. A* **1969**, 2403.

73. O'Connor, J. M.; Casey, C. P. *Chem. Rev.* **1987**, *87*, 307.

74. Rerek, M. E.; Ji, L.-N.; Basolo, F. *J. Chem. Soc., Chem. Commun.* **1983**, 1208.

75. Basolo, F. *New J. Chem.* **1994**, *16*, 19.

76. Kowaleski, R. M.; Rheingold, A. L.; Trogler, W. C.; Basolo, F. *J. Am. Chem. Soc.* **1986**, *108*, 2460.

77. Gamelas, C. A.; Herdtweck, E.; Lopes, J. P.; Romão, C. C. *Organometallics.* **1999**, *18*, 506.

78. Nesmeyanov, A. N.; Ustynyuk, N. A.; Makarova, L. G.; Andrianov, V. G.; Struchkov, Y.,T.; Andrae, S. *J. Organometal. Chem.* **1978**, *159*, 189.

79. Merola, J. S.; Kacmarcik, R. T.; Van Engan, D. *J. Am. Chem. Soc.* **1986**, *108*, 329.

80. Husebo, T. L.; Jensen, C. M. *Organometallics* **1995**, *14*, 1087.

81. Schmid, C.; Alt, H. G.; Milius, W. *J. Organometal. Chem.* **1997**, *544*, 139.

82. Licht, E. H.; Alt, H. G.; Milius, W.; Abu-Orabi, S. *J. Organometal. Chem.* **1998**, *560*, 69.

83. Alt, H. G.; Han, J. S.; Rogers, R. D. *J. Organometal. Chem.* **1993**, *454*, 165.

84. Casey, C. P.; O'Connor, J. M. *Organometallics* **1985**, *4*, 384.

85. Casey, C. P.; O'Connor, J. M.; Jones, W. D.; Haller, K. J. *Organometallics* **1983**, *2*, 535.

86. Bang, H.; Lynch, T. J.; Basolo, F. *Organometallics* **1992**, *11*, 40.

87. Herrmann, W. A.; Kuhn, F. E.; Romão, C. C. *J. Organometal. Chem.* **1995**, *489*, C56.

88. Zhou, Y.; Dewey, M. A.; Gladysz, J. A. *Organometallics* **1993**, *12*, 3918.

89. Lee, S. W.; Richmond, M. G. *Inorg. Chem.* **1991**, *30*, 2237.

90. Cotton, F. A.; Marks, T. J. *J. Am. Chem. Soc.* **1969**, *91*, 3178.

91. Belmont, J. A.; Wrighton, M. S. *Organometallics* **1986**, *5*, 1421.

92. Blenkiron, P.; Enright, G. D.; Taylor, N. J.; Carty, A. J. *Organometallics* **1996**, *15*, 2855.

93. Caddy, P.; Green, M.; O'Brien, E.; Smart, L. E.; Woodward, P. *Angew. Chem. Int. Ed. Engl.* **1977**, *16*, 648.

94. Merola, J. S.; Kacmarcik, R. T. *Organometallics* **1989**, *8*, 778.

95. Habib, A.; Tanke, R. S.; Holt, E. M.; Crabtree, R. H. *Organometallics* **1989**, *8*, 1225.

96. Foo, T.; Bergman, R. G. *Organometallics* **1992**, *11*, 1811.

97. Bellomo, S.; Ceccon, A.; Gambaro, A.; Santi, S.; Venzo, A. *J. Organometal. Chem.* **1993**, *453*, C4.

98. Bonifaci, C.; Carta, G.; Ceccon, A.; Gambaro, A.; Santi, S.; Venzo, A. *Organometallics* **1996**, *16*, 1630.

99. Cecchetto, P.; Ceccon, A.; Gambaro, A.; Santi, S.; Ganis, P.; Gobetto, R.; Valle, G.; Venzo, A. *Organometallics* **1998**, *17*, 752.

100. Huber, T. A.; Bélanger-Gariépy, F.; Zargarian, D. *Organometallics* **1995**, *14*, 4997.

101. Huber, T. A.; Bayrakdarian, M.; Dion, S.; Dubuc, I.; Bélanger-Gariépy, F.; Zargarian, D. *Organometallics* **1997**, *16*, 5811.

102. O'Hare, D. *Organometallics* **1987**, *6*, 1766.

103. Ackermann, M. N.; Ajmera, R. K.; Barnes, H. E.; Gallucci, J. C.; Wojcicki, A. *Organometallics* **1999**, *18*, 787.

104. Saegusa, T.; Ito, Y.; Tomita, S. *J. Am. Chem. Soc.* **1971**, *93*, 5656.

105. Kitching, W.; Hegarty, B. F. *J. Organometal. Chem.* **1969**, *16*, P39.

106. Kitching, W.; Hegarty, B. F.; Doddrell, D. *J. Organometal. Chem.* **1970**, *21*, 29.

107. Cotton, F. A.; Hunter, D. L.; Jamerson, J. D. *Inorg. Chim. Acta* **1975**, *15*, 245.

108. Halterman, R. L. *Chem. Rev.* **1992**, *92*, 965.

109. Britovsek, G. J. P.; Gibson, V. C.; Wass, D. F. *Angew. Chem. Intl. Ed.* **1999**, *38*, 428.

110. Lee, H.; Desrosiers, P. J.; Guzei, I.; Rheingold, A. L.; Parkin, G. *J. Am. Chem. Soc.* **1998**, *120*, 3255.

111. Mikhailov, B. M.; Baryshnikova, T. K.; Bogdanov, V. S.; Negrebetskii, V. V. *Dokl. Akad. Nauk. SSSR.* **1972**, *207*, 613.

112. Mikhailov, B. M.; Baryshnikova, T. K.; Bogdanov, V. S. *Z. Obshch. Khim.* **1972**, *43*, 1949.

113. Rufanov, K.; Avtomonov, E.; Kazennova, N.; Kotov, V.; Khvorost, A.; Lemenovskii, D.; Lorberth, J. *J. Organometal. Chem.* **1997**, *536-537*, 361.

114. Herberich, G. E.; Barday, E.; Fischer, A. *J. Organometal. Chem.* **1998**, *567*, 127.

115. Barday, E.; Frange, B.; Hanquet, B.; Herberich, G. E. *J. Organometal. Chem.* **1999**, *572*, 225.

116. Duchateau, R.; Lancaster, S. J.; Thornton-Pett, M.; Bochmann, M. *Organometallics* **1997**, *16*, 4995.

117. Knizek, J.; Krossing, I.; Nöth, H.; Ponikwar, W. *Eur. J. Inorg. Chem.* **1998**, 505.

118. Thiyagarajan, B.; Jordan, R. F.; Young, V. G. *Organometallics* **1998**, *17*, 281.

119. Sommer, L. H.; Marans, N. S. *J. Am. Chem. Soc.* **1951**, *73*, 5135.

120. Rakita, P. E.; Davison, A. *Inorg. Chem.* **1969**, *8*, 1164.

121. Larrabee, R. B.; Dowden, B. F. *Tetrahedron Lett.* **1970**, *12*, 915.

122. Ashe, A. J., III. *Tetrahedron. Lett.* **1970**, *24*, 2105.

123. Davison, A.; Rakita, P. E. *J. Organometal. Chem.* **1970**, *23*, 407.

124. Amor, F.; Okuda, J. *J. Organometal. Chem.* **1996**, *520*, 245.

125. Foster, P.; Rausch, M. D.; Chien, J. C. W. *J. Organometal. Chem.* **1997**, *527*, 71.

126. Jin, R.; Wang, B.; Zhou, X.; Wang, R.; Wang, H. *Youji Huaxue.* **1993**, *13*, 35; Chemical Abstracts *118*: 234133c (1993).

127. Sergeyev, N. M.; Grishin, K.; Luzikov, Y. N.; Ustynyuk, Y. A. *J. Organometal. Chem.* **1972**, *38*, C1.

128. Rakita, P. E.; Taylor, G. A. *J. Organometal. Chem.* **1973**, *61*, 71.

129. Hogan, J. C., Ph.D. Thesis, Boston College (1969).

130. Angus, P. C.; Stobart, S. R. *J. Chem. Soc., Dalton Trans.* **1973**, 2374.

131. Orrell, K. G.; Šik, V.; Dunster, M. O.; Abel, E. W. *J. Chem. Soc., Faraday Trans.II.* **1975**, *71*, 631.

132. Kashin, A. N.; Khutoryanskii, V. A.; Bakunin, V. N.; Beletskaya, I. P.; Reutov, O. A. *J. Organometal. Chem.* **1977**, *128*, 359.

133. Kashin, A. N.; Bakunin, V. N.; Khutoryanskii, V. A.; Beletskaya, I. P.; Reutov, O. A. *J. Organometal. Chem.* **1979**, *171*, 309.

134. McMaster, A. D.; Stobart, S. R. *J. Chem. Soc., Dalton Trans.* **1982**, 2275.

135. Veith, M.; Olbrich, M.; Shihua, W.; Huch, V. *J. Chem. Soc., Dalton Trans.* **1996**, 161.

136. Herrmann, W. A.; Geisberger, M. R.; Kühn, F. E.; Artus, G. R. J.; Herdtweck, E. *Z. Anorg. Allg. Chem.* **1997**, *623*, 1229.

137. Nifant'ev, I. E.; Ivchenko, P. V. *Organometallics* **1997**, *16*, 713.

138. Morris, R. J.; Bock, P. L.; Jefferis, J. M.; Goedde, D. M. *Polyhedron* **1997**, *16*, 3699.

139. Heuer, L.; Bode, U. K.; Jones, P. G.; Schmutzler, R. *Z. Naturforsch.* **1989**, *44b*, 1082.

140. Fallis, K. A.; Anderson, G. K.; Rath, N. P. *Organometallics* **1992**, *11*, 885.

141. Aumann, R.; Jasper, B.; Fröhlich, R. *Organometallics* **1995**, *14*, 231.

142. Stradiotto, M.; Kozak, C. M.; McGlinchey, M. J. *J. Organometal. Chem.* **1998**, *564*, 101.

143. McMaster, A. D.; Stobart, S. R. *J. Am. Chem. Soc.* **1982**, *104*, 2109.

144. Kashin, A. N.; Bakunin, V. N.; Beletskaya, I. P.; Reutov, O. A. *Izv. Akad. Nauk. SSSR, Ser. Khim.* **1977**, *11*, 2638.

145. Harkte, K.; Schilling-Pindur, A. *Liebigs Ann. Chem.* **1984**, 552.

146. Feast, W. J.; Preston, W. E. *J. Chem. Soc., Chem. Commun.* **1974**, 985.

147. Castañer, J.; Riera, J.; Fajarí, L. *J. Org. Chem.* **1993**, *58*, 1377.

148. Woell, J. B.; Boudjouk, P. *J. Org. Chem.* **1980**, *45*, 5213.

149. Stradiotto, M.; Hughes, D. W.; Bain, A. D.; Brook, M. A.; McGlinchey, M. J. *Organometallics* **1997**, *16*, 5563.

150. Kerber, R. C.; Garcia, R.; Nobre, A. L. *Organometallics* **1996**, *15*, 5756.

151. Welker, M. E. *Chem. Rev.* **1992**, *92*, 97.

152. Wright, M. E. *Organometallics* **1983**, *2*, 558.

153. Ibbott, D. G.; Payne, N. C.; Shaver, A. *Inorg. Chem.* **1981**, *20*, 2193.

154. Churchill, M. R.; Ni Chang, S. W. Y. *J. Am. Chem. Soc.* **1973**, *95*, 5931.

155. Muir, K. W.; Sim, G. A. *Chem. Ind.* **1964**, 1581.

156. Glass, R. S.; McConnell, W. W. *Organometallics* **1984**, *3*, 1630.

157. Gilman, H.; Gist, L. A. *J. Org. Chem.* **1957**, *22*, 250.

158. Atwood, J. L.; McMaster, A. D.; Rogers, R. D.; Stobart, S. R. *Organometallics* **1984**, *3*, 1500.

159. Chen, Y.; Rausch, M. D.; Chien, J. C. W. *Organometallics* **1993**, *12*, 4607.

160. Rigby, S. S.; Girard, L.; Bain, A. D.; McGlinchey, M. J. *Organometallics* **1995**, *14*, 3798.

161. Christopher, J. N.; Jordan, R. F.; Petersen, J. L.; Young, V. G. *Organometallics* **1997**, *16*, 3044.

162. Stradiotto, M.; Rigby, S. S.; Hughes, D. W.; Brook, M. A.; Bain, A. D.; McGlinchey, M. J. *Organometallics* **1996**, *15*, 5645.

163. Stradiotto, M.; Brook, M. A.; McGlinchey, M. J. *New J. Chem.* **1999**, 317.

164. Mislow, K. *Acc. Chem. Res.* **1975**, *9*, 26.

165. In a hypercube (or *tesseract*) all cube edges are of equal length and all internal angles are 90°; it is difficult to represent such a 4-dimensional figure in 2-dimensions but an intriguing photograph merits examination: MacKay, D. M. *Electronic Engineering* **1960**, *32*, 344.

166. Gust, D.; Patton, A. *J. Am. Chem. Soc.* **1978**, *100*, 8175.

167. Smonou, I.; Khan, S.; Foote, C. S.; Elemes, Y.; Mavridis, I. M.; Pantidou, A.; Orfanopoulos, M. *J. Am. Chem. Soc.* **1995**, *117*, 7081.

168. Shirota, Y.; Nagata, J.; Nakano, Y.; Nogami, T.; Mikawa, H. *J. Chem. Soc., Perkin Trans. I.* **1977**, 14.

169. Sato, T.; Shiro, M.; Koyama, H. *J. Chem. Soc. (B)* **1968**, 935.

170. Schmid, G. H.; Toyonaga, B.; Siew, P. Y. Nyburg, S. C. *Acta Cryst.* **1983**, *C39*, 889.

171. Dhar, D, N. *Chem. Rev.* **1967**, *67*, 611.

172. Agarwal, A.; Barnes, J. A.; Fletcher, J. L.; McGlinchey, M. J.; Sayer, B. G. *Can. J. Chem.* **1977**, *55*, 2575.

173. Waugh, J. S.; Fessenden, R. W. *J. Am. Chem. Soc.* **1957**, *79*, 846.

174. Waugh, J. S.; Fessenden, R. W. *J. Am. Chem. Soc.* **1958**, *80*, 6697.

175. Johnson, C. E., Jr.; Bovey, F. A. *J. Chem. Phys.* **1958**, *29*, 1012.

176. Ruffolo, R.; Kainz, S.; Gupta, H. K.; Brook, M. A.; McGlinchey, M. J. *J. Organometal. Chem.* **1997**, *547*, 217.

177. Corriu, R. J. P.; Moreau, J. J. E.; Praet, H. *Organometallics* **1989**, *8*, 2779.

178. Olah, G. A. *Angew. Chem. Int. Ed. Engl.* **1995**, *34*, 1393.

179. Kondratenko, M.; El Hafa, H.; Gruselle, M.; Vaissermann, J.; Jaouen, G.; McGlinchey, M. J. *J. Am. Chem. Soc.* **1995**, *117*, 6907.

180. Schleyer, P. v. R. *Science* **1996**, *275*, 39.

181. Lambert, J. A.; Kania, L.; Zhang, S. *Chem. Rev.* **1995**, *95*, 1191.

182. Lambert, J. B.; Zhao, Y. *J. Am. Chem. Soc.* **1996**, *118*, 7867.

183. Lambert, J. B.; Zhao, Y. *Angew. Chem. Intl. Ed. Engl.* **1997**, *36*, 400.

184. Flynn, C. R.; Michl, J. *J. Am. Chem. Soc.* **1974**, *96*, 3280.

185. Palensky, F. J.; Morrison, H. A. *J. Am. Chem. Soc.* **1977**, *99*, 3507.

186. Alder, K.; Fremery, M. *Tetrahedron* **1961**, *14*, 190.

187. Dolbier, W. R., Jr.; Anapolle, K. E.; McCullagh, L.; Matsui, K.; Reimann, J. M.; Rolison, D. *J. Org. Chem.* **1979**, 44, 2845.

188. Rakita, P. E.; Taylor, G. A. *Inorg. Chem.* **1972**, *11*, 2136.

189. Taylor, G. A.; Rakita, P. E. *J. Organometal. Chem.* **1974**, *78*, 281.

190. Andrews, M. N.; Rakita, P. E.; Taylor, G. A. *Tetrahedron Lett.* **1973**, *21*, 1851.

191. Andrews, M. N.; Rakita, P. E.; Taylor, G. A. *Inorg. Chim. Acta.* **1975**, *13*, 191.

192. Jones, D. W. *J. Chem. Soc. C* **1969**, 1729.

193. Collett, M. J.; Jones, D. W.; Renyard, S. J. *J. Chem. Soc., Perkin Trans. I.* **1986**, 1471.

194. Jones, D. W.; Marmon, R. J. *J. Chem. Soc., Perkin Trans. I.* **1993**, 681.

195. Rigby, S. S.; Stradiotto, M.; Brydges, S.; Pole, D. L.; Top, S.; Bain, A. D.; McGlinchey, M. J. *J. Org. Chem.* **1998**, *63*, 3735.

196. Rigby, S. S.; Gupta, H. K.; Werstiuk, N. H.; Bain, A. D.; McGlinchey, M. J. *Polyhedron* **1995**, *14*, 2787.

197. Rigby, S. S.; Gupta, H. K.; Werstiuk, N. H.; Bain, A. D.; McGlinchey, M. J. *Inorg. Chim. Acta.* **1996**, *251*, 355.

198. Capparelli, M. V.; Machado, R.; De Sanctis, Y.; Arce, A. J. *Acta Cryst.* **1996**, *C52*, 947.

199. Warrener, R. N.; Harrison, P. A.; Russell, R. A. *J. Chem. Soc., Chem. Commun.* **1982**, 1134.

200. Warrener, R. N.; Pitt, I. G.; Russell, R. A. *J. Chem. Soc., Chem. Commun.* **1982**, 1136.

201. Warrener, R. N.; Pitt, I. G.; Russell, R. A. *Aust. J. Chem.* **1993**, *46*, 1845.

202. Olmstead, M. M.; Hitchcock, S. R.; Nantz, M. H. *Acta Cryst.* **1996**, *C52*, 1523.

203. Malaba, D.; Djebli, A.; Chen, L.; Zarate, E. A.; Tessier, C. A.; Youngs, W. J. *Organometallics* **1993**, *12*, 1266.

204. Malaba, D.; Tessier, C. A.; Youngs, W. J. *Organometallics* **1996**, *15*, 2918.

205. Simmross, U.; Müllen, K. *Chem. Ber.* **1993**, *126*, 969.

206. Rutsch, W.; Escher, A.; Neuenschwander, M. *Chimia* **1983**, *37*, 160.

207. Escher, A.; Rutsch, W.; Neuenschwander, M. *Helv. Chim. Acta* **1986**, *69*, 1644.

208. McGovern, P. A.; Vollhardt, K. P. C. *J. Chem. Soc., Chem. Commun.* **1996**, 1593.

209. Baumgarten, M.; Tyutyulkov., N. *Chem. Eur. J.* **1998**, *4*, 987.

210. Ustynyuk, Yu. A.; Luzikov, Yu. N.; Mstislavsky, U. J.; Azizov, A. A.; Pribytkova, J. M. *J. Organometal. Chem.* **1975**, *96*, 335.

211. Jutzi, P.; Sauer, J. *J. Organometal. Chem.* **1973**, *50*, 29.

212. Wey, H. G.; Butenschön, H. *Angew. Chem. Int. Ed. Engl.* **1991**, *30*, 880.

213. Brands, M.; Wey, H. G.; Butenschön, H. *J. Chem. Soc., Chem. Commun.* **1991**, 1541.

214. Brands, M.; Wey, H. G.; Goddard, R.; Butenschön, H. *Inorg. Chim. Acta* **1994**, *220*, 175.

215. Brands, M.; Wey, H. G.; Krömer, R.; Krüger, C.; Butenschön, H.; *Liebigs Ann.* **1995**, 253.

216. Fischer, E. O.; Kriebitzsch, N. *Z. Naturforsch.* **1960**, *15b*, 465.

217. Berno, P.; Ceccon, A.; Gambaro, A.; Venzo, A. *Tetrahedron. Lett.* **1988**, *29*, 3489.

218. Rausch, M. D.; Moser, G. A.; Zaiko, E. F.; Lipman, A. L. *J. Organometal. Chem.* **1970**, *23*, 185.

219. Kerber, R. C.; Waldbaum, B. *Organometallics* **1995**, *14*, 4742.

220. Nesmeyanov, A. N.; Ustynyuk, N. A.; Novikova, L. N.; Andrianov, V. G.; Struchkov, Y. T.; Ustynyuk, Y. A.; Oprunenko, Y. F.; Luzikov, Y. N. *J. Organometal. Chem.* **1982**, *226*, 239.

221. Kunz, V.; Nowacki, W. *Helv. Chim. Acta* **1967**, *50*, 1052.

222. Trifonova, O. I.; Ochertyanova, E. A.; Akhmedov, N. G.; Roznyatovsky, V. A.; Laikov, D. N.; Ustynyuk, N. A.; Ustynyuk, Y. A. *Inorg. Chim. Acta.* **1998**, *280*, 328.

223. Bonifaci, C.; Ceccon, A.; Gambaro, A.; Ganis, P.; Santi, S.; Valle, G.; Venzo, A. *Organometallics* **1993**, *12*, 4211.

224. Bonifaci, C.; Ceccon, A.; Gambaro, A.; Ganis, P.; Santi, S.; Valle, G.; Venzo, A. *J. Organometal. Chem.* **1995**, *492*, 35.

225. Fatiadi, A. J. *Synthesis.* **1986**, 249.

226. Sennikov, P. G.; Kuznetsov, V. A.; Egorochkin, A. N.; Sirotkin, N. I.; Nazarova, R. G.; Razuvaev, G. A. *J. Organometal. Chem.* **1980**, *190*, 167.

227. Fatiadi, A. J. *Synthesis.* **1987**, 959.

228. Kündig, E. P.; Kondratenko, M.; Romanens, P. *Angew. Chem. Int. Ed.* **1998**, *37*, 3146.

229. Guttenberger, J.-F.; Strohmeier, W. *Chem. Ber.* **1967**, *100*, 2807.

230. Sneeden, R.P.A. *Organochromium Compounds;* Academic Press: New York, 1975, p.193.

231. Wege, D.; Wilkinson, S. P. *Aust. J. Chem.* **1973**, *26*, 1751.

232. Bly, R. S.; Maier, T. L. *J. Org. Chem.* **1978**, *43*, 614.

233. Merkert, J. W.; Geiger, W. E.; Paddon-Row, M. N.; Oliver, A. M.; Rheingold, A. L. *Organometallics* **1992**, *11*, 4109.

234. McGlinchey, M. J.; Girard, L.; Ruffolo, R. *Coord. Chem. Revs.* **1995**, *143*, 331.

235. Melikyan, G. G.; Bright, S.; Monroe, T.; Hardcastle, K. I.; Cuirash, J. *Angew. Chem. Int. Ed.* **1998**, *37*, 161.

236. Ruffolo, R.; Decken, A.; Girard, L.; Gupta, H. K.; Brook, M. A.; McGlinchey, M. J. *Organometallics* **1994**, *13*, 4328.

237. Epiotis, N. D.; Shaik, S. *J. Am. Chem. Soc.* **1977**, *99*, 4936.

238. Stradiotto, M.; Brook, M. A.; McGlinchey, M. J. *Inorg. Chem. Commun.* **1998**, *1*, 105.

239. Brieger, G.; Bennett, J. N. *Chem. Rev.* **1980**, *80*, 63.

240. Malacria, M. *Chem. Rev.* **1996**, *96*, 289.

241. Funk, R. L.; Vollhardt, K. P. C. *J. Am. Chem. Soc.* **1980**, *102*, 5253.

242. Cruciani, P.; Aubert, C.; Malacria, M. *J. Org. Chem.* **1995**, *60*, 2664.

243. Brosius, A. D.; Overman, L. E.; Schwink, L. *J. Am. Chem. Soc.* **1999**, *121*, 700.

244. Batey, R. A.; Thadani, A. N.; Lough, A. J. *J. Am. Chem. Soc.* **1999**, *121*, 450.

245. Padwa, A.; Goldstein, S.; Pulwer, M. *J. Org. Chem.* **1982**, *47*, 3893.

246. Jones, D. W.; Ryder, T. C. L. M. *J. Chem. Soc., Chem. Commun.* **1997**, 1169.

247. Carey, F. A.; Sundberg, R. J. *Advanced Organic Chemistry, Part B: Reactions and Synthesis;* Plenum Press: New York, 1993, p.286.

248. Shibasaki, M.; Sasai, H.; Arai, T. Angew. Chem. Int. Ed. Engl. **1997**, 36, 1237.

249. SMART (1996), Release 4.05; Siemens Energy And Automation Inc., Madison, WI 53719.

250. SAINT (1996), Release 4.05; Siemens Energy And Automation Inc., Madison, WI 53719.

251. Sheldrick, G. M. SADABS (Siemens Area Detector Absorption Corrections) (1996); Siemens Crystallographic Research Systems, Madison, WI 53719.

252. Sheldrick, G. M. Siemens SHELXTL (1994), Version 5.03; Siemens Crystallographic Research Systems, Madison, WI 53719.

253. Haszeldine, R. N.; Parish, R. V.; Taylor, R. J. *J. Chem. Soc., Dalton. Trans.* **1974**, 2311.

254. Haszeldine, R. N.; Parish, R. V.; Parry, D. J. *J. Chem. Soc. (A).* **1969**, 683.

255. Nicolet, P.; Sanchez, J.-Y.; Benaboura, A.; Abadie, M. J. M. *Synthesis* **1987**, 202.

256. Majerus, G.; Yax, E.; Ourisson, G. *Bull. Soc. Chim. Fr.* **1967**, 4147.

APPENDIX: X-RAY CRYSTALLOGRAPHIC DATA

Refinement Data and Metrical Parameters

Table A1. Crystal Data and Structure Refinement Parameters for 1.134, 2.2 and 3.20.

	1.134	2.2	3.20
Empirical formula	$C_{18}H_{16}N_4Si_1$	$C_{22}H_{12}N_4O_1Fe_1$	$C_{27}H_{22}Si_1$
Molecular Weight	316.44	420.21	374.54
Description	colorless prism	yellow plate	colorless fragment
Temperature, K	293(2)	300(2)	300(2)
Crystal system	triclinic	triclinic	orthorhombic
Space group	$P(\bar{1})$	$P(\bar{1})$	$P2_12_12_1$
a, Å	8.0200(8)	9.079(4)	9.6561(1)
b, Å	8.4380(6)	14.888(9)	20.5988(3)
c, Å	13.601(1)	15.018(9)	20.9879(3)
α, deg.	80.644(8)	72.56(5)	90.000
β, deg.	81.245(9)	85.96(4)	90.000
γ, deg.	79.100(7)	88.63(4)	90.000
Volume, $Å^3$	884.8(1)	1932(1)	4175.6(1)
Z	2	4	8
Calcd Density, g/cm^3	1.188	1.445	1.192
Scan Mode	2θ–ω scans	ω-scans	ω-scans
θ - range, deg.	3.32 to 55.00	1.42 to 26.40	1.39 to 25.00
Index ranges	$-9 \le h \le 8$	$-11 \le h \le 11$	$-12 \le h \le 11$
	$-9 \le k \le 9$	$-18 \le k \le 18$	$-25 \le k \le 25$
	$-15 \le l \le 15$	$-18 \le l \le 18$	$-26 \le l \le 26$
No. Refl. collected	2420	13298	30305
No. Indep. Refl.	2232	5974	7347
Data / restr. / param.	2232 / 0 / 209	5974 / 0 / 524	7272 / 0 / 514
Goodness-of-fit on F^2	1.191	0.861	1.065
Final R indices ($I>2\sigma(I)$)*	R1 = 0.0707;	R1 = 0.0471;	R1 = 0.0683;
	wR2 = 0.01684	wR2 = 0.0954	wR2 = 0.1002
R indices (all data)*	R1 = 0.1012;	R1 = 0.0744;	R1 = 0.1524;
	wR2 = 0.1918	wR2 = 0.1109	wR2 = 0.1280
Mean shift/error	<0.001	<0.002	<0.002
Max. shift/error	<0.001	<0.002	<0.002
Trans. (max., min.)	0.982, 0.867	0.942, 0.846	0.981, 0.710
Largest diff. Peak, $e/Å^3$	0.266	0.62	0.16
Largest diff. Hole, $e/Å^3$	-0.249	-0.34	-0.18

*$R1 = \Sigma(\|Fo\| - \|Fc\|)/\Sigma|Fo|$; $wR2 = [\Sigma[w(Fo^2-Fc^2)^2]/\Sigma[w(Fo^2)^2]]^{0.5}$; $P = (Fo^2+2Fc^2)/3$)

Table A2. Crystal Data and Structure Refinement Parameters for 3.22, 3.24 and 4.34.

	3.22	3.24	4.34
Empirical formula	$C_{48}H_{26}N_{12}Si$	$C_{51}H_{34}N_{12}Si_1O_3$	$C_{20}H_{20}N_4Si_1$
Molecular Weight	798.90	890.99	344.49
Description	colorless needle	colorless fragment	colorless prism
Temperature, K	300(2)	300(2)	299(2)
Crystal system	monoclinic	monoclinic	monoclinic
Space group	$P2_1/c$	$P2_1/c$	$P2_1/c$
a, Å	13.9562(3)	14.0079(5)	9.601(1)
b, Å	15.0799(4)	14.7086(4)	14.782(2)
c, Å	23.1845(2)	23.3079(7)	13.977(2)
α, deg.	90.000	90.000	90.000
β, deg.	102.979(1)	102.395(1)	105.040(3)
γ, deg.	90.000	90.000	90.000
Volume, $Å^3$	4754.7(2)	4690.3(3)	1915.7(5)
Z	4	4	4
Calcd Density, g/cm^3	1.116	1.262	1.194
Scan Mode	ω-scans	ω-scans	ω-scans
θ - range, deg.	1.50 to 20.00	1.50 to 23.00	2.04 to 22.50
Index ranges	$-15 \le h \le 15$	$-17 \le h \le 17$	$-10 \le h \le 10$
	$-16 \le k \le 12$	$-18 \le k \le 17$	$-15 \le k \le 15$
	$-25 \le l \le 25$	$-29 \le l \le 29$	$-14 \le l \le 15$
No. Refl. collected	20188	27620	11384
No. Indep. Refl.	4448	6518	2501
Data / restr. / param.	4405 / 0 / 549	6451 / 0 / 605	2501 / 0 / 226
Goodness-of-fit on F^2	1.059	1.067	0.854
Final R indices ($I>2\sigma(I)$)*	R1 = 0.0776;	R1 = 0.0628;	R1 = 0.0448;
	wR2 = 0.2053	wR2 = 0.1445	wR2 = 0.0870
R indices (all data)*	R1 = 0.1333;	R1 = 0.1177;	R1 = 0.1104;
	wR2 = 0.2477	wR2 = 0.1816	wR2 = 0.1016
Mean shift/error	0.005	<0.001	<0.001
Max. shift/error	<0.001	<0.001	<0.001
Trans. (max., min.)	0.895, 0.775	0.991, 0.810	0.979, 0.690
Largest diff. Peak, $e/Å^3$	0.803	0.489	0.152
Largest diff. Hole, $e/Å^3$	-0.317	-0.259	-0.195

*$R1 = \Sigma(\|Fo\| - \|Fc\|)/\Sigma|Fo|$; $wR2 = [\Sigma[w(Fo^2-Fc^2)^2]/\Sigma[w(Fo^2)^2]]^{0.5}$; $P = (Fo^2+2Fc^2)/3$)

Table A3. Crystal Data and Structure Refinement Parameters for 4.38 and 4.54.

	4.38	4.54
Empirical formula	$C_{17}H_{20}O_3Si_1Cr_1$	$C_{28}H_{22}Co_2Si_2O_6N_4$
Molecular Weight	352.42	684.54
Description	yellow plate	red plate
Temperature, K	299(2)	300(2)
Crystal system	triclinic	triclinic
Space group	$P(\bar{1})$	$P(\bar{1})$
a, Å	9.691(11)	8.606(3)
b, Å	9.877(9)	9.345(5)
c, Å	10.395(12)	22.115(9)
α, deg.	67.98(3)	97.09(3)
β, deg.	81.98(2)	95.51(2)
γ, deg.	82.94(2)	110.05(3)
Volume, Å^3	910(2)	1639(1)
Z	2	2
Calcd Density, g/cm^3	1.285	1.387
Scan Mode	ω-scans	ω-scans
θ - range for collection, deg.	2.12 to 22.50	0.94 to 22.50
Index ranges	$-11 \le h \le 12$ $-12 \le k \le 12$ $-12 \le l \le 13$	$-10 \le h \le 10$ $-11 \le k \le 11$ $-27 \le l \le 27$
No. Reflections collected	5572	12055
No. Indep. reflections	2376	4192
Data / restraints / parameters	2353 / 0 / 200	4172 / 0 / 380
Goodness-of-fit on F^2	0.995	1.021
Final R indices ($I>2\sigma(I)$)*	R1 = 0.0672; wR2 = 0.1507	R1 = 0.0440; wR2 = 0.1020
R indices (all data)*	R1 = 0.1317; wR2 = 0.1644	R1 = 0.0732; wR2 = 0.1184
Mean shift/error	0.005	<0.002
Max. shift/error	<0.001	<0.001
Transmission (max., min.)	0.901, 0.571	0.823, 0.635
Largest diff. Peak, e/Å^3	0.31	0.33
Largest diff. Hole, e/Å^3	-0.29	-0.25

*$R1 = \Sigma(\|Fo\| - \|Fc\|)/\Sigma|Fo|$; $wR2 = [\Sigma[w(Fo^2-Fc^2)^2]/\Sigma[w(Fo^2)^2]]^{0.5}$; $P = (Fo^2+2Fc^2)/3$)

Table A4. Complete Listing of Bond Lengths [Å] for 1.134.

Si(1)-C(14)	1.830(8)
Si(1)-C(13)	1.844(8)
Si(1)-C(12)	1.865(8)
Si(1)-C(7)	1.918(6)
N(51)-C(51)	1.144(7)
N(52)-C(52)	1.129(7)
N(61)-C(61)	1.136(8)
N(62)-C(62)	1.129(7)
C(1)-C(2)	1.497(8)
C(1)-C(7)	1.537(8)
C(1)-C(6)	1.582(8)
C(2)-C(8)	1.384(9)
C(2)-C(3)	1.392(9)
C(3)-C(11)	1.372(9)
C(3)-C(4)	1.489(8)
C(4)-C(7)	1.545(8)
C(4)-C(5)	1.593(8)
C(5)-C(51)	1.458(9)
C(5)-C(52)	1.481(9)
C(5)-C(6)	1.608(8)
C(6)-C(62)	1.490(8)
C(6)-C(61)	1.492(9)
C(8)-C(9)	1.419(12)
C(9)-C(10)	1.382(13)
C(10)-C(11)	1.358(12)

Table A5. Complete Listing of Bond Angles [deg] for 1.134.

C(14)-Si(1)-C(13)	111.6(4)
C(14)-Si(1)-C(12)	109.2(5)
C(13)-Si(1)-C(12)	109.2(4)
C(14)-Si(1)-C(7)	109.3(3)
C(13)-Si(1)-C(7)	104.9(3)
C(12)-Si(1)-C(7)	112.6(3)
C(2)-C(1)-C(7)	101.3(5)
C(2)-C(1)-C(6)	105.2(4)
C(7)-C(1)-C(6)	100.5(4)
C(8)-C(2)-C(3)	120.5(6)
C(8)-C(2)-C(1)	132.4(7)
C(3)-C(2)-C(1)	107.1(5)
C(11)-C(3)-C(2)	121.9(7)
C(11)-C(3)-C(4)	131.7(7)
C(2)-C(3)-C(4)	106.4(5)
C(3)-C(4)-C(7)	102.2(5)
C(3)-C(4)-C(5)	107.0(5)
C(7)-C(4)-C(5)	100.6(4)
C(51)-C(5)-C(52)	109.8(5)
C(51)-C(5)-C(4)	109.3(5)
C(52)-C(5)-C(4)	111.8(5)
C(51)-C(5)-C(6)	112.7(5)
C(52)-C(5)-C(6)	112.8(5)
C(4)-C(5)-C(6)	100.1(4)
C(62)-C(6)-C(61)	106.1(5)
C(62)-C(6)-C(1)	113.0(5)
C(61)-C(6)-C(1)	110.8(5)
C(62)-C(6)-C(5)	112.5(5)
C(61)-C(6)-C(5)	111.4(5)
C(1)-C(6)-C(5)	103.3(4)
C(1)-C(7)-C(4)	93.9(4)
C(1)-C(7)-Si(1)	118.7(4)
C(4)-C(7)-Si(1)	116.7(4)
C(2)-C(8)-C(9)	117.2(8)
C(10)-C(9)-C(8)	120.1(9)
C(11)-C(10)-C(9)	122.3(9)
C(10)-C(11)-C(3)	117.9(9)
N(51)-C(51)-C(5)	178.0(7)
N(52)-C(52)-C(5)	178.2(7)
N(61)-C(61)-C(6)	178.9(7)
N(62)-C(62)-C(6)	175.2(7)

Table A6. Atomic Coordinates (x 10^4) and Equivalent Isotropic Displacement Parameters ($Å^2$ x 10^3) for 1.134. U(eq) is defined as one third of the trace of the orthogonalized Uij tensor.

	x	y	z	U(eq)
Si(1)	0019(2)	5061(2)	7317(2)	59(1)
N(51)	2763(8)	0618(7)	4925(5)	69(2)
N(52)	4805(8)	-1999(8)	7583(5)	70(2)
N(61)	5792(8)	3304(7)	4716(5)	75(2)
N(62)	7652(7)	0996(7)	7420(4)	65(2)
C(1)	3705(7)	3557(7)	7162(4)	42(2)
C(2)	3491(8)	2831(8)	8244(5)	49(2)
C(3)	2426(8)	1677(8)	8334(4)	51(2)
C(4)	1953(7)	1713(7)	7312(4)	46(2)
C(5)	3600(7)	0856(7)	6663(4)	42(2)
C(6)	4852(7)	2161(7)	6593(4)	41(2)
C(7)	1944(7)	3516(7)	6860(4)	45(2)
C(8)	4144(9)	3103(9)	9076(6)	67(2)
C(9)	3706(14)	2139(15)	10002(6)	107(4)
C(10)	2641(14)	1010(12)	10052(7)	100(3)
C(11)	2023(10)	0739(9)	9231(6)	78(2)
C(12)	-1043(11)	4334(10)	8583(6)	97(3)
C(13)	-1488(10)	5287(10)	6386(6)	93(3)
C(14)	0723(11)	6987(10)	7356(9)	128(4)
C(51)	3155(8)	0704(7)	5686(5)	50(2)
C(52)	4293(8)	-0771(9)	7171(5)	47(2)
C(61)	5401(8)	2802(8)	5528(5)	52(2)
C(62)	6454(8)	1445(8)	7045(4)	45(2)

Table A7. Complete Listing of Bond lengths [Å] for 2.2.

Fe(1)-C(18)	1.757(5)	C(12)-C(13)	1.401(7)
Fe(1)-C(17)	1.756(5)	C(12)-C(16)	1.420(7)
Fe(1)-C(7)	2.053(4)	C(13)-C(14)	1.392(7)
Fe(1)-C(12)	2.087(5)	C(14)-C(15)	1.397(7)
Fe(1)-C(15)	2.092(4)	C(15)-C(16)	1.406(7)
Fe(1)-C(13)	2.100(5)	C(21)-C(22)	1.516(5)
Fe(1)-C(16)	2.098(4)	C(21)-C(27)	1.562(5)
Fe(1)-C(14)	2.105(5)	C(21)-C(26)	1.590(5)
Fe(2)-C(38)	1.719(7)	C(22)-C(23)	1.377(6)
Fe(2)-C(37)	1.733(9)	C(22)-C(28)	1.391(5)
Fe(2)-C(27)	2.042(4)	C(23)-C(31)	1.379(6)
Fe(2)-C(35)	2.067(7)	C(23)-C(24)	1.509(5)
Fe(2)-C(34)	2.074(6)	C(24)-C(27)	1.543(5)
Fe(2)-C(32)	2.072(6)	C(24)-C(25)	1.606(5)
Fe(2)-C(33)	2.068(5)	C(25)-C(54)	1.481(5)
Fe(2)-C(36)	2.085(6)	C(25)-C(53)	1.482(5)
O(17)-C(17)	1.152(5)	C(25)-C(26)	1.604(6)
O(18)-C(18)	1.137(5)	C(26)-C(64)	1.479(5)
O(37)-C(37)	1.160(8)	C(26)-C(63)	1.484(6)
O(38)-C(38)	1.142(7)	C(28)-C(29)	1.388(7)
N(51)-C(51)	1.138(5)	C(29)-C(30)	1.380(7)
N(52)-C(52)	1.133(5)	C(30)-C(31)	1.394(7)
N(53)-C(53)	1.133(5)	C(32)-C(36)	1.313(9)
N(54)-C(54)	1.131(5)	C(32)-C(33)	1.342(9)
N(61)-C(61)	1.134(5)	C(33)-C(34)	1.397(10)
N(62)-C(62)	1.129(5)	C(34)-C(35)	1.455(10)
N(63)-C(63)	1.139(5)	C(35)-C(36)	1.343(8)
N(64)-C(64)	1.135(5)		
C(1)-C(2)	1.510(5)		
C(1)-C(7)	1.550(5)		
C(1)-C(6)	1.594(5)		
C(2)-C(3)	1.387(5)		
C(2)-C(8)	1.388(5)		
C(3)-C(11)	1.371(5)		
C(3)-C(4)	1.508(5)		
C(4)-C(7)	1.550(5)		
C(4)-C(5)	1.602(5)		
C(5)-C(52)	1.479(5)		
C(5)-C(51)	1.473(5)		
C(5)-C(6)	1.613(5)		
C(6)-C(62)	1.482(5)		
C(6)-C(61)	1.480(6)		
C(8)-C(9)	1.393(7)		
C(9)-C(10)	1.374(7)		
C(10)-C(11)	1.395(6)		

Table A8. Complete Listing of Bond Angles [deg] for 2.2.

C(18)-Fe(1)-C(17)	94.8(2)	C(35)-Fe(2)-C(33)	66.4(3)
C(18)-Fe(1)-C(7)	90.6(2)	C(34)-Fe(2)-C(33)	39.4(3)
C(17)-Fe(1)-C(7)	97.0(2)	C(32)-Fe(2)-C(33)	37.8(3)
C(18)-Fe(1)-C(12)	157.6(2)	C(38)-Fe(2)-C(36)	143.3(4)
C(17)-Fe(1)-C(12)	102.0(2)	C(37)-Fe(2)-C(36)	125.1(4)
C(7)-Fe(1)-C(12)	101.8(2)	C(27)-Fe(2)-C(36)	88.3(2)
C(18)-Fe(1)-C(15)	93.7(2)	C(35)-Fe(2)-C(36)	37.7(2)
C(17)-Fe(1)-C(15)	113.5(2)	C(34)-Fe(2)-C(36)	65.1(3)
C(7)-Fe(1)-C(15)	148.7(2)	C(32)-Fe(2)-C(36)	36.8(2)
C(12)-Fe(1)-C(15)	66.1(2)	C(33)-Fe(2)-C(36)	63.7(3)
C(18)-Fe(1)-C(13)	124.8(2)	C(2)-C(1)-C(7)	101.7(3)
C(17)-Fe(1)-C(13)	140.2(2)	C(2)-C(1)-C(6)	106.1(3)
C(7)-Fe(1)-C(13)	86.9(2)	C(7)-C(1)-C(6)	100.2(3)
C(12)-Fe(1)-C(13)	39.1(2)	C(3)-C(2)-C(8)	120.7(4)
C(15)-Fe(1)-C(13)	65.4(2)	C(3)-C(2)-C(1)	107.5(3)
C(18)-Fe(1)-C(16)	127.4(2)	C(8)-C(2)-C(1)	131.8(4)
C(17)-Fe(1)-C(16)	88.8(2)	C(11)-C(3)-C(2)	121.7(4)
C(7)-Fe(1)-C(16)	141.0(2)	C(11)-C(3)-C(4)	132.1(4)
C(12)-Fe(1)-C(16)	39.7(2)	C(2)-C(3)-C(4)	106.2(3)
C(15)-Fe(1)-C(16)	39.2(2)	C(3)-C(4)-C(7)	102.2(3)
C(13)-Fe(1)-C(16)	65.6(2)	C(3)-C(4)-C(5)	105.7(3)
C(18)-Fe(1)-C(14)	92.9(2)	C(7)-C(4)-C(5)	100.8(3)
C(17)-Fe(1)-C(14)	151.9(2)	C(52)-C(5)-C(51)	108.3(3)
C(7)-Fe(1)-C(14)	110.0(2)	C(52)-C(5)-C(4)	113.1(3)
C(12)-Fe(1)-C(14)	65.5(2)	C(51)-C(5)-C(4)	110.9(3)
C(15)-Fe(1)-C(14)	38.9(2)	C(52)-C(5)-C(6)	111.0(3)
C(13)-Fe(1)-C(14)	38.7(2)	C(51)-C(5)-C(6)	112.1(3)
C(16)-Fe(1)-C(14)	65.3(2)	C(4)-C(5)-C(6)	101.4(3)
C(38)-Fe(2)-C(37)	91.5(5)	C(62)-C(6)-C(61)	108.5(3)
C(38)-Fe(2)-C(27)	95.7(2)	C(62)-C(6)-C(1)	111.7(3)
C(37)-Fe(2)-C(27)	87.8(2)	C(61)-C(6)-C(1)	110.3(3)
C(38)-Fe(2)-C(35)	106.3(4)	C(62)-C(6)-C(5)	113.7(3)
C(37)-Fe(2)-C(35)	158.3(3)	C(61)-C(6)-C(5)	110.7(3)
C(27)-Fe(2)-C(35)	102.2(2)	C(1)-C(6)-C(5)	101.9(3)
C(38)-Fe(2)-C(34)	92.0(3)	C(1)-C(7)-C(4)	93.6(3)
C(37)-Fe(2)-C(34)	128.2(4)	C(1)-C(7)-Fe(1)	117.0(2)
C(27)-Fe(2)-C(34)	143.0(3)	C(4)-C(7)-Fe(1)	120.9(3)
C(35)-Fe(2)-C(34)	41.1(3)	C(9)-C(8)-C(2)	117.5(4)
C(38)-Fe(2)-C(32)	154.0(3)	C(10)-C(9)-C(8)	121.4(4)
C(37)-Fe(2)-C(32)	95.1(4)	C(9)-C(10)-C(11)	120.9(4)
C(27)-Fe(2)-C(32)	109.6(3)	C(3)-C(11)-C(10)	117.7(4)
C(35)-Fe(2)-C(32)	63.5(3)	C(13)-C(12)-C(16)	107.4(5)
C(34)-Fe(2)-C(32)	64.3(3)	C(13)-C(12)-Fe(1)	70.9(3)
C(38)-Fe(2)-C(33)	116.6(3)	C(16)-C(12)-Fe(1)	70.6(3)
C(37)-Fe(2)-C(33)	94.8(3)	C(14)-C(13)-C(12)	108.5(5)
C(27)-Fe(2)-C(33)	147.4(3)	C(14)-C(13)-Fe(1)	70.9(3)

Table A8. Complete Listing of Bond Angles [deg] for 2.2 (continued).

C(13)-C(14)-Fe(1)	70.5(3)	C(33)-C(34)-Fe(2)	70.1(3)
C(15)-C(14)-Fe(1)	70.1(3)	C(35)-C(34)-Fe(2)	69.2(3)
C(16)-C(15)-C(14)	108.0(5)	C(36)-C(35)-C(34)	106.1(6)
C(16)-C(15)-Fe(1)	70.6(2)	C(36)-C(35)-Fe(2)	71.9(4)
C(14)-C(15)-Fe(1)	71.0(3)	C(34)-C(35)-Fe(2)	69.7(4)
C(15)-C(16)-C(12)	107.6(5)	C(32)-C(36)-C(35)	110.3(6)
C(15)-C(16)-Fe(1)	70.2(3)	C(32)-C(36)-Fe(2)	71.1(4)
C(12)-C(16)-Fe(1)	69.8(3)	C(35)-C(36)-Fe(2)	70.4(4)
O(17)-C(17)-Fe(1)	172.1(4)	O(37)-C(37)-Fe(2)	178.1(6)
O(18)-C(18)-Fe(1)	177.3(4)	O(38)-C(38)-Fe(2)	175.0(6)
C(22)-C(21)-C(27)	101.3(3)	N(51)-C(51)-C(5)	178.0(4)
C(22)-C(21)-C(26)	106.2(3)	N(52)-C(52)-C(5)	178.1(5)
C(27)-C(21)-C(26)	99.7(3)	N(53)-C(53)-C(25)	173.0(4)
C(23)-C(22)-C(28)	121.9(4)	N(54)-C(54)-C(25)	177.8(4)
C(23)-C(22)-C(21)	107.3(3)	N(61)-C(61)-C(6)	176.6(4)
C(28)-C(22)-C(21)	130.8(5)	N(62)-C(62)-C(6)	177.2(4)
C(22)-C(23)-C(31)	121.7(4)	N(63)-C(63)-C(26)	176.1(5)
C(22)-C(23)-C(24)	107.0(3)	N(64)-C(64)-C(26)	177.7(5)
C(31)-C(23)-C(24)	131.3(5)	C(12)-C(13)-Fe(1)	69.9(3)
C(23)-C(24)-C(27)	101.8(3)	C(13)-C(14)-C(15)	108.5(5)
C(23)-C(24)-C(25)	106.5(3)	C(33)-C(34)-C(35)	105.0(5)
C(27)-C(24)-C(25)	100.0(3)	C(34)-C(33)-Fe(2)	70.5(3)
C(54)-C(25)-C(53)	109.0(3)		
C(54)-C(25)-C(26)	111.5(3)		
C(53)-C(25)-C(26)	113.8(3)		
C(54)-C(25)-C(24)	113.6(3)		
C(53)-C(25)-C(24)	106.9(3)		
C(26)-C(25)-C(24)	101.8(3)		
C(64)-C(26)-C(63)	107.5(4)		
C(64)-C(26)-C(21)	112.8(3)		
C(63)-C(26)-C(21)	108.4(3)		
C(64)-C(26)-C(25)	113.3(3)		
C(63)-C(26)-C(25)	112.5(3)		
C(21)-C(26)-C(25)	102.2(3)		
C(24)-C(27)-C(21)	93.9(3)		
C(24)-C(27)-Fe(2)	118.8(3)		
C(21)-C(27)-Fe(2)	120.5(3)		
C(29)-C(28)-C(22)	116.4(5)		
C(30)-C(29)-C(28)	121.6(4)		
C(29)-C(30)-C(31)	121.5(5)		
C(23)-C(31)-C(30)	116.8(5)		
C(36)-C(32)-C(33)	111.2(7)		
C(36)-C(32)-Fe(2)	72.1(3)		
C(33)-C(32)-Fe(2)	70.9(4)		
C(32)-C(33)-C(34)	107.3(6)		
C(32)-C(33)-Fe(2)	71.3(3)		

Table A9. Atomic Coordinates (x 10^4) and Equivalent Isotropic Displacement Parameters ($Å^2$ x 10^3) for 2.2. U(eq) is defined as one third of the trace of the orthogonalized Uij tensor.

	x	y	z	U(eq)
Fe(1)	-85(1)	3821(1)	3353(1)	35(1)
Fe(2)	7489(1)	8546(1)	1533(1)	53(1)
O(17)	-1868(4)	5069(2)	4150(3)	78(1)
O(18)	-1317(4)	4456(3)	1543(2)	75(1)
O(37)	4719(10)	9564(6)	1352(6)	235(5)
O(38)	8600(11)	9726(5)	-253(4)	263(5)
N(51)	-3454(4)	1100(3)	2558(2)	55(1)
N(52)	-6189(4)	1302(3)	4919(3)	62(1)
N(53)	5314(4)	5099(3)	2357(2)	50(1)
N(54)	7030(4)	5114(3)	-401(2)	51(1)
N(61)	-629(4)	75(3)	4021(3)	50(1)
N(62)	-3372(5)	208(3)	6428(3)	67(1)
N(63)	2481(5)	6849(3)	1199(3)	65(1)
N(64)	4386(5)	6817(3)	-1475(3)	68(1)
C(1)	-1384(4)	2030(3)	4789(2)	30(1)
C(2)	-2390(4)	2582(3)	5277(2)	32(1)
C(3)	-3442(4)	3022(3)	4662(3)	30(1)
C(4)	-3104(4)	2735(3)	3788(2)	30(1)
C(5)	-3571(4)	1651(3)	4056(2)	30(1)
C(6)	-2320(4)	1150(3)	4753(2)	32(1)
C(7)	-1398(4)	2646(3)	3755(2)	29(1)
C(8)	-2403(5)	2694(3)	6162(3)	46(1)
C(9)	-3482(6)	3282(4)	6395(3)	58(2)
C(10)	-4516(6)	3718(4)	5780(3)	58(2)
C(11)	-4532(5)	3576(3)	4904(3)	43(1)
C(12)	1570(5)	3433(4)	4294(3)	67(2)
C(13)	1721(5)	2899(4)	3666(4)	61(1)
C(14)	1966(5)	3510(4)	2766(4)	63(1)
C(15)	1967(5)	4432(4)	2816(4)	64(2)
C(16)	1747(5)	4394(4)	3763(4)	66(2)
C(17)	-1235(5)	4527(3)	3858(3)	48(1)
C(18)	-863(5)	4195(3)	2263(3)	43(1)
C(21)	5746(5)	7873(3)	118(3)	37(1)
C(22)	7086(5)	7954(3)	-563(3)	39(1)
C(23)	8111(5)	7307(3)	-122(3)	38(1)
C(24)	7425(4)	6791(3)	834(2)	31(1)
C(25)	6145(4)	6142(3)	672(2)	28(1)
C(26)	4960(5)	6912(3)	175(2)	36(1)
C(27)	6477(4)	7572(3)	1075(2)	32(1)
C(28)	7366(6)	8548(3)	-1468(3)	58(1)
C(29)	8765(7)	8491(4)	-1885(3)	69(2)

Table A9. Atomic Coordinates (x 10^4) and Equivalent Isotropic Displacement Parameters ($Å^2$ x 10^3) for 2.2 (continued). U(eq) is defined as one third of the trace of the orthogonalized Uij tensor.

	x	y	z	U(eq)
C(30)	9803(7)	7855(4)	-1434(3)	70(2)
C(31)	9486(5)	7230(3)	-546(3)	52(1)
C(32)	7372(8)	8123(6)	2982(4)	100(2)
C(33)	8107(10)	8940(5)	2661(5)	102(3)
C(34)	9368(9)	8783(7)	2138(5)	121(3)
C(35)	9279(7)	7801(6)	2165(5)	94(2)
C(36)	8053(8)	7458(4)	2701(4)	80(2)
C(37)	5835(10)	9162(6)	1436(6)	133(4)
C(38)	8145(11)	9225(5)	443(4)	147(4)
C(51)	-3523(4)	1329(3)	3217(3)	36(1)
C(52)	-5063(5)	1462(3)	4533(3)	39(1)
C(53)	5612(4)	5528(3)	1607(3)	34(1)
C(54)	6645(4)	5545(3)	78(2)	33(1)
C(61)	-1388(5)	520(3)	4351(3)	35(1)
C(62)	-2924(5)	598(3)	5696(3)	39(1)
C(63)	3547(5)	6849(3)	751(3)	42(1)
C(64)	4609(5)	6852(3)	-752(3)	42(1)

Table A10. Complete Listing of Bond Lengths [Å] for 3.20.

Si(1)-C(8)	1.889(4)	C(29)-C(30)	1.505(6)
Si(1)-C(15)	1.895(5)	C(29)-C(35A)	1.507(6)
Si(1)-C(1)	1.896(5)	C(30)-C(31)	1.324(6)
Si(2)-C(29)	1.894(5)	C(31)-C(31A)	1.448(6)
Si(2)-C(36)	1.898(5)	C(31A)-C(32)	1.397(7)
Si(2)-C(22)	1.911(4)	C(31A)-C(35A)	1.404(6)
C(1)-C(2)	1.486(6)	C(32)-C(33)	1.390(7)
C(1)-C(7A)	1.496(6)	C(33)-C(34)	1.389(7)
C(2)-C(3)	1.339(6)	C(34)-C(35)	1.375(7)
C(3)-C(3A)	1.449(7)	C(35)-C(35A)	1.376(6)
C(3A)-C(4)	1.386(7)	C(36)-C(37)	1.508(7)
C(3A)-C(7A)	1.395(6)	C(36)-C(42A)	1.510(6)
C(4)-C(5)	1.377(8)	C(37)-C(38)	1.346(7)
C(5)-C(6)	1.362(8)	C(38)-C(38A)	1.461(7)
C(6)-C(7)	1.394(7)	C(38A)-C(42A)	1.405(6)
C(7)-C(7A)	1.394(6)	C(38A)-C(39)	1.404(7)
C(8)-C(9)	1.499(6)	C(39)-C(40)	1.373(7)
C(8)-C(14A)	1.503(6)	C(40)-C(41)	1.374(7)
C(9)-C(10)	1.327(6)	C(41)-C(42)	1.395(7)
C(10)-C(10A)	1.453(7)	C(42)-C(42A)	1.376(6)
C(10A)-C(11)	1.388(7)		
C(10A)-C(14A)	1.402(6)		
C(11)-C(12)	1.375(7)		
C(12)-C(13)	1.373(7)		
C(13)-C(14)	1.393(7)		
C(14)-C(14A)	1.374(7)		
C(15)-C(21A)	1.501(6)		
C(15)-C(16)	1.517(7)		
C(16)-C(17)	1.326(7)		
C(17)-C(17A)	1.457(8)		
C(17A)-C(18)	1.393(7)		
C(17A)-C(21A)	1.405(6)		
C(18)-C(19)	1.373(8)		
C(19)-C(20)	1.373(8)		
C(20)-C(21)	1.377(7)		
C(21)-C(21A)	1.386(7)		
C(22)-C(28A)	1.488(6)		
C(22)-C(23)	1.497(6)		
C(23)-C(24)	1.331(6)		
C(24)-C(24A)	1.455(7)		
C(24A)-C(25)	1.391(7)		
C(24A)-C(28A)	1.403(6)		
C(25)-C(26)	1.377(7)		
C(26)-C(27)	1.387(7)		
C(27)-C(28)	1.383(7)		
C(28)-C(28A)	1.372(6)		

Table A11. Complete Listing of Bond Angles [deg] for 3.20.

C(8)-Si(1)-C(15)	108.9(2)	C(19)-C(20)-C(21)	120.1(6)
C(8)-Si(1)-C(1)	113.6(2)	C(20)-C(21)-C(21A)	120.1(5)
C(15)-Si(1)-C(1)	111.1(2)	C(21)-C(21A)-C(17A)	119.3(5)
C(29)-Si(2)-C(36)	112.2(2)	C(21)-C(21A)-C(15)	130.9(5)
C(29)-Si(2)-C(22)	112.8(2)	C(17A)-C(21A)-C(15)	109.7(5)
C(36)-Si(2)-C(22)	108.7(2)	C(28A)-C(22)-C(23)	103.0(4)
C(2)-C(1)-C(7A)	102.5(4)	C(28A)-C(22)-Si(2)	112.3(3)
C(2)-C(1)-Si(1)	106.3(3)	C(23)-C(22)-Si(2)	106.5(3)
C(7A)-C(1)-Si(1)	108.6(3)	C(24)-C(23)-C(22)	110.7(5)
C(3)-C(2)-C(1)	110.7(5)	C(23)-C(24)-C(24A)	109.4(5)
C(2)-C(3)-C(3A)	109.4(5)	C(25)-C(24A)-C(28A)	120.7(5)
C(4)-C(3A)-C(7A)	119.7(5)	C(25)-C(24A)-C(24)	131.2(5)
C(4)-C(3A)-C(3)	132.2(6)	C(28A)-C(24A)-C(24)	108.1(5)
C(7A)-C(3A)-C(3)	108.0(5)	C(26)-C(25)-C(24A)	118.4(5)
C(5)-C(4)-C(3A)	118.9(6)	C(25)-C(26)-C(27)	120.7(6)
C(6)-C(5)-C(4)	122.4(6)	C(26)-C(27)-C(28)	120.9(6)
C(5)-C(6)-C(7)	119.4(6)	C(28A)-C(28)-C(27)	119.1(5)
C(7A)-C(7)-C(6)	119.2(5)	C(28)-C(28A)-C(24A)	120.2(5)
C(7)-C(7A)-C(3A)	120.3(5)	C(28)-C(28A)-C(22)	131.4(5)
C(7)-C(7A)-C(1)	131.1(5)	C(24A)-C(28A)-C(22)	108.4(4)
C(3A)-C(7A)-C(1)	108.6(5)	C(30)-C(29)-C(35A)	102.4(4)
C(9)-C(8)-C(14A)	102.0(4)	C(30)-C(29)-Si(2)	105.9(3)
C(9)-C(8)-Si(1)	106.9(3)	C(35A)-C(29)-Si(2)	108.3(3)
C(14A)-C(8)-Si(1)	112.5(3)	C(31)-C(30)-C(29)	110.1(5)
C(10)-C(9)-C(8)	111.5(5)	C(30)-C(31)-C(31A)	110.9(4)
C(9)-C(10)-C(10A)	109.5(5)	C(32)-C(31A)-C(35A)	120.1(5)
C(11)-C(10A)-C(14A)	120.0(5)	C(32)-C(31A)-C(31)	132.3(5)
C(11)-C(10A)-C(10)	131.9(5)	C(35A)-C(31A)-C(31)	107.6(5)
C(14A)-C(10A)-C(10)	108.1(5)	C(33)-C(32)-C(31A)	118.7(5)
C(12)-C(11)-C(10A)	119.3(5)	C(34)-C(33)-C(32)	120.4(5)
C(13)-C(12)-C(11)	120.6(6)	C(35)-C(34)-C(33)	121.0(5)
C(12)-C(13)-C(14)	120.9(6)	C(34)-C(35)-C(35A)	119.5(5)
C(14A)-C(14)-C(13)	118.8(5)	C(35)-C(35A)-C(31A)	120.3(5)
C(14)-C(14A)-C(10A)	120.3(5)	C(35)-C(35A)-C(29)	131.3(5)
C(14)-C(14A)-C(8)	131.0(5)	C(31A)-C(35A)-C(29)	108.3(4)
C(10A)-C(14A)-C(8)	108.7(4)	C(37)-C(36)-C(42A)	101.7(4)
C(21A)-C(15)-C(16)	101.7(4)	C(37)-C(36)-Si(2)	113.1(4)
C(21A)-C(15)-Si(1)	114.5(3)	C(42A)-C(36)-Si(2)	112.7(3)
C(16)-C(15)-Si(1)	112.8(4)	C(38)-C(37)-C(36)	111.3(5)
C(17)-C(16)-C(15)	110.8(5)	C(37)-C(38)-C(38A)	109.5(5)
C(16)-C(17)-C(17A)	110.5(5)	C(42A)-C(38A)-C(39)	119.6(5)

Table A11. Complete Listing of Bond Angles [deg] for 3.20 (continued).

C(18)-C(17A)-C(21A)	119.9(6)	C(42A)-C(38A)-C(38)	107.8(5)
C(18)-C(17A)-C(17)	132.8(6)	C(39)-C(38A)-C(38)	132.6(5)
C(21A)-C(17A)-C(17)	107.2(5)	C(40)-C(39)-C(38A)	118.9(5)
C(19)-C(18)-C(17A)	119.1(6)	C(41)-C(40)-C(39)	121.7(6)
C(18)-C(19)-C(20)	121.4(6)	C(40)-C(41)-C(42)	120.0(6)
C(42A)-C(42)-C(41)	119.6(5)	C(42)-C(42A)-C(36)	130.0(5)
C(38A)-C(42A)-C(36)	109.6(5)	C(42)-C(42A)-C(38A)	120.3(5)

Table A12. Atomic Coordinates (x 10^4) and Equivalent Isotropic Displacement Parameters ($Å^2$ x 10^3) for 3.20. U(eq) is defined as one third of the trace of the orthogonalized Uij tensor.

	x	y	z	U(eq)
Si(1)	-6899(1)	-3540(1)	-340(1)	48(1)
Si(2)	-8532(1)	-8511(1)	-426(1)	47(1)
C(1)	-5516(5)	-4108(2)	-22(2)	52(1)
C(2)	-4164(5)	-3807(3)	-186(3)	63(2)
C(3)	-3572(5)	-3548(3)	332(3)	73(2)
C(3A)	-4404(5)	-3697(3)	888(3)	61(2)
C(4)	-4224(6)	-3566(3)	1530(3)	87(2)
C(5)	-5163(7)	-3813(4)	1961(3)	95(2)
C(6)	-6239(7)	-4199(3)	1781(3)	85(2)
C(7)	-6435(6)	-4336(3)	1136(3)	70(2)
C(7A)	-5525(5)	-4074(2)	690(2)	54(1)
C(8)	-8719(4)	-3793(2)	-121(2)	55(1)
C(9)	-9655(5)	-3244(2)	-306(3)	64(2)
C(10)	-10501(5)	-3412(3)	-776(3)	65(2)
C(10A)	-10280(5)	-4091(2)	-936(2)	56(1)
C(11)	-10870(5)	-4488(3)	-1396(3)	70(2)
C(12)	-10460(6)	-5126(3)	-1437(3)	80(2)
C(13)	-9482(6)	-5371(3)	-1027(3)	80(2)
C(14)	-8866(5)	-4977(3)	-567(3)	70(2)
C(14A)	-9249(4)	-4336(2)	-532(2)	52(1)
C(15)	-6777(5)	-3459(2)	-1237(2)	55(1)
C(16)	-6481(7)	-4099(3)	-1567(3)	77(2)
C(17)	-5301(7)	-4070(3)	-1888(3)	78(2)
C(17A)	-4705(6)	-3422(3)	-1847(2)	61(2)
C(18)	-3503(7)	-3146(4)	-2096(3)	80(2)
C(19)	-3210(6)	-2508(4)	-1964(3)	93(2)
C(20)	-4064(7)	-2141(3)	-1586(3)	80(2)
C(21)	-5258(5)	-2406(3)	-1339(2)	65(2)
C(21A)	-5595(5)	-3047(3)	-1466(2)	49(1)
C(22)	-6700(4)	-8779(2)	-201(2)	52(1)
C(23)	-5759(5)	-8227(2)	-368(3)	61(1)
C(24)	-4917(5)	-8391(3)	-843(3)	65(2)
C(24A)	-5141(5)	-9068(3)	-1010(2)	55(1)
C(25)	-4522(5)	-9460(3)	-1469(3)	73(2)
C(26)	-4962(6)	-10094(3)	-1525(3)	85(2)
C(27)	-5983(6)	-10338(3)	-1126(3)	80(2)
C(28)	-6597(5)	-9950(3)	-669(3)	67(2)
C(28A)	-6187(5)	-9315(2)	-613(2)	52(1)
C(29)	-9910(5)	-9096(2)	-138(2)	54(1)

Table A12. Atomic Coordinates (x 10^4) and Equivalent Isotropic Displacement Parameters ($Å^2$ x 10^3) for 3.20 (continued). U(eq) is defined as one third of the trace of the orthogonalized Uij tensor.

	x	y	z	U(eq)
C(30)	-11276(5)	-8786(3)	-302(3)	67(2)
C(31)	-11872(4)	-8556(3)	219(3)	65(2)
C(31A)	-11065(5)	-8715(2)	780(2)	53(1)
C(32)	-11252(6)	-8578(3)	1426(3)	77(2)
C(33)	-10324(7)	-8838(3)	1863(3)	80(2)
C(34)	-9220(6)	-9216(3)	1657(3)	71(2)
C(35)	-9014(5)	-9336(2)	1020(3)	62(2)
C(35A)	-9922(5)	-9083(2)	580(2)	50(1)
C(36)	-8609(5)	-8381(2)	-1321(2)	54(1)
C(37)	-8876(6)	-8998(3)	-1688(2)	66(2)
C(38)	-10069(6)	-8963(3)	-2018(2)	67(2)
C(38A)	-10691(6)	-8323(3)	-1927(2)	56(1)
C(39)	-11936(5)	-8046(3)	-2142(3)	71(2)
C(40)	-12259(6)	-7425(3)	-1958(3)	75(2)
C(41)	-11408(6)	-7073(3)	-1563(3)	75(2)
C(42)	-10175(5)	-7344(3)	-1342(2)	60(2)
C(42A)	-9820(5)	-7965(3)	-1522(2)	50(1)

Table A13. Complete Listing of Bond Lengths [Å] for 3.22.

Si(1)-C(60B)	1.73(4)	C(22)-C(22A)	1.462(12)
Si(1)-C(27)	1.878(7)	C(22)-C(22B)	1.469(12)
Si(1)-C(7)	1.903(7)	C(28)-C(29)	1.396(12)
Si(1)-C(47)	1.908(7)	C(29)-C(30)	1.378(13)
Si(1)-C(60A)	1.92(2)	C(30)-C(31)	1.373(12)
N(3A)-C(3A)	1.141(10)	C(41)-C(46)	1.503(10)
N(3B)-C(3B)	1.155(10)	C(41)-C(47)	1.545(10)
N(2A)-C(2A)	1.151(10)	C(41)-C(42)	1.587(10)
N(2B)-C(2B)	1.125(10)	C(46)-C(45)	1.378(10)
N(23A)-C(23A)	1.146(9)	C(46)-C(48)	1.403(11)
N(23B)-C(23B)	1.120(10)	C(45)-C(51)	1.360(11)
N(22A)-C(22A)	1.142(10)	C(45)-C(44)	1.497(10)
N(22B)-C(22B)	1.128(9)	C(44)-C(47)	1.548(9)
N(43A)-C(43A)	1.133(11)	C(44)-C(43)	1.584(10)
N(43B)-C(43B)	1.133(10)	C(43)-C(43A)	1.467(13)
N(42A)-C(42A)	1.132(10)	C(43)-C(43B)	1.479(12)
N(42B)-C(42B)	1.140(10)	C(43)-C(42)	1.610(10)
C(1)-C(6)	1.485(10)	C(42)-C(42A)	1.481(12)
C(1)-C(7)	1.546(9)	C(42)-C(42B)	1.493(13)
C(1)-C(2)	1.577(10)	C(48)-C(49)	1.394(13)
C(6)-C(8)	1.368(11)	C(49)-C(50)	1.373(14)
C(6)-C(5)	1.372(10)	C(50)-C(51)	1.380(13)
C(5)-C(11)	1.372(11)	C(60A)-C(61A)	1.36(3)
C(5)-C(4)	1.477(10)	C(61A)-C(62A)	1.26(3)
C(4)-C(7)	1.552(9)	C(60B)-C(61B)	1.51(5)
C(4)-C(3)	1.575(10)	C(61B)-C(62B)	1.30(3)
C(3)-C(3B)	1.455(12)	C(3)-C(3A)	1.484(12)
C(23)-C(23A)	1.479(12)	C(23)-C(23B)	1.482(12)
C(23)-C(22)	1.598(10)	C(3)-C(2)	1.599(10)
C(2)-C(2B)	1.443(12)		
C(2)-C(2A)	1.444(12)		
C(8)-C(9)	1.393(14)		
C(9)-C(10)	1.39(2)		
C(10)-C(11)	1.356(13)		
C(21)-C(26)	1.496(10)		
C(21)-C(27)	1.555(9)		
C(21)-C(22)	1.579(10)		
C(26)-C(28)	1.370(11)		
C(26)-C(25)	1.389(10)		
C(25)-C(31)	1.360(10)		
C(25)-C(24)	1.506(10)		
C(24)-C(27)	1.546(9)		
C(24)-C(23)	1.574(10)		

Table A14. Complete Listing of Bond Angles [deg] for 3.22.

C(60B)-Si(1)-C(27)	107(2)	C(27)-C(21)-C(22)	100.8(5)
C(60B)-Si(1)-C(7)	111(2)	C(28)-C(26)-C(25)	121.9(8)
C(27)-Si(1)-C(7)	101.4(3)	C(28)-C(26)-C(21)	131.2(8)
C(60B)-Si(1)-C(47)	112.5(14)	C(25)-C(26)-C(21)	106.9(6)
C(27)-Si(1)-C(47)	113.2(3)	C(31)-C(25)-C(26)	119.9(7)
C(7)-Si(1)-C(47)	110.5(3)	C(31)-C(25)-C(24)	133.6(8)
C(27)-Si(1)-C(60A)	107.3(7)	C(26)-C(25)-C(24)	106.5(6)
C(7)-Si(1)-C(60A)	115.7(7)	C(25)-C(24)-C(27)	102.3(6)
C(47)-Si(1)-C(60A)	108.6(6)	C(25)-C(24)-C(23)	106.6(6)
C(6)-C(1)-C(7)	101.8(6)	C(27)-C(24)-C(23)	99.5(5)
C(6)-C(1)-C(2)	104.8(6)	C(23A)-C(23)-C(23B)	107.3(6)
C(7)-C(1)-C(2)	102.6(5)	C(23A)-C(23)-C(24)	108.5(6)
C(8)-C(6)-C(5)	121.7(8)	C(23B)-C(23)-C(24)	112.4(6)
C(8)-C(6)-C(1)	131.9(8)	C(23A)-C(23)-C(22)	110.9(6)
C(5)-C(6)-C(1)	106.3(7)	C(23B)-C(23)-C(22)	114.9(6)
C(11)-C(5)-C(6)	121.8(8)	C(24)-C(23)-C(22)	102.7(5)
C(11)-C(5)-C(4)	130.6(8)	N(23A)-C(23A)-C(23)	177.2(8)
C(6)-C(5)-C(4)	107.5(6)	N(23B)-C(23B)-C(23)	177.6(10)
C(5)-C(4)-C(7)	102.2(6)	C(22A)-C(22)-C(22B)	109.8(7)
C(5)-C(4)-C(3)	106.9(6)	C(22A)-C(22)-C(21)	107.7(6)
C(7)-C(4)-C(3)	100.0(5)	C(22B)-C(22)-C(21)	112.5(6)
C(3B)-C(3)-C(3A)	108.1(7)	C(22A)-C(22)-C(23)	113.4(6)
C(3B)-C(3)-C(4)	112.6(6)	C(22B)-C(22)-C(23)	112.0(6)
C(3A)-C(3)-C(4)	110.1(6)	C(21)-C(22)-C(23)	101.2(5)
C(3B)-C(3)-C(2)	113.5(6)	N(22A)-C(22A)-C(22)	173.4(8)
C(3A)-C(3)-C(2)	110.9(6)	N(22B)-C(22B)-C(22)	177.5(9)
C(4)-C(3)-C(2)	101.7(5)	C(24)-C(27)-C(21)	93.1(5)
N(3A)-C(3A)-C(3)	176.5(9)	C(24)-C(27)-Si(1)	121.9(5)
N(3B)-C(3B)-C(3)	176.9(9)	C(21)-C(27)-Si(1)	122.3(5)
C(2B)-C(2)-C(2A)	108.5(6)	C(26)-C(28)-C(29)	117.1(8)
C(2B)-C(2)-C(1)	111.5(6)	C(30)-C(29)-C(28)	121.3(9)
C(2A)-C(2)-C(1)	109.7(6)	C(31)-C(30)-C(29)	120.0(9)
C(2B)-C(2)-C(3)	113.1(6)	C(25)-C(31)-C(30)	119.8(9)
C(2A)-C(2)-C(3)	112.7(6)	C(46)-C(41)-C(47)	102.0(6)
C(1)-C(2)-C(3)	101.3(5)	C(46)-C(41)-C(42)	104.8(5)
N(2A)-C(2A)-C(2)	175.1(9)	C(47)-C(41)-C(42)	101.1(6)
N(2B)-C(2B)-C(2)	176.9(10)	C(45)-C(46)-C(48)	121.2(8)
C(1)-C(7)-C(4)	92.2(5)	C(45)-C(46)-C(41)	107.6(7)
C(1)-C(7)-Si(1)	116.6(5)	C(48)-C(46)-C(41)	131.1(8)
C(4)-C(7)-Si(1)	120.6(5)	C(51)-C(45)-C(46)	121.6(8)
C(6)-C(8)-C(9)	116.9(10)	C(51)-C(45)-C(44)	131.9(8)
C(10)-C(9)-C(8)	120.4(10)	C(46)-C(45)-C(44)	106.0(6)
C(11)-C(10)-C(9)	122.1(10)	C(45)-C(44)-C(47)	101.7(6)
C(10)-C(11)-C(5)	117.2(9)	C(45)-C(44)-C(43)	106.6(6)
C(26)-C(21)-C(27)	102.3(6)	C(47)-C(44)-C(43)	101.0(5)
C(26)-C(21)-C(22)	105.6(6)	C(43A)-C(43)-C(43B)	109.1(6)

Table A14. Complete Listing of Bond Angles [deg] for 3.22 (continued).

C(43A)-C(43)-C(44)	109.3(7)
C(43B)-C(43)-C(44)	112.0(6)
C(43A)-C(43)-C(42)	112.0(6)
C(43B)-C(43)-C(42)	112.3(6)
C(44)-C(43)-C(42)	102.1(5)
N(43A)-C(43A)-C(43)	177.0(11)
N(43B)-C(43B)-C(43)	177.0(9)
C(42A)-C(42)-C(42B)	107.3(6)
C(42A)-C(42)-C(41)	110.7(6)
C(42B)-C(42)-C(41)	111.4(6)
C(42A)-C(42)-C(43)	113.7(7)
C(42B)-C(42)-C(43)	112.7(6)
C(41)-C(42)-C(43)	101.1(5)
N(42A)-C(42A)-C(42)	176.7(10)
N(42B)-C(42B)-C(42)	179.0(9)
C(41)-C(47)-C(44)	93.2(5)
C(41)-C(47)-Si(1)	119.7(5)
C(44)-C(47)-Si(1)	115.1(5)
C(49)-C(48)-C(46)	116.1(9)
C(50)-C(49)-C(48)	121.7(10)
C(49)-C(50)-C(51)	121.1(9)
C(45)-C(51)-C(50)	118.2(9)
C(61A)-C(60A)-Si(1)	118(2)
C(62A)-C(61A)-C(60A)	118(3)
C(61B)-C(60B)-Si(1)	125(3)
C(62B)-C(61B)-C(60B)	134(3)

Table A15. Atomic Coordinates (x 10^4) and Equivalent Isotropic Displacement Parameters ($Å^2$ x 10^3) for 3.22. U(eq) is defined as one third of the trace of the orthogonalized Uij tensor.

	x	y	z	U(eq)
Si(1)	2320(1)	7439(1)	1753(1)	35(1)
N(3A)	3831(7)	8593(5)	3898(3)	74(2)
N(3B)	986(7)	8116(6)	4225(4)	88(3)
N(2A)	2856(6)	10493(5)	3026(4)	76(2)
N(2B)	-46(7)	9896(5)	3155(4)	89(3)
N(23A)	-404(6)	8958(5)	238(3)	69(2)
N(23B)	1623(6)	9154(6)	-872(4)	85(3)
N(22A)	915(6)	10566(5)	1242(3)	67(2)
N(22B)	3055(6)	10779(6)	152(4)	85(3)
N(43A)	5069(8)	5851(6)	831(5)	104(3)
N(43B)	5413(6)	4273(5)	2405(4)	76(2)
N(42A)	6254(6)	7722(5)	1773(4)	86(3)
N(42B)	6531(6)	6112(5)	3287(4)	81(3)
C(1)	1392(5)	8802(5)	2354(3)	41(2)
C(6)	495(6)	8251(5)	2308(4)	47(2)
C(5)	766(5)	7548(5)	2685(3)	43(2)
C(4)	1829(5)	7632(5)	2945(3)	40(2)
C(3)	1956(6)	8416(5)	3405(3)	41(2)
C(3A)	3009(7)	8525(5)	3698(4)	49(2)
C(3B)	1410(7)	8272(5)	3862(4)	57(2)
C(2)	1568(5)	9243(4)	2986(3)	38(2)
C(2A)	2292(7)	9938(6)	3032(4)	55(2)
C(2B)	674(7)	9621(5)	3093(4)	58(2)
C(7)	2207(5)	8088(4)	2438(3)	36(2)
C(8)	-459(7)	8377(7)	2011(4)	76(3)
C(9)	-1146(7)	7759(9)	2110(6)	97(4)
C(10)	-860(9)	7068(8)	2507(6)	92(3)
C(11)	89(7)	6952(6)	2799(4)	67(3)
C(21)	2720(5)	9123(4)	1150(3)	37(2)
C(26)	3473(6)	8741(5)	852(3)	41(2)
C(25)	2997(5)	8110(5)	453(3)	40(2)
C(24)	1940(5)	8102(5)	503(3)	41(2)
C(23)	1470(5)	8995(5)	221(3)	40(2)
C(23A)	410(7)	8988(5)	220(3)	48(2)
C(23B)	1555(6)	9103(6)	-401(4)	58(2)
C(22)	2039(5)	9725(5)	670(3)	42(2)
C(22A)	1396(6)	10230(5)	967(4)	47(2)
C(22B)	2605(6)	10336(5)	381(4)	52(2)
C(27)	2030(5)	8317(4)	1165(3)	32(2)

Table A15. Atomic Coordinates (x 10^4) and Equivalent Isotropic Displacement Parameters ($Å^2$ x 10^3) for 3.22 (continued). U(eq) is defined as one third of the trace of the orthogonalized Uij tensor.

	x	y	z	U(eq)
C(28)	4444(6)	8948(6)	901(4)	60(2)
C(29)	4942(7)	8492(7)	534(5)	73(3)
C(30)	4478(8)	7852(8)	145(5)	80(3)
C(31)	3503(7)	7663(6)	107(4)	62(2)
C(41)	4364(5)	7080(5)	2444(3)	43(2)
C(46)	3986(6)	6439(5)	2838(4)	45(2)
C(45)	3523(5)	5758(5)	2486(4)	44(2)
C(44)	3674(5)	5937(4)	1878(4)	45(2)
C(43)	4806(5)	5785(5)	1906(3)	45(2)
C(43A)	4979(7)	5823(6)	1305(5)	68(3)
C(43B)	5154(6)	4921(6)	2175(4)	54(2)
C(42)	5303(5)	6609(5)	2304(3)	44(2)
C(42A)	5840(6)	7224(6)	1991(4)	59(2)
C(42B)	6004(7)	6324(5)	2859(5)	57(2)
C(47)	3612(5)	6961(4)	1849(3)	38(2)
C(48)	4078(6)	6431(6)	3453(4)	65(3)
C(49)	3663(8)	5707(9)	3680(5)	82(3)
C(50)	3193(7)	5042(7)	3321(7)	81(3)
C(51)	3136(6)	5052(6)	2719(5)	65(3)
C(60A)	1384(15)	6497(15)	1522(10)	25(7)
C(61A)	1359(15)	6089(12)	996(9)	94(7)
C(62A)	568(26)	6105(21)	609(14)	170(12)
C(60B)	1419(31)	6635(28)	1578(22)	91(21)
C(61B)	412(15)	6781(13)	1187(9)	68(8)
C(62B)	7(19)	6593(16)	641(11)	78(8)

Table A16. Complete Listing of Bond Lengths [Å] for 3.24$(CH_3COCH_3)_2$.

Si(1)-O(1)	1.603(3)	C(23)-C(23A)	1.477(6)
Si(1)-C(47)	1.884(4)	C(28)-C(29)	1.386(6)
Si(1)-C(27)	1.894(4)	C(29)-C(30)	1.373(7)
Si(1)-C(7)	1.895(4)	C(30)-C(31)	1.383(7)
N(2A)-C(2A)	1.140(5)	C(44)-C(45)	1.500(6)
N(2B)-C(2B)	1.136(5)	C(44)-C(47)	1.557(5)
N(3A)-C(3A)	1.138(6)	C(44)-C(43)	1.597(5)
N(3B)-C(3B)	1.135(5)	C(45)-C(48)	1.371(6)
N(22A)-C(22A)	1.141(6)	C(45)-C(46)	1.391(5)
N(22B)-C(22B)	1.136(5)	C(46)-C(51)	1.386(6)
N(23A)-C(23A)	1.138(5)	C(46)-C(41)	1.499(5)
N(23B)-C(23B)	1.139(5)	C(41)-C(47)	1.540(5)
N(42A)-C(42A)	1.134(5)	C(41)-C(42)	1.595(5)
N(42B)-C(42B)	1.139(5)	C(42)-C(42A)	1.468(6)
N(43A)-C(43A)	1.138(5)	C(42)-C(42B)	1.479(6)
N(43B)-C(43B)	1.140(5)	C(42)-C(43)	1.615(6)
C(4)-C(5)	1.512(6)	C(43)-C(43A)	1.462(6)
C(4)-C(7)	1.556(5)	C(43)-C(43B)	1.484(6)
C(4)-C(3)	1.589(6)	C(48)-C(49)	1.391(7)
C(5)-C(8)	1.382(6)	C(49)-C(50)	1.365(7)
C(5)-C(6)	1.392(6)	C(50)-C(51)	1.385(6)
C(6)-C(11)	1.382(6)	C(90)-C(91)	1.51(3)
C(6)-C(1)	1.506(5)	C(91)-O(2)	1.39(2)
C(1)-C(7)	1.551(5)	C(91)-C(92)	1.51(2)
C(1)-C(2)	1.587(5)	C(93)-C(94)	1.489(11)
C(2)-C(2B)	1.468(6)	C(94)-O(3)	1.212(8)
C(2)-C(2A)	1.468(6)	C(94)-C(95)	1.508(11)
C(2)-C(3)	1.612(5)		
C(3)-C(3B)	1.463(6)		
C(3)-C(3A)	1.469(6)		
C(8)-C(9)	1.386(7)		
C(9)-C(10)	1.383(7)		
C(10)-C(11)	1.373(7)		
C(24)-C(25)	1.506(5)		
C(24)-C(27)	1.554(5)		
C(24)-C(23)	1.582(5)		
C(25)-C(28)	1.389(6)		
C(25)-C(26)	1.389(5)		
C(26)-C(31)	1.380(6)		
C(26)-C(21)	1.508(6)		
C(21)-C(27)	1.557(5)		
C(21)-C(22)	1.590(5)		
C(22)-C(22A)	1.468(6)		
C(22)-C(22B)	1.481(6)		
C(22)-C(23)	1.617(6)		
C(23)-C(23B)	1.473(6)		

Table A17. Complete Listing of Bond Angles [deg] for 3.24$(CH_3COCH_3)_2$.

O(1)-Si(1)-C(47)	104.4(2)	C(26)-C(25)-C(24)	107.3(3)
O(1)-Si(1)-C(27)	108.9(2)	C(31)-C(26)-C(25)	121.1(4)
C(47)-Si(1)-C(27)	113.2(2)	C(31)-C(26)-C(21)	131.8(4)
O(1)-Si(1)-C(7)	116.0(2)	C(25)-C(26)-C(21)	106.8(3)
C(47)-Si(1)-C(7)	103.3(2)	C(26)-C(21)-C(27)	101.5(3)
C(27)-Si(1)-C(7)	110.9(2)	C(26)-C(21)-C(22)	106.1(3)
C(5)-C(4)-C(7)	101.5(3)	C(27)-C(21)-C(22)	100.1(3)
C(5)-C(4)-C(3)	106.2(3)	C(22A)-C(22)-C(22B)	108.7(3)
C(7)-C(4)-C(3)	101.0(3)	C(22A)-C(22)-C(21)	109.2(3)
C(8)-C(5)-C(6)	121.8(4)	C(22B)-C(22)-C(21)	112.5(3)
C(8)-C(5)-C(4)	131.9(4)	C(22A)-C(22)-C(23)	113.0(3)
C(6)-C(5)-C(4)	106.1(3)	C(22B)-C(22)-C(23)	111.3(3)
C(11)-C(6)-C(5)	120.8(4)	C(21)-C(22)-C(23)	102.0(3)
C(11)-C(6)-C(1)	131.6(4)	N(22A)-C(22A)-C(22)	175.5(5)
C(5)-C(6)-C(1)	107.5(3)	N(22B)-C(22B)-C(22)	177.0(4)
C(6)-C(1)-C(7)	101.9(3)	C(23B)-C(23)-C(23A)	107.4(3)
C(6)-C(1)-C(2)	106.6(3)	C(23B)-C(23)-C(24)	111.9(3)
C(7)-C(1)-C(2)	99.7(3)	C(23A)-C(23)-C(24)	110.8(3)
C(2B)-C(2)-C(2A)	108.9(3)	C(23B)-C(23)-C(22)	112.8(3)
C(2B)-C(2)-C(1)	108.3(3)	C(23A)-C(23)-C(22)	112.2(3)
C(2A)-C(2)-C(1)	112.0(3)	C(24)-C(23)-C(22)	101.9(3)
C(2B)-C(2)-C(3)	111.0(3)	N(23A)-C(23A)-C(23)	178.1(5)
C(2A)-C(2)-C(3)	114.4(3)	N(23B)-C(23B)-C(23)	178.0(5)
C(1)-C(2)-C(3)	102.0(3)	C(24)-C(27)-C(21)	93.9(3)
N(2A)-C(2A)-C(2)	175.5(5)	C(24)-C(27)-Si(1)	120.7(3)
N(2B)-C(2B)-C(2)	174.3(5)	C(21)-C(27)-Si(1)	113.9(3)
C(3B)-C(3)-C(3A)	108.7(4)	C(29)-C(28)-C(25)	117.7(4)
C(3B)-C(3)-C(4)	107.1(3)	C(30)-C(29)-C(28)	121.4(5)
C(3A)-C(3)-C(4)	111.2(3)	C(29)-C(30)-C(31)	121.0(4)
C(3B)-C(3)-C(2)	113.3(3)	C(26)-C(31)-C(30)	118.0(4)
C(3A)-C(3)-C(2)	114.5(3)	C(45)-C(44)-C(47)	102.6(3)
C(4)-C(3)-C(2)	101.7(3)	C(45)-C(44)-C(43)	105.3(3)
N(3A)-C(3A)-C(3)	175.2(5)	C(47)-C(44)-C(43)	100.1(3)
N(3B)-C(3B)-C(3)	172.7(5)	C(48)-C(45)-C(46)	121.2(4)
C(1)-C(7)-C(4)	93.6(3)	C(48)-C(45)-C(44)	132.0(4)
C(1)-C(7)-Si(1)	119.7(3)	C(46)-C(45)-C(44)	106.5(3)
C(4)-C(7)-Si(1)	117.5(3)	C(51)-C(46)-C(45)	120.8(4)

Table A17. Complete Listing of Bond Angles [deg] for 3.24(CH_3COCH_3)$_2$ (continued).

C(5)-C(8)-C(9)	116.9(5)	C(51)-C(46)-C(41)	131.9(4)
C(10)-C(9)-C(8)	120.9(5)	C(45)-C(46)-C(41)	107.1(3)
C(11)-C(10)-C(9)	122.2(5)	C(46)-C(41)-C(47)	102.6(3)
C(10)-C(11)-C(6)	117.3(5)	C(46)-C(41)-C(42)	106.4(3)
C(25)-C(24)-C(27)	101.9(3)	C(47)-C(41)-C(42)	99.7(3)
C(25)-C(24)-C(23)	106.3(3)	C(42A)-C(42)-C(42B)	108.7(3)
C(27)-C(24)-C(23)	99.8(3)	C(42A)-C(42)-C(41)	109.5(3)
C(28)-C(25)-C(26)	120.6(4)	C(42B)-C(42)-C(41)	112.1(3)
C(28)-C(25)-C(24)	131.7(4)	C(42A)-C(42)-C(43)	111.1(3)
C(42B)-C(42)-C(43)	113.6(3)	C(41)-C(42)-C(43)	101.8(3)
N(42A)-C(42A)-C(42)	177.1(4)	N(42B)-C(42B)-C(42)	176.9(5)
C(43A)-C(43)-C(43B)	109.8(3)	C(43A)-C(43)-C(44)	107.6(3)
C(43B)-C(43)-C(44)	112.3(3)	C(43A)-C(43)-C(42)	112.9(3)
C(43B)-C(43)-C(42)	112.5(3)	C(44)-C(43)-C(42)	101.5(3)
N(43A)-C(43A)-C(43)	173.6(5)	N(43B)-C(43B)-C(43)	177.6(5)
C(41)-C(47)-C(44)	93.6(3)	C(41)-C(47)-Si(1)	121.5(3)
C(44)-C(47)-Si(1)	121.0(3)	C(45)-C(48)-C(49)	117.9(5)
C(50)-C(49)-C(48)	120.9(5)	C(49)-C(50)-C(51)	121.9(4)
C(50)-C(51)-C(46)	117.3(4)	O(2)-C(91)-C(92)	99(2)
O(2)-C(91)-C(90)	132(2)	C(92)-C(91)-C(90)	127(2)
O(3)-C(94)-C(93)	118.8(8)	O(3)-C(94)-C(95)	123.2(8)
C(93)-C(94)-C(95)	118.0(9)		

Table A18. Atomic Coordinates (x 10^4) and Equivalent Isotropic Displacement Parameters ($Å^2$ x 10^3) for 3.24(CH_3COCH_3)$_2$. U(eq) is defined as one third of the trace of the orthogonalized Uij tensor.

	x	y	z	U(eq)
Si(1)	2324(1)	2452(1)	1893(1)	30(1)
O(1)	1563(2)	3274(2)	1732(1)	57(1)
N(2A)	949(3)	1568(3)	4306(2)	69(1)
N(2B)	3792(3)	1192(3)	3957(2)	60(1)
N(3A)	2(4)	-371(3)	3173(2)	81(2)
N(3B)	2917(3)	-703(3)	2968(2)	56(1)
N(22A)	5033(3)	4085(3)	970(2)	68(1)
N(22B)	5473(3)	5644(3)	2557(2)	57(1)
N(23A)	6173(3)	2137(3)	1869(2)	59(1)
N(23B)	6523(3)	3755(3)	3397(2)	63(1)
N(42A)	-442(3)	1085(3)	305(2)	70(1)
N(42B)	1578(3)	1149(3)	-829(2)	66(1)
N(43A)	895(3)	-668(3)	1189(2)	63(1)
N(43B)	2979(3)	-687(3)	52(2)	67(1)
C(4)	1372(3)	980(3)	2427(2)	34(1)
C(5)	465(3)	1549(3)	2402(2)	39(1)
C(6)	739(3)	2251(3)	2804(2)	36(1)
C(1)	1817(3)	2151(3)	3059(2)	33(1)
C(2)	1935(3)	1306(3)	3491(2)	34(1)
C(2A)	1370(3)	1420(3)	3949(2)	45(1)
C(2B)	2973(3)	1212(3)	3771(2)	38(1)
C(3)	1575(3)	477(3)	3045(2)	35(1)
C(3A)	696(4)	8(3)	3140(2)	47(1)
C(3B)	2337(3)	-201(3)	3037(2)	41(1)
C(7)	2186(3)	1719(3)	2539(2)	29(1)
C(8)	-494(3)	1429(3)	2108(2)	55(1)
C(9)	-1172(4)	2048(4)	2226(3)	70(2)
C(10)	-896(4)	2739(4)	2630(3)	67(2)
C(11)	54(3)	2854(3)	2928(2)	50(1)
C(24)	4351(3)	2794(3)	2597(2)	30(1)
C(25)	3962(3)	3447(3)	2989(2)	32(1)
C(26)	3526(3)	4162(3)	2640(2)	35(1)
C(21)	3665(3)	3977(3)	2027(2)	33(1)
C(22)	4798(3)	4120(3)	2049(2)	34(1)
C(22A)	4967(3)	4097(3)	1449(2)	44(1)
C(22B)	5168(3)	4995(3)	2325(2)	39(1)
C(23)	5280(3)	3266(3)	2444(2)	34(1)
C(23A)	5786(3)	2639(3)	2113(2)	39(1)
C(23B)	5992(3)	3545(3)	2976(2)	41(1)
C(27)	3611(3)	2920(3)	2003(2)	30(1)

Table A18. Atomic Coordinates (x 10^4) and Equivalent Isotropic Displacement Parameters ($Å^2$ x 10^3) for 3.24$(CH_3COCH_3)_2$ (continued). U(eq) is defined as one third of the trace of the orthogonalized Uij tensor.

	x	y	z	U(eq)
C(28)	4061(3)	3476(3)	3595(2)	46(1)
C(29)	3669(4)	4216(4)	3831(2)	56(1)
C(30)	3211(4)	4908(4)	3481(2)	58(1)
C(31)	3147(3)	4901(3)	2881(2)	47(1)
C(44)	2690(3)	858(3)	1167(2)	33(1)
C(45)	3418(3)	1316(3)	877(2)	34(1)
C(46)	2924(3)	2019(3)	539(2)	35(1)
C(41)	1887(3)	1993(3)	612(2)	33(1)
C(42)	1400(3)	1115(3)	266(2)	34(1)
C(42A)	356(3)	1089(3)	276(2)	43(1)
C(42B)	1504(3)	1111(3)	-352(2)	44(1)
C(43)	1986(3)	303(3)	656(2)	35(1)
C(43A)	1355(3)	-269(3)	930(2)	41(1)
C(43B)	2539(3)	-272(3)	317(2)	42(1)
C(47)	1999(3)	1654(3)	1248(2)	32(1)
C(48)	4367(3)	1111(3)	863(2)	46(1)
C(49)	4826(4)	1635(4)	505(2)	61(2)
C(50)	4348(4)	2337(4)	183(2)	56(1)
C(51)	3383(3)	2542(3)	184(2)	47(1)
C(90)	-1210(17)	173(13)	4380(9)	411(21)
C(91)	-1790(13)	900(14)	3996(7)	267(12)
C(92)	-1649(9)	1916(9)	4061(6)	227(6)
C(93)	7369(8)	3063(6)	648(4)	170(4)
C(94)	7261(6)	4039(6)	476(3)	105(2)
C(95)	6453(6)	4295(8)	-38(4)	164(4)
O(2)	-2704(11)	886(8)	3617(5)	296(6)
O(3)	7823(4)	4588(3)	752(2)	109(2)

Table A19. Complete Listing of Bond Lengths [Å] for 4.34.

Si(1)-C(15)	1.850(3)
Si(1)-C(14)	1.857(3)
Si(1)-C(16)	1.859(3)
Si(1)-C(7)	1.913(3)
N(21)-C(21)	1.133(4)
N(22)-C(22)	1.130(4)
N(31)-C(31)	1.136(4)
N(32)-C(32)	1.135(4)
C(1)-C(6)	1.511(4)
C(1)-C(12)	1.519(4)
C(1)-C(7)	1.547(4)
C(1)-C(2)	1.608(4)
C(2)-C(21)	1.479(4)
C(2)-C(22)	1.481(5)
C(2)-C(3)	1.591(4)
C(3)-C(31)	1.468(4)
C(3)-C(32)	1.479(4)
C(3)-C(4)	1.612(4)
C(4)-C(13)	1.505(4)
C(4)-C(5)	1.509(4)
C(4)-C(7)	1.554(4)
C(5)-C(6)	1.377(4)
C(5)-C(11)	1.387(4)
C(6)-C(8)	1.379(4)
C(8)-C(9)	1.393(4)
C(9)-C(10)	1.368(5)
C(10)-C(11)	1.388(5)

Table A20. Complete Listing of Bond Angles [deg] for 4.34.

C(32)-C(3)-C(2)	112.8(3)	C(21)-C(2)-C(1)	110.7(3)
C(31)-C(3)-C(4)	110.8(3)	C(22)-C(2)-C(1)	110.6(3)
C(32)-C(3)-C(4)	111.8(2)	C(3)-C(2)-C(1)	102.3(2)
C(2)-C(3)-C(4)	102.7(2)	C(31)-C(3)-C(32)	106.3(3)
C(13)-C(4)-C(5)	116.8(3)	C(31)-C(3)-C(2)	112.5(3)
C(13)-C(4)-C(7)	120.9(3)		
C(5)-C(4)-C(7)	101.2(2)		
C(13)-C(4)-C(3)	111.8(3)		
C(5)-C(4)-C(3)	103.8(2)		
C(7)-C(4)-C(3)	99.7(2)		
C(6)-C(5)-C(11)	121.4(3)		
C(6)-C(5)-C(4)	107.3(3)		
C(11)-C(5)-C(4)	131.3(3)		
C(5)-C(6)-C(8)	121.1(3)		
C(5)-C(6)-C(1)	107.9(3)		
C(8)-C(6)-C(1)	131.0(3)		
C(1)-C(7)-C(4)	95.2(2)		
C(1)-C(7)-Si(1)	117.9(2)		
C(4)-C(7)-Si(1)	119.6(2)		
C(6)-C(8)-C(9)	118.0(3)		
C(10)-C(9)-C(8)	120.5(4)		
C(9)-C(10)-C(11)	122.1(4)		
C(5)-C(11)-C(10)	117.0(3)		
N(21)-C(21)-C(2)	178.9(4)		
N(22)-C(22)-C(2)	176.4(4)		
N(31)-C(31)-C(3)	177.1(4)		
N(32)-C(32)-C(3)	177.4(4)		
C(15)-Si(1)-C(14)	109.63(17)		
C(15)-Si(1)-C(16)	108.03(17)		
C(14)-Si(1)-C(16)	108.70(17)		
C(15)-Si(1)-C(7)	109.15(15)		
C(14)-Si(1)-C(7)	111.80(14)		
C(16)-Si(1)-C(7)	109.46(15)		
C(6)-C(1)-C(12)	116.3(3)		
C(6)-C(1)-C(7)	100.5(2)		
C(12)-C(1)-C(7)	120.7(3)		
C(6)-C(1)-C(2)	103.5(2)		
C(12)-C(1)-C(2)	112.3(3)		
C(7)-C(1)-C(2)	101.0(2)		
C(21)-C(2)-C(22)	107.5(3)		
C(21)-C(2)-C(3)	111.7(3)		
C(22)-C(2)-C(3)	114.0(3)		

Table A21. Atomic Coordinates (x 10^4) and Equivalent Isotropic Displacement Parameters ($Å^2$ x 10^3) for 4.34. U(eq) is defined as one third of the trace of the orthogonalized Uij tensor.

	x	y	z	U(eq)
Si(1)	4431(1)	746(1)	1941(1)	54(1)
N(21)	3947(3)	1425(2)	5710(2)	85(1)
N(22)	-317(4)	2062(2)	4122(2)	88(1)
N(31)	3369(3)	-950(2)	5127(2)	82(1)
N(32)	-933(3)	-422(2)	3713(2)	79(1)
C(1)	2536(3)	1490(2)	3126(2)	46(1)
C(2)	1979(3)	1147(2)	4054(2)	46(1)
C(3)	1705(3)	99(2)	3821(2)	43(1)
C(4)	2086(3)	-11(2)	2770(2)	42(1)
C(5)	922(3)	524(2)	2063(2)	44(1)
C(6)	1209(3)	1426(2)	2266(2)	46(1)
C(7)	3385(3)	651(2)	2930(2)	41(1)
C(8)	324(4)	2090(3)	1740(3)	64(1)
C(9)	-865(4)	1820(3)	990(3)	77(1)
C(10)	-1149(4)	922(3)	799(3)	76(1)
C(11)	-274(4)	248(3)	1330(2)	62(1)
C(12)	3259(3)	2411(2)	3309(2)	68(1)
C(13)	2242(3)	-989(2)	2516(2)	62(1)
C(14)	3256(3)	1116(2)	730(2)	76(1)
C(15)	5242(4)	-365(2)	1797(3)	90(1)
C(16)	5918(3)	1579(3)	2348(3)	88(1)
C(21)	3093(4)	1296(2)	4994(3)	58(1)
C(22)	675(4)	1653(3)	4117(2)	58(1)
C(31)	2637(3)	-480(2)	4575(3)	53(1)
C(32)	205(4)	-177(2)	3764(2)	52(1)

Table A22. Complete Listing of Bond Lengths [Å] for 4.38.

Cr(1)-C(66)	1.822(9)
Cr(1)-C(55)	1.826(9)
Cr(1)-C(44)	1.836(8)
Cr(1)-C(5)	2.172(8)
Cr(1)-C(6)	2.205(9)
Cr(1)-C(4)	2.217(6)
Cr(1)-C(7)	2.237(8)
Cr(1)-C(3A)	2.280(7)
Cr(1)-C(7A)	2.293(6)
Si(1)-C(10)	1.831(7)
Si(1)-C(8)	1.847(8)
Si(1)-C(9)	1.853(9)
Si(1)-C(1)	1.938(7)
O(55)-C(55)	1.168(8)
O(44)-C(44)	1.154(7)
O(66)-C(66)	1.170(8)
C(1)-C(2)	1.479(9)
C(1)-C(7A)	1.496(8)
C(1)-C(11)	1.540(8)
C(2)-C(3)	1.339(10)
C(3)-C(3A)	1.455(10)
C(3)-C(33)	1.508(9)
C(3A)-C(7A)	1.413(8)
C(3A)-C(4)	1.419(10)
C(4)-C(5)	1.400(11)
C(5)-C(6)	1.395(12)
C(6)-C(7)	1.384(11)
C(7A)-C(7)	1.403(9)

Table A23. Complete Listing of Bond Angles [deg] for 4.38.

C(6)-Cr(1)-C(7A)	65.0(3)	C(5)-Cr(1)-C(7)	65.8(4)
C(4)-Cr(1)-C(7A)	65.8(3)	C(6)-Cr(1)-C(7)	36.3(3)
C(7)-Cr(1)-C(7A)	36.0(2)	C(4)-Cr(1)-C(7)	78.9(3)
C(3A)-Cr(1)-C(7A)	36.0(2)	C(66)-Cr(1)-C(3A)	89.7(3)
C(10)-Si(1)-C(8)	109.9(4)	C(55)-Cr(1)-C(3A)	148.1(3)
C(10)-Si(1)-C(9)	110.4(4)	C(44)-Cr(1)-C(3A)	123.7(3)
C(8)-Si(1)-C(9)	109.3(4)	C(5)-Cr(1)-C(3A)	65.4(3)
C(10)-Si(1)-C(1)	108.7(3)	C(6)-Cr(1)-C(3A)	77.7(3)
C(8)-Si(1)-C(1)	109.8(3)	C(4)-Cr(1)-C(3A)	36.8(3)
C(9)-Si(1)-C(1)	108.6(4)	C(7)-Cr(1)-C(3A)	65.5(3)
C(2)-C(1)-C(7A)	100.9(5)	C(66)-Cr(1)-C(7A)	112.9(3)
C(2)-C(1)-C(11)	116.1(7)	C(55)-Cr(1)-C(7A)	158.2(3)
C(7A)-C(1)-C(11)	115.4(6)	C(44)-Cr(1)-C(7A)	95.3(3)
C(2)-C(1)-Si(1)	106.3(4)	C(5)-Cr(1)-C(7A)	76.5(3)
C(7A)-C(1)-Si(1)	107.4(4)	C(3A)-C(4)-Cr(1)	74.0(4)
C(11)-C(1)-Si(1)	109.8(5)	C(4)-C(5)-C(6)	123.1(9)
C(3)-C(2)-C(1)	114.2(7)	C(4)-C(5)-Cr(1)	73.2(4)
C(2)-C(3)-C(3A)	107.0(7)	C(6)-C(5)-Cr(1)	72.7(5)
C(2)-C(3)-C(33)	128.9(8)	C(7)-C(6)-C(5)	119.0(9)
C(3A)-C(3)-C(33)	124.0(8)	C(7)-C(6)-Cr(1)	73.1(5)
C(7A)-C(3A)-C(4)	119.9(7)	C(5)-C(6)-Cr(1)	70.1(5)
C(7A)-C(3A)-C(3)	108.5(6)	C(7)-C(7A)-C(3A)	120.4(6)
C(4)-C(3A)-C(3)	131.6(8)	C(7)-C(7A)-C(1)	130.4(7)
C(7A)-C(3A)-Cr(1)	72.5(4)	C(3A)-C(7A)-C(1)	109.1(6)
C(4)-C(3A)-Cr(1)	69.2(4)	C(7)-C(7A)-Cr(1)	69.8(4)
C(3)-C(3A)-Cr(1)	130.1(4)	C(3A)-C(7A)-Cr(1)	71.5(4)
C(5)-C(4)-C(3A)	117.3(8)	C(1)-C(7A)-Cr(1)	135.0(4)
C(5)-C(4)-Cr(1)	69.7(4)	C(6)-C(7)-C(7A)	120.2(8)
C(66)-Cr(1)-C(55)	88.6(3)	C(6)-C(7)-Cr(1)	70.6(5)
C(66)-Cr(1)-C(44)	89.2(3)	C(7A)-C(7)-Cr(1)	74.1(4)
C(55)-Cr(1)-C(44)	88.1(3)	O(44)-C(44)-Cr(1)	177.1(7)
C(66)-Cr(1)-C(5)	122.9(5)	O(55)-C(55)-Cr(1)	179.5(6)
C(55)-Cr(1)-C(5)	89.1(3)	O(66)-C(66)-Cr(1)	179.3(7)
C(44)-Cr(1)-C(5)	147.7(5)		
C(66)-Cr(1)-C(6)	159.7(4)		
C(55)-Cr(1)-C(6)	93.7(3)		
C(44)-Cr(1)-C(6)	111.0(4)		
C(5)-Cr(1)-C(6)	37.2(3)		
C(66)-Cr(1)-C(4)	92.9(3)		
C(55)-Cr(1)-C(4)	111.6(3)		
C(44)-Cr(1)-C(4)	160.3(3)		
C(5)-Cr(1)-C(4)	37.2(3)		
C(6)-Cr(1)-C(4)	67.5(3)		
C(66)-Cr(1)-C(7)	148.4(3)		
C(55)-Cr(1)-C(7)	122.8(3)		
C(44)-Cr(1)-C(7)	89.1(3)		

Table A24. Atomic Coordinates (x 10^4) and Equivalent Isotropic Displacement Parameters ($Å^2$ x 10^3) for 4.38. U(eq) is defined as one third of the trace of the orthogonalized Uij tensor.

	x	y	z	U(eq)
Cr(1)	2689(1)	4432(1)	8836(1)	58(1)
Si(1)	2108(2)	888(2)	6507(2)	60(1)
O(55)	2048(6)	5998(6)	10846(6)	104(2)
O(44)	927(7)	6837(6)	6920(6)	117(2)
O(66)	5169(7)	6198(6)	7600(6)	96(2)
C(1)	2675(8)	2744(6)	6404(7)	51(2)
C(2)	4213(9)	2683(7)	6089(8)	69(2)
C(3)	4909(8)	2528(7)	7168(10)	66(2)
C(3A)	3869(8)	2525(6)	8322(7)	49(2)
C(4)	4004(10)	2364(7)	9715(10)	76(3)
C(5)	2770(16)	2365(8)	10595(9)	100(4)
C(6)	1443(12)	2584(9)	10143(11)	92(3)
C(7A)	2528(7)	2733(6)	7860(7)	43(2)
C(7)	1327(9)	2794(7)	8768(9)	69(2)
C(8)	191(8)	852(9)	6893(10)	114(3)
C(9)	2639(10)	686(9)	4802(9)	116(3)
C(10)	2967(9)	-590(7)	7890(9)	101(3)
C(11)	1844(9)	4014(7)	5364(8)	99(3)
C(33)	6464(8)	2313(9)	7266(10)	113(3)
C(44)	1615(9)	5893(8)	7633(8)	76(2)
C(55)	2292(7)	5389(8)	10060(8)	66(2)
C(66)	4201(9)	5504(8)	8077(8)	64(2)

Table A25. Complete Listing of Bond Lengths [Å] for 4.54.

Co(1)-C(17)	1.794(5)	O(17)-C(17)	1.127(6)
Co(1)-C(16)	1.810(6)	O(18)-C(18)	1.127(6)
Co(1)-C(18)	1.823(7)	O(19)-C(19)	1.133(6)
Co(1)-C(15)	1.991(4)	C(20)-O(20)	1.140(7)
Co(1)-C(14)	1.998(4)	C(21)-O(21)	1.139(6)
Co(1)-Co(2)	2.484(1)		
Co(2)-C(20)	1.785(7)		
Co(2)-C(19)	1.798(6)		
Co(2)-C(21)	1.805(7)		
Co(2)-C(15)	2.006(4)		
Co(2)-C(14)	2.008(4)		
Si(1)-C(14)	1.853(5)		
Si(1)-C(12)	1.864(5)		
Si(1)-C(13)	1.868(5)		
Si(1)-C(7)	1.918(4)		
Si(2)-C(23)	1.863(5)		
Si(2)-C(15)	1.869(4)		
Si(2)-C(24)	1.869(6)		
Si(2)-C(22)	1.873(5)		
N(51)-C(51)	1.140(6)		
N(52)-C(52)	1.127(5)		
N(61)-C(61)	1.119(5)		
N(62)-C(62)	1.137(5)		
C(1)-C(2)	1.502(5)		
C(1)-C(7)	1.550(5)		
C(1)-C(6)	1.603(5)		
C(2)-C(8)	1.384(6)		
C(2)-C(3)	1.385(6)		
C(3)-C(11)	1.395(6)		
C(3)-C(4)	1.516(6)		
C(4)-C(7)	1.540(6)		
C(4)-C(5)	1.588(5)		
C(5)-C(52)	1.484(6)		
C(5)-C(51)	1.488(6)		
C(5)-C(6)	1.608(5)		
C(6)-C(62)	1.481(6)		
C(6)-C(61)	1.483(6)		
C(8)-C(9)	1.393(7)		
C(9)-C(10)	1.371(7)		
C(10)-C(11)	1.400(7)		
C(14)-C(15)	1.323(6)		
O(16)-C(16)	1.138(6)		

Table A26. Complete Listing of Bond Angles [deg] for 4.54.

C(17)-Co(1)-C(16)	100.1(2)	C(8)-C(2)-C(1)	132.1(4)
C(17)-Co(1)-C(18)	97.2(2)	C(3)-C(2)-C(1)	106.5(3)
C(16)-Co(1)-C(18)	105.1(3)	C(2)-C(3)-C(11)	121.3(4)
C(17)-Co(1)-C(15)	101.1(2)	C(2)-C(3)-C(4)	106.9(4)
C(16)-Co(1)-C(15)	140.5(2)	C(11)-C(3)-C(4)	131.8(4)
C(18)-Co(1)-C(15)	104.9(2)	C(3)-C(4)-C(7)	100.8(3)
C(17)-Co(1)-C(14)	100.9(2)	C(3)-C(4)-C(5)	106.8(3)
C(16)-Co(1)-C(14)	104.4(2)	C(7)-C(4)-C(5)	101.7(3)
C(18)-Co(1)-C(14)	141.9(2)	C(52)-C(5)-C(51)	107.7(3)
C(15)-Co(1)-C(14)	38.7(2)	C(52)-C(5)-C(4)	112.7(3)
C(17)-Co(1)-Co(2)	150.8(2)	C(51)-C(5)-C(4)	110.1(3)
C(16)-Co(1)-Co(2)	97.6(2)	C(52)-C(5)-C(6)	113.3(3)
C(18)-Co(1)-Co(2)	100.4(2)	C(51)-C(5)-C(6)	111.5(3)
C(15)-Co(1)-Co(2)	51.86(12)	C(4)-C(5)-C(6)	101.4(3)
C(14)-Co(1)-Co(2)	51.87(12)	C(62)-C(6)-C(61)	108.9(3)
C(20)-Co(2)-C(19)	98.6(3)	C(62)-C(6)-C(1)	112.1(3)
C(20)-Co(2)-C(21)	99.5(3)	C(61)-C(6)-C(1)	110.4(3)
C(19)-Co(2)-C(21)	104.7(3)	C(62)-C(6)-C(5)	111.1(3)
C(20)-Co(2)-C(15)	102.5(2)	C(61)-C(6)-C(5)	112.4(3)
C(19)-Co(2)-C(15)	140.9(2)	C(1)-C(6)-C(5)	101.8(3)
C(21)-Co(2)-C(15)	103.8(2)	C(4)-C(7)-C(1)	93.5(3)
C(20)-Co(2)-C(14)	102.4(2)	C(4)-C(7)-Si(1)	114.3(3)
C(19)-Co(2)-C(14)	104.9(2)	C(1)-C(7)-Si(1)	119.0(3)
C(21)-Co(2)-C(14)	139.7(2)	C(2)-C(8)-C(9)	117.3(5)
C(15)-Co(2)-C(14)	38.5(2)	C(10)-C(9)-C(8)	121.7(5)
C(20)-Co(2)-Co(1)	151.9(2)	C(9)-C(10)-C(11)	121.3(5)
C(19)-Co(2)-Co(1)	98.7(2)	C(3)-C(11)-C(10)	116.9(5)
C(21)-Co(2)-Co(1)	97.4(2)	C(15)-C(14)-Si(1)	148.0(3)
C(15)-Co(2)-Co(1)	51.30(13)	C(15)-C(14)-Co(1)	70.3(3)
C(14)-Co(2)-Co(1)	51.49(13)	Si(1)-C(14)-Co(1)	132.2(2)
C(14)-Si(1)-C(12)	110.2(2)	C(15)-C(14)-Co(2)	70.7(3)
C(14)-Si(1)-C(13)	108.5(2)	Si(1)-C(14)-Co(2)	130.3(2)
C(12)-Si(1)-C(13)	110.0(3)	Co(1)-C(14)-Co(2)	76.6(2)
C(14)-Si(1)-C(7)	106.6(2)	C(14)-C(15)-Si(2)	147.8(3)
C(12)-Si(1)-C(7)	113.5(2)	C(14)-C(15)-Co(1)	70.9(3)
C(13)-Si(1)-C(7)	107.8(2)	Si(2)-C(15)-Co(1)	132.3(3)
C(23)-Si(2)-C(15)	108.2(2)	C(14)-C(15)-Co(2)	70.8(2)
C(23)-Si(2)-C(24)	110.9(3)	Si(2)-C(15)-Co(2)	129.8(2)
C(15)-Si(2)-C(24)	108.5(2)	Co(1)-C(15)-Co(2)	76.8(2)

Table A26. Complete Listing of Bond Angles [deg] for 4.54 (continued).

C(23)-Si(2)-C(22)	109.8(3)	O(16)-C(16)-Co(1)	178.5(6)
C(15)-Si(2)-C(22)	109.0(2)	O(17)-C(17)-Co(1)	177.9(5)
C(24)-Si(2)-C(22)	110.4(3)	O(18)-C(18)-Co(1)	178.5(6)
C(2)-C(1)-C(7)	101.1(3)	O(19)-C(19)-Co(2)	177.7(7)
C(2)-C(1)-C(6)	105.9(3)	O(20)-C(20)-Co(2)	179.7(7)
C(7)-C(1)-C(6)	101.5(3)	O(21)-C(21)-Co(2)	178.4(5)
C(8)-C(2)-C(3)	121.4(4)	N(51)-C(51)-C(5)	177.2(5)
N(52)-C(52)-C(5)	178.8(5)	N(62)-C(62)-C(6)	177.9(5)
N(61)-C(61)-C(6)	176.7(5)		

Table A27. Atomic Coordinates (x 10^4) and Equivalent Isotropic Displacement Parameters ($Å^2$ x 10^3) for 4.54. U(eq) is defined as one third of the trace of the orthogonalized Uij tensor.

	x	y	z	U(eq)
Co(1)	9791(1)	2828(1)	1873(1)	58(1)
Co(2)	9163(1)	4123(1)	1016(1)	60(1)
Si(1)	8704(2)	6006(2)	2422(1)	58(1)
Si(2)	5463(2)	1414(2)	1322(1)	68(1)
N(51)	3190(5)	3140(6)	3402(2)	93(2)
N(52)	5360(5)	6983(5)	4838(2)	70(1)
N(61)	6323(6)	1612(5)	3912(2)	83(1)
N(62)	8641(5)	5636(5)	5307(2)	63(1)
C(1)	8790(5)	5281(4)	3704(2)	42(1)
C(2)	9578(5)	6988(5)	3936(2)	44(1)
C(3)	8384(5)	7615(5)	3778(2)	48(1)
C(4)	6850(5)	6293(5)	3436(2)	51(1)
C(5)	6021(5)	5308(5)	3934(2)	44(1)
C(6)	7423(5)	4616(5)	4141(2)	43(1)
C(7)	7668(5)	5250(5)	3107(2)	45(1)
C(8)	11146(5)	7901(6)	4251(2)	63(1)
C(9)	11502(7)	9488(7)	4376(2)	81(2)
C(10)	10324(8)	10120(6)	4224(3)	82(2)
C(11)	8720(7)	9198(6)	3922(2)	68(1)
C(12)	10931(6)	7320(7)	2641(3)	105(2)
C(13)	7453(8)	7032(6)	2050(3)	100(2)
C(14)	8553(5)	4287(5)	1869(2)	49(1)
C(15)	7600(5)	2926(5)	1545(2)	52(1)
O(16)	13330(5)	4835(6)	2245(2)	128(2)
C(16)	11959(7)	4067(7)	2109(2)	84(2)
O(17)	8999(5)	1665(5)	3015(2)	108(2)
C(17)	9326(6)	2101(6)	2574(3)	69(1)
O(18)	9923(6)	-27(6)	1182(2)	121(2)
C(18)	9856(6)	1064(8)	1440(3)	80(2)
O(19)	12476(6)	6528(6)	1115(2)	150(2)
C(19)	11181(7)	5619(7)	1074(2)	90(2)
C(20)	7932(8)	5020(8)	624(3)	94(2)
O(20)	7140(6)	5586(7)	373(2)	145(2)
C(21)	9122(7)	2669(7)	390(3)	83(2)
O(21)	9127(6)	1775(6)	-10(2)	130(2)
C(22)	5623(6)	-328(6)	853(3)	89(2)

Table A27. Atomic Coordinates (x 10^4) and Equivalent Isotropic Displacement Parameters ($Å^2$ x 10^3) for 4.54 (continued). U(eq) is defined as one third of the trace of the orthogonalized Uij tensor.

	x	y	z	U(eq)
C(23)	4606(7)	893(7)	2040(3)	114(2)
C(24)	4123(6)	2220(7)	861(3)	95(2)
C(51)	4420(6)	4062(6)	3644(2)	59(1)
C(52)	5654(5)	6255(5)	4452(2)	49(1)
C(61)	6777(5)	2903(6)	4025(2)	52(1)
C(62)	8110(5)	5168(5)	4802(2)	44(1)